Investigations of Photoswitchable Platform Molecules on Au(111) Surfaces by Scanning Tunneling Microscopy

Dissertation

zur Erlangung des Doktorgrades
der Mathematisch-Naturwissenschaftlichen Fakultät
der Christian-Albrechts-Universität zu Kiel
vorgelegt von

Talina Rusch

Kiel 2020

Erster Gutachter:	Prof. Dr. Olaf M. Magnussen
Zweiter Gutachter:	Prof. Dr. Rainer Herges
Tag der mündlichen Prüfung:	02.04.2020

Abstract

The functionalization of surfaces by self-assembled monolayers is of great interest for the bottom-up preparation of functional nanosystems. In this thesis structural investigations of photoswitchable self-assembled monolayers on Au(111) and investigations of their switching behavior via scanning tunneling microscopy under ambient conditions are presented.

Initially, adsorbate layers of five different triazatriangulenium-based (TATA) azobenzene derivatives with varying coupling units between the photoswitch and the surface were investigated. They all exhibit highly-ordered hexagonal monolayers with a $(\sqrt{19} \times \sqrt{19})$ $R23.4^\circ$ superstructure and IRRAS measurements confirm that the reversible isomerization mechanism is retained upon metal-surface adsorption. When exploring the gold mediated thermal relaxation a significant dependency of the relaxation rates on the coupling of the azobenzene to the gold surface was shown. An electronically isolating linker group therefore enables a high stability of the *cis* configuration against thermal backswitching.

Based on these results, the *trans*-to-*cis* isomerization of monolayers consisting of the isolated azobenzene derivative was investigated by molecular scale STM. The analysis of the high-resolution STM images revealed that the *trans*-to-*cis* isomerization does not occur randomly but is dependent on the isomeric state of the neighboring molecules. Therefore, the irradiation with UV-light results in a formation of *trans* and *cis* clusters.

Furthermore, the coadsorption of the highly stable isolated azobenene TATA with TATA-based molecules with different vertical functions is shown. The molecules can be mixed without affecting the in-plane order, allowing a facile preparation of stochastically mixed bifunctional adsorbate layers.

Finally, a molecule composed of an azobenzene unit spanned between two molecular pillars mounted on TATA platforms was adsorbed on Au(111). A preparation under defined deposition conditions results in a $(\sqrt{31} \times \sqrt{31})$ $R8.9^\circ$ superstructure. UV/Vis and NEXAFS measurements show the reversible switching of the azobenzene and indicate differences in the rotatability of the isomers, making it a horizontally oriented switch as well as an altitudinal rotor.

Kurfassung

Die Funktionalisierung von Oberflächen durch selbstorganisierte Monoschichten ist für die Bottom-up-Präparation von funktionellen Nanosystemen von großem Interesse. In dieser Arbeit werden strukturelle Untersuchungen von photoschaltbaren selbstorganisierten Monolagen auf Au(111) und Untersuchungen ihres Schaltverhaltens mittels Rastertunnelmikroskopie unter Umgebungsbedingungen vorgestellt.
Zunächst wurden Adsorbatschichten von fünf verschiedenen Azobenzol-Derivaten auf Triazatriangulenium (TATA)-Basis mit unterschiedlichen elektronischen Kopplungseinheiten zwischen dem Photoschalter und der Oberfläche untersucht. Sie alle weisen hochgeordnete hexagonale Monolagen mit einer $(\sqrt{19} \times \sqrt{19})$ $R23.4°$-Überstruktur auf und IRRAS-Messungen bestätigen, dass der reversible Isomerisierungsmechanismus bei der Adsorption auf die Metalloberflächen erhalten bleibt. Bei der Untersuchung der goldvermittelten thermischen Relaxation zeigte sich eine signifikante Abhängigkeit der Relaxationsraten von der Kopplung des Azobenzols an die Goldoberfläche. Eine elektronisch isolierende Verbindungseinheit ermöglicht daher eine hohe Stabilität der *cis*-Konfiguration gegenüber thermischer Rückschaltung.
Basierend auf diesen Ergebnissen wurde die *trans-cis*-Isomerisierung von Monolagen, die aus dem isolierten Azobenzol-Derivat bestehen, mittels STM auf molekularer Ebene untersucht. Die Analyse der hochauflösenden STM-Bilder ergab, dass die *trans* zu *cis*-Isomerisierung nicht zufällig erfolgt, sondern vom Konfigurationszustand der Nachbarmoleküle abhängt. Die Belichtung mit UV-Licht führt daher zu einer Bildung von *trans*- und *cis*-Clustern.
Darüber hinaus wird die Koadsorption des hochstabilen isolierten Azobenzol-TATA mit TATA-basierten Molekülen mit unterschiedlichen vertikalen Funktionen gezeigt. Die Moleküle können gemischt werden, ohne die Anordnung auf der Goldoberfläche zu beeinflussen, sodass eine einfache Herstellung von stochastisch gemischten bifunktionalen Adsorbatschichten möglich ist.
Schließlich wurde ein Molekül, das aus einer Azobenzol-Einheit besteht, die zwischen zwei auf TATA-Plattformen montierten molekularen Säulen gespannt ist, auf Au(111) adsorbiert. Eine Präparation unter definierten Adsorptionsbedingungen führt zu einer $(\sqrt{31} \times \sqrt{31})$ $R8.9°$-Überstruktur. UV/Vis- und NEXAFS-Messungen belegen die reversible Umschaltung des Azobenzols und deuten auf Unterschiede in der Rotierbarkeit der Isomere hin, sodass es sich sowohl um einen horizontal ausgerichteten Schalter als auch um einen altitudinalen Rotor handelt.

Contents

1 | Introduction

The preparation and characterization of self-assembled monolayers are integral parts of today's research [1–5]. A reason for this is that the targeted control of surface properties with tailored molecular functionalities seems to be a promising answer to the rapidly increasing demand for miniaturization in the existing technologies [6–9]. A photoswitchable unit embedded into the adsorbate layer can be used to switch surface properties on and off in a targeted manner. Furthermore, such photoswitchable molecules can serve as building blocks in molecular machines [10, 11]. The relevance of this interdisciplinary research area was underlined in 2016 by the award of the Nobel Prize to B. Feringa, J.-P. Sauvage and J. F. Stoddart "for the design and synthesis of molecular machines" [12].
In comparison to statically functionalized systems, switchable systems require a more precise control over the adsorption geometry to fine tune the coupling between the substrate and functional groups and avoid steric hindrance when switching. The platform concept, which was introduced in 2009 offers a successful strategy for vertically mounting spaced out functionalities on surfaces while enabling control over the vertical as well as lateral spacings [13]. The modularity of the molecular architecture allows a precise adjustment of the adsorption geometry and coupling to the substrate [14–18].

The objective of this thesis is to gain insight into the switching and adsorption behavior of well-known azobenzenes mounted on such molecular platforms on an Au(111) substrate. The studies presented here were carried out within the Collaborative Research Centre 677 - "Function by Switching" and are thus part of a joint effort of several research groups. The focus

of my work lies on the preparation of photoswitchable adsorbate layers and their characterization by scanning tunneling microscopy (STM) under ambient conditions.
Since its development by Gerd Binnig and Heinrich Rohrer, the scanning tunnelling microscope has become a versatile and important method for the investigation of surfaces [19, 20]. In this work it has been used to investigate systems with different coupling to the metallic substrate, bifunctional systems and the switching behavior of azobenzene-functionalized adsorbate layers. Prior to this, however, preparation conditions to form the adsorbate layers had to be found. The aim was to obtain an adsorbate layer as homogeneous as possible with a low defect density. For this purpose, different preparation procedures were employed and assessed by STM.
The systems examined are the following: The investigation of five different azobenzene derivatives is shown in chapter 4. They form a series of conjugation strengths, including an isolated and a fully conjugated system. The functionalities are mounted on a triazatriangulenium (TATA) platform with laterally spacings controlled by octyl side chains. This study explores the influence of electronic coupling on the relaxation behavior by systematic measurements of adsorbate layers consisting of the differently conjugated molecules.
Based on the results from chapter 4, the isolated system was chosen for an in-depth study of the *trans*-to-*cis* photoswitching behavior. Direct molecular scale STM observations of the switching process were complemented by UV/vis and IRRA spectroscopy measurements as well as calculations. These results are presented in chapter 5.
Chapter 6 covers the results of coadsorption experiments, in which the isolated azobenzene-TATA was mixed with the fully conjugated species, the bare platform and pyridine mounted on a TATA platform, respectively.
The seventh chapter deals with the extension of the platform concept to horizontally mounted functionalities, specifically, a molecule composed of an azobenzene unit as a bridge between two molecular pillars mounted on TATA platforms.

2 | Scientific Background

2.1 Molecular Switches - Azobenzene

Molecules that can convert between different states due to external influences can be found in biological systems in many variations [4, 21]. Since these so-called molecular switches create functions in the smallest of spaces, attempts have been made for decades to use them in a controlled manner for miniaturization. In the present work only photochromic molecular switches were investigated. They perform structural as well as electronic changes via excitation with light of a suitable wavelength [22–25]. The molecules can be reversibly switched between at least two states via a *trans-cis* isomerization, a photocyclization or a combination of both [4].

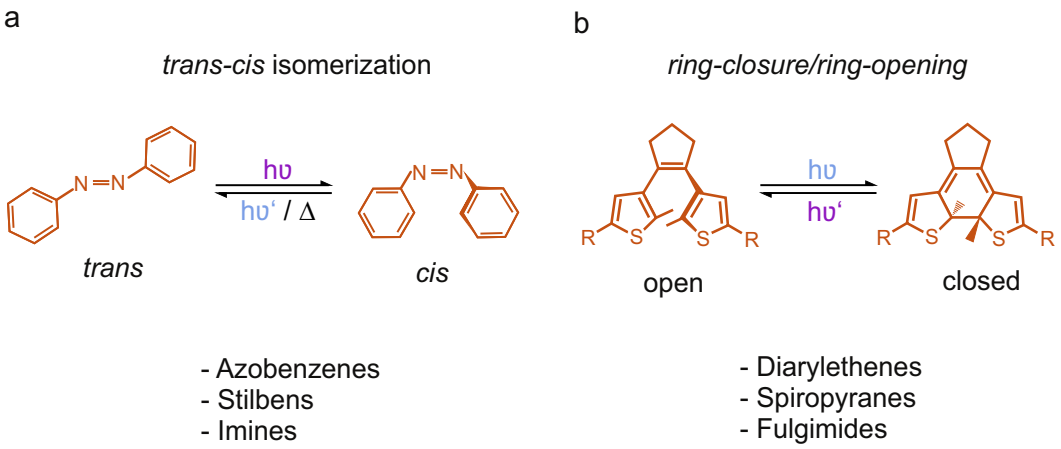

Figure 2.1: Switching mechanisms of photochromic molecules: (a) *trans-cis* isomerization of azobenzene, (b) photocyclization of diarylethene. Based on [26].

Figure 2.1 shows examples of photochromic systems that can undergo a

trans-cis isomerization (Fig. 2.1a) or a photocyclization (Fig 2.1b). These molecular switches and their derivatives have been studied extensively over the past decades.
Diarylethene is shown as an example of photocyclic reaction. In this type of isomerization a chemical bond is created (ring-closing) or broken (ring-opening). It can cyclize at 331 nm irradiation and ring-opening takes place at 552 nm.
As an example of *trans-cis* isomerization, Figure 2.1a shows one of the most prominent molecular switches, azobenzene, which was investigated in the CRC 677 and also in the course of this work. In contrast to diarylethene, azobenzene undergoes a large geometric change during isomerization and is therefore well suited for investigation with surface sensitive methods. It was investigated 1937 by Hartley [27] and the photochemical *trans-cis* isomerization was first described by Krollpfeiffer et al. [28]. The *trans* and the *cis* isomer of azobenzene exhibit well-separated absorption bands in the UV and visible region. The *trans-cis* isomerization takes place by irradiation with a wavelength of 365 nm. The *cis* $\rightarrow$ *trans* reaction can be activated by photoinduced isomerization with 455 nm as well as thermally. The two isomeric states differ not only in their geometry but also in their electronic properties: The *trans* form is planar without a dipole moment μ while the *cis* form is non-planar and has a dipole moment of about μ = 3.2 D [29]. The planar *trans* form is thermodynamically more stable by 56 kJ/mol than the *cis* isomer. For years there has been much debate about the pathway for azobenzene photoisomerization [30–32], which can be either inversion, rotation, concerted inversion or inversion-assisted rotation (see Fig. 2.2) [33, 34].

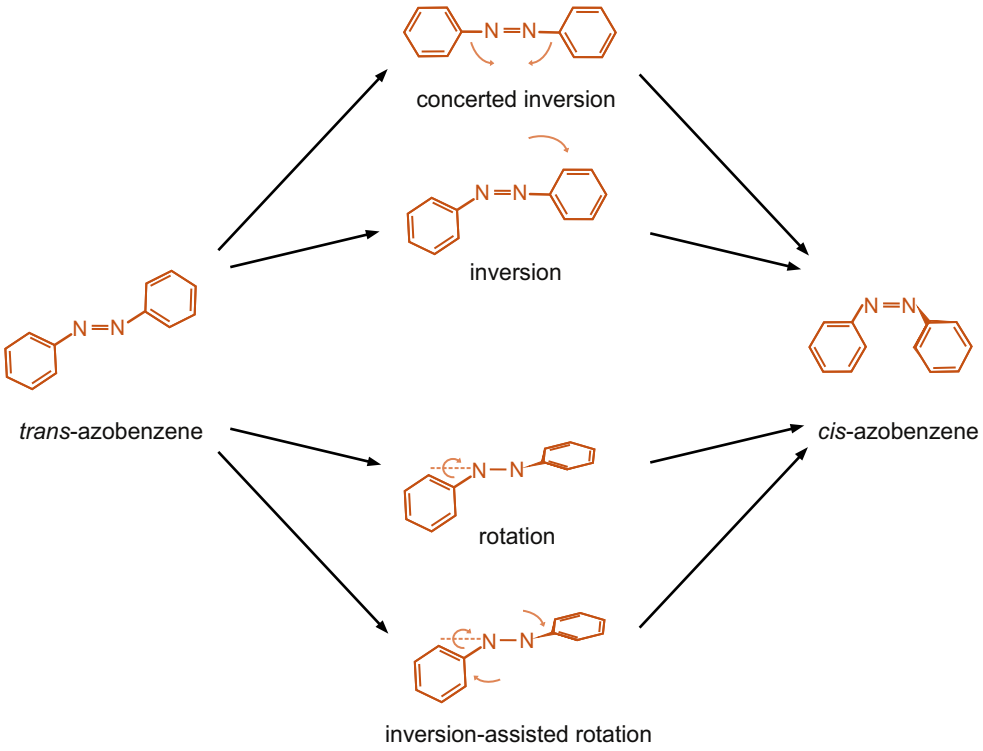

Figure 2.2: Four proposed pathways for the *trans-cis* isomerization of azobenzene. Based on [34].

The rotational pathway is caused by rotation of the N-N-single bond, while the inversional pathway is based on the inversion of an N-atom. In the concerted inversion mechanism, a linear transition state is created by increasing both N=N-C bond angles to 180°. In inversion-assisted rotation the C-N=N-C dihedral angle and the N=N-C angles change simultaneously. All four mechanisms predict photostationary states which consist of both isomers. Which pathway occurs depends on the respective azobenzene derivative and the chemical environment (e.g. solvent polarity). Also multiple isomerization pathways have been suggested to explain experimental observations [31]. Many studies concluded that the employed pathway depends on the isomerization and relaxation route. The photochemical isomerization of azobenzene follows an excitation from the ground state (singlet state S_0) to the S_1 ($n \rightarrow \pi^*$) and the S_2 ($\pi \rightarrow \pi^*$) states [35]. Computational studies showed the existence of triplet excited states [34, 36].

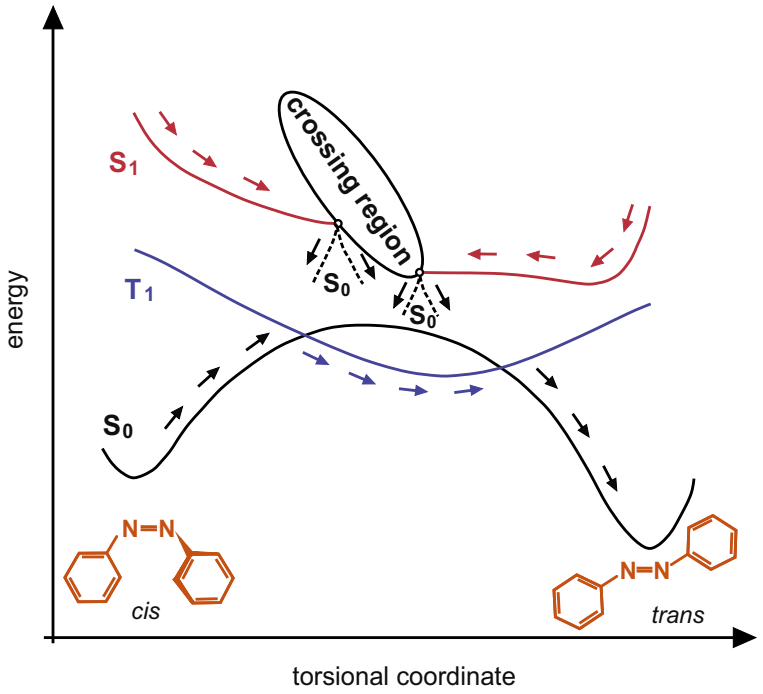

Figure 2.3: S_0, S_1 and T_1 reaction paths for the *cis-trans* isomerization in azobenzene. The crossing region contains different S_1/S_0 conical intersections. Based on [36].

Figure 2.3 shows a schematic of a suggested decay and isomerization route of the ground state S_0 and the low-lying singlet S_1 and triplet T_1 excited states of azobenzene. Four S_1/S_0 conical intersections are located in the marked crossing region.
All in all, the distinctive properties of azobenzene, especially the reversible switching with light and the large change in geometry during isomerization, make it a suitable molecule for surface functionalization.

2.2 Self-Assembled Monolayers

A simple method to make surface properties controllable is the functionalization by means of self-assembled monolayers (SAMs). SAMs are molecular assemblies that are formed by the adsorption of a surface-active material to a substrate and order without external intervention via local interactions [1, 37, 38]. SAMs can be formed by a wet-chemical process or vapor deposition [2]. In the former case, the substrate is immersed into a solution of the respective molecules. In this procedure, the solvent, the concentration of the solution, the duration of immersion of the substrate and the temperature have an influence on the adsorption and the process of self-organization [39]. All adsorbate layers investigated in this thesis were prepared using this method.

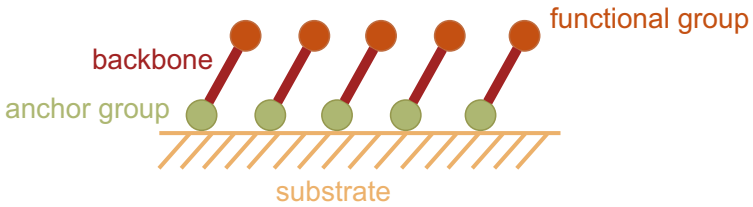

Figure 2.4: Schematic illustration of the structure of self-assembled monolayers. The molecules are attached to the surface via an anchor group (green). The backbone (red) creates a spacing between the surface of the substrate (yellow) and the functional unit (orange).

Figure 2.4 shows a schematic illustration of the basic structure of a SAM. The large variety of applications, e.g. for corrosion inhibition, coating of colloidal particles, molecular electronics and biorelated applications [1, 2, 39, 40], is mainly based on the ability to tailor the anchoring group as well as the functionality of the single molecules and the wide range of investigated molecule-substrate systems. The choice of an anchoring group also determines the type of binding to the substrate, either via physisorption or via chemisorption. In the latter case, the molecules bind covalently to the substrate and in the former case the molecules can be attached by non-covalent interactions like van-der-Waals or π-π interactions. The binding energies are therefore significantly higher in chemisorbed systems (about

190 kJ/mol) than in physisorbed ones (about 4-40 kJ/mol), but also in physisorbed systems the binding energy can be quite high for example in extended π-systems in molecular platforms [41, 42]. A well studied approach to bind azobenzenes covalently to surfaces is the use of thiolates. Especially, thiol bonds on gold surfaces were investigated because the bond is very stable due to the great affinity of sulfur to gold. Furthermore, gold is particularly suitable as a substrate for SAMs in general because of its chemical inertness. Azobenzenes can also be brought directly on gold surfaces as monolayers, but the close contact with the substrate hinders the photoinduced switching [4]. Therefore, an attempt was made to create a distance to the gold surface using azobenzene-functionalized alkanthiols and to avoid direct contact between the azobenzene and the gold. The packing density of SAMs consisting of functionalized alkanthiols is very high, so that the molecules are upright, almost perpendicular to the surface. However, photoisomerization is sterically hindered by the high packing density. In order to reduce the packing density and thus increase the switching efficiency, functionalized alkanethiols were mixed with shorter molecules and adsorbed on the surface. The shorter alkyl chains serve as lateral spacers and allow the functional groups more free volume for the photoisomerization. Unfortunately, mixing the alkanethiols on the surface does not produce a homogeneous monolayer, but also phase-separated areas. Therefore, only a reduced switching efficiency could be demonstrated for these monolayers. This shows that the formation of highly ordered, functional SAMs requires precise control over the adsorption geometry. But using thiols, the in-plane order and orientation are difficult to adjust [40, 43, 44].
Several strategies have therefore been developed to control the exact positioning of molecular building blocks [4, 45–47].

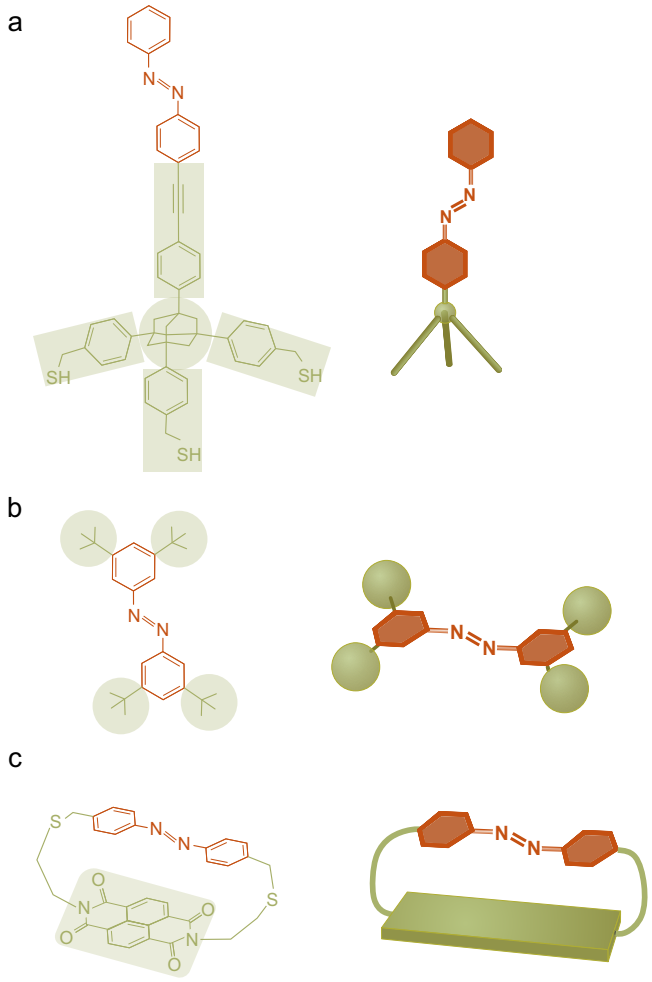

Figure 2.5: Examples of molecular architectures that permit decoupling of a functional unit from a substrate. Azobenzene (a) mounted on a tripodal platform [48], (b) mounted on bulky spacer groups, namely tetra-*tert*-butyl [49], and (c) embedded in a cyclophane-type molecule [50].

Figure 2.5 shows examples of different approaches that result in an adsorption geometry where the functional unit is mechanically decoupled from the surface.

Many studies focus on molecular architectures with multiple anchor groups (Fig. 2.5a, b). Tripodal adsorbates are one of these architectures. They consist of a tetrahedral core with three substituents used as a tripodal scaffold and one oriented perpendicular to the surface. This fourth substituent is the functional group. The molecules can be attached to a surface via three anchoring groups. The distance between the functionality and the anchors

can be varied by using different rigid spacers such as aromatic units or phenylene ethylene species [46, 51]. For the core, carbon [52–54], silicon [55, 56] or adamantane [57, 58] atoms have been reported [47]. Kitagawa and co-workers examined the adsorption of multiple tripods and found that all three sulfur atoms of the anchoring unit bind to the Au(111) surface [59]. Functionalized tripodal scaffolds can form well-ordered SAMs with the functionality standing upright in respect to the surface [57, 60]. Several research groups have investigated azobenzene-terminated tripodal derivatives [61–64]. The group of P. Tegeder showed that a SAM on Au(111) consisting of an azobenzene unit connected to a tripodal scaffold with an adamantane core (see Fig. 2.5a) can perform reversible photoinduced switching [48].

Another well-studied approach for maintaining the photoswitchability of azobenzenes on surfaces is the use of bulky spacer molecules, namely tetra-*tert*-butyl [26, 65, 66]. Adsorbed on Au(111), the four spacers maintain the azobenzene unit above the surface in such a way that it has no direct contact with it (see Fig. 2.5b). Tetra-*tert*-butyl-azobenzenes (TBA) can form highly ordered monolayers on gold surfaces that are switchable by irradiation [49, 67, 68] and directly with an STM tip [26, 69, 70]. However, reversible photoinduced switching could not be observed, only thermal backswitching can take place [67, 68, 71–73].

Cyclophane-type structures were developed to decouple the functional unit even more than tetra-*tert*-butyl units from the metallic surface. They create a greater distance between the azobenzene and the surface than the bulky spacer molecules by using a double-decker structure. Matino et al. demonstrated the electronic decoupling of the azobenzene from an Au(111) surface via scanning tunneling spectroscopy studies [74]. Figure 2.5c shows an example of an azobenzene containing cyclophane. The lower deck contains a naphthalene diimide phane which is adsorbed to the surface due to dispersion interactions while the azobenzene is expected to be separated from the surface as the upper deck. STM investigations performed under ultra-high vacuum conditions at low temperature proved that the molecules adsorb in the expected way with the upper deck being the azobenzenophane. Un-

fortunately, reversible photoinduced switching was not reported so far. Another approach which like the cyclophane type molecules uses only one anchor group is the platform concept [13]. It employs a planar molecule as an anchor unit to which a functional unit can be attached to.

2.3 The Platform Concept

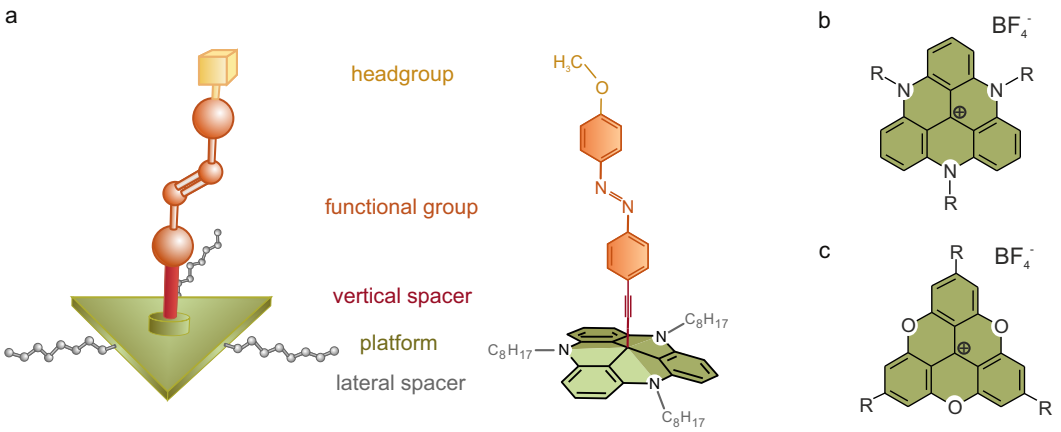

Figure 2.6: Schematic illustration of the platform approach. (a) Basic principle of the architecture, (b) molecular structure of the triazatriangulenium ion and (c) molecular structure of the trioxatriangulenium ion.

Figure 2.6a shows the architecture of the so called platform molecules: The basic principle is, that the functional group is attached perpendicular to a molecular platform (green triangle), which provides a free volume for the functionality of the molecule. Between them sits a rotatable spacer (red), which is used to provide a defined distance between the substrate and the functional unit. The side chains of the platform molecule (grey) are variable in length to adjust the intermolecular distance on the surface. There is also the possibility to attach a headgroup (yellow) to the functional unit which can be used as a marker for different measuring methods.
Molecules that have been used as molecular platforms are triazatriangulenium (TATA) (Fig. 2.6b) and trioxatriangulenium (TOTA) (Fig. 2.6c). Both platforms contain a central carbon atom to which an ethynyl spacer with a functional group can be attached via a covalent bond. In addition, side

groups can be attached to the three nitrogen atoms of the TATA and in para-position relative to the central carbon atom to the TOTA.
A synthesis of triazatriangulenium salts was first published by B. W. Laursen and F. C. Krebs [75] and further investigations were performed in the working group of J. Lacour [76]. Compared to TATA, TOTA has a lower molecular mass and a lower sublimation energy. In addition, the bond strength of the functional group attached vertically to the carbon atom is greater in TOTA, making it more suitable for the adsorption in ultra-high vacuum [77].
In the course of this work, only TATA-based molecules were investigated on Au(111) surfaces. The molecules are adsorbed due to dispersive interactions and thereby not covalently attached like thiol-based systems. In the collaborative research centre 677 TATA-based molecules were characterized in detail in solution as well as adsorbed on surfaces [13–15, 78–81].
Scanning tunneling microscopy measurements have shown that TATA cations form highly ordered hexagonal monolayers upon adsorption and the phenyl rings as well as the nitrogen atoms are preferrably located on top of the gold atoms [13, 18]. As mentioned above, the intermolecular distance can be tuned by varying the alkyl chains attached to the nitrogen atoms of the TATA platform. Thereby, the change in the distance proceeds stepwise and not continuously. For example, propyl TATA molecules form a $(\sqrt{13} \times \sqrt{13})$ $R13.9^\circ$ superstructure (intermolecular distance d = 1.04 nm), whereas everything between butyl and decyl TATA forms a $\sqrt{19} \times \sqrt{19})$ $R23.4^\circ$ superstructure (d = 1.26 nm). Undecyl TATA can exhibit both, a $(\sqrt{19} \times \sqrt{19})$ $R23.4^\circ$ and a $(\sqrt{21} \times \sqrt{21})$ $R10.9^\circ$ superstructure, while dodecyl TATA monolayers exhibit only a $(\sqrt{21} \times \sqrt{21})$ $R10.9^\circ$ superstructure (d = 1.32 nm) [18]. The alkyl chains cannot be completely adsorbed on the substrate because there is too little space between the molecules. Therefore, they overlap partially and can also lie on the platforms. A vertical functionalization by different groups, e.g. azobenzene, imine and diazocine, has no influence on the formed superstructure and thus on the intermolecular distances [14, 17, 78, 82–86].

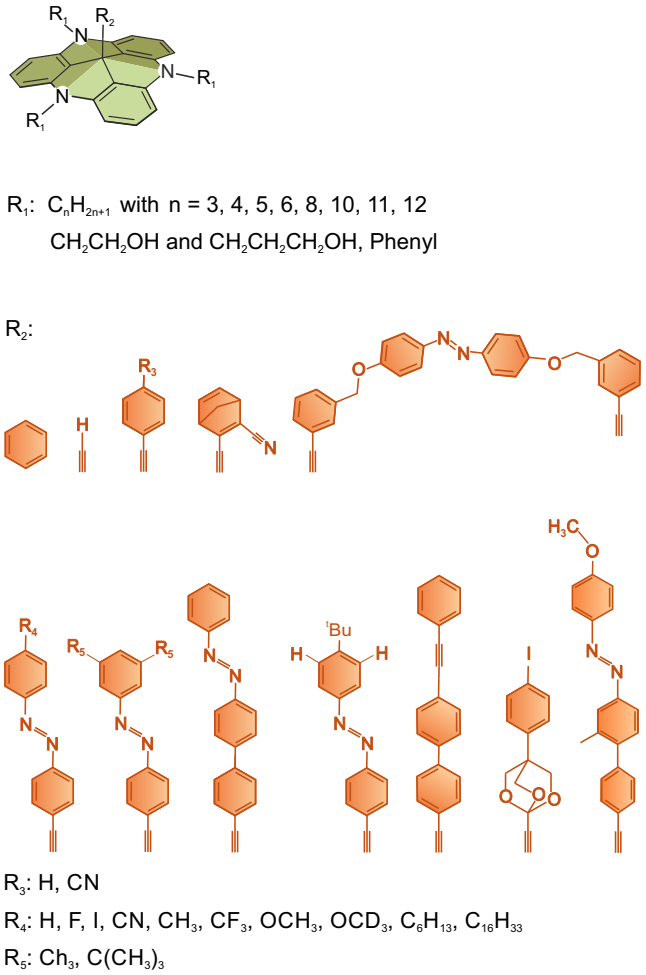

Figure 2.7: Schematic of a sample of TATA derivatives that have already been synthesized using the platform approach.

Many studies have focused on octyl-TATA functionalized molecules on surfaces. Due to the large intermolecular distance there is no steric hindrance and thus the photoswitchability of the functionalities stays intact.
Another huge advantage of the platform concept is, that it achieves modularity due to the variety of possibilities to design a molecule by choosing between different functionalities, molecular platforms, headgroups and side chains. Figure 2.7 shows examples of molecules that already have been synthesized by the research group of Prof. Dr. R. Herges and adsorbed on surfaces. Several surface sensitive methods have been used to characterize the molecules, for instance UV/visible spectroscopy [87], surface-enhanced

Raman spectroscopy (SERS) [14], cyclic voltammetry [81], near edge X-ray absorption fine structure (NEXAFS) [88], STM [13, 42, 78] and infrared reflection absorption spectroscopy (IRRAS) [17]. For the latter, methoxy groups have shown to be a particulary suitable markers. The C-O stretching vibration perpendicular to the surface leads to a strong absorbance band in the IRRA spectrum. This is the reason why the molecules in the following publications have a methoxy group attached to the functional unit. However, the work of this thesis focuses on the investigation of different platform molecules adsorbed on gold surfaces via scanning tunneling microscopy.

2.4 Scanning Tunneling Microscopy

The scanning tunneling microscope (STM) uses the quantum mechanical tunneling effect to display conductive surfaces as three-dimensional real-space images with atomic resolution. It was developed by Heinrich Rohrer and Gerhard Binnig, who both received the Nobel Prize for this work in 1981 [19, 89]. A metallic, ideally monoatomically sharp tip is approached to a metallic surface within a few angstroms. This allows electrons to tunnel from occupied states to unoccupied states on the other side of the potential barrier. When a voltage U_{bias} is applied, the Fermi levels of tip and sample are shifted against each other by the value of U_{bias} and a tunnel current I_t can be measured.

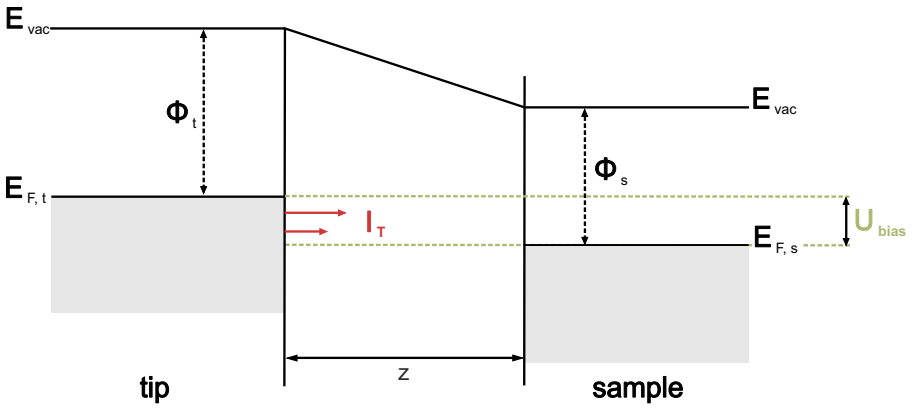

Figure 2.8: Schematic illustration of the energy levels during tunnelling. Φ_t and Φ_s denote the work functions of the tip and the sample with respect to the vacuum energy level E_{vac}. $E_{F,t}$ and $E_{F,s}$ describe the Fermi energies of the tip and the sample. I_t illustrates the tunnel current when positive voltage U_{bias} is applied to the sample.

When a positive voltage is applied, electrons tunnel from occupied states of the tip to unoccupied states of the sample, and vice versa when a negative voltage is applied. The measured tunnel current depends on the probability of tunneling through the barrier and is also exponentially dependent on the distance z between the sample and the tip:

$$I_t \propto |\Psi|^2 \propto U_{bias} \cdot e^{-2z\sqrt{\frac{2m_e \cdot \Phi}{\hbar^2}}}. \tag{2.1}$$

Here, Φ denotes the effective barrier height, m_e the free electron mass and $\hbar$ Planck's constant divided by 2π. The resulting high distance sensitivity is utilized when performing the STM measurement. The sample surface is scanned contact-free by means of piezo elements. Depending on the scanning method, different samples can be examined or different information can be obtained from the data. Essentially, a distinction is made between two measuring modes: the constant current and the constant height mode.

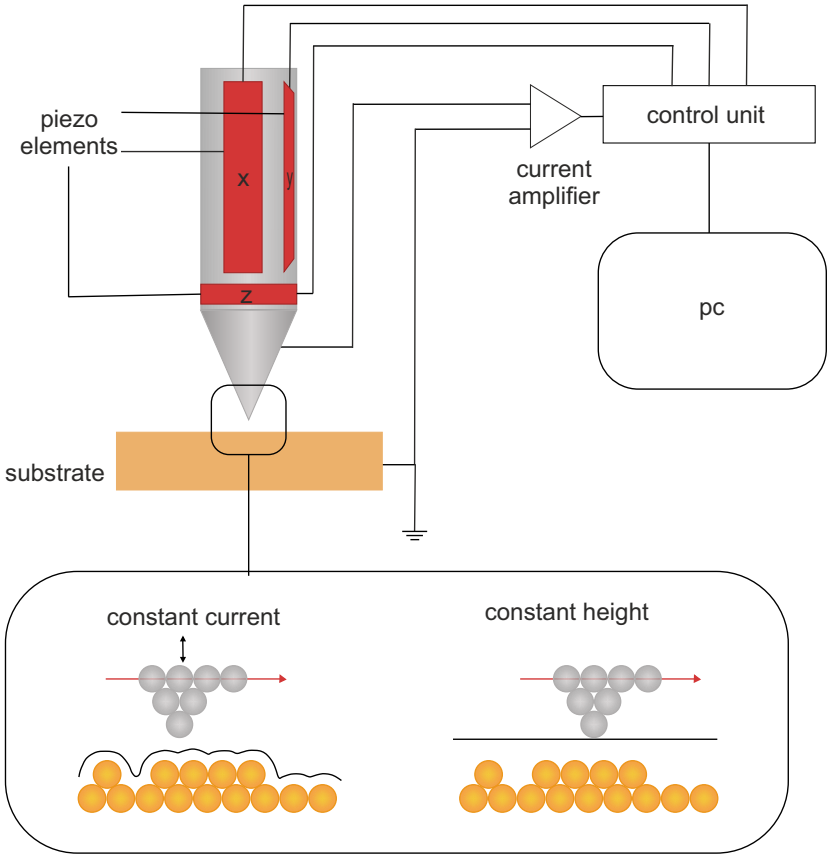

Figure 2.9: Schematic illustration of the STM working principle and both scanning modes.

In the constant current mode, the distance between the tip and the sample is adjusted via a feedback loop so that the tunnel current remains constant. A topography image can be calculated from the control voltages at the piezo elements which are adjusting the position of the tip. Due to the adjustment of the height, rough surfaces can be measured well in this mode.

In the constant height mode the distance between the tip and the average sample surface remains unchanged and from the measured tunnel current the surface topography image can be generated. The advantage of this measuring mode is that it is possible to scan at a high speed. However, this can only be used for atomically smooth surfaces. The adsorbate layers investigated in this work were therefore measured in constant current mode.
Since STM images reflect not only the geometry but also the electronic properties, the topography images obtained may differ significantly from the real topography [90]. Thus, the topographical representation of the STM data is called apparent height. A major difference between apparent and absolute height is mainly observed when complex molecules are adsorbed onto the surface. This is for example due to the fact that the adsorbate-surface interaction influences the work function of the substrate [91, 92] as well as the adsorbate molecular orbitals [93] leading to a shift in their energy and therefore influence the local density of states probed in the STM experiments. All in all the interpretation of STM images is challenging because the contrast depends on the applied voltage, the surface, the tip, the adsorbates and their associated interactions [94, 95].
With the STM it is not only possible to create images of surfaces, but also to measure magnetic properties [96, 97], identify molecules [98, 99] as well as manipulate single atoms with the tip (e.g. switching or moving) [65, 100]. It can be used in a vacuum at low temperature, under ambient conditions and in liquids, including electrochemically. All data shown in this thesis were recorded under ambient conditions.
Due to the small changes in ambient temperature, the images are often distorted due to thermal expansion. This so-called thermal drift is caused by slow contractions or expansions of the sample and microscope material and results in variations in length of several nanometers during a few seconds [101]. By using low-expansion materials and components with large thermal masses, the drift can be reduced. Since the thermal drift is particularly high when the sample or tip is inserted into the microscope, it is reduced after long scanning when the system is stabilized and thermal equilibrium is reached.
A low drift was especially important for the measurements in chapter 5, as

it allowed the same sample area to be scanned over a longer period of time and a quantitative analysis of the data to be conducted.
A detailed description of the fundamentals of STM can be found in the literature [20, 102–105].

3 | Experimental Details

The preparation and characterization of functional surfaces consisting of one or two different functionalities and the investigation of the photoisomerization behavior of azobenzene SAMs were the main objectives of this thesis. Thus, different TATA-based molecules, most of them with azobenzene as a functional unit, were adsorbed on Au(111) surfaces by self-assembly.
This chapter provides an overview of the procedure for preparing the adsorbate layers, the experimental setup and the data analysis performed.

3.1 Sample Preparation

Au(111) single crystals from MaTeck GmbH Jülich, which have an orientation accuracy of $\leq 0.3°$, were used as substrates for all scanning tunneling microscopic investigations of this work. The crystals used have a diameter of 10 mm and are 3 mm high. To ensure a smooth surface of the crystals, they were electro-polished in an interval approximately of four weeks. For this procedure, the crystal was immersed in 0.1 M sulfuric acid on a platinum grid in the center of a ring-shaped platinum wire acting as cathode. The substrate was then oxizied by applying a voltage of 4V between the crystal and the cathode. The potential was kept at this level for 20 seconds. Afterwards, the substrate was rinsed with Milli-Q water (18.2 MΩ, TOC value less than 10 ppb) and placed in 0.1 M HCl for four minutes. This procedure is however only suitable to smooth out small roughnesses. If a large roughness was observed during STM measurements, about 10 to 50 nm of gold had to be removed by another method. Here, the crystal was immersed in a solution of 2.5 parts ethylene glycol, 1.5 parts ethanol and one part 33%

HCl at 60°C. The crystal was again contacted by placing it on a platinum grid, a zylindric platinum sheet placed also in the prepared solution around the gold crystal acted as the cathode. The potential applied between the crystal and the cathode was chosen to provide a current between 3 and 4.5 A and kept at this level for 20 seconds. Afterwards, the crystal was rinsed as described before. Subsequent to both processes, the crystal was heated with a butane flame for at least four minutes. This increases the surface mobility of the gold atoms, making the surface atomically smooth and terraces of up to several hundred nanometres are formed. In addition, reconstructions are formed on the Au(111) surface, which are either visible below the adsorbate layer during STM measurement or dissolve in gold islands.

All glassware used for polishing and preparation was cleaned beforehand by placing it in a mixture of 2/3 sulphuric acid and 1/3 hydrogen peroxide for at least 24 hours. This ensures that the impurities from previous preparations (solvents and molecular residues) are removed. Subsequently, the working materials were thoroughly rinsed with and afterwards placed in Milli-Q water and heated while immersed. This rinsing and heating process was repeated four times. It removes the acid residues from the glassware, which can then be stored in cleaned containers for an extended period of time. The titanium forceps used were heated with butane gas for cleaning before each preparation. The gold crystals were also heated before each preparation using a butane gas flame to remove previous adsorbate layers and smooth the gold surface as described above. After the crystals had cooled in air for five minutes, they were placed in a solution consisting of the respective molecules. In most cases, the corresponding solutions were previously prepared in a larger beaker at a defined concentration and then filled into a smaller beaker with a ground lid for the respective preparation using a sterile pipette (5 ml pipette from ThermoFisher Scientific). This allowed prepared solutions to be used for several experiments over a longer period of time. For some molecules, such as the pyridine-TATA [106] or the norbornadiene-TATA [85], the solutions were prepared immediately before the gold crystal was immersed and were not stored because the molecules in the solution were not stable over a longer period of time.

Although the concentration, temperature and duration of immersion have an impact on the preparation of the adsorbate layers, it has been shown that the choice of solvent has the greatest influence on the formation of the adsorbate layer. This could be observed by STM measurements on adsorbate layers consisting of different TATA-based molecules. An example is shown in Fig. 3.1. It shows STM images of tert-butyl-Imin-TATA [82] SAMs on an Au(111) surface. Prepared with toluene despite several systematic variations in temperature, concentration and immersion time, only isolated molecules and bilayers can be seen on the gold surface (Fig. 3.1a). Prepared with tetrahydrofuran, however, a complete monolayer of the molecules is obtained (Fig. 3.1b).

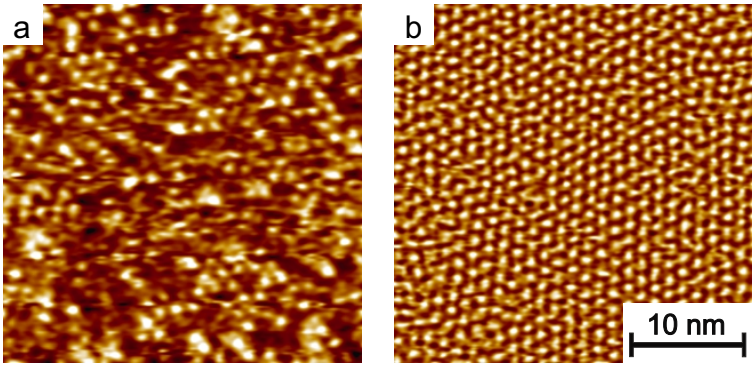

Figure 3.1: STM images of tert-butyl-Imin-TATA on Au(111), (30 x 30) nm^2, prepared with (a) toluene and (b) THF.

Therefore, the search for a suitable preparation condition began with the variation of the solvent. As soon as an adsorbate layer had formed, an attempt was made to form a complete highly ordered monolayer by varying the concentration, immersion time and temperature. An advantage when preparing under high temperatures is that it inhibits the formation of bilayers. However, it must be ensured that the temperature is insufficient to cause bond breaking within the molecules. In addition, attempts were made to achieve the shortest possible immersion times in order not to prolong the preparation process unnecessarily. At the same time, however, the immersion time must be long enough for a fully ordered layer to form. The time of immersion varied between half an hour and 72 hours, the tempera-

ture was between room temperature and 80°C. After that, the crystals were rinsed three times with the pure solvent to remove excess molecules from the surface. They were then dried in air and placed in the STM setup for immediate measurement.
The preparation of the mixed adlayers (see chapter 6) was similar to the procedure described above. The only difference in coadsorption is that the solution in which the crystals are inserted contains two different types of molecules with different concentrations. In this type of preparation, the different types of molecules adsorb simultaneously and therefore competitive onto the surface. Further details about specific sample preparation and measurements are given in the following chapters of the results sections.

3.2 STM Setup

A PicoPlus 4500 and a PicoPlus 5500 Scanning Probe Microscope from Agilent Inc., Santa Clara, USA, were used for the STM measurements. The microscopes stand on freely suspended plates, each of which is housed in an insulating box. Both microscopes are equipped with a glass cylinder in which the sample can be enclosed. This means that the samples can be stored and measured in the assembly for several days without signs of major impurities. All measurements shown in this work were performed in air at room temperature with tunnel currents in the range of 10-50 pA and bias voltages between 200-900 mV. A platinum-iridium wire (70:30) was used as tip material (Chempur, diameter 0.25 mm). This was cut mechanically with a side cutter.

Chapter 5 shows STM data of adsorbate layers that were irradiated with light by LEDs. In order to be able to expose samples during the measurement, an irradiation unit was added to the STM setup. Due to the heat development and the temperature fluctuation when the LEDs were switched on, they could not be mounted in the immediate vicinity of the sample holder. Furthermore, there is only a small space between the scanner and the sample (3 cm height) and the LEDs could not be placed in the glass

cylinder of the STM due to space constraints. To circumvent these obstacles, the light was fed in via two quartz fibers (custom-made by Light Guide Optics). The diameter of the fibers was chosen so that the bending radius is small enough for the quartz fibers to fit into the glass cylinder and large enough to transmit a sufficient intensity (max. 200 μW 455 nm and max. 15 μW 365 nm). To be able to use two different light sources, two LEDs (one ultraviolet, 365 nm, and one blue, 455 nm) were each focused to 445 μm using a lens and directed to the input of an SMA connector using a prism. Figure 3.2 shows the setup of the STM schematically. The two quartz fibers

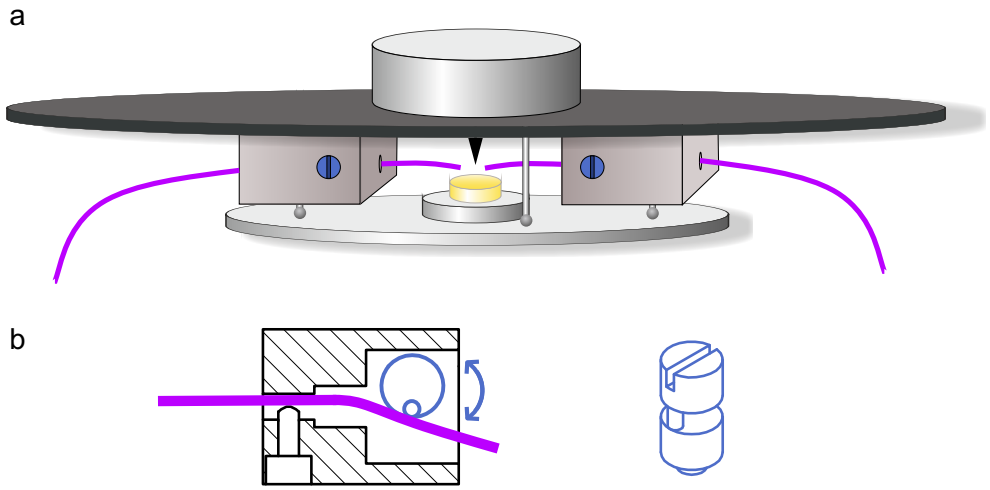

Figure 3.2: (a) Schematic illustration of STM setup with additional irradiation unit. The violet lines represent the two quartz fibers. (b) Cut surface of the holder (left) and enlarged view of the eccentric (right).

are aligned opposite to each other so that the shading of the sample by the tip is as low as possible. The angle at which the light hits the sample can be varied via an eccentric in the quartz fiber guide (Fig. 3.2). The angle at which the quartz fibers emerge from the holder was adjusted to provide maximum illumination of the surface. The adjustment of the angle was tested before each measurement using a light active sensor placed in the place of the sample.

For the correspoding IRRAS measurements, LEDs similar to the ones added in the STM setup were used. The LEDs were power controlled using a

microcontroller-based operating unit. The intensity could thus be regulated continuously between 0 and 6 mW cm^{-2}.
The aim of the STM experiments was to observe individual molecules during the switching process. For this purpose, the measurements had to be performed at the same location over a period of up to 6 hours. There were two approaches to exposure: Exposure during scanning and exposure with the tip retracted. In the case of the former, it can be observed that only a few switching events take place. This can be explained by a shadowing of the sample by the tip. In the case of the latter the tip was retracted by approximately 1000 nm and then approached again. Due to the drift, the exact same position was not approached. Therefore, defects, gold islands or stepped edges were used to identify the same sample area and to continue measurements there. After a few hours of measurement with the same tip, the drift was sufficiently low that after an exposure time of 5 minutes, it could be returned to a position within 40 nm of the previous site. The (80 x 80) nm^2 measuring range was chosen so that the area is large enough to be found on the sample at low drift and small enough to get a high resolution of the molecules. The tip had to remain stable for the entire duration of the experiment because it was no longer possible to travel to the same location after a installing a replacement. The mounted sample was first measured for approx. 1-3 hours until a thermodynamic equilibrium settled and drift was very low. Slight contaminations at the tip can be released by a short voltage pulse. This was also done in the switching experiments. Since the impurities subsequently remain on the sample, a different sample region, at least 800 nm away from the measuring area, was initially selected. Then a voltage pulse of 4.5 V was set several times for 0.04 ms and then, after a higher resolution of the surface was visible, the measuring range was changed again. However, this procedure only works with low drift. If the original measuring region was not found again, the experiment had to be carried out again from the beginning.

3.3 Data Analysis

The scanners used for measurement were calibrated approximately every three months. Measurements were made on graphite samples, values for the lattice constants were determined using the SPIP software (Scanning Probe Image Processor, Image Metrology A/S, Horsholm, Denmark), compared with the literature value and a correction factor was determined. Subsequently, the recorded STM data were drift corrected with SPIP using a plug-in developed by Niklas Jepsen in Prof. Magnussen's working group. To determine the lattice constants, a Fourier transformation was performed with SPIP and the angles between rotational domains were also evaluated. In addition, SPIP has a tool for detecting individual peaks and calculating their geometric center. This tool was used to evaluate the data on the laterally mounted switch decribed in chapter 7. The geometric centres of the peaks were determined and subsequently the distances between molecules were calculated by means of a radial distribution function in Matlab. These two functions were also used for the evaluation of the data shown in chapter 6. However, in order to determine the switching probability as a function of the surrounding neighbors, it was necessary to record two different molecular states and to be able to query individual positions in a hexagonal grid. Since this is not possible with SPIP, scripts for Python 3.6 were developed for the evaluation of the data shown in chapter 5. These scripts make it possible to detect molecules in a given hexagonal lattice and to convert them into a two-dimensional array with the values 0 and 1 indicating the isomeric states of the respective molecule. Based on this, a Python script could then be used to query states dependent on the neighbors. Some images, however, show a strong piezo creep, especially after approaching the sample with the tip. Since this could not be corrected, these data were converted manually.
Further details on the evaluation procedures can be found in the supporting information of the respective chapters.

4 | Long-Distance Rate Acceleration by Bulk Gold

This chapter is based on an article published in Angewandte Chemie International Edition [83].

We report on a very unusual case of surface catalysis involving azobenzenes in contact with a Au(111) surface. A rate acceleration of the cis-trans isomerization on gold up to a factor of 1300 compared to solution is observed. By using carefully designed molecular frameworks, the electronic coupling to the surface can be systematically tuned. The isomerization kinetics of molecules with very weak coupling to the metal is similar to that found in solution. For their counterparts with strong coupling, the relaxation rate is shown to depend on the spin-density distribution in the triplet states of the molecules. This suggests that an intersystem crossing is involved in the relaxation process. Aside from their impact on catalytic processes, these effects could be used to trigger reactions over long distances.

The majority of chemical processes in nature and in industry involve catalysis. Often, there is no other way to form stable products from stable reactants under mild conditions. Most technologically relevant reactions employ

heterogeneous catalysis, where the reacting molecules interact with atoms or ions on surfaces, forming intermediates [107]. This opens up reaction pathways with lower barriers and faster reaction rates than in the uncatalyzed processes. A number of reactions on surfaces have been studied and their mechanisms have been elucidated in detail [107, 108]. Here, we report on a very unusual case of surface catalysis involving azobenzene units in contact with a Au(111) surface. We observe a drastic rate acceleration (up to a factor of 1300 compared to solution) of *cis–trans* isomerization on gold, even though the reacting N=N double bonds are located 14 $\AA$ above and are separated by eleven covalent bonds from the Au(111) surface. To elucidate this extraordinary long-range acceleration of the reaction rate, we employ carefully designed molecular frameworks [13]. The modularity of this unique system allows a precise adjustment of intermolecular distances and coupling [18, 78]. Furthermore, the electronic coupling to the surface is systematically tuned by changing the p-conjugation of the coupling unit, while the distance between the gold surface and the azobenzene unit remains almost the same. Surprisingly, the isomerization kinetics of molecules with strong coupling to the metal follows a different mechanism than the one observed for their counterparts with no or very weak coupling. Specifically, activation energies drop to very low values and frequency factors become explicitly dependent on an electronic matrix element that can be correlated with the spin-density distribution in the triplet states of the molecules. Besides their impact on catalytic processes, these effects could be used to trigger chemical reactions over a long distance. Similar remote effects have not been considered in catalytic processes so far. However, they could be operative in a number of reactions on metallic surfaces or nanoparticles. Catalysts increase the rates of chemical reactions by creating a new and energetically more favorable reaction path with lower activation energies. In heterogeneous catalysis, this new path involves the adsorption of reactants at a surface, where chemical bonds within the molecule are broken and new bonds with surface atoms are formed. Although the majority of chemical reactions follow the Eyring theory or RKKM-type transition state theories, there are a few examples of chemical reactions that substantially deviate from the theoretically predicted behavior [109]. Their reaction rates

mainly depend on quantum-mechanical transition probabilities and not the height of an energy barrier. Characteristic features are apparently small frequency factors and low activation energies, corresponding to reaction rates that are almost temperature-independent. Such processes have mostly been observed at low temperatures (<50 K) [110–112]. Herein, we show that bulk gold can mediate similar phenomena at temperatures around 300 K. Moreover, by modifying the electronic coupling between the reaction center and the Au surface, we are able to shift the isomerization kinetics from a classical, solution-like behavior to a new regime involving a drastically lowered barrier and increased reaction rates. In our studies, we employ azobenzene-functionalized TATA (azo-TATA) molecules (Figure 1, top).

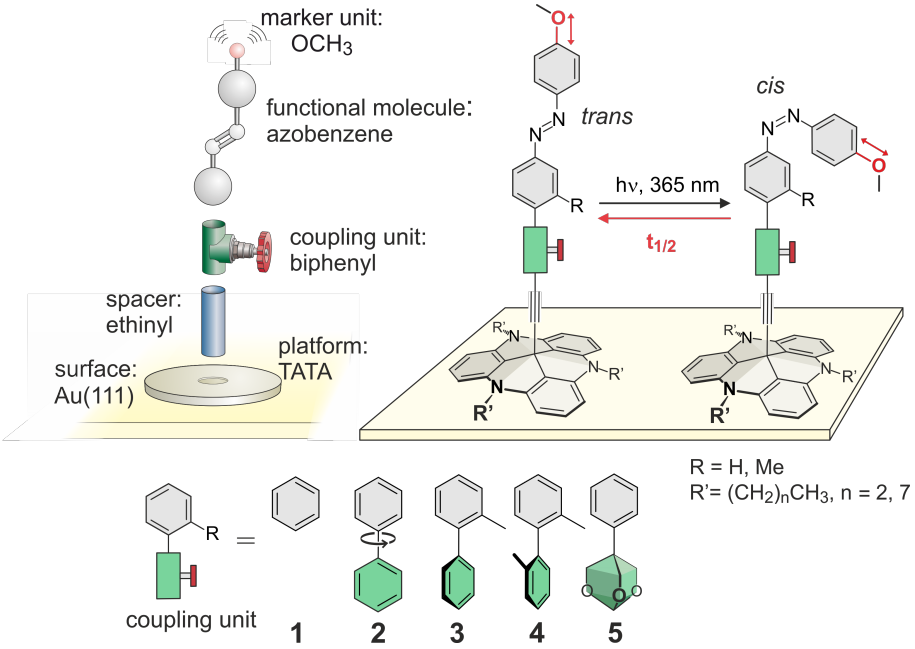

Figure 4.1: Modular design to tune the electronic coupling of azobenzene units with the metal surface: TATA platforms define the intermolecular distances on the surface (by the size of the side chain: a=octyl, b=propyl) and ethinyl spacers provide a freestanding upright orientation of the reacting azobenzene molecules. Coupling units (green) control the electronic coupling of azobenzenes with the surface. Methoxy groups allow to identify the configuration of the azobenzene (*cis* or *trans*) by IRRAS.

The *cis–trans* isomerization kinetics of **1a** and **2a** have recently been investigated in solution and for adsorbed monolayers, finding that the thermal

cis-to-*trans* relaxation of the molecules adsorbed on bulk Au(111) is considerably faster than in solution [17, 81, 87]. Assuming that this rate acceleration involves electronic coupling to the metal [81], we synthesized three new azo-TATA compounds with different coupling units inserted between the TATA platform and the azobenzene unit (Figure 1 and Supporting Information). Biphenyl groups were chosen to tune the electronic coupling of the azo group to the surface, because 4,4' substituted biphenyls retain the upright alignment of the azobenzene with respect to the surface and, most importantly, upon addition of an increasing number of methyl groups (n=0–4) in ortho position, the phenyl groups are twisted out of coplanarity, which decreases their conductivity (Supporting Information, Figure S124) [113–115].

To shut off p-conjugation completely, we inserted a trioxabicyclo[2,2,2] unit which separates the p-systems of azobenzene and the ethinyl spacer with sp3-hybridized C and O atoms. The new compounds (3a–5a, 1b, 2b, 5b) were completely characterized in solution and bulk material with NMR, UV/Vis, and vibrational spectroscopy (see Supporting Information). Scanning Tunneling Microscopy (STM) shows that, in agreement with previous results [13, 18, 88] optimized selfassembly conditions result in monolayers of **1a**-**5a** with $(\sqrt{19} \times \sqrt{19})$ *R*23.4° superstructures and low defect densities (see Figures 2 and S125). X-ray spectroscopy studies (XPS, NEXAFS) prove that the adlayers are of high purity with the molecules being oriented perpendicular to the surface, as shown in Figure 2 (Figures S126 and S127). The vertical alignment of the azobenzene with respect to the surface has been confirmed in previous studies as well (tilt angle: 6° ±16°) [88].

The well-defined molecular orientation together with the surface selection rule allows to monitor the photochemical (365 nm) *trans*-to-*cis* isomerization as well as the ensuing thermal *cis*-to-*trans* relaxation by Infrared Reflection Absorption Spectroscopy (IRRAS) [116, 117]. The relaxation leads to orientational changes of the C_{phenyl}-$O_{methoxy}$ bond relative to the surface and thus, temporal changes in the intensity of the corresponding band in the IRRA spectrum. The rates of the thermal *cis*-to-*trans* relaxation were determined at five different temperatures (Figures 2 and S129). From these data, activation energies and frequency factors were obtained for compounds **1a**-

5a (Figures 3 and S128). For adsorbate layers of compounds **1a**, **2a**, and **3a** on Au(111), the rates show only small changes in the investigated temperature range. Correspondingly, the activation energies and frequency factors are exceptionally small and typical for non-adiabatic reactions, where the rates are controlled by quantum-mechanical transition probabilities rather than classical energy barriers. On the contrary, the largely decoupled compounds **4a** and **5a** show a significantly stronger temperature dependence of the reaction rate, close to the rates observed in solution. The combined surface-kinetic data thus show that at a fixed temperature, the half-life of the adsorbed species can be changed by up to four orders of magnitude through adjusting the electronic coupling between the platform and the azo unit. In contrast, the half-lives of the five compounds in solution vary only slightly with the coupling unit.

The fundamental change in the *cis*-to-*trans* reaction observed across compounds **1a**-**5a** can be correlated with the degree of electronic coupling to the surface. Particularly remarkable is the change in kinetics between compounds **3a** and **4a** (Figure 3, right). Since both are structurally closely related and only differ in a methyl group, the kinetic data in solution are very similar. Absorbed on the metal surface, however, their half-lives ($t_{1/2}$), frequency factors (A), and activation energies (E_A) differ drastically (Figure 3). Electronic coupling to the metal surface is still operative in **3a**, whereas the almost orthogonal arrangement of the phenyl rings in **4a** interrupts π-conjugation and electronic coupling. The change from non-standard kinetics in **3a** to classical Arrhenius behaviour in **4a** is thereby clearly related to the breakdown of molecule-substrate coupling. The different activation energies of the compounds **4a**-**5a** in solution and adsorbed on a surface can be explained by the dissimilar environments.

Different hypotheses for the acceleration of *cis*-to-*trans* relaxation processes in molecular adsorbates were discussed. It is known that dense monolayers of azobenzenes on surfaces exhibit increased *cis*-to-*trans* isomerization rates, because intermolecular steric repulsion is larger in the bent *cis* than in the more straight *trans* configuration [118, 119]. Even though this is unlikely to account for the large rate accelarations, we performed further experiments to probe this hypothesis. The large octyl side groups at the TATA

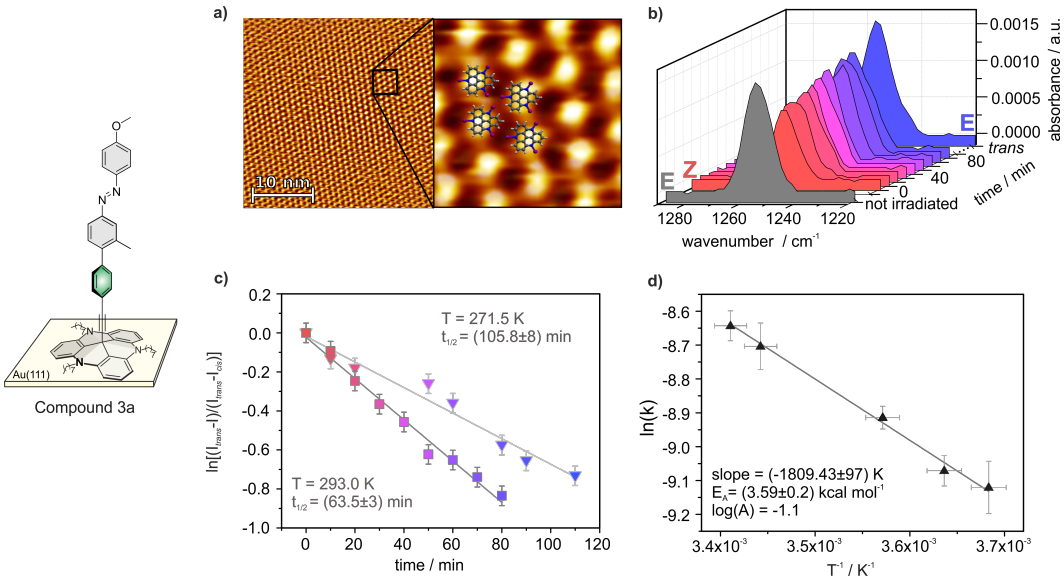

Figure 4.2: a) STM image and model of a monolayer of azo-TATA **3a** on Au(111). The molecules exhibit an intermolecular distance of 12.6 *Å*. b) PMIRRAS signal of the C-O stretching vibration region before irradiation (gray) and after irradiation with light of 365 nm as a function of time (red to blue). The blue spectrum was obtained after irradiation with 440 nm light. In both cases, the irradiation time was 10 min. c) PM-IRRAS intensity of the C-O stretching vibration as a function of time at two different temperatures (271.5 K and 293.0 K). Half-lives ($t_{1/2}$) are derived by a linear regression. d) Arrhenius plot of reaction rates k at five different temperatures. The activation barrier E_a and the frequency factor A are derived by a linear regression.

platform were replaced by smaller propyl groups (**1b**, **2b**, **5b**), which results in a smaller intermolecular distance in the self-assembled monolayers on Au(111) (octyl: 12.6 *Å* vs. propyl 10.4 *Å*) [13, 17, 78]. However, the measured rate accelerations on gold are similar (Figure S129). Steric constraints can therefore be excluded. Moreover, steric confinement would not explain the very low barriers and frequency factors. Traces of absorbed water are also not responsible for the rate acceleration [120]. On the contrary, coincidental water on adsorbed azobenzenes decreases the relaxation rate [121]. Added water also slows down the reaction rates in solution (Figure S133). It is known that charge transfer can accelerate the *cis-trans* isomerization rates of azobenzenes. Azobenzenes that are either oxidized to the corre-

Parameter \ Molecule		1	2	3	4	5	6
In solution	$t_{1/2}$ (290.5 K)	18.7 h	25.6 h	37.9 h	49.9 h	64.8 h	15.3 h
	k_{obs} (290.5 K)	$1.03 \cdot 10^{-5}$ s^{-1}	$7.52 \cdot 10^{-6}$ s^{-1}	$5.08 \cdot 10^{-6}$ s^{-1}	$3.85 \cdot 10^{-6}$ s^{-1}	$2.97 \cdot 10^{-6}$ s^{-1}	$1.26 \cdot 10^{-5}$ s^{-1}
	E_A (kcal/mol)	24.1	22.6	21.7	21.2	21.5	23.5
	log(A)	13.12	14.02	11.04	10.58	10.67	11.70
On Au(111)	$t_{1/2}$ (290.5 K)	45.3 s	14.9 min	69.6 min	48.4 h	61.6 h	
	k_{obs} (290.5 K)	$1.53 \cdot 10^{-2}$ s^{-1}	$7.73 \cdot 10^{-4}$ s^{-1}	$1.66 \cdot 10^{-4}$ s^{-1}	$3.97 \cdot 10^{-6}$ s^{-1}	$3.13 \cdot 10^{-6}$ s^{-1}	
	E_A (kcal/mol)	2.5	2.6	3.6	13.7	14.7	
	log(A)	0.1	-1.2	-1.1	4.9	5.6	
spin density (δ_S)		$6.1 \cdot 10^{-2}$	$8.1 \cdot 10^{-3}$	$4.9 \cdot 10^{-3}$	$1.0 \cdot 10^{-6}$	$-3.4 \cdot 10^{-5}$	

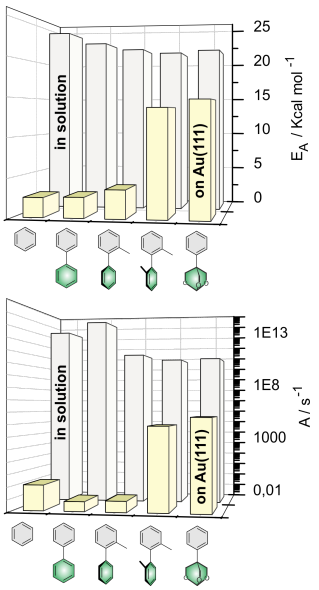

Figure 4.3: Kinetic data of the *cis-trans* isomerization of compounds **1a**–**5a** and **6** in solution and adsorbed on Au(111). Half-lives ($t_{1/2}$), observed rates (k_{obs}), activation energy (E_a), and frequency factors (A) for azo-TATA compounds (sorted by decreased coupling between platform and azobenzene) are determined in solution (gray), and adsorbed on Au(111) (yellow). Spin densities (δ_s) of textbf1a–textbf5a in the triplet state are calculated with DFT (M08HX/def2-TZVP) and integrated over all atoms within the platform unit and the ethinyl spacer. For compound **6**, $t_{1/2}$, E_a, and A are presented in solution. More data points and error margins are given in the Supporting Information (Figure S129).

sponding radical cations or reduced to the radical anions exhibit very fast thermal isomerization rates [122, 123]. The low *cis-trans* activation barriers of azobenzenes directly absorbed on gold nanoparticles [124, 125] or lying flat on Au(111) [49] or Bi(111) [126] surfaces have been explained by a transfer of electron density from the azobenzene to the metal [125]. To investigate if such a charge transfer would be operative in our system, we synthesized azobenzene **6**, where an Au^+ ion is directly connected to the ethinyl group (Scheme S5). According to the NBO analysis of **6**, the azoethinyl group carries approximately half an elementary charge (-0.508 *e*). Kinetic analysis, however, reveals that the activation energy (20.3 kcal mol^+) and the frequency factor ($\log(A/s^{-1})$ = 13.78; see Figure 3, right) are in the usual range expected for undisturbedazobenzenes [127]. The strongest argument

against static charge transfer is the fact that the IR vibrational frequencies of the *cis* and the *trans* azo-TATA molecules in solution and absorbed on the surface are virtually identical (Figure S123).

The appearance of two different regimes in Figure 3 suggests the existence of two distinct mechanisms. It will be shown that the delocalization of the electronic wavefunction of the azobenzene unit over the entire molecule into the gold plays a key role in this context. A convenient measure of the delocalization is the spin density δ_s at the TATA platform computed for the triplet state (Figure S124): the wavefunction amplitude localized in the bulk gold is approximately proportional to the square root of δ_s for the triplet (T_1) as well as for the singlet (S_0) electronic state (see Supporting Information, Section 1). The plot of $\log(k_{obs})$ vs. $\log(\delta_s)$ shown in Figure 4 reveals that the observed rate constant k_{obs} can be written as a sum of a rate constant k, which is associated with a thermally activated process exhibiting standard Arrhenius-type behaviour, and a rate constant $k^{'}$, which additionally depends upon the square of the spin density at the TATA platform:

The parameters A ($10^{5.6}$ s^{-1}) and E_A (14.7 kcal mol^{-1}) for the regime associated with k are taken from compound **5a**, serving as a reference system for a surface-deposited azo-TATA molecule with an electronically decoupled azobenzene unit (Figure 3). For $k^{'}$, a significantly reduced apparent barrier height $E_A^{'}$ of 2.7 $\pm$ 0.1 kcal mol^{-1} and a prefactor $A^{'}$ of 894 $\pm$ 110 s^{-1} are found by fitting our data to Equation (1) (Figures S130 and S131).

$$k_{obs} = k + k^{'} = A \cdot exp\left(\frac{-E_A}{RT}\right) + \delta_s^2 \cdot A^{'} \cdot exp\left(\frac{-E_A^{'}}{RT}\right) \tag{4.1}$$

The described findings strongly suggest that an electronic transition mediated by the bulk gold is involved in the reaction mechanism associated with the rate constant $k^{'}$. Two different mechanisms can be imagined: a gold-mediated intersystem crossing (ISC) between the singlet (S_0) and triplet (T_1) states of the azobenzene or a transient charge transfer (CT) between the gold and azo-TATA. By considering the coupling between the different electronic states to be a weak perturbation, $k^{'}$ can be assumed to be proportional to the square of the coupling element that enables the electronic

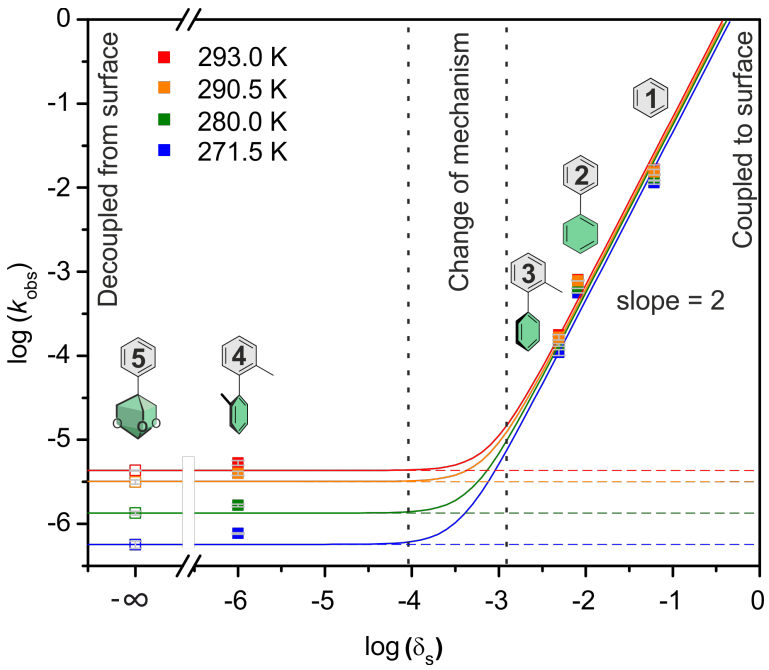

Figure 4.4: Log(k_{obs}) as a function of log(δ_s) for compounds **1a**- **5a**. δ_s is the spin density of the triplet state of **1a**-**5a** integrated over all atoms of the platform and the ethinyl spacer, calculated with DFT (M08HX/def2-TZVP). Compound **5** serves as a reference molecule without electronic coupling to the surface and a very small value for δ_s (dashed lines). Continuous lines are fitted according to Equation (1).

transition (see Supporting Information, Section 1). Since the ISC as well as the CT are enabled by the coupling to the bulk gold, the value of the coupling element is determined by the respective wavefunction amplitudes localized in the bulk gold. The coupling matrix element for the ISC involves the S_0 and T_1 wavefunctions and is thus proportional to δ_s. In contrast, the coupling matrix element for the CT involves the S_0 wavefunction and the wavefunction of the CT state and is proportional to the square root of δ_s (see Supporting Information, Section 1). Thus, only the ISC mechanism is consistent with the observed quadratic δ_s dependence of k'.

The rate enhancement induced by bulk gold described above represents a new type of catalysis. Unlike in conventional heterogeneous catalysis, there is no direct chemical involvement of the surface (no chemical bonds to the surface are made or broken). Instead, the bulk metal opens an alternative pathway with almost vanishing barriers by the mixing of molecular states

with the quantum states of gold. Particularly exceptional is the fact that the state transitions occur at room temperature, without photochemical activation, and over a large distance (14 $\AA$, 11 bonds). We used a well-defined, controllable environment to investigate these non-classical effects systematically and propose that a change in spin state is responsible for the drastic rate acceleration. It is quite likely that similar effects are operative in a number of catalytic processes where molecules react at metal surfaces. Likewise, the controlled coupling of molecules to the conducting band of materials could open new ways to trigger reactions with spatiotemporal control. Such effects may also be exploited to efficiently catalyze chemical reactions or to remote-control molecular machines on surfaces [128, 129].

Acknowledgements
We thank the Deutsche Forschungsgemeinschaft (SFB 677) for funding this research, the Helmholtz-Zentrum Berlin for the supply of beamtime at the HE-SGM beamline (XPS and NEXAFS measurements), and Martin Kirk for fruitful discussions.

Conflict of interest
The authors declare no conflict of interest.

Supporting information available via the internet at `https://doi.org/10.1002/anie.201814342`.

5 | Observation of Collective Photoswitching in Free-standing TATA-based Azobenzenes on Au(111)

Light-induced transitions between the trans and cis isomer of TATA-based azobenzene derivatives on Au(111) surfaces were observed directly by scanning tunneling microscopy, allowing atomic-scale studies of the photoisomerization kinetics. Although the azobenzene units in these adlayers are free-standing and spaced at uniform distances of 1.26 nm, their photoswitching depends on the isomeric state of the surrounding molecules and, specifically, is accelerated by neighboring cis isomers. These collective effects are supported by ab initio calculations indicating that the electronic excitation preferably localizes on the n-π^* state of trans isomers with neighboring cis azobenzenes.

The development of photo-controlled surfaces consisting of highly ordered molecular switches is an important step towards integrating machine-like functions in solid-state devices and thus has received much interest. Self-assembled monolayers (SAMs) of azobenzene and its derivatives have been intensely investigated for this purpose.[65, 130–132] Switching between the *trans* and *cis* of adsorbed azobenzene derivatives were not only identified by various spectroscopic methods but also at the nanoscale via scanning probe microscopy.[44, 48, 61, 67, 69, 133, 134] While in densely packed aliphatic azobenzene SAMs switching is prevented[135], densely packed aromatic azobenzene SAMs exhibited reversible, collective photoswitching.[43, 44,

136, 137] The latter is surprising and was attributed largely to steric effects, caused by the rigidity of the molecule and stabilization of the *cis* isomer by intermolecular interactions.[44, 138, 139] Furthermore, excitonic coupling was proposed to lead to cooperativity in diluted aliphatic azobenzene SAMs.[140]

We here report collective photoswitching in adlayers of freestanding well-separated azobenzene derivatives, bound to Au(111) surfaces via a triazatriangulenium (TATA) platform (Fig. 5.1a). In the employed molecule, ((E)-12c-[(4-4-[(4-methoxyphenyl)diazenyl]phenyl-2,6,7-trioxabicyclo[2.2.2]octane-1-yl)ethynyl]-4,8,12-tri-n-octyl-4,8,12-triazatriangulene (compound **1**), the azobenzene switch is linked to the TATA platform via an isolating trioxabicyclo [2.2.2] unit. The molecules were shown to adsorb intactly on the

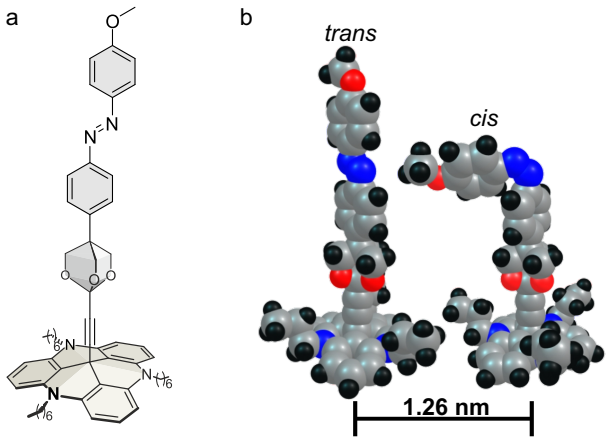

Figure 5.1: (a) Studied compound **1**. (b) Illustration of a *cis* and *trans* isomer, placed at the distance of neighboring adsorbates in the **1** adlayer. The depicted molecular geometries shows the Van-der-Waals spheres and were calculated using DFT (M062X-D3/def2-TZVP) [83].

surface in form of a well-ordered hexagonal $(\sqrt{19} \times \sqrt{19})$ $R23.4°$ superstructure with a nearest neighbor distance of (12.6 ± 0.5) $\AA$, and are reversibly switchable without steric hindrance (see Fig. 5.1b) [83]. The absence of steric effects is expected because of the open arrangement of the molecules on the surface (see Fig. 5.1b) and is supported by quantitative studies of mixed adlayers of **1** and TATA-derivatives with different vertical groups, which find random distributions of the adsorbed molecules.[86] The isolating unit leads to a weak electronic coupling between the azobenzene

unit and the Au surface, resulting in a high stability of the *cis* state against thermal back-isomerization ($t_{1/2}$ = 61.1 h at 290.5 K), which enables direct observations of the switching process via STM.

In the initial state, obtained immediately after preparation, **1** SAMs on Au(111) show a well-ordered hexagonal adlayer in scanning tunneling microscopy (STM) images, in which all molecules appear equal (Supporting Information, Fig. 9.2).

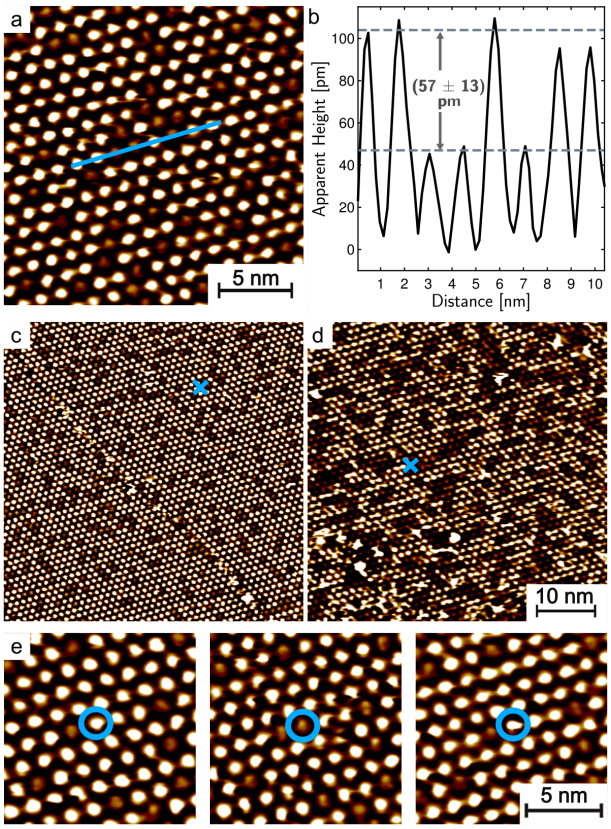

Figure 5.2: STM images of self-assembled monolayers of **1** on Au(111) after irradiation with 365 nm at 6 μW/cm^2 (a,c) after 28 min. and (d) after 71 min. of irradiation. Blue crosses mark the same area on the surface. (b) Cross section, taken along the blue line in (a). (e) Series of STM images, showing the same surface area after 28, 32, and 38 min. of UV irradiation, respectively, illustrating light-induced dynamic changes between *trans* and *cis* state. In all experiments, the tip was withdrawn from the surface during irradiation.

Upon irradiation of the sample with UV light (365 nm, 6μW cm^{-2}), the lateral arrangement of the molecules remains unchanged, but the appearance

of the adlayer distinctly changes: instead of a single molecular species, two type of molecules with different apparent heights are visible (Fig. 5.2a,b). These height changes can be reversed by irradiation with blue light (440 nm), indicating that they correspond to the reversible switching of the molecules, rather than to irreversible light-induced reactions, as e.g. photochemical cleavage [141]. The molecules with lower apparent height become more numerous with UV irradiation time (Fig. 5.2c, d) and thus can be assigned to the *cis*-isomer; the higher molecules therefore correspond to the *trans* isomer. Without further irradiation, the spatial distribution of the isomers does not change, indicating that the switching is not induced by the STM imaging. Furthermore, significant changes are only observed in experiments, where the tip is withdrawn from the surface during irradiation. In sequences of STM images recorded during irradiation only minor *trans* - *cis* isomerization was observed, which we attribute to shading by the STM tip.

Observations of the same surface area before and after a UV irradiation sequence show that the apparent heights of the molecules not always change from high to low, but also occasionally from low to high (Fig. 5.2e, example marked by blue circle). This is not surprising, as there is a finite probability that 365 nm irradiation induces *cis* - *trans* photoisomerization. According to more quantitative analysis of the dynamic fluctuations between the two isomers, during a total change in *cis* coverage from $\theta_{cis}(t_1)$ = 0.15 to $\theta_{cis}(t_2)$ = 0.32 approximately 7% of the *cis* isomers that were present on the surface at t_1 changed to the *trans* state.

The isomers are not randomly distributed on the surface, but seem to form clusters, especially after a longer period of irradiation (Fig. 5.2d). This was verified quantitatively by a statistic analysis of the spatial distributions in the STM images for *cis* coverages of 0.15 and 0.32 (Fig. 5.3, see supporting information for details).

First, we determined the Warren Cowley coefficients, which are a measure for the short-range order [142]. Second, we determined the coverages of small ensembles of *cis* isomers (monomers, dimers, trimers, surrounded by *trans* isomers) and compared those to the coverages, obtained for a random distribution with the same *cis*/*trans* ratio on the surface. At a surface

coverage of 0.15 *cis* molecules, only slightly deviations from a random distribution are found.

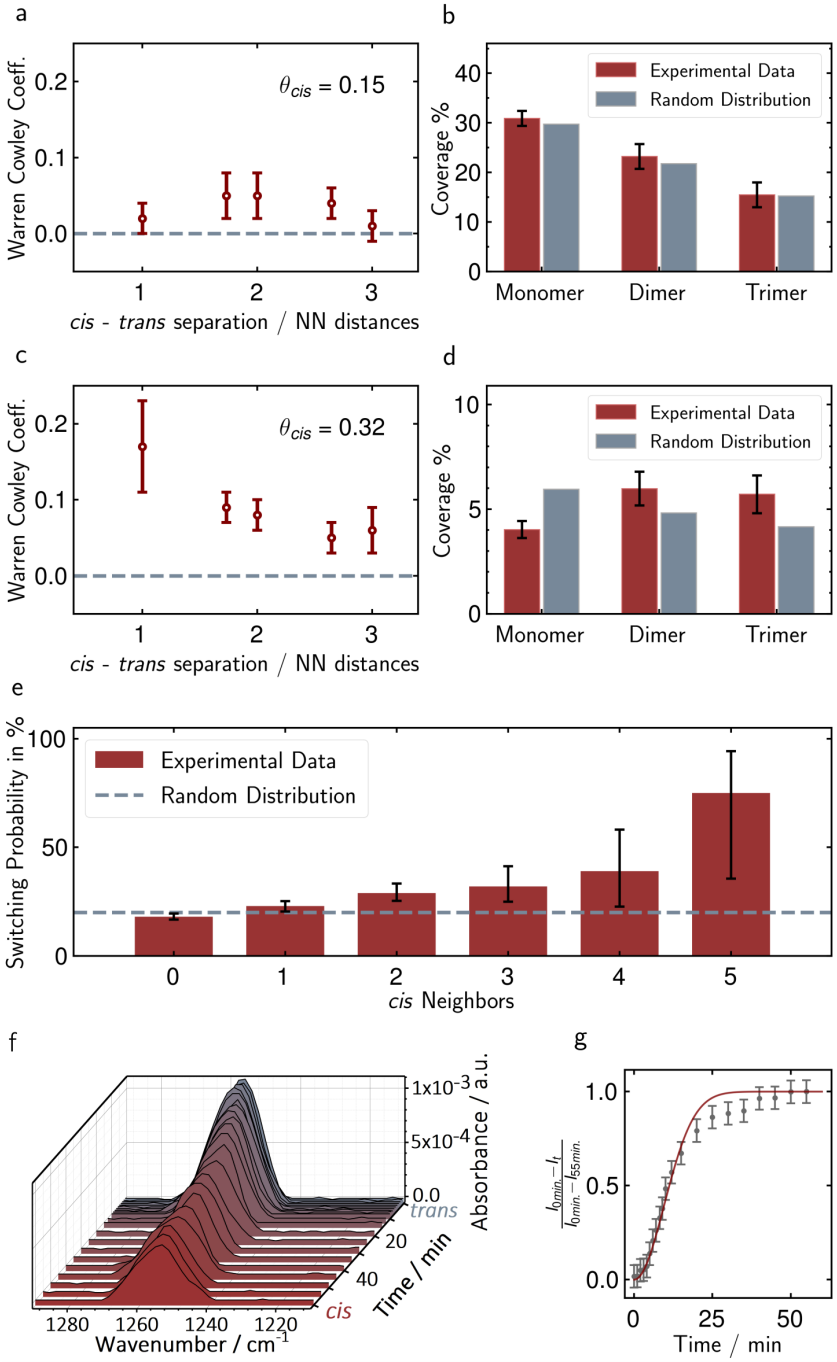

Figure 5.3: Quantitative analysis of photoswitching. (a, c) Warren Cowley coefficients of STM images at 0.15 and 0.32 *cis* coverage, (b, d) corresponding distributions of small ensembles, (e) switching probability as a function of neighboring molecules in *cis* state (a *trans* molecule with 6 *cis* neighbors could not be observed). The dashed line indicates the value expected for fully stochastic switching. (f) IRRAS spectra of the C_{phenyl}-$O_{methoxy}$ stretching band of **1** on Au(111) during transition from the *trans* saturated state (grey) to the *cis* saturated state (red) upon 365 nm irradiation (at 10 μW/cm^2). (g) Corresponding change in *cis* coverage as a function of time, fitted by an Avrami growth model (solid line).

The Warren Cowley coefficients are all close to zero for the first five nearest neighbor distances (Fig. 5.3a), as expected for a statistic distribution. Furthermore, the coverages of small ensembles match those simulated for a random distribution within the statistical errors (Fig. 5.3b). In contrast, clear cluster formation is observed at 0.32 *cis* coverage. Here, the Warren Cowley coefficients deviate significantly from zero (Fig. 5.3c) and the surface fraction of dimers and trimers is clearly enhanced at the expense of the fraction of monomers in comparison to a random distribution (Fig. 5.3d).
Both the Warren Cowley coefficients as well as the increased coverage of multimers and lowered coverage of monomers indicates that neighboring adsorbates in the *cis* state accelerate the rate of *trans* - *cis* photoisomerization. This can also be demonstrated by direct analysis of the changes in isomeric state as a function of the state of the adjacent molecules (Fig. 5.3e). Here, we assume that only the direct neighbors in the adlayer affect the switching and determine from sequences of *in situ* STM images, recorded in the same surface area, the probability that a molecule that is at time t_1 in the *trans* state is found at time t_2, i.e., after irradiation, in the *cis* state. If the switching probability is independent of the state of the adjacent molecules, every molecule in the *trans*-state will switch with the same probability, namely 20% for a coverage change from $\theta_{cis}(t_1) = 0.15$ to $\theta_{cis}(t_2) = 0.32$ (see supporting information). However, the experimental data clearly shows an influence of neighboring *cis* isomers on the switching probability. Although the errors for molecules with 3 to 5 *cis* neighbors are high due to poor statistics (only a few switching events of these types are seen in the images), the trends towards higher *trans-cis* switching probability with an increasing number of neighboring molecules in the *cis* state are obvious. These studies, in which the temporal evolution of the isomerization state is directly monitored, also rule out other explanations of the cooperative effect, such as a decreased *cis-trans* backisomerization in the presence of *cis* neighbors.
The cooperative effects observed on the atomic scale also manifest in the macroscopic photoisomerization kinetics of **1** SAMs. We illustrate this by measurements with infrared reflection absorption spectroscopy (IRRAS), where we record the intensity of the stretching vibration of the terminal

C_{phenyl}-$O_{methoxy}$ group attached to the azobenzene unit. Because of the rigid and well-defined molecular structure, transitions between *trans* and *cis* state lead to defined orientation changes of this group relative to the surface and, thus, changes in the IR band's intensity, which allow monitoring the photoisomerization [17, 83]. In Fig. 5.3f spectra of the C_{phenyl}-$O_{methoxy}$ stretch region during the UV-induced transition from a *trans* saturated adlayer (grey), prepared by irradiation with 440 nm light, to the *cis* saturated state (red) are shown. Upon irradiation with light of 365 nm the band intensity gradually decreases by nearly 60 %. These data allow to quantify the kinetics of the transition. Taking the different irradiation intensity into account, the time-dependent changes in the *cis* coverage are in agreement with those in the STM images. Interestingly, the data do not show a simple exponential buildup of the *cis* state, as would be expected in the absence of interactions between the molecules, but a more sigmoidal dependence with a pronounced induction period (Fig. 5.3g). It can be well described by a Avrami-type of 2D growth with instantaneous nucleation (solid line) [143, 144]. In this model, transition to the *cis* state occurs only at boundaries to existing *cis* molecules, starting from initial nuclei, which we identify with residual *cis* isomers in the *trans* saturated adlayer. Obviously, this behavior implies pronounced acceleration of the switching by neighboring *cis* isomers.

These collaborative effects cannot be explained by simple steric effects, because the large lateral distance of the molecules prevents direct contact between the functional groups (Fig. 5.1b). Furthermore, no indication for excitonic coupling is found in UV/Vis spectra of **1** SAMs (Fig. 9.5). Thus more subtle interactions have to be considered, which we examine in more detail by *ab initio* calculations (see the SI for details). In a first approach, we consider a system of 14 vertical azobenzene units. The ground state interaction between a central *cis* and the surrounding *trans* isomers is mediated mainly by electrostatic and dispersion interactions between the methoxy groups of the bent *cis* and the N=N moiety of the *trans* azobenzenes. Consistent with the above statements, due to the large separation between the azobenzenes, these interactions remain weak, only -5 kJ/mol for a *cis-trans* pair as compared to -0.2 kJ/mol for a *trans-trans* pair. Interestingly, the cal-

culations reveal that the *trans-cis* interaction stabilizes the lone pair on the interacting *trans*. Consequently, the n-π^* excitation on this *trans* isomer is the highest in the $n - \pi^*$ manifold (Fig. 5.4). While the $n - \pi^*$ states are localized on individual photochromes, the π-π^* states are delocalized on several photochromes.

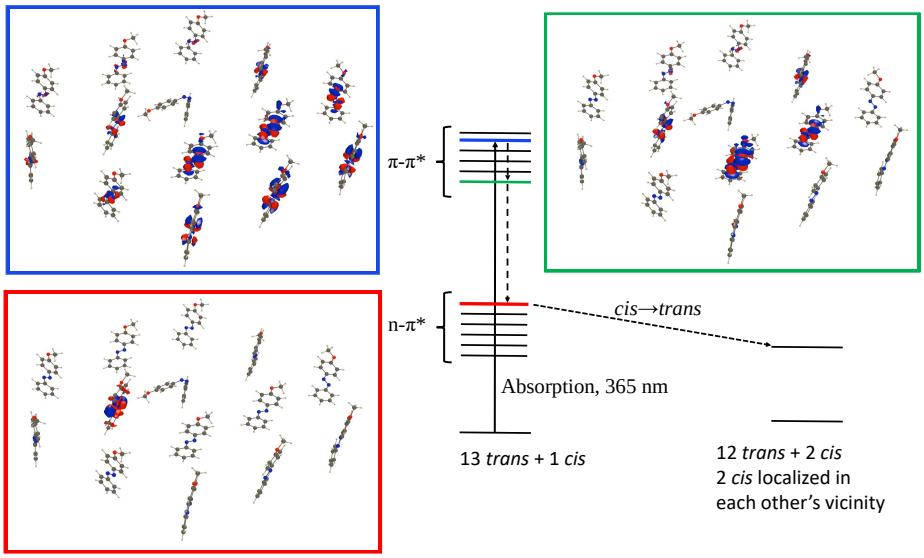

Figure 5.4: Excited states ordering and electron density differences for the model system of 13 *trans* and one *cis* isomers. The electron density differences ($\rho^{ES} - \rho^{GS}$ determined on the FC geometry) are shown for the π-π^* with highest oscillator strength (blue highlight), lowest π-π^* state (green highlight) and the first $n - \pi^*$ state (red highlight), which is localized on the interacting *cis-trans* pair.

Irradiation by UV light first induces the π-π^* manifold, followed by a fast fall to the lowest π-π^*, which is localized on azobenzenes surrounding the *cis*. In the subsequent de-excitation to $n - \pi^*$, the $n - \pi^*$ state localized on the *trans* isomer interacting with a *cis* isomer could act as a "trap". Relaxation of this excited state will eventually lead to *cis* clusters on the surface. This is of course a qualitative analysis and not all the photochromes would exactly follow this pathway. Nevertheless, such a localization processes are well known in light harvesting systems and it was shown that they can proceed also in systems with large spatial separation [145–147].

In a second, more local approach, we evaluated the impact of the surrounding photochromes - modelled as embedding point charges - on the $n - \pi^*$ excited state of a central *trans* surrounded by six *trans* azobenzenes or by five *trans* and one *cis* isomer, respectively. At the CASPT2/ANO-S level, the tilting of the C-N=N-C dihedral angle of the central photochrome is barrierless in the $n - \pi^*$ excited state, a statement holding for both arrangements. However, the geometry optimization of the all *trans* case ends in a local minimum, while the same calculation for the *cis*-containing cluster leads to a direct relaxation to the conical intersection. Of course, the molecule surrounded by all-*trans* has likely enough kinetic energy in its excited state to escape from the shallow minimum and switch as well. Nevertheless, these different topologies of the potential energy surfaces hint that the surrounding molecules tune the excited state of the switch so as to tilt the probability toward the formation of *cis* clusters. Which of these two effects dominate is hard to determine, but both explain the observed *cis* clustering.

In conclusion, our results demonstrate that cooperative switching can occur even in freestanding photoswitches with spacings larger than 1 nm, where direct contact between the switchable groups can be excluded. Based on ab initio calculations, we attribute this observation to intermolecular electronic coupling, similar as in light-harvesting systems. Understanding and controlling such effects will be of central importance for nanoscale applications of such switches, e.g. for data storage or functional molecular machines. These may on the one hand require independent operation of the molecular units and thus suppression of cooperative switching. On the other hand, such collective phenomena may be exploited for the design of increasingly complex functional systems that involve molecular scale signal processing or cascade effects.

Supporting Information

The Supporting Information is available.

Acknowledgements

We gratefully acknowledge financial support by the Deutsche Forschungsgemeinschaft (DFG) via SFB677. This work used the computational ressources of the CCIPL installed in Nantes and HPCC in Banska Bystrica.

6 | Molecular Platforms as Versatile Building Blocks for Multifunctional Photoswitchable Surfaces

This chapter is based on an article published in Chemical Communications [86].

Controlled attachment of photoswitchable molecules to solid surfaces is a promising route for the realization of complex machine-like molecular functions. A central next step here is the preparation of adlayers with multiple chemical functions that have defined intermolecular spacings and orientations and interact with each other in a controlled way, resulting in novel advanced system properties. We demonstrate that this is possible using molecular platforms with vertical functional units. Employing molecular components with identical triazatriangulenium-based units, we prepared mixed adlayers of platforms carrying a stable photoswitch and bare platforms, platforms with vertical pyridine units, and platforms with metastable switches, respectively. All these mixed layers are highly hexagonally ordered, can be easily varied in composition, and exhibit a stochastic arrangement of the two molecular components.

Translating the working principles of biomolecular systems into artificial molecular machines is a topic of great current interest. Molecular switches - elementary building blocks of such machines - are nowadays well developed and have been embedded in a wide range of materials [23, 26, 148, 149]. An important next step toward more complex machine-like functions is the combination of different types of switches or of switches with other functional units. This may allow the realization of novel functions that arise from cooperative effects, but requires precise control of the position and orientation of the corresponding groups relative to each other.

The most obvious approach is combining the different functional groups in the same molecule. Spectacular cooperative effects have been demonstrated this way [150–153], however, the synthesis of such multifunctional molecules is challenging and has to be tailor-made for a specific application. Mounting the different functionalities parallel to each other on surfaces offers an attractive alternative (Fig. 6.1a). Various methods have been developed that allow surface attachment of molecular switches in defined orientation while maintaining the switching properties [45, 47, 154–156]. In principle, arbitrary combinations of functions are easily obtainable by coadsorption. However, this strategy has been barely pursued for molecular switches. Apart from coadorption systems, in which switchable molecules were diluted by embedding them in a matrix of inert aliphatic spacers [79, 140, 157, 158], no mixed adlayers were reported up to now. We here demonstrate that well-defined mixed adlayers of photoswitchable and other functional molecules can be prepared by the platform concept, developed by our group [13, 16, 17, 78, 80, 81, 83, 88]. This approach provides a modular system for the preparation of adlayers in which the functional units are free-standing and oriented perpendicular to the surface. As platform we employ octyl triazatriangulenium (TATA), the functional groups are covalently bound to the TATA's central carbon atom. The bare octyl-TATA platform adsorbs strongly in planar geometry on Au(111) surfaces and forms at saturation coverage a highly ordered $(\sqrt{19} \times \sqrt{19})$ $R23.4^\circ$ superstructure with an intermolecular spacing of 1.25 nm [13, 78]. The same adlayer structure is found for TATA derivatives with vertically functional groups, demonstrating that the lateral arrangement is determined by the size of the

adsorbing platform. Only for TATA derivatives with very bulky attached groups different adlayer structures were observed [16, 159]. In addition, the lateral distances between the adsorbed TATA platforms may be varied via the length of the alkyl side chains [18]. TATA based azobenzene-containing molecules remain reversibly photoswitchable in the adlayer and exhibit a high switching efficiency and fast photoisomerization kinetics, demonstrating that the diameter of the TATA molecule ensures a sufficiently large free volume of the perpendicular azobenzene group [17, 81, 83].
Due to these properties, TATA derivatives with different functional groups should be ideally suited for the preparation of mixed multifunctional adlayers. We test this by performing systematic investigations of binary adlayers on Au(111), consisting of TATA-based coadsorbed molecules with different functionalities (Fig. 6.1b). In these studies we mix an azobenzene-TATA

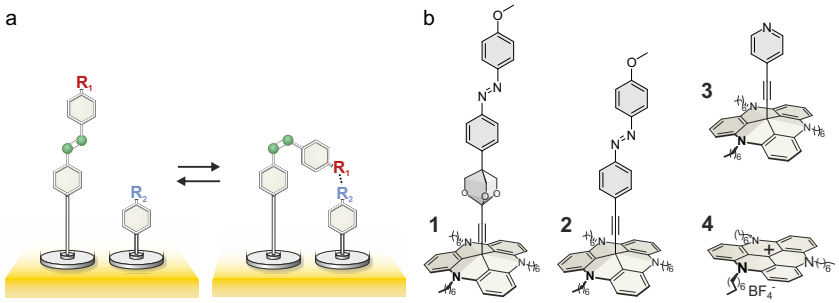

Figure 6.1: (a) Schematic illustration of cooperativity achieved by defined coadsorption on surfaces. (b) TATA derivatives used for preparation of mixed monolayers on Au(111).

with an intermediate trioxabicyclo[2,2,2] unit (**1**) with (i) a fully conjugated azobenzene-TATA (**2**), (ii) a pyridine-TATA (**3**), and (iii) the bare TATA platform (**4**). Adsorbed **1** and **2** molecules can both be photoswitched between the *trans* and *cis* isomer, but differ by more than three orders in thermal stability of the metastable *cis* state (at 290 K the half-life of **1** is 61.6 h, that of **2** is 45.3 s) [83]. This difference is attributed to a much stronger electronic coupling of the azobenzene group to the Au(111) surface in the conjugated compound **2** than in compound **1**, where the azobenzene is decoupled by the isolating trioxabicyclo[2,2,2] unit.
The synthesis of compounds **1**, **2** and **4** are described in detail in previous publications [13, 17, 75, 76, 83], that of **3** is given in the supporting informa-

tion †. All compounds were characterized by NMR and mass spectroscopy and show no major signs of impurities. The adlayers were prepared by immersing flame annealed Au(111) single crystals for 1 hour at temperatures between room temperature and 80 °C in solutions of the compounds in toluene. To vary the mixing ratio of the two compounds i and j in the adlayer, the ratio of the corresponding concentrations c_j and c_i was varied, while maintaining the total concentration $c_i + c_j$ at 10 μM. The structure and composition of the resulting adlayers were characterized under ambient conditions by molecular resolution scanning tunneling microscopy (STM) in constant current mode, using Pt/Ir tips. Details on the sample preparation and characterization can be found in the supporting information.

Control experiments of single component adlayers of **1** to **4**, prepared under identical conditions, reveal in all cases well-ordered homogeneous monolayers with $(\sqrt{19} \times \sqrt{19})$ $R23.4°$ structure (see Fig. 9.19). For the three binary systems the high-resolution STM images reveal homogeneous monolayers, in which the two types of molecules exhibit a different apparent height (Figure 6.2). Thus, mixed adlayers can be prepared and structurally analysed by STM. All samples show hexagonally ordered adlayer structures with lattice constants of (1.26 $\pm$ 0.03) nm, (1.28 $\pm$ 0.05) nm and (1.28 $\pm$ 0.05) nm and angles of 12° $\pm$ 4°, 15° $\pm$ 8° and 16° $\pm$ 7° between rotational domains for **1/2**, **1/3** and **1/4** adlayers, respectively. These results are in good agreement with a $(\sqrt{19} \times \sqrt{19})$ $R23.4°$ superstructure and demonstrate that also in the mixed adlayers the lateral intermolecular distances are determined by the TATA platform. Taken into account that the photoisomerization kinetics of single-component adlayers of 1 and 2 is almost identical to that of these molecules in solution [17, 83] and dilution of photoswitchable groups on the surface generally results in improved photoswitching [140], fast and reversible switching in these adlayers is expected.

In the following, we discuss the molecular composition and the arrangement of the two species in the adlayer, starting with **1/2** adlayers. To analyze this, samples with 5 different mixing ratios of compounds **1** and **2** were prepared and characterized using STM (Fig. 6.3, top row). By varying the ratio of the concentration of **1** and **2** in solution (c_1/c_2) we can change the ratio

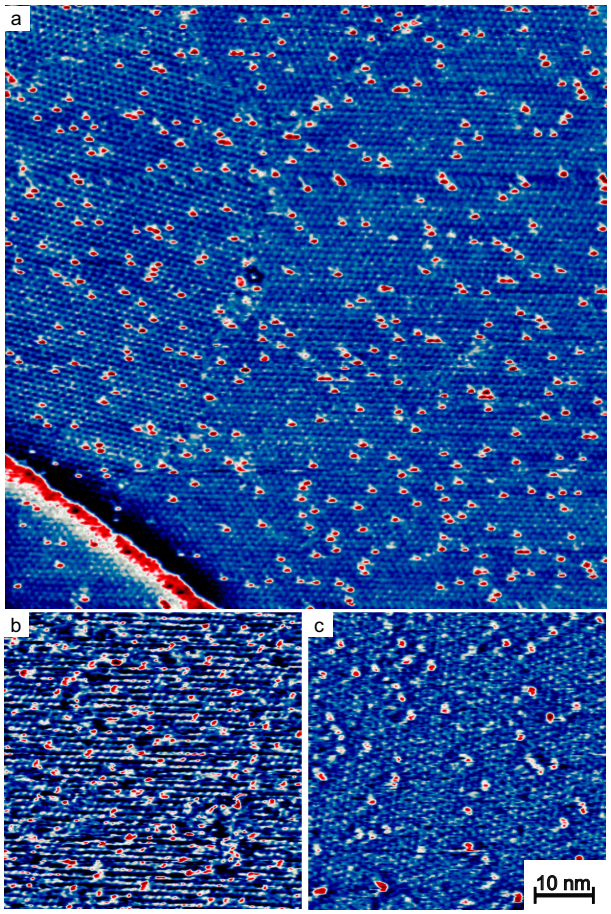

Figure 6.2: STM images of self-assembled monolayers on Au(111) prepared by coadsorption from (a) 9.8 μM **1** and 0.2 μM **2** solution (100 $\times$ 100 nm^2), (b) 5 μM **1** and 5 μM **3** solution (50 $\times$ 50 nm^2) and (c) 5 μM **1** and 5 μM **4** solution (50 $\times$ 50 nm^2).

of their coverages on the surface (θ_1/θ_2) and thus identify the molecular species in the STM images. At all coverage ratios the two type of species can be clearly distinguished by their substantial difference in apparent height of (220 $\pm$ 40) pm (Fig. 9.20 a). The molecules with the greater apparent height correspond to compound **2**, because the amount of those molecules in the adlayer decreases with decreasing amount in solution. *Vice versa*, the molecules with the lower apparent height correspond to compound **1**. This contrast is not caused by the geometric height of the molecules, which is larger for compound **1** (see Fig. 6.1), but has to be attributed to an electronic effect, specifically the higher electronic conductivity of the fully conjugated vertical group in **2**. Thus, the STM observations directly confirm that the

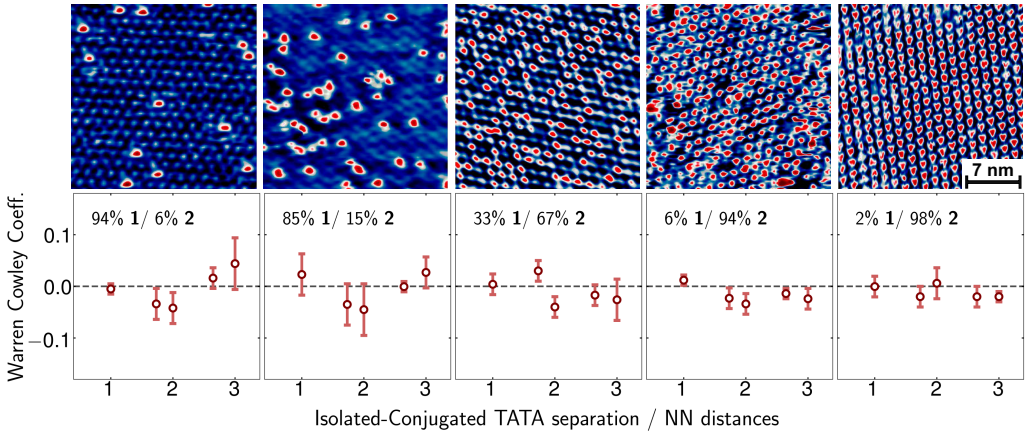

Figure 6.3: Top: Exemplary STM images of five different compositions of mixed monolayers consisting of **1** and **2** (20 x 20 nm^2). Bottom: Corresponding Warren Cowley coefficients, calculated from the STM data for the surface compositions shown above, as a function of the intermolecular distance (in units of the TATA-TATA distance of 1.25 nm). A coefficient of 0 (dashed line) is expected for a random distribution.

conjugation in the vertical unit of **1** is broken by the trioxabicyclo[2,2,2] isolator unit.

Quantitative analysis of the STM data indicates that the coverage ratio θ_1/θ_2 is approximately a factor 0.5 smaller than the concentration ratio c_1/c_2 of the solutions used for the adlayer self-assembly (Fig. 6.4). On the basis of previous studies, which reveal that the adsorption energy of TATA on Au(111) is high ($\approx$ 180 kJ/mol [160]) although its surface diffusion is fast [41], we assume that the molecules are strongly irreversible adsorbed and the observed coverage ratios results from a kinetic effect. Specifically, our observation indicates a faster adsorption of **2** as compared to **1**, which we attribute to the involved mass transport in solution. Because of the lower molar mass of **2**, a higher diffusion coefficient is expected. Alternatively, the difference between coverage ratio and concentration ratio in solution may be explained by an equilibration process, in which molecules of the initially formed adlayer subsequent exchange with molecules in solution via desorption and re-adsorption. However, the pronounced differences in the behaviour of **1/2**, **1/3**, and **1/4** adlayers would be difficult to explain in this scenario, because the binding to the Au substrate and the lateral interactions are governed by the TATA platform, whereas the different ver-

tical groups have a negligible influence. To quantify whether the molecules aggregate in the adlayer or are randomly distributed on the Au(111) surface, the Warren Cowley coefficients, which describe the short-range order, were calculated as a function of the intermolecular distances (Fig. 6.3, bottom; see Supporting Information for details). These coefficients give the probability to find a molecule of one type in a defined distance to a molecule of the other type and normalize that probability by the coverage ratio of these molecules. For a random distribution the Warren Cowley coefficient will be zero for all distances. According to our analysis, the coefficients are close to zero within the experimental errors at all concentration ratios and thus indicate that the molecules are stochastically distributed on the surface.
Similar studies were performed for **1**/**3** and **1**/**4** binary adlayers, albeit over a smaller range of concentration ratios (Fig. 9.21). In both systems, the molecules **1** appear higher in the STM images than the surrounding molecules **3** and **4**, respectively. The significantly larger apparent height of **1** relative to the bare platform **4** (100 $\pm$ 30) pm (Fig. 9.20c) may be expected, taken into account that the conjugation in the vertical group of **1** is only interrupted 410 pm above the TATA's central C atom. More surprising is the larger apparent height of **1** relative to **3** ((60 $\pm$ 20) pm, Fig. 9.20b), since the vertical extension of the conjugated pyridine unit in **3** exceeds that of the part of **1**, which is strongly electronically coupled to the Au surface. The observed height contrast suggests that the trioxabicyclo[2,2,2] group does not fully disrupt electronic transport through the vertical unit in **1**.
The comparison between the ratio of the molecules in solution and that on the surface shows that both **3** and **4** adsorbed significantly faster than **1**, leading to a much weaker dependence of the coverage ratio on the concentration ratio than for **1**/**2** adlayers (Fig. 6.4). This behaviour is in agreement with the much lower molecular mass of compounds **3** and **4** and thus supports our assumption that this effect is related to the different diffusion velocity of the species rather than differences in the adsorption energies. The Warren Cowley coefficients of **1**/**3** and **1**/**4** adlayers show that also in these systems the molecules are randomly distributed on the surface (Fig. 9.21 bottom). Thus, even bare TATA platforms mix perfectly stochastically with the azobenzene-functionalized TATA molecules.

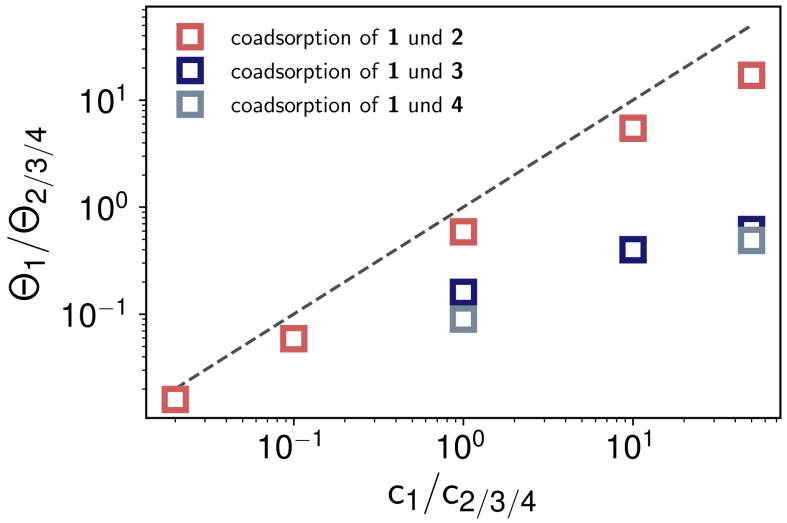

Figure 6.4: The composition of the monolayers θ_1/θ_i (i = 2, 3, 4) as function of the concentration ratio c_1/c_i in solution. The dashed line illustrates the behaviour expected for equal adsorption rates of the two species. The statistical errors are within the symbol size.

In summary, our study demonstrated that TATA-based molecules provide a versatile construction kit for the preparation of structurally well-defined adlayers that exhibit multiple functional groups. As illustrated here for azobenzene derivatives and pyridine, the TATA platform enables vertical mounting of the functional groups at fixed in-plane distances. It exclusively determines the lateral arrangement in the adlayer, independent of the attached functional unit. As a consequence, the molecules are not only homogeneously and statistically distributed in the adlayer but also have a sufficient free volume for performing advanced functions, such as the photoswitching of the azobenzene units. Furthermore, the molecular composition of the mixed adlayers and thus the fraction of specific functions on the surface can be varied over a wide range by the concentration ratio in solution.

Considering that many TATA-based molecules, including various types of photoswitches (imines, diazocins) and other functionalities (e.g. metal complexes) [82, 84, 161], have been shown to form similar adlayer structures, the concept demonstrated here should be easily transferable to other

binary systems and even adlayers consisting of three of more different molecular species. Suitable design of the attached vertical units should allow the realization of cooperative functions, for example photoswitching of the chemical reactivity via blocking or activation of a neighbouring group (Fig. 6.1a). The latter does not require in-plane order but only a precise positioning of the different functional groups relative to each other and thus can be readily realized in stochastically mixed layers as prepared in this work. For example, **1**/**3** adlayers, in which Co porphyrins are attached to adsorbed **3** [162], access to the metal center may potentially be modified by *trans-cis* isomerization of the azobenzene unit in **1**, which would allow to photoswitch the electrocatalytic O2 reduction reaction. Furthermore, an even better controlled lateral arrangement of the different functions may be obtained by combining the platform concept with principles of two-dimensional supramolecular organization. For planar adsorbate molecules without vertical functions, assembly of two different species into well-defined ordered surface arrangements have been achieved using molecular recognition via hydrogen bonding [163, 164], coordinative bonding via metal atoms [130, 165], or ionic interactions between charged molecular building blocks [166]. Transferring these principles to vertically functionalized platforms will require synthesis of platforms with different lateral ligands that interact with each other.

We gratefully acknowledge financial support by the Deutsche Forschungsgemeinschaft (DFG) via the collaborative research centre SFB677, project B09.

Conflicts of interest

There are no conflicts to declare.

7 | Ordered Adlayers of a Combined Lateral Switch and Rotor

This chapter is based on an article published in The Journal of Physical Chemistry C [159].

Rotors and switches are elementary building blocks of molecular machines. To achieve more advanced functions, these units have to be integrated into solid-state devices, which triggered interest in mounting these functional units in well-defined geometries onto surfaces. While vertically oriented switches and rotors have been obtained by various strategies, the design of surface-parallel switches and of altitudinal rotors with an in-plane oriented rotation axis has proven to be more difficult. We here demonstrate a molecular adlayer system with highly defined geometry and laterally oriented functional groups that combines facile photoswitching and rotation. We employ a custom-designed molecule with two platforms and pillars that span an azobenzene unit between them. The molecules form well-ordered monolayers on Au(111) with the azobenzene units parallel to and above the surface. Spectroscopic data and density functional calculations suggest that in the trans configuration, at room temperature, the azo unit is freely rotating. Upon irradiation with UV light, the azo unit switches to the bent cis configuration and rotation stops. Irradiation

with 430 nm restores the rotating trans state. Notably, the photochemistry is not quenched by the metal surface. This approach offers a promising strategy to operate molecular machines on metal surfaces with light, which is still a major problem in molecular nanotechnology.

7.1 Introduction

Similar to their counterparts in the macroscopic world, molecular motors and machines must be properly embedded in their environment to achieve sophisticated functions. A first step in building artificial molecular machines thus is the integration of functional molecular units into solids or onto surfaces. Extensive advances in this field have already been made, especially in the attachment of molecular rotors and switches to surfaces via self-assembly. Free rotation and molecular switching are among the most fundamental functions achievable in self-assembled layers on surfaces, but applications of such systems for more complex machine-like functions are still limited. For this, systems with precisely defined positions and orientations have to be developed. That requires going beyond conventional self-assembly approaches, such as surface attachment of functional units via flexible alkanethiol or siloxane based molecules.
Several strategies have been used to mount molecular switches or rotors perpendicular or parallel to solid surfaces, which in the case of rotors, correspond to an azimuthal or altitudinal rotation axis, respectively (Figure 7.1a).
Both geometries have been realized (Figure 7.1b, c) [47, 167, 168]. Azimuthal rotors on surfaces were demonstrated by Michl and coworkers, who used vertical channels in crystal surfaces to insert the axes of rotors [169]. Alternative approaches to mount rotors and switches perpendicular to surfaces use molecular building blocks that ensure a vertical geometry, for example tripods [47, 154, 170], bulky spacer groups [46, 55, 156, 171], or the platform concept developed by our group (Figure 7.1b, right) [13, 16, 75, 78, 80, 88]. The latter employs planar units that adsorb on the surface in form of highly

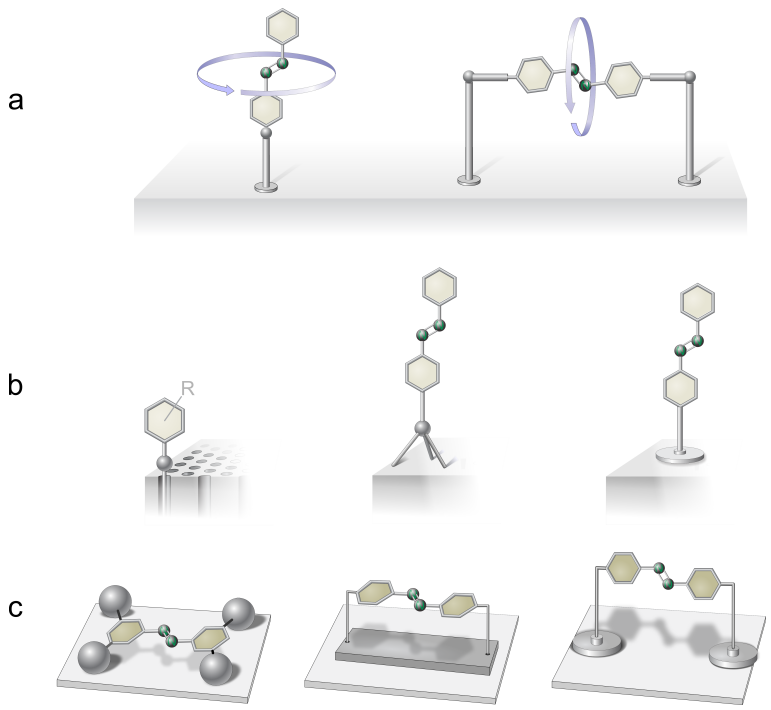

Figure 7.1: Schematic illustrations of (a) surface-mounted molecular switches and rotors with vertical and lateral orientation. Concepts for realizing these (b) vertical and (c) lateral functions on surfaces.

ordered monolayers and provide posts for vertical functions that are freely rotating and – with suitable functional groups – photoswitchable.
Altitudinal rotors and surface-parallel switches require a different construction strategy [47, 167, 172–174]. Zheng et al. have been the first to present a concept for such systems [172]. They employed two vertical poles to mount an altitudinal rotor parallel to the surface. However, apart from this seminal work, very few examples of such systems exist [167, 173, 175]. In case of molecular switches on metals, azobenzenes and other photochromes adsorb in a planar geometry [69, 70], but their photochemistry is quenched by electronic coupling to the substrate. Several approaches have been developed to decouple the photoactive parts from the surface and thus restore the photochemistry[74, 176, 177]. Tegeder et al. employed azobenzene units with large substituents as vertical spacers (airbag approach) [4, 68, 71, 72], but distortions of the molecule upon adsorption lead to strong suppression of the photoisomerization. Furthermore, cyclophane type structures were

used to enforce a distance between the metal surface and the photoactive part of the molecule to prevent electronic coupling[50]. Switching or rotation of the decoupled units was not reported, however.
In this work, we demonstrate that modification of our platform concept allows vertical mounting of a functional unit while retaining its capability to both switch and rotate. Here, two platforms with two pillars span the axis of a rotor, consisting of a photoswitchable *p,p′* -substituted azobenzene unit (Figure 7.1c, right). This is realized by using compound **1**, which we recently introduced[106]. In this molecule, an azobenzene is spanned between two phenyl-functionalized triazatriangulenium (TATA) platforms (Figure 7.2). Ether bridges attached the phenyls *meta* positions on both sides to the azobenzene's *para* positions. The alkoxy group interrupts the conjugation between platform and azobenzene and decouples the azo unit from the metal surface. According to photophysical experiments in solution, the azobenzene is still reversibly switchable with a high switching efficiency and low fatigue.

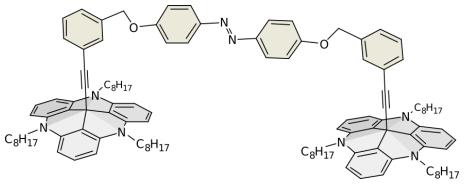

Figure 7.2: Studied compound **1**: azobenzene unit spanned between two phenyl posts, mounted on TATA platforms.

In the following, we present a detailed study of the adlayers structure and photoswitching by scanning tunneling microscopy (STM), X-ray photoelectron spectroscopy (XPS), near edge X-ray absorption fine structure spectroscopy (NEXAFS), ultraviolet-visible spectroscopy (UV/Vis), and supporting quantum chemical calculations. Preparation of molecular monolayers with a well-defined adsorption geometry and long-range order is nontrivial for complex non-planar molecules, such as compound **1**. We show that by optimizing the self-assembly conditions ordered adlayers with high packing density of these molecules can be prepared on Au(111) surfaces, in

which the azobenzene units are oriented parallel to the surface and to each other. Furthermore, we provide evidence that the azobenzene is rotatable in the slender *trans* configuration. Upon irradiation with UV light, reversible isomerization to the bent *cis* configuration occurs, which appears to block the rotation.

7.2 Experimental Section

Adlayer preparation. The synthesis of 1,2-Bis[4-[[3-(4,8,12-tris-*n*-octyl-4,8,12-triazatriangu-lenium-benzyloxy)-12c-ethynyl]phenyl]]diazene (**1**) has been described in detail in a previous publication [106]. The crude product was purified by column chromatography and according to NMR analysis there are no major signs for impurities. For the STM, XPS and NEXAFS measurements, circular Au(111) single crystals with surface diameters of 10 to 12 mm, oriented within 0.3° (MaTeck) were used as substrates for the self assembled monolayer (SAM) formation. The single crystals were cleaned before each preparation by flame annealing in butane gas. UV/Vis experiments were performed on ultrathin Au films of 10 nm nominal thickness with a 1-2 nm Ti adhesion layer on quartz glas (Phasis Sàrl), described in more detail in a previous publication [87]. The substrates were cleaned by repeated rinsing with acetone (Uvasol, spectroscopy grade, Merck). The glassware used for all the preparations of the SAMs was cleaned in piranha solution (1/3 hydrogen peroxide, 2/3 sulfuric acid) and thoroughly rinsed with Milli-Q water prior to use. The adsorbate layers were then prepared by immersion of the substrate in 50 - 100 μM solutions in acetone for 1 to 3 days at 20 °C to 25 °C. Afterwards, the samples were rinsed with pure acetone to remove excess molecules physisorbed on top of the SAM, dried under ambient conditions, and immediately transferred into the experimental setup.

STM. STM studies were performed under ambient conditions with a PicoPlus STM (Agilent, Santa Clara, USA) and mechanically cut Pt/Ir (70:30) tips. The measurements were carried out in constant current mode at tun-

neling currents of 20 to 90 pA and bias voltages of 200 to 700 mV. The STM data was analyzed using Scanning Probe Imaging Processor Software (SPIP, Image Metrology). Lateral drift was corrected with a dedicated software, developed by our group. Radial distribution functions were obtained from sets of 14-30 images with sizes ranging from 3600 nm^2 to 8100 nm^2 using Matlab R2016a.

XPS. The XPS and NEXAFS measurements were performed at the BESSY II synchrotron radiation facility using the PREVAC endstation at the beamline HE-SGM. The experimental station is equipped with a hemispherical VG Scienta R3000 photoelectron analyzer. The energy resolution E/DE of the beamline with 150 μm slits is 800. XP survey spectra were recorded at 700 eV photon energy using an analyzer pass energy of 100 eV, whereas for the C 1s and N 1s spectra the photon energy was 350 eV and 500 eV, respectively with a pass energy of 50 eV. All spectra were acquired at normal electron emission. For determination of the relative composition of the TATA adlayers, the XP spectra were energy-corrected using the Au $4f_{7/2}$ line at a binding energy of 84.0 eV as reference. Background correction was performed using a Shirley background for the Au 4f signals and a linear background for all other signals. Peak fitting was performed using the CASA XPS Tool. The fitting parameter are shown in the supporting information (Tab. 9.7). For the quantitative determination of the adlayer coverage the peaks were integrated and normalized by the number of recorded scans to obtain the intensity per scan (IPS). In order to secure that small changes in beam energy and beam spot size do not influence the comparison, the IPS values were divided by the respective IPS of the gold peaks, measured directly after the N 1s or C 1s signal.

NEXAFS. The NEXAFS spectra were normalized by setting the pre-edge background to 1 (i.e., for the C K-edge determined at (275.0 $\pm$ 2.5) eV and the N K-edge at (388.75 $\pm$ 2.5) eV). To correct for the photon flux, all spectra were divided by the spectrum obtained for a freshly sputtered clean gold substrate and then edge-step normalized (using the average intensities for the C K-edge between (275 $\pm$ 0.5) eV and (325 $\pm$ 0.5) eV and for the N K-

edge between (395 ± 0.5) eV and (420 ± 0.5) eV as pre- and post-edge). The normalized spectra were fitted employing a step function for the absorption edge and Gaussians for the π^* and σ^* resonances in order to determine the intensity I of specific resonances (Fig. 9.25). The series of spectra of a specific sample measured at different angles of incidence were fitted with the same parameter set, i.e., the energies of the resonances were allowed to vary in maximum by 0.2 eV and the half-widths at full maximum by 0.3 eV, as in agreement with the estimated experimental resolution. For determination of the orientation of the molecular orbitals, the dependence of the intensities I of the π^* resonances on the angle of incidence θ were finally fitted to model functions:

$$I = A \cdot [P \cdot \cos^2\theta \cdot (1 - \frac{3}{2} \cdot \sin^2\alpha) + \frac{1}{2} \cdot \sin^2\alpha] \tag{7.1}$$

with the specific amplitudes of the resonances A, the degree of polarization P = 0.91, and the tilt angle of the transition dipole moment of the molecule with respect to the surface normal α.

UV/Vis. The UV/Vis spectroscopy measurements were carried out with a Cary 4000 double-beam spectrometer (Varian Inc.) using the methodology of our previous studies [87]. The intensities of the spectrometer beam were $< 10^{-7}$ mW cm^{-2}, i.e., six orders of magnitude lower than those employed for the photoisomerization. The spectra were obtained under ambient conditions and in transmission, with the Au thin film oriented perpendicular and the quartz backside of the sample facing towards the incident monochromatic probe beam. The *trans-cis* and *cis-trans* photoisomerization in the SAM was induced by irradiating the sample from the backside at an angle of 45° with LEDs with emission maxima at 365 nm (Nichia Corporation) and 455 nm (Luxeon), respectively. This resulted in intensities up to 0.41 mW cm^{-2} (365nm) and 0.38 mW cm^{-2} (455 nm) at the sample. Photoisomerization of the molecules in solution was recorded with the same setup, using a cuvette with a thickness of 1 mm in the place of the quartz sample holder. In all spectral measurements the spectral resolution $\Delta\lambda$ was set to 1 nm with an integration time of 0.1 s. The spectral bandwidth was 5 nm. To

reduce the contribution of the substrate, the initially obtained absorption spectrum of the pristine nonfunctionalized substrate was subtracted. The photoisomerization kinetics were measured by monitoring the absorption of the sample at a fixed wavelength of 355 nm with a time resolution of 1 s. While probing the molecules, UV and blue light were alternately turned on and off, which was accompanied by instantaneous jumps of the signal, caused by stray light. These jumps were removed in the presented data.

Calculations. All semi-empirical geometry optimizations were conducted with the code GFN-xTB (version 1, as published in JCTC 2017) [178], designed for accurate geometries, frequencies, and non-covalent interactions. Simulated annealing was performed as implemented in the code with 3 annealing blocks with electronic temperatures of 149, 650, and 1000 K, respectively, and a run time of 50 ps each, also making use of the SHAKE algorithm [179] for all bonds. Single point energie calculations were performed with ORCA 4.0.1 [180]. For the single point energies the ωB97X-D3 [181] density functional approximation was used in conjunction with a large def2-TZVPP orbital basis set [182], as this DFA performed well in Grimme's latest study on noncovalent interactions [183]. To speed up the calculations, density fitting together with the chain of spheres approximations as implemented in ORCA (RIJCOSX)[184] was used, with a fine grid (gridX6 in ORCA nomenclature) and the all-purpose def2 fitting basis set (def2/J in ORCA terminology) [185].
Density functional theory (DFT) geometry optimizations without underlying Au(111) surface were conducted with the standard level of theory B3LY[186] and a 6-31G* basis set[187] with Gaussian09 Rev. D01 [188]. For single point energies the Minnesota density functional M06-2X [189] with dispersion correction (D3) [190] was used with a large triple zeta basis def2-TZVPP [182]. These calculations were carried out with Turbomole7.2 [191] and the usage of resolution-of-identity (RI) with multipole accelerated RI-J (marij) to speed up the calculations. For the DFT calculations on a single layer of Au(111), Turbomole7.2 was used with the same adjustments as above but with the time saving GGA PBE [192–195], dispersion correction (D3) and a small def2-SVP basis set [182]. Afterwards single point calcu-

lations (M06-2X(D3)/def2-TZVPP) were carried out by removing the gold slab to get comparable energies of the isomers.

7.3 Results

STM A high coverage and low defect density are preferable to determine the overall adsorption geometry of **1** on the Au(111) surface as well as the adsorption sites. To identify the preparation condition that yields the SAM most suitable to achieve this goal, several samples prepared via three different methods were studied by STM. Characteristic examples of the appearance of these samples are presented in Figure 7.3. In all STM images

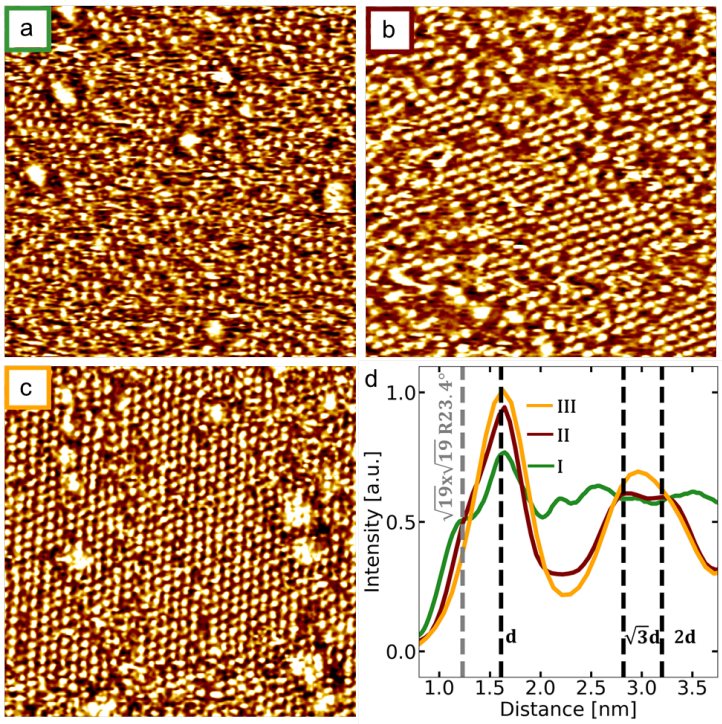

Figure 7.3: STM images of **1** adlayers on Au(111), prepared by (a) method I, (b) method II, and (c) method III (50 × 50 nm^2, U_{bias} = 0.3 V, I_t = 30 pA). (d) Corresponding radial distribution functions. The dashed vertical lines highlight the first 3 intermolecular distances for a $\sqrt{31} \times \sqrt{31}$ $R8.9°$ superstructure and the nearest neighbor distance for the unfunctionalized platforms ($(\sqrt{19} \times \sqrt{19})$ $R23.4°$ superstructure).

discrete maxima of uniform size are observed. As we will demonstrate

below, these can be attributed to individual molecules of **1**. In addition, larger features are observed, which can be assigned to small Au monolayer islands, caused by the lifting of the Au(111) surface reconstruction during adlayer formation [78].

Preparation by immersion for 48 h at 20 °C (method I, Figure 7.3a), results in a largely disordered monolayer, in which only small patches exhibit hexagonal order. It can be assumed that in this case compound **1** adsorbs in the thermodynamically stable *trans* configuration on the surface. On samples prepared with additional permanent irradiation during the immersion with 365 nm (method II, Figure 7.3b) we find larger hexagonally ordered patches with some disordered areas at the edges of those patches. Uncovered areas between the ordered domains can also be observed. Although one expects the majority of the adsorbed molecules **1** to be in the *cis* state under these preparation conditions, the better ordering is most probably caused by a slight heating of the sample rather then due to photoisomerization of the molecules. Non-irradiated samples which were heated to 25 °C during the preparation and immersed for 72 hours (method III, Figure 7.3c) exhibited even better order with large hexagonally ordered domains and only a few disordered areas, mainly at areas between different rotational domains. Preparation at even higher temperatures resulted in adlayers of low coverages without ordered structures and thus was not studied in more detail.

The increasing order in the adlayer is corroborated by a quantitative analysis of the hexagonally ordered domains in larger sets of STM images. Here, the average number of molecules per domain increases from 28 to 45 for adlayers prepared by method I and II, respectively, while for method III even 280 molecules per domain were found. The same trend manifests in the intermolecular distances, which were determined from the radial distribution function of the molecule positions, calculated from the STM data (Figure 7.3d). All studied samples show a pronounced peak at about 1.6 nm, which corresponds to the nearest neighbor distance of the molecules in the hexagonally-ordered domains. From the well-ordered samples prepared by method III, an intermolecular distance of d = (1.62 $\pm$ 0.04) nm is determined. This distance as well as the experimentally measured angle between

rotational domains of 17° ± 3° are in good agreement with a ($\sqrt{31} \times \sqrt{31}$) *R*8.9° superstructure on the Au(111) substrate. For samples of type II and III, also the corresponding distances to next-nearest neighbors and beyond (at $\sqrt{3}$d, 2d) manifest as clear peaks in the pair correlation function, further supporting this structure. However, interesting deviations are found in the more disordered areas, specifically in the samples prepared by method I. For these, the radial distribution function shows an additional edge, located at about 1.25 nm, i.e., below the 1.6 nm intermolecular spacing of the ordered domains. An intermolecular distance of 1.25 nm was also found for adlayers of bare and functionalized octyl-TATA [18, 78]. We assign this spacing to shorter distances between molecules of **1** in the disordered regions, where a greater variability in the local environment exist and the distance between the molecules thus may vary. In type II samples, only a very weak shoulder in the correlation function is visible at 1.25 nm, in type III samples, this distance is not observable at all.

The surface coverage of **1** increases with the degree of order. Specifically, type I samples have a coverage θ of (0.26 ± 0.03) nm^{-2}, type II samples (0.33 ± 0.03) nm^{-2} and type III samples (0.36 ± 0.02) nm^{-2}. The latter is ≈80% of the ideal coverage of a ($\sqrt{31} \times \sqrt{31}$) *R*8.9° superstructure of (0.45 ± 0.02) nm^{-2}, but in good agreement with the experimental coverages obtained by XPS (see below). Because type III adlayers had unsurpassed high coverage and low defect density, this method was employed for the preparation of the adlayers in all spectroscopic studies. The decrease in coverage with reduced long-range order reflects the lower surface density in the disordered areas. Nevertheless, as just discussed, the lowest intermolecular distances of 1.25 nm are found only in those locations. That seemingly paradoxical situation originates in the specific molecular geometry and will be discussed in more detail below. For all preparation methods the observed adlayer structures strongly differ from that of bare octyl-TATA or octyl-TATA platforms with vertical functions, which all form well-ordered ($\sqrt{19} \times \sqrt{19}$) *R*23.4° adlayers [13, 18, 78, 83]. This indicates that the molecule, especially the azobenzene bridge between the two TATA platforms, remains intact upon adsorption.

High-resolution STM images, obtained at higher bias voltages (500-700 mV), reveal the intramolecular structure of the molecules. Figure 7.4a, recorded

in the center of an extended $(\sqrt{31} \times \sqrt{31})$ $R8.9°$ domain, show two peaks in each $(\sqrt{31} \times \sqrt{31})$ $R8.9°$ unit cell, arranged in a honeycomb structure. We assign each of those peaks to one of the two TATA units of **1**, corresponding to one molecule **1** per unit cell. The attached azobenzene unit is not directly visible in these STM images due to the electronic decoupling. The surface density of the adsorbing octyl-TATA platforms in this arrangement is 23% higher than in the well-ordered $(\sqrt{19} \times \sqrt{19})$ $R23.4°$ adlayers of bare octyl-TATA. Only in the more disordered areas, where the local coverage of **1** is

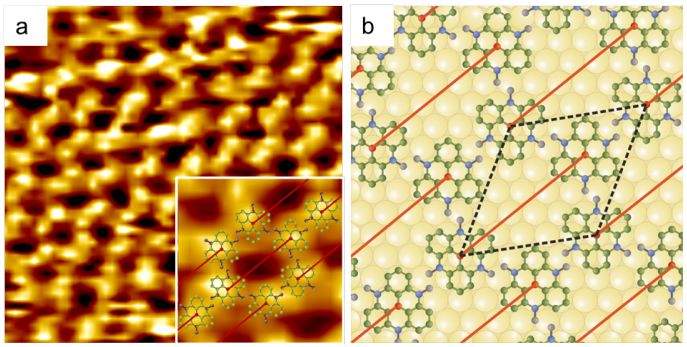

Figure 7.4: (a) High-resolution STM image of a **1** adlayer, revealing the intramolecular structure ((15 × 15) nm^2, U_{bias} = 0.7 V, I_t = 50 pA). (b) Model of the in-plane arrangement of the TATA platforms of **1** in the adlayer on the Au(111) surface. For clarity, only the first C atom of the octyl side chains is shown (in gray). The suggested positions of the vertical phenyl-azobenzene-phenyl units are indicated by red lines. The inset in (a) shows the proposed structure overlaid on a (2.2 x 2.2)nm^2 area of the STM image.

lower, the characteristic $\sqrt{19}$ distance of 1.25 nm can be apparently achieved (e.g., by a parallel arrangement of both molecules where both TATA units are offset by the same 1.25 nm distance from the corresponding TATA units of the neighboring molecule, Fig. 9.22). On the basis of these data, we propose an arrangement as indicated in Figure 7.4b, where the TATA platforms adopt a honeycomb structure with a nearest neighbor distance of 0.92 nm. We assume that the azobenzene bridge links the two TATA platforms on opposite sides of the honeycomb (Figure 7.4b, red lines), as their distance of 18.5 $\AA$ is close to the natural spacing of these units in the free molecule **1**. Further rationalization for this adsorbate structure will be provided in the discussion.

For the free molecule in solution, the spacing between the two platforms of each **1** molecule, in *cis* state differs from that in the *trans* state. To assess if the **1** adlayer structure, especially the spacing between the two TATA groups of an adsorbed molecule, was influenced by photoisomerization, the samples were irradiated with 365 nm light. No differences were found, i.e., STM images of irradiated samples exhibit the same inter- and intramolecular distances as non-irradiated samples. Since the two states cannot be distinguished by STM, NEXAFS and UV/Vis spectroscopy measurements were conducted to establish if the molecules can switch reversibly between the *trans* and the *cis* state. Prior to the NEXAFS and UV/Vis studies, XPS experiments were carried out in order to validate the surface coverage and confirm that the adsorbed molecules are intact.

XPS High-resolution XPS spectra of the C 1s (Figure 7.5a) and N 1s region (Figure 7.5b) were used to probe the adlayer composition. In the N 1s spectra two species can be recognized under the main line. The one with the lower binding energy at 399.4 eV (red line) can be assigned to nitrogen atoms directly connected to carbon atoms representing the nitrogens of the TATA platform [17, 88], whereas the other signal with higher binding energy at 400.0 eV (blue line) refers to nitrogen atoms directly bonded to another nitrogen atom. According to literature, this signal corresponds to the nitrogen atoms of the azo moiety [14, 196]. This clearly indicates that the azo group is still intact after the adsorption process. The ratio of the relative intensities (2.7:1) almost conforms to the expected values (3:1), which was calculated based on the molecular structure. The small deviation is within the error bars of the fit. The slightly lower value may result from attenuation of the TATA nitrogens signal by atoms located above the TATA platforms.
The high resolution C 1s spectrum contains two signals. The most prominent signal at 284.6 eV (red line) corresponds to the aliphatic and aromatic carbon atoms with only carbon-carbon bonds and the signal at 285.7 eV (blue line) is due to the carbon atoms, which have bonds to nitrogen or oxygen atoms. Actually, two different species (C-O) and (C-N) for the second

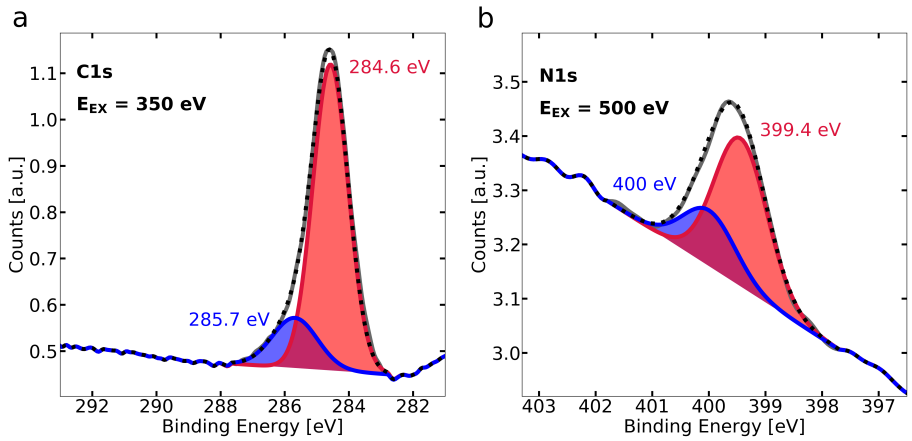

Figure 7.5: XP spectra of the **1** monolayer on Au(111), showing (a) the C 1s and (b) the N 1s lines.

signal would be anticipated, but the resolution of the spectrum is insufficient to separate them. However, within the error bars of the quantitative analysis, the ratio of the relative intensities (4.8:1) fits approximately to the values expected on the basis of the molecular composition (5:1).

To confirm the adlayer coverage inferred from the STM measurements, quantitative XPS measurements were employed. For this, a well known azo-TATA compound ((E)-12c-[4-(4-methoxyphenyldiazenyl)-phenyl]ethynyl-4,8,12-tri-*n*-octyl-4,8,12-triazatriangulene, **2** was used as a reference [17]. Self-assembled monolayers of **2** form a highly ordered $(\sqrt{19} \times \sqrt{19})$ $R23.4°$ superstructure on Au(111) surfaces with an ideal coverage of 0.73 molecules per nm^{-2}, corresponding to 3.6 N atoms per nm^{-2} and 42.4 C atoms per nm^{-2}. Because the defect densities of optimal prepared **1** and **2** monolayers are similar according to the STM studies, comparison with this reference should provide the local coverage of **1** in the ideal ordered adlayer structure. For both compounds, **2** and **1**, N 1s and C 1s spectra were recorded on the same Au(111) single crystal and subsequently fitted. From the intensity ratio of the N 1s peaks for **1** and **2** (see Tab. 9.5, Tab. 9.6), a surface coverage of 0.45 molecules per nm^{-2} was obtained, which is in good agreement with the ideal coverage of a $(\sqrt{31} \times \sqrt{31})$ $R8.9°$ superstructure with one molecule **1** per unit cell. The surface coverage obtained from the C 1s peaks is ≈30% lower (0.32 molecules per nm^{-2}). However, this quantity is expected to be

more inaccurate than that obtained from the N 1s spectra, since the transfer of the samples into the vacuum could lead to an uptake of carbon containing impurities.

NEXAFS NEXAFS spectra (Figure 7.6) were measured at the carbon and nitrogen K-edges for **1** monolayers on Au(111) single crystals. The C K-edge of **1** (Figure 7.6b) shows one intensive π^* resonance at 285.5 eV. Above the edge several broad σ^* resonances can be observed, the most pronounced one located at 293 eV. Measurements with different angles of incidence indicate an angular dependency of the π^* resonance, where the intensity slightly decreases at an angle of 90°. These results are in accordance with previous studies of TATA compounds [88]. The spectra of the N K-edge of non-irradiated **1** monolayers on Au(111) (Figure 7.6a) exhibit three π^* resonances. The smaller resonances at 400.7 eV and 402.5 eV originates from the TATA platform nitrogen atoms and show the same polarization as observed for the pure platform molecule [88]. With higher angles of incidence the intensity of these π^* resonances decrease, which also is well known for adsorbed TATA platforms.

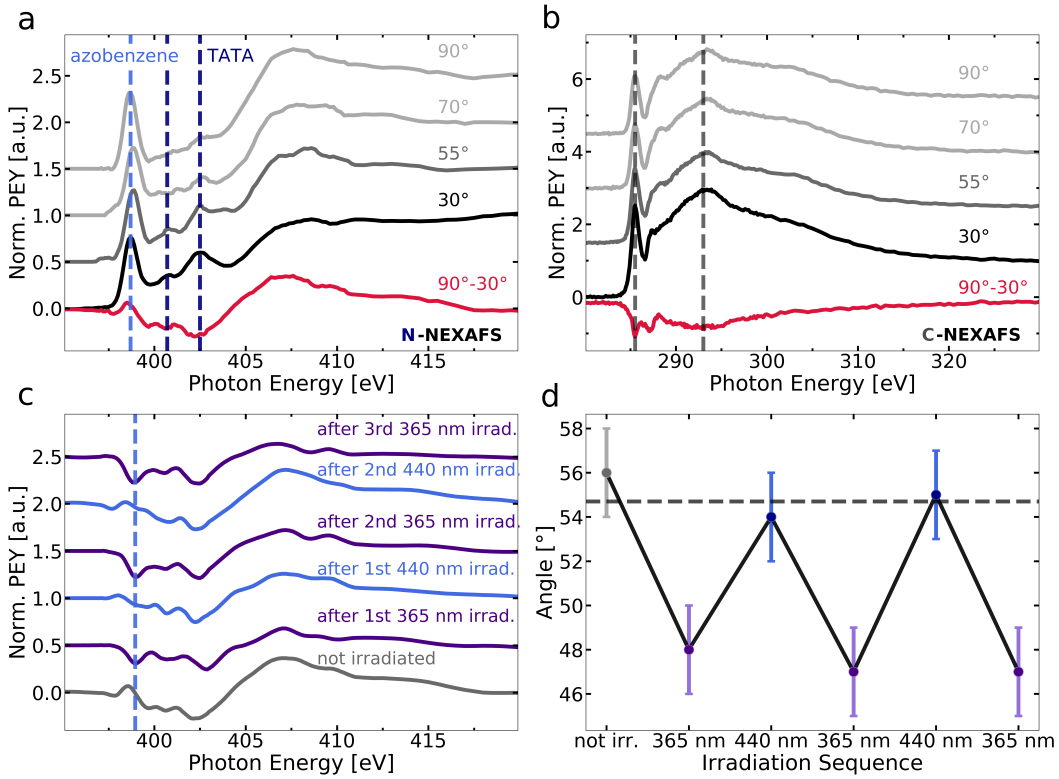

Figure 7.6: NEXAFS of the **1** adlayer on Au(111). (a) N and (b) C K-edge at different angles. The red lines show the differences of the spectra measured at 90 and 30°. (c) Changes of the N K-edge difference spectra during an experiment, where the sample was alternately irradiated by UV (365 nm) and blue (440 nm) light, resulting in transitions between the *trans* and *cis* state of the azobenzene unit. (d) Calculated effective angle between the transition dipole moment of the N 1s core level excitation to the azobenzene's LUMO and the surface normal for the sequence of spectra shown in (c). The dashed line indicates the magic angle for an isotropically oriented dipole moment.

The energy position (398.7 eV) of the first π^* resonance corresponds well to the characteristic π^* resonance reported in the literature for azobenzene units [88] and thus is assigned to the N 1s $\rightarrow \pi^*$ transition of the azo moiety, i.e., the excitation from the N 1s core level to the LUMO. Its intensity depends on the direction of the electric field vector of the incident polarized light relative to the direction of the transition dipole moment of this excitation, which varies with the angle of incidence of the polarized X-ray beam. It is thus expected that the intensity of this azo-resonance depends

on this angle, if the molecule and the transition dipole moment of the considered resonance show a preferred orientation to the surface. However, in contrast to adlayers with vertical oriented azobenzene groups, a significant change of the azo-resonance at 398.7 eV with incident angle is missing for the studied range of 30-90° (Figure 7.6a).
Quantitative calculation of the angle of the transition dipole moment of this resonance (excitation from N 1s core level to the LUMO of the azobenzene) relative to the surface normal yields a nominal value of 56° (Equation 7.1, Fig. 9.25). Within the experimental error, this is identical to the so called "magic angle" (54.7°), which would be obtained for an isotropic orientation of the dipole moment. Taking into account that the azobenzene unit is mounted at the same height above the surface at the two phenyl-TATA moieties and its axis thus is parallel oriented to surface, this result indicates that the azobenzene unit is freely rotatable around the $C_{azob.}$-O bonds.
To study the photoisomerization of adsorbed **1**, the sample was irradiated with UV-light of 365 nm, which results in clear changes in the polarization of the first π^* resonance at 398.7 eV (Figure 7.6c). Specifically, the intensity of this azo-resonance decreases at an angle of 90° in comparison to that at 30°. This correspond to a decrease in the calculated dipole moments angle to 47°, indicating a change in orientation of the azobenzene groups of the molecules **1**. This change in geometry can be assigned to a *trans-cis* isomerization of the azobenzene and is fully reversible: If the sample is subsequently irradiated with light of 440 nm, the polarization of the π^* resonance at 398.7 eV switches back, indicating that the orientation of the transition dipole moment is reverted to the original state. The high reversibility of this processes is proven by repetitive irradiation experiments, where the angle of the dipole moment to the surface alternated reproducible between approximately 55° and 47° during photoinduced changes between the *cis* and *trans* state (Figure 7.6d). Besides the change in intensity a shift of the respective azo-π^* resonance from 398.7 eV to 398.9 eV could be observed after irradiation with light of 365 nm. As shown by Moldt et al. [121], this small peak shift can be attributed to a binding energy change of the N 1s core level upon the *cis-trans* isomerization of the azobenzene. After irradiation with light of 440 nm the peak shifts back to 398.7 eV, confirming again

the high reversibility of the **1** photoisomerization in the adlayer.

UV/Vis Further confirmation and kinetic data on the photoswitching were obtained by UV/Vis spectroscopy. Spectra of **1** in cyclopentane solution (Figure 9.5a, dashed lines) are shown for the photostationary state (PSS) after 365 and 455 nm irradiation, corresponding to a state containing predominantly *cis*- and *trans*-azobenzene, respectively. In good agreement with previous data of azobenzene-functionalized TATA derivatives [87], the π-π^* ($\sim$ 300-400 nm) and the n-π^* ($\sim$ 400-500 nm) bands are observed. Photoisomerization to the *cis* state results in a significant reduction of the π-π^* and a slight increase of the n-π^* band. Additionally, a band centered at 264 nm is observed, which belongs to the TATA moiety (in the following called TATA band), but is blue-shifted by 21 nm with respect to that of TATA platforms with vertically oriented azobenzene groups [87].

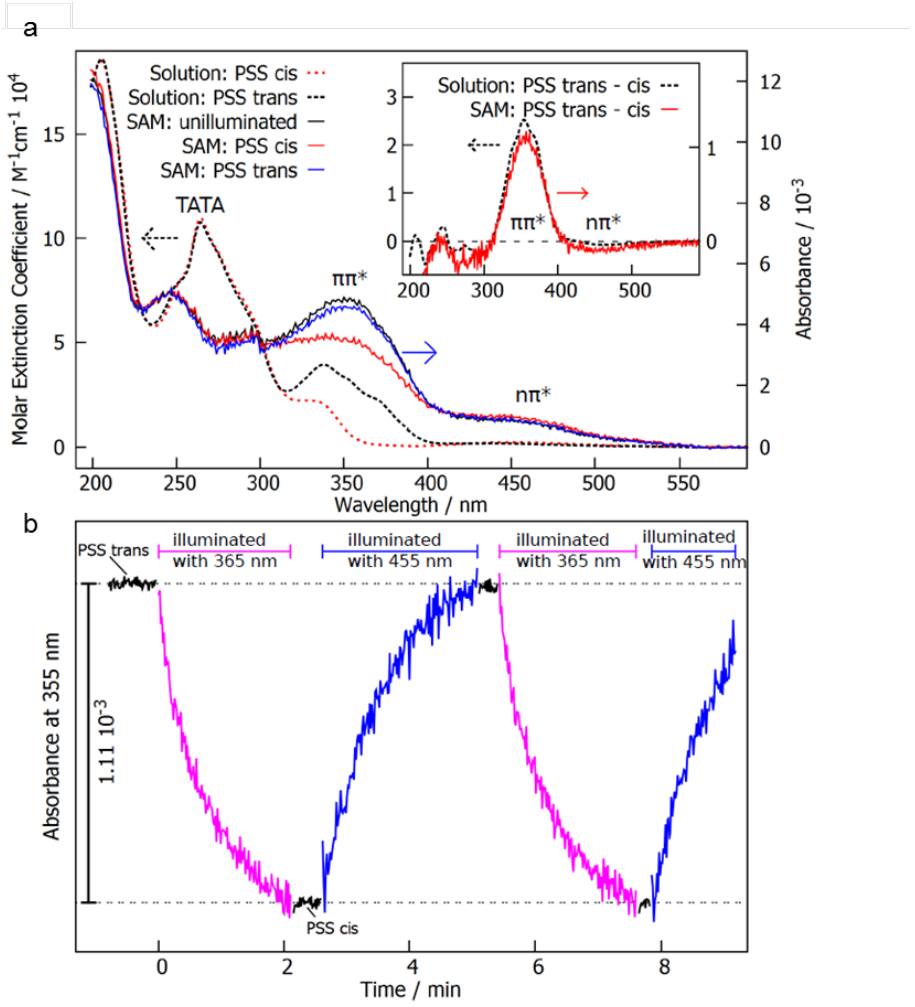

Figure 7.7: (a) UV/Vis spectra of **1** in cyclopentane solution (dashed lines, axis on the left side) and as adlayer on Au films (solid lines, axis on the right side), recorded directly after preparation and in the *cis* and *trans* state, prepared by irradiation with UV (365 nm, (2.69 $\pm$ 0.07) mW cm^{-2} for solution, (0.41 $\pm$ 0.02) mW cm^{-2} for SAM) and blue light (455 nm, (2.63 $\pm$ 0.15) mW cm^{-2} for solution, (0.38 $\pm$ 0.05) mW cm^{-2} for SAM), respectively. Background signals of the solvent or substrate are subtracted. The inset shows the *trans-cis* difference spectra in solution (dashed line) and in the adlayer (solid line). (b) Time dependent changes of the absorbance signal at 355 nm of the **1** adlayer during irradiation with UV and blue light, showing fast and highly reversible photoswitching.

In UV/Vis spectra of **1** adlayers on Au (Figure 9.5a, solid lines) the π-π^* transition can be clearly resolved. The spectra change in a similar way upon irradiation with UV and blue light as those obtained in solution, confirming

the photoswitching of the adsorbed molecules. Even the change in the n-π^* band can be observed. Compared to solution, the n-π^* band is more pronounced relative to the π-π^* band whereas the TATA band is significantly less pronounced. In addition, the TATA band is even more blue-shifted (from 264 nm to 246 nm) than in solution. For a better comparison of the photoswitching of **1** in solution and in the monolayer, the difference between the UV/Vis spectra in the *trans* and *cis* state is shown for both cases in the inset of Figure 9.5a. In contrast to TATAs with vertically mounted azobenzene groups [87], the π-π^* band maxima in the difference spectra of the **1** adlayer and **1** in solution are not shifted with respect to each other. Furthermore, the larger relative change of the n-π^* band in the **1** adlayer as compared to **1** in solution becomes apparent.

From the spectral data, the surface coverage of **1** on the Au surface can be estimated by comparison of the absorbance of the **1** adlayer with the extinction coefficient ϵ of **1** in solution [87]. For this, the area under a band in the difference spectra of solution and adlayer were determined. Here, we assume that the extinction change $\Delta\epsilon$ of the SAM is similar to that in solution. This seems justified in view of the identical spectral position of the π-π^* band and the very similar photoisomerization cross sections (see below) of **1** in the SAM and in solution, which indicate an effective decoupling of the azobenzene switch from the surface. For the calculation of the surface concentration of **1** from these data, it must be taken into account that the molecules are isotropically distributed in solution, whereas the adsorbed molecules and thus their transition dipole moments have a defined orientation. Due to the structure of the molecules, a planar orientation of the platforms and azobenzene units and thus of the π-π^* dipole moment is expected, resulting in appropriate correction factors (for the employed spectrometer geometry 3/2 for the solution, 1 for the adlayer). From the measured signals, a coverage θ of (0.37 ± 0.04) nm^{-2} is obtained, which is in excellent agreement with the STM and XPS results.

The photoisomerization kinetic of adsorbed **1** on gold was studied by monitoring the absorption as a function of time during alternating irradiation by UV (365 nm) and blue light (455 nm). The experiments were performed at a fixed wavelength λ = 355 nm, where the change of the π-π^* band

is largest. Highly reversible and reproducible absorption changes were observed (Figure 9.5b). Fits of these data by single-exponential decay functions (not shown) perfectly describe the experimental curves, revealing that the *trans-cis* photoisomerization in the adlayer can be described by well-defined first-order transitions. The corresponding effective photoisomerization cross sections are $\sigma_{eff,trans-cis}$ = (28±7) $\cdot 10^{-18}$ cm^2 for the *trans-cis* and $\sigma_{eff,cis-trans}$ = (20±3) $\cdot 10^{-18}$ cm^2 for the *cis-trans* transition, respectively. These values are very similar to those for azobenzene-TATA compounds in solution and adlayers of TATA-based molecules with vertically attached azobenzenes [87], indicating effective electronic decoupling of the azobenzene unit from the Au substrate.
In the same way, the thermal relaxation of **1** adlayers from the *cis* to the *trans* state was measured. Because of the slow kinetics of this process and temporal drift in the small signal from the monolayer, only a rough estimation of the characteristic relaxation time of $\leq$ 150 min. at room temperature could be obtained. Nevertheless, these experiments demonstrate that the adsorbed molecules **1** have a similar stability against thermal backisomerization as the molecules in solution.

Quantum chemical calculations To assist the determination of the complex 3D adlayer structure, quantum chemical calculations were performed, using a two-pronged approach. First, semiempiric calculations were used to obtain the energetically most favorable geometric conformation of the entire **1** molecule, including the six octyl side chains, by simulated annealing. Then, the side chains were neglected and the geometry of the simplified molecule was calculated by density functional theory, using standard local geometry optimization techniques. This allows to combine the advantages of both approaches, i.e., the capability of exhaustive conformer searches by semiempirics and the increased accuracy of DFT. In the following we will present and compare the results of both approaches.
In the semiempiric approach, a geometry optimization for molecule **1** on a single layer of Au(111) was carried out, with the distance of the two central carbon atoms of the TATA platforms being fixed to the 18.5 $\AA$, obtained from the STM measurements. Although geometry optimization of the free

unrestrained molecule **1** in the *trans* configuration with DFT (B3LYP/6-31G*) find 19.8 $\AA$ for this distance (Fig. 9.27), the state with 18.5 $\AA$ is only 0.5 kcal/mol higher in energy (at the M06-2X(D3)/def2-TZVPP level), indicating that the molecules can easily accommodate the strain induced by the geometric constrains, resulting from the in-plane arrangement of the TATA platforms. In the next step, the gold surface was removed, the internal coordinates of the TATA platforms fixed, and the most stable thermally accessible conformer determined by simulated annealing (Fig. 9.26). With the thus obtained structures, single point energies were calculated by DFT (ωB97X-D3/def2-TZVPP) to obtain more accurate relative conformer energies. From these single point energies, the most stable conformer was determined, redeposited on an Au(111) surface and reoptimized to account for molecule-surface interactions. The geometries obtained in this manner were used to judge whether the *trans* configuration can freely rotate. In both *trans* and *cis* state the molecule is strained, manifesting in a slight bending of the phenyl pillars (on average 12° and 10° relative to the surface normal for the *cis* and *trans* isomer, respectively). This strain results from the imperfect match of the length of the azobenzene bridge with the spacing of the corresponding TATA platforms in the tightly packed honeycomb lattice and is more pronounced for the bend *cis* than for the straight *trans* configuration.

The geometry optimizations conducted with DFT employed a simplified version of **1**, where the octyl side chains were substituted by protons. This approach is based on the assumption that the flexible alkyl side chains interact only weakly with the azobenzene bridge. In addition, the gold surface was initially omitted and the positions of the TATA platforms were geometrically constrained by keeping the outer carbon atoms of the platforms in a virtual plane simulating the surface and fixing the distance of the central TATA carbon atoms to 18.5 $\AA$. Within this approach, three *trans* isomer conformations were obtained, which differ significantly in geometry, especially also in the altitudinal orientation of the azobenzene, but are isoenergetic within the precision of the calculations (Fig. 9.27, top). The four most stable conformers of the *cis* isomer (Fig. 9.27, bottom) vary more in energy due to larger structural variations of the azo group geometry. For a final opti-

mization of selected conformations the virtual surface was replaced by a single Au(111) layer with fixed positions of the gold atoms. The resulting *trans* isomer (Figure 7.8a) stays nearly the same. This indicates a negligible influence of the metal substrate, as may be expected for the rather large and uniform azobenzene-metal spacing ($\approx 9\mathring{A}$ relative to the topmost Au layer). For the *cis* isomer two configurations were considered, with the azo group pointing either towards or away from the surface (Figure 7.8b,c). The latter is lower in energy and additionally supported by the facile photoswitching of the molecule, observed in the NEXAFS and UV/VIS measurements. In the former conformation the azo group is physisorbed on the Au surface, which should quench the isomerization process [73]. Isomerization could still be possible for this configuration via indirect transient excitation [197, 198]. However, a configuration where the *cis* azo group is pointing away from the surface is more likely, because the intramolecular excitation process still occurs according to the UV/Vis data. Overall, the resulting structures obtained by the semiempiric and by the DFT calculations are very similar.

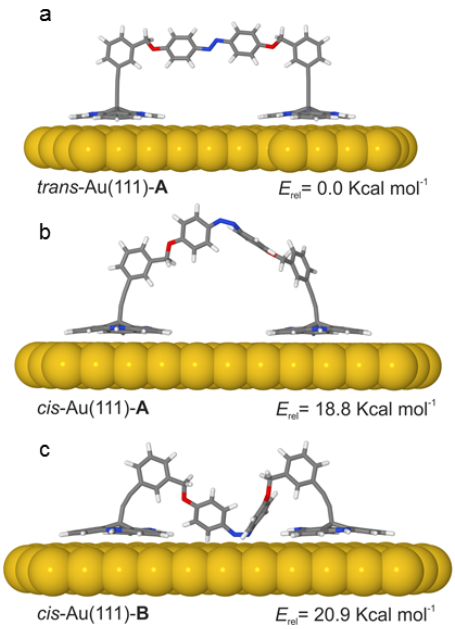

Figure 7.8: Optimized (PBE(D3)/def2-SVP) structures of the (a) *trans* and (b,c) *cis* isomer of **1** on the Au surface. Relative energies were conducted by DFT single point energy calculations (M06-2X(D3)/def2-TZVPP) with removed Au layer.

These results support a free rotation of the azobenzene in the *trans* configuration. In the *cis* isomer the strongly bent conformation probably restricts this rotation geometrically. Unfortunately, this cannot easily be proven by the current calculations, due to the many degrees of freedom of molecule **1**. Especially, the presence of the six octyl side chains, including the side chains of neighboring molecules in the densely-packed monolayer, is expected to significantly influence the rotation of the bridging azobenzene (see below).

7.4 Discussion

The results obtained by the various microscopic, spectroscopic, and computational methods provide a comprehensive characterization of **1** monolayers on Au(111). On the basis of these studies a detailed microscopic picture

emerges, which demonstrates the successful design of a system with combined vertical switching and altitudinal rotation as well as defined long-range order. In the following we discuss first the molecular arrangement and then rotation and switching in the adlayer.

The observed lateral arrangement in the adlayer is in good agreement with expectations based on the molecular geometry. As all other TATA-based compounds, the TATA moieties of the molecules **1** adsorb planar on Au(111) substrates, with the vertical attached units pointing away from the surface. Under optimized preparation conditions, the molecules arrange in a densely-packed, hexagonal ($\sqrt{31} \times \sqrt{31}$) $R8.9^\circ$ superstructure with one molecule **1** in the unit cell. The TATA surface density in this structure is substantially higher than that for bare octyl-TATA platforms under ambient conditions. However, it has been shown that the packing density in TATA adlayers is variable and depends on the space requirements of the alkyl side chains [18]. In particular, for octyl-TATA adlayers in electrochemical environment an even ≈30% denser ($2\sqrt{3}$x$2\sqrt{3}$) structure was found at negative potentials, where the octyl chains were extended away from the surface [42]. That the arrangement proposed in Figure 7.4b is sterically feasible, was also confirmed by quantum chemical calculations.

The honeycomb lattice of TATA units in the ($\sqrt{31} \times \sqrt{31}$) $R8.9^\circ$ adlayer has never been observed for adlayers of pure TATA or molecules, consisting of a single TATA platform with a vertically attached group. We rationalize this by a lateral structure, in which the adsorbed **1** molecules are parallel but staggered with respect to each other. This type of arrangement has also been found for planar dumbbell-shaped molecules [199]. Taking into account the high flexibility and the many degrees of freedom of **1**, the formation of adlayers with large well-ordered domains is unusual. In many cases, a much more disordered arrangement was found for similarly complex, anisotrop 3D molecules [172]. We attribute the good in-plane order to the pronounced self-assembly and high room temperature mobility of the TATA platforms on Au(111). Apparently, these enable ordering even in this system, where two platforms are interconnected by a molecular bridge. However, the defect density in the **1** adlayer is much more sensitive to the self-assembly conditions and even in the optimal case much larger than for

molecules with a single TATA platform.

As demonstrated by the DFT and quantum chemical calculations, a $(\sqrt{31} \times \sqrt{31})$ *R*8.9° honeycomb structure, in which the azobenzene is parallel to the surface and spans across the remaining empty surface site (Figure 7.4b), is in good agreement with the natural dimensions of the *trans* isomer of **1**. It implies a geometry where the *trans* azobenzene is oriented parallel to the Au(111) surface and well separated from it. However, the space between the azobenzene unit and the metal is not empty, but largely filled by the alkyl side chains of the TATA platforms. These most likely physisorb on the Au surface due to dispersive interactions and may lead to additional lateral binding between neighboring **1** adsorbates. Considering that 6 octyl chains are present in each $(\sqrt{31} \times \sqrt{31})$ *R*8.9° unit cell and assuming a similar density as in liquid alkanes, the average height of this physisorbed layer is $\approx 9\mathring{A}$, i.e., the bridge should already be partially embedded.

Adlayers of **1** exhibit fast and highly reversible photoisomerization between the *trans* and *cis* state. This is in marked contrast to pure azobenzene and tetra-*tert*-butyl-azobenzene, which also feature a planar adsorption geometry on Au(111) surfaces [4, 69, 70], but strongly hindered photoisomerization in the adsorbed state [67, 68, 71–73]. The facile photoswitching in our system can be attributed to the larger spatial and electronic decoupling of the azobenzene unit from the metal substrate. The latter is also supported by the UV/Vis spectra of adsorbed **1**, which are even less affected than those of azobenzene mounted vertical on TATA platforms [87] and indistinguishable from those of **1** in solution. Altogether, our data demonstrate that our platform-based method is a highly successful approach to mount vertically oriented photoswitches on metal surfaces.

In the $(\sqrt{31} \times \sqrt{31})$ *R*8.9° adlayer the *trans-cis* isomerization does not induce changes in the positions of the molecules TATA units on the surface. This is understandable in view of the tight TATA packing and the high flexibility of the vertical functional unit. Even if the molecules are adsorbed in the *cis* state (i.e., prepared by method II), the same structure is formed. Probably, the arrangement of the TATA units into the honeycomb arrangement is preferred over an in-plane geometry with a shorter distance between the two TATA units of the molecule, which would only be sterically possible

by breaking the hexagonal symmetry of the adlayer structure. Nevertheless, photoinduced changes between the two TATA units may in principle be possible for isolated molecules at low coverage, since the surface mobility of TATA on a clean Au(111) surface is high. However, such experiments would require STM measurements on **1** at cryogenic temperatures, which is outside the scope of the present study.
According to the NEXAFS results, the azobenzene is isotropically oriented in the *trans* isomer of **1**, suggesting that it is rotatable around its main axis. This is supported by the calculations and expected in view of the flexible mounting on the phenyl pillars. In contrast, the *cis* isomer clearly shows a preferred orientation. The corresponding configurations are strongly bend and – contrary to the *trans* isomer – the azo group thus is located far away from the rotation axis. Rotation of the *cis* azobenzene should therefore be strongly impeded by the octyl side chain. For a similar reason, an orientation where the azo group is orientated towards the Au surface (as in Figure 7.8c) seems unlikely. The latter should also strongly quench the photoisomerization, which is at variance with the spectroscopic studies. Finally, the NEXAFS data also provide clear evidence that photoisomerization leads to highly reversible changes in the angular distribution. This is only possible, if the *trans* isomer's orientation is redistributed after backisomerization, corroborating that the *trans* azobenzene bridge not only is rotatable, as suggested by DFT and quantum chemical calculations, but indeed rotates at room temperature.

7.5 Conclusion

With this study we demonstrated the successful assembly of a combined lateral photoswitch and altitudinal rotor on a metal surface. By extending our platform concept to molecules containing several platform units, we could mount the functional azobenzene groups parallel to the Au(111) substrate at a distance defined by the height of the molecular phenyl pillars attached to the TATA platforms. This approach leads to electronic decoupling of the azobenzene from the surface, enabling facile photoswitching.

Because the azobenzene is rotatable in the *trans* but not in the *cis* state, we can fully reversibly switch the altitudinal rotation on and off by irradiation with UV and blue light, respectively. This capability may be of interest for the realization of higher molecular functions. For example, one may attach additional functions to the rotor unit which would be either permanently oriented in a defined direction (e.g., towards or away from the surface) or have an isotropic orientation, dependent on the switching state. This would allow switching the chemical availability of these functions to species in the environment above the metal surface. Furthermore, the well-ordered adlayer structure allows mounting the molecules in arrays with parallel arranged functional units. This may enable higher functions that employ cooperative effects. Using intrinsically anisotropic substrates, e.g. Au(110) surface, even macroscopic directionality may seem feasible.

Supporting Information Available

Model of adsorbed molecules on Au(111), results from quantitative XPS measurements, fitting parameters for XPS data, SP spectra showing the survey, N1s NEXAFS spectra of the LUMO resonance of the azo moiety, N-NEXAFS spectra, models of calculated local enery minima (Figures S1-S6 and Tables S1-S4).

Acknowledgements

We gratefully acknowledge financial support by the Deutsche Forschungsgemeinschaft (DFG) via the collaborative research centre SFB677, project B09. Furthermore we would like to thank the HZB for provision of beamtime at the BESSYII/HE-SGM and Christof Wöll for the provision of the Prevac endstation. RH is gratefull for support by SPP 1928.

8 | Conclusion

The four studies presented in this thesis address the creation and systematic analysis of photoswitchable self-assembled monolayers as a step towards sophisticated machine-like functions. The studied systems employ the platform concept introduced in 2009 by the research group of Prof. Dr. Herges [98] to prepare highly ordered functionalized surfaces of free-standing functional units. In these systems, the functional unit is attached perpendicularly to a molecular platform of triazatriangulenium ions. The lateral intermolecular spacings are controlled by alkyl side chains. This concept thus provides the means to design well-defined adsorption geometries.
The presented work was carried out within the scope of the Collaborative Research Centre 677 - "Function by Switching". The studies shown are therefore the results of a joint work of research groups in organic, inorganic and theoretical chemistry as well as interface physics. As part of the joint project, the aim of this work was the preparation of highly-ordered self-assembled monolayers consisting of azobenzene derivatives on Au(111) surfaces with a low defect density and their characterization via scanning tunneling microscopy under ambient conditions.

In chapter 3 the dependence of the relaxation rate of the azobenzene's *cis* isomer on the electronic coupling to the gold substrate was systematically investigated. Therefore different coupling units were embedded between the platform and the switching unit. Five different molecules were examined, which contained coupling units from fully conjugated to isolated in gradations. STM studies revealed that all molecules formed a hexagonal, highly ordered $\sqrt{19} \times \sqrt{19}\, R23.4^\circ$ superstructure on Au(111) surfaces. Since all molecules were connected to the substrate via octyl-TATA platforms, this

study confirmed that functionalization of the TATA platforms did not affect the arrangement of the molecules.
The *cis*-to-*trans* relaxation behavior of these systems was examined using IRRAS. The systematic investigation of the influence of conjugation on the relaxation time showed that the weaker the coupling of azobenzene to gold, the slower the molecule switches back into the *trans* state. The molecule with the weakest conjugation had a half-life of about 62 hours. This comparatively high stability of the *cis* configuration against thermal backswitching made it possible to study the switching behavior of these molecules by using STM. In order to irradiate the sample with UV light during the measurement a custom built irradiation unit was added to the STM setup. Thus, the same surface area could be observed before and after the isomerization process.
Chapter 4 shows the results of those experiments: Direct molecular scale STM observations of the photoswitching of adlayers consisting of the azobenzene functionalized TATA derivatives with an electronically isolating linker group were obtained. By comparing the same surface area before and after exposure to UV light of 365 nm wavelength, it could be demonstrated that the *trans*-to-*cis* isomerization does not occur randomly but is dependent on the state of the neighboring molecules in the monolayer, resulting in a formation of *trans* and *cis* clusters. Additionally, a quantitative analysis of the high-resolution STM data revealed that the switching probability increases with the number of neighboring molecules in *cis* state. *Ab initio* calculations indicate that the electronic excitation preferably localizes on the n-π^* state of *trans* isomers with neighboring *cis* azobenzenes.
With a better insight into the switching behaviour of isolated azobenzene TATA, mixed layers of these molecules were prepared and are shown in the next chapter. Specifically, the stable isolated azobenzene TATAs were coadsorbed with unfunctionalized platforms, platforms with pyridine units and platforms with fully conjugated azobenzene units, respectively. The ratio of the respective molecules in the solution was systematically changed to obtain different coverages on the surface. For all three systems we found that the TATA derivatives are perfectly mixable and randomly distributed on the surface. They all form the expected highly-ordered hexagonal $\sqrt{19} \times \sqrt{19}$

*R*23.4° superstructure on Au(111) surfaces. Due to the differences in the apparent heights, the molecules could be distinguished and ascribed to a functional unit.
Like the investigations dicussed before the last study examines an adsorbate layer of TATA-based azobenzene derivatives. In contrast to the molecules analyzed in the previous chapters, the azobenzene unit was not vertically but horizontally oriented with respect to the surface. The synthesis of the molecule under investigation was already published in 2015 as part of the CRC 677 [106]. It consists of an azobenzene unit placed between two molecular pillars, each of which is attached to an octyl-TATA platform. STM investigations have shown that the molecules form a highly ordered adsorbate layer on Au(111) surfaces. In both *cis* and *trans* state, a $\sqrt{31} \times \sqrt{31}$ *R*8.9° superstructure was observed. This means that the connected platforms do not change their position when the isomerization state of the azobenzene changes. Using NEXAFS and UV/vis spectroscopy, reversible switching could be demonstrated. In addition, the NEXAFS data showed an isotropic orientation distribution of the *trans* isomer but not of the *cis* isomer. It follows that the azobenzene unit rotates parallel to the surface when it's in the *trans* state. This rotation can be suppressed by switching to the *cis* state. Hence, an altitudinal rotor was realized which can reversibly be turned on and off by photoswitching with a suitable wave length. The platform concept was therefore extended from vertically to horizontally oriented switches and rotors.

In summary, the preparation of different highly-ordered photoswitchable adsorbate layers on Au(111) surfaces was realized and confirmed by scanning tunneling microscopy. Not only the structure of monoatomic adsorbate layers but also of binary layers prepared by coadsorption was investigated. The platform concept was also extended by a photoswitchable altitudinal rotor. Furthermore, the STM was complemented by an irradiation unit, which allowed to obtain high-resolution STM data of adsorbate layers before and after exposure to UV light. These data showed the neighbor-dependent switching behavior of TATA-based azobenzene derivatives on Au(111) surfaces. The observation of this collective switching behavior can lead to a

better understanding also on a macroscopic level.
All in all, the investigations performed have provided significant insights into the adsorption and switching behavior of TATA-based azobenzene derivatives on Au(111). This may be fundamental to further improve photo-controlled surfaces and to integrate them in solid-state devices.

9 | Supporting Information

9.1 Observation of collective photoswitching in free-standing TATA-based azobenzenes on Au(111)

Experimental Section

Sample Preparation

Compound **1**, which has a trioxabicyclo [2.2.2] unit implemented between the ethinyl spacer and the azobenzene group, was described in Ref. [83], where its synthesis and properties in solution are given in detail. The self-assembled monlayers were prepared on Au(111) single crystals with surface diameters of 10 mm and oriented within $\pm 0.3^{\circ}$ (MaTeck). For the IRRAS measurements, glass substrates with a 5 nm titanium adlayer and a 200 nm evaporated gold film from EMF corporation (Ithaca, NY) were used. All glassware used for the preparation was previously placed in 1/3 hydrogen peroxide mixed with 2/3 of sulfuric acid for at least 24 hours and carefully rinsed with Milli-Q water afterwards. The respective substrates were cleaned by flame annealing in butane gas and then immersed in 10 μM solutions of **1** in toluene (Merck, Uvasol) for 1 hour at 80 °C. Afterwards, the samples were rinsed with pure toluene, dried under ambient conditions and immediately thereafter, embedded into the STM or IRRAS setup.

IRRAS

The surface-adsorbed molecules were investigated using a Bruker VERTEX 70 FTIR spectrometer equipped with a polarization modulation accessory (PMA) 50 unit (Bruker Optik GmbH, Ettlingen, Germany). This instrument allows IRRAS and PM-IRRAS data to be recorded with a spectral range

of 4000-800 cm^{-1}. IRRAS data were collected with a liquid-nitrogen-cooled MCT detector in a horizontal reflection unit for grazing incidence (Bruker A518). The sample chamber was purged with dry nitrogen before and during measurements. A deuterated hexadecanethiol SAM on Au(111) was used as a reference for the background spectrum for conventional IRRAS spectra. Each displayed spectrum is the average of 2048 measured spectra. A p-polarized beam at an incident angle of 80° to the surface normal was used for measurements. All spectra were recorded with 4 cm^{-1} resolution. PM-IRRAS data were collected with the PMA 50 accessory and a liquid-nitrogen-cooled MCT detector. The PEM maximum efficiency was set for the half-wave at 1750/3000 cm^{-1} for analysis of the area from 1400/2000 to 1000 cm^{-1}. All spectra were recorded with 4 cm^{-1} resolution. Processing of IRRAS and PM-IRRAS data was carried out using the OPUS software Version 6.5 (Bruker, Germany). Baseline correction of the resulting IRRAS data was performed by the rubber band method in an interactive mode. PM-IRRAS data were processed by the implicit removal of the Bessel function through manual baseline correction. For the *trans - cis* isomerization of compound adsorbed on Au(111) the prepared samples were irradiated within the spectrometer using LEDs (peak wavelength: 365 ($\pm$ 9) nm or 440 ($\pm$ 5) nm). For the reference measurements (I_{trans} and I_{cis}) of the *trans* and the *cis* saturated state Nichia NC4U133(T) LEDs (power dissipation: 12 W, luminous flux: 10 lm) were used. The IRRAS measurements were conducted at 294 K. The temperature of the sample was measured during the IRRAS measurements and irradiation experiments. No significant changes ($\Delta T = \pm 1$) were observed. At first, the sample was irradiated with light of 365 nm with 10 μW cm^{-2} for a certain period (1 min, 2 min, or 5 min) depending on the progress of the isomerization. Subsequently a PM-IRRA spectrum was measured for the determination of the C_{phenyl}-$O_{methoxy}$ stretch intensity. By repeating this procedure several times, the photoinduced *trans*/*cis*-isomerization was retraced by IRRA spectroscopy.

UV/Vis

The UV/Vis spectroscopy measurements were carried out with a Cary 4000 double-beam spectrometer (Varian Inc.) using the methodology of our pre-

vious studies.[87] The intensities of the spectrometer beam were $< 10^{-7}$ mW cm^{-2}, i.e., six orders of magnitude lower than those employed for the photoisomerization. The spectra for the **1** SAM were obtained on 10 nm thin (111)-oriented Au films on quartz under ambient conditions, using transmission geometry. The *trans-cis* and *cis-trans* photoisomerization was induced by irradiating the sample with 365 nm / 0.41 mW cm^{-2} (Nichia Corporation) and 455 nm / 0.38 mW cm^{-2} (Luxeon) LEDs, respectively. Photoisomerization of the molecules in solution was recorded with the same setup, using a cuvette with a thickness of 1 mm in place of the quartz sample holder. The spectra were measured at 1 nm resolution with an integration time of 0.1 s and a spectral bandwidth of 5 nm.

STM

The STM measurements were performed under ambient conditions with a PicoPlus STM (Agilent, Santa Clara, USA) and mechanically cut Pt/Ir (70:30) tips and carried out in constant current mode at tunneling currents of 30 to 50 pA and bias voltages of 200 to 400 mV.

STM images of highly oriented graphite were used for the in-plane calibration and the lateral drift was corrected with a dedicated software, developed by our group. The lattice constants and angles between rotational domains were analyzed using SPIP 6.7.6 (Image Metrology).

Two ultraviolet (365 nm) LEDs were used to irradiate the samples. The light was coupled via lenses into two 400 μm diameter quartz fibers. The ends of these fibers were mounted opposite of each other around the sample (Fig. 9.1), allowing to irradiate the sample. The intensity was calibrated using a photoactive sensor placed in the STM setup instead of the sample. The angle of incidence of the light from the quartz fibers can be adjusted and was set were between 7 and 10 degrees before each measurement. A these angles the intensity at the position of the tip was still high and shading by the tip small.

Despite the shallow incident angles only a few switching events could be observed when the tip was in tunneling contact during sample irradiation. This can be explained by (partial) shading of the imaged area by the tip. Because the typical tip radius is in the range of 1 μm (tunneling occurs via

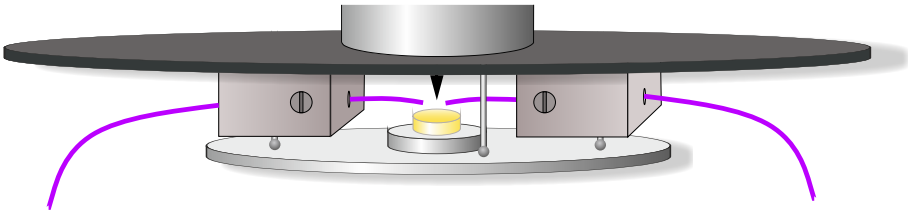

Figure 9.1: Schematic illustration of STM's UV irradiation setup, with the two quartz fibers shown in purple.

nanoscale protrusions on this sphere), the tip-sample distance in tunneling contact a few nm, and the typical size of the imaged area 50 nm, geometric shading occurs even at angles of 7-10 deg. To ensure sufficiently exposure of the sample, the tip was withdrawn from the surface by approximately 800 nm between irradiation periods and approached again after exposure. In order to arrive at the same sample area again after approaching, the thermal drift must be low. Therefore, at the beginning of a sequence of measurements, the sample was first imaged with the measuring tip for one to two hours. This time was used to find a suitable area for the irradiation experiments. Since the adlayer is initially very homogeneous, it was important to find larger defects or long gold steps, which can be recognized even after changes in the isomeric states of the adsorbed molecules. Fig. 9.3 shows an unprocessed STM image from the evaluated measurement sequence. The step edge and the domain boundary served as distinct markers to recover the identical position on the sample surface after irradiation.
The STM images were drift corrected with SPIP (Scanning Probe Image Processor, Image Metrology A/S, Horsholm, Denmark) using a plug-in developed in our group. In addition, SPIP and Python 3.6 were used to reduce noise and increase contrast, especially in Fig. 5.2d and 9.4b.

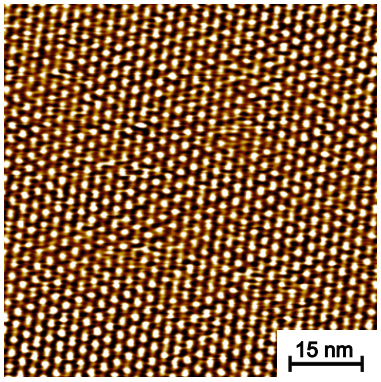

Figure 9.2: STM image of a self-assembled monolayer of **1** on Au(111) (35 x 35) nm^2 before irradiation.

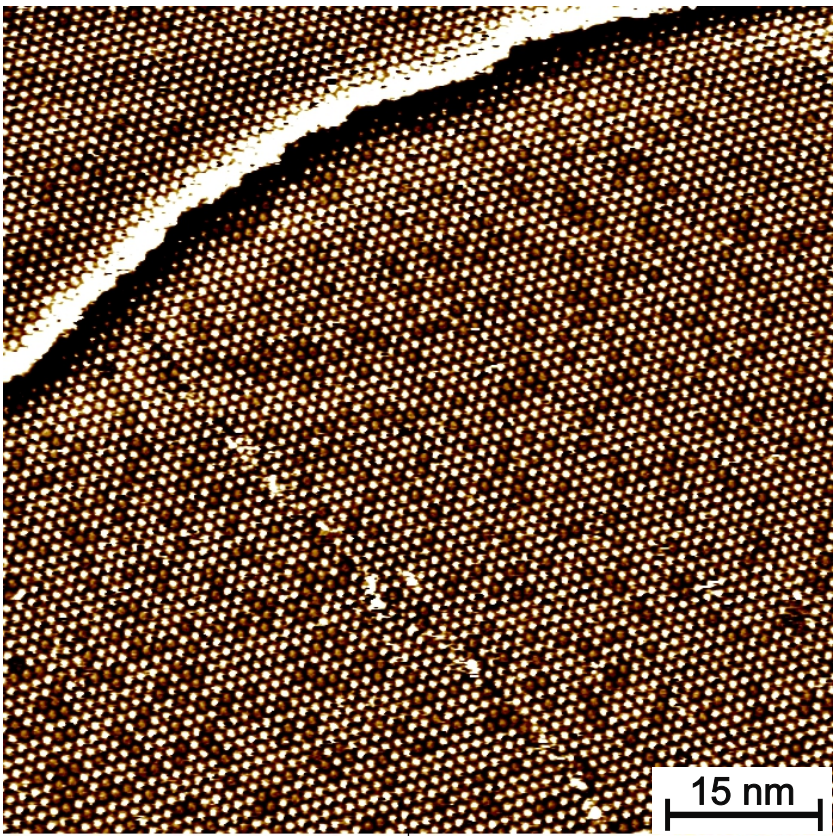

Figure 9.3: Unprocessed STM image of **1** on Au(111) after 28 minutes of irradiation with 365 nm at 6 $\mu W/cm^2$, (80 x 80) nm^2, I_t=30 pA, U_{bias}=0.3 V.

Quantitative Image Analysis

The statistical analysis focused on low to intermediate coverages, where most *cis* isomers are located in small clusters (monomers, dimers, trimers) embedded in a *trans* matrix. At higher coverages, a large variety of different *cis* clusters coexist, which differ in size and shape, leading to small numbers for each configuration and thus poor statistics. In addition, we molecular-resolution STM images were experimentally more difficult to obtain at high *cis* coverage, resulting again in low counting statistics.
The images were first transferred to a mathematical grid with a 1-0 matrix (Fig. 9.4a-d). Only sections that did not show rotational domains or gold steps were used for the quantitative analysis. Ensemble sizes, switching probabilities and Warren Cowley coefficients were calculated from these, using home-build software written in Python.

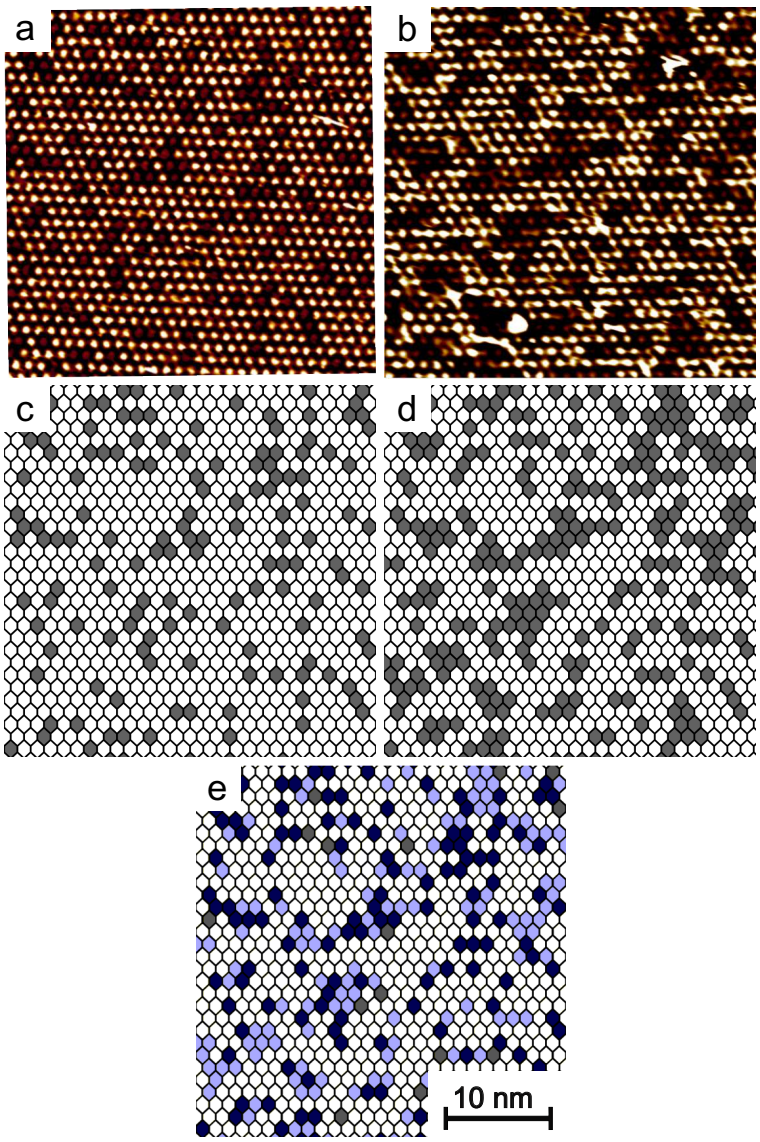

Figure 9.4: (a) STM image of a self-assembled monolayer of **1** on Au(111) after 28 minutes of irradiation with 365 nm at 6 μW/cm^2 and (b) after additional irradiation of 43 minutes with 365 nm at 6 μW/cm^2. (c, d) Data from (a) and (b) converted to a 1-0-matrix. The grey hexagons represent molecules in *cis* state and the white hexagons molecules in *trans* state. (e) Difference image of (c) and (d). The dark blue hexagons show *cis* and the white hexagons *trans* molecules from (c) that are unchanged. The light blue hexagons illustrate the molecules that isomerized from *trans* to *cis*, the grey hexagons illustrate the molecules that switched in the opposite direction.

Warren Cowley Coefficients

The Warren Cowley coefficients $\alpha(r)$ can be used as a measure of short-range order for binary mixed adlayers and were calculated as follows:[142]

$$\alpha(r) = 1 - \rho_{cis,trans}(r) \cdot \frac{1}{\theta_{cis}} \tag{9.1}$$

Here, $\rho_{cis,trans}(r)$ is the probability to find a molecule in *cis* state in a defined distance to a molecule in *trans* state, θ_{cis} is the coverage of *cis* isomers, and r is a particular lattice distance. In our study, $\alpha(r)$ was determined for r values of 1, $\sqrt{3}$, 2, $\sqrt{7}$, and 3 nearest neighbour distances). The Warren Cowley coefficients and ensemble sizes were determined using images from different surface areas. The errors were calculated by error propagation using the standard deviation from the mean.

Multimer Analysis

For the multimer analysis we generated random distributions for different ratios of $\frac{\theta_{cis}}{\theta_{trans}}$ and determined from those the coverage of small multimers. To keep the statistical error small, a large grid (1000×1000) was used. For verification purposes, we also calculated the average expected number of monomers, dimers, and trimers according to Ref. [200]. The results obtained by the simulation are in agreement with the calculated ones. The advantage of simulation is that the probability for large multimers can easily and quickly be determined.

Switching Probability

For the analysis of the switching probability as a function of the number of neighboring molecules in *cis* state, images taken in the same surface area before (t_1) and after (t_2) irradiation were used. As a result of this irradiation the *cis* coverage increased from $\theta_{cis}(t_1)$ to $\theta_{cis}(t_2)$. In the data analysis, first the molecules in *trans* state that at time t_1 have a certain number i (i = 1 to 6) of neighbors in *cis* state were identified. Of these n_i molecules k_i were found to have switched at t_2 to the *cis* state (graphically illustrated in Fig. 9.4e). From these data, the switching probability for molecules with i *cis* neighbors was determined as k_i/n_i.

Neighbours in *cis* state i	total number of molecules n_i	number of switching molecules k_i	ratio in %	90% confidence interval [p_l, p_u] in %
0	2174	392	18.0	[16.7, 19.5]
1	826	188	22.8	[20.4, 25.5]
2	347	101	29.1	[25.3, 33.3]
3	86	28	32.6	[24.9, 41.3]
4	18	7	38.9	[22.7, 58.1]
5	4	3	75.0	[35.6, 94.2]
6	0	0		

Table 9.1: Switching probability as a function of the isomerisation state of the nearest neighbors, obtained from the statistical analysis of the STM data. To determine the switching probability, several image sections with a total of 4046 molecules were analysed.

The errors in Fig. 3e of the manuscript correspond to the 90% confidence interval and were calculated using the Wilson confidence interval for a binomial distribution [201]:

$$p_{u,l} = \frac{k_i + \frac{c^2}{2}}{n_i + c^2} \pm \frac{c\sqrt{n_i}}{n_i + c^2} \cdot \sqrt{\frac{k_i}{n_i} \cdot (1 - \frac{k_i}{n_i}) + \frac{c^2}{4n_i}} \tag{9.2}$$

with $p_{u,l}$ being the upper and lower boundary of the confidence interval and c the $1 - \frac{\alpha}{2}$ quantile of a standard normal distribution. A confidence level of α = 90% was considered and therefore c = 1.644.

IRRAS Studies of the macroscopic kinetics

The macroscopic kinetics of the photoinduced *trans-cis*-isomerization of the **1** SAM was quantified in a similar way as in our previous study.[83]. First, the integrated intensity I of the C_{phenyl}-$O_{methoxy}$ stretch band in the spectra was determined as a function of irradiation time t. Due to the surface selection rule, the IRRAS signal depends on the surface-normal component of the transition dipole vector of the methoxy group. Upon switching from the *trans* into the *cis* state, the orientation of the methoxy group relative to the surface changes, resulting in an intensity change. However, even in the *cis* state the transition dipole moment retains a (smaller) surface-normal component. Thus, even a SAM consisting only of *cis* isomers will exhibit a C_{phenyl}-$O_{methoxy}$ stretch band. To determine the *cis* fraction in the SAM we therefore subtract the band intensity of the photostationary state, which is reached at $t \leq 50s$, and normalize this value by the difference in intensity before and after UV irradiation, $I(t) - I(54s)$.

This procedure is not fully exact, because even at 365 nm *cis-trans* reisomerization occurs at a low rate (as directly observable in the STM images), leading to a photostationary equilibrium with a *cis* isomer coverage $\theta_{cis} < 100\%$. For isolated molecules in solution, the *cis* fraction in the photostationary state is 85%, according to NMR measurements. For **1** SAMs an even higher *cis* fraction is expected, taking into account that θ_{cis} is high in the photostationary state and that the collective effects thus lead to an increase $k_{trans-cis}$ as compared to isolated molecules.

For the following modelling we ignore the deviation of θ_{cis} from 100%. This is justified, because (i) we are only interested in the qualitative behavior of $\theta_{cis}(t)$ and (ii) the collective effects mainly manifest at very low coverage. Here, the $\theta_{cis}(t)$ curve is not substantially affected by the saturation value. For the high coverage regime we do not expect a perfect agreement with the experimental data anyway, because of the simplicity of the employed models (see below).

To describe the IRRAS data shown in Fig. 3g, a number of different kinetic models were tested. Because a simple exponential function cannot reproduce the curve and the STM data indicate collaborative effects, several models that include adsorbate interactions were employed. These include

(i) the model by Hauser et al.[202, 203], which describes the high-spin to low-spin relaxation in spin-crossover systems,[204] and essential results in a sigmoidal function and (ii-iv) models for the growth of two-dimensional films, based on the Avrami theorem, (ii) in the limit of instantaneous nucleation, (iii) in the limit of progressive nucleation, and (iv) in the general form with an intermediate island nucleation rate. Performing fits by these models, we found that the Avrami model with instantaneous nucleation described best the time-depend changes in *cis* coverage, determined from the IRRAS data. In this model, $\theta_{cis}(t)$ is given by:

$$\theta_{cis} = 1 - e^{-k \cdot t^2} \tag{9.3}$$

The best fit with this model is shown in Fig. 3g and corresponds to a value of the single parameter k = 0.00547. Although deviations from the measured data in the area of high *cis* coverage can be seen in the fitted curve, this is not unexpected in view of the simplifications in this model, e.g., the assumption of growth in form of circular islands growing centers, which is not the case according to the STM observations.

UV/Vis spectroscopy results

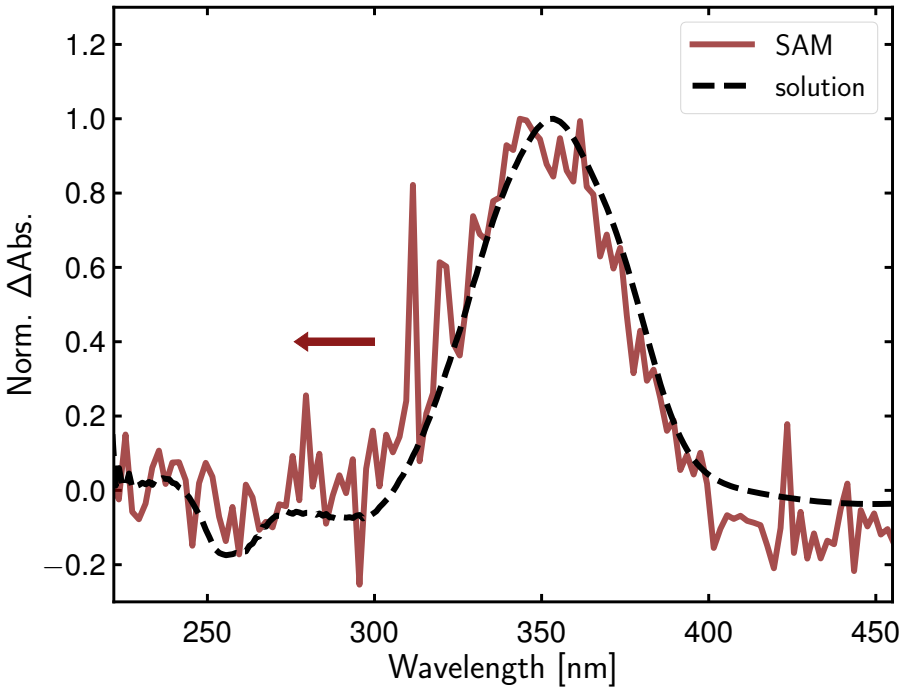

Figure 9.5: Normalized UV/Vis difference spectra (*trans* spectra minus *cis* spectra) for **1** in acetonitrile solution (dashed line) and as SAM on 10 nm thin Au substrate (solid line).The characteristic peak around is caused by the $\pi - \pi^*$ transition of the azobenzene unit and centered at 353.5 nm for the free **1** molecule in solution and at 349.8 nm for the **1** SAM, respectively. Please note that the absorbances of the **1** SAM are only in the range 10^{-4}, leading to substantial noise in the spectra.

Theoretical Calculations

Methodology

Our methodology relied on Density Functional Theory (DFT) for the ground state geometry optimization. As the considered system is a large gold slab with p-methoxyazobenzene molecules grafted onto an anchoring platform, the AZB are well separated from the surface. In our model, we simulate this by a single hexagonal cell consisting of (at least) seven AZB. The distance between the dyes was set to reflect the experimental setup, i.e., 1.26 nm. The *trans* isomer was first optimized isolated in the gas phase and its geometry was used to create the cell. At such a distance the main interactions between the AZB molecules are of electrostatic and dispersion nature. We used the standard hybrid B3LYP functional [186] together with 6-31G(d) atomic basis set to perform the DFT calculations. While electrostatics is reasonably described with such a standard DFT approach, the dispersion effects were accounted for using an empirical correction, namely the so called DFT-D3-BJ correction [205]. To simulate the anchoring of the AZB the bottom hydrogen atom was frozen during the optimizations. Likewise, to prevent unrealistic tilting of the dyes, the nitrogen atom the closest from the surface was kept fixed. Test calculations revealed that freezing this nitrogen atom or the vicinal carbon atom led to essentially the same results. This set up allows the system to explore potential energy surface for rotations around H-N(C) axis but prevents it from "collapsing". All DFT calculations have been performed with Gaussian16 [206].

In order to gain additional insights into the origin of the interaction between the monomers we performed a decomposition of the interaction energy at the SAPT0/cc-pVDZ level of theory [207, 208] in PSI4 software [209].

To further investigate larger clusters of the *cis* isomers we performed calculation of the system with 14 AZB. This allows us to fully embed central 4 AZB and study their orientations. Since this system was too large to be treated by first principles, we used semi-empirical PM7 method [210] to obtain the structures and energies of these larger clusters. PM7 includes parameters for weak interactions.

For the excited state calculations, we opted for the Complete Active Space SCF (CASSCF) method [211]. The active space of 10 electrons in 8 orbitals was used and state-averaging over the three lowest states was always performed. These states are: the ground state, and both the $n - \pi^*$ and $\pi - \pi^*$ excited states. The active space includes the lowest π, π^* orbital pairs together with the two possible combinations of the nitrogen lone pairs. The dynamic electron correlation was accounted by multistate perturbation theory (CASPT2) [212]. To avoid intruder state problems the default value of IPEA (ionization energy, electron affinity) shift 0.25 au was introduced. Due to the size of the system, the multi-reference calculation was performed on the central AZB and all neighboring molecules were represented as a point charges. In these CASSCF and CASPT2 calculations the ANO-S-DZVP basis set was applied. All CAS calculations were performed with the OpenMolCas package [213].

Larger system of several *trans* monomers is needed for calculating exciton coupling effects. To this end we used geometry of the system with 14 AZB (see above) and ωB97X-D functional [181] in combination with 6-31G(d) basis set. From the 42 converged excited states, the lowest 14 correspond to the n-π^* states, the next 14 to the $\pi - \pi^*$ transitions. The n-π^* states are localized on individual AZBs, while $\pi - \pi^*$ states are linear combinations of excitations on different monomers.

Ground state characterization. We started by calculating the relative energies of the different motifs in the ground electronic state. The DFT calculations clearly show a preference for two neighboring *cis* isomers compared to two separated *cis* isomers. As can be seen in the graph below (Figure 9.6), one would expect by simple addition that a central+peripheral *cis* block to be 41.5+49.8=91.3 kJ.mol^{-1} less stable than the all-*trans* cell in the ground electronic state. However, when two *cis* isomers are close, the structure is relatively stabilized by 83.5-91.3 = -7.8 kJ.mol^{-1}. In contrast, when the two *cis* isomers do not interact directly, the cooperative effect is much smaller, with 97.2-2x49.8=-2.4 kJ.mol^{-1}. Although these are relative total energies for

the final photochromic states, this simulation shows a thermodynamic preference for the clustering of *cis* AZB, hinting that if they are formed, there is no thermodynamic reason that would make them unstable. In addition, in contrast to the all-*trans* cell in which the rotation of the monomers is unhindered at room temperature, two neighboring *cis* isomers cannot rotate freely. In fact, one can build two different relative orientations for the cell with two neighboring *cis* AZB: the first with parallel orientation of both *cis* and the second being the anti-parallel counterpart. Irrespective of these orientations, the cell with the neighboring *cis* isomers is stabilized by stronger dispersion interactions with the neighboring *trans* dyes (as compared to the all-*trans* case), with short contacts of less than 0.3 nm. This qualitatively explains the stabilization of -7.8 kJ.mol^{-1}.

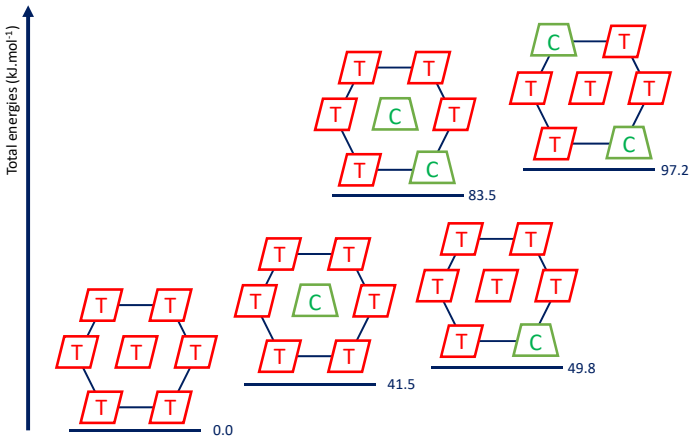

Figure 9.6: Relative energies of various clusters of *cis* and *trans* AZB.

In addition, we have considered the thermal inversion, which is the usually preferred ground state isomerization mechanism. The barrier for the *trans* to *cis* reaction is 179 kJ.mol^{-1} and does not depend on nature (*cis* or *trans*) of the surrounding molecules. The barrier for the thermal backreaction, relevant for our purposes, is of course smaller. In the case of the vicinal *cis* motif (2 in Figure 9.7), the barrier reaches 137 kJ.mol^{-1} which is larger than the one computed when only one central *cis* isomer back-transforms (131

kJ.mol^{-1}, case 1 on the same figure). These barriers indicate that the back reaction will likely be slow in all cases, especially with vicinal *cis* isomers.

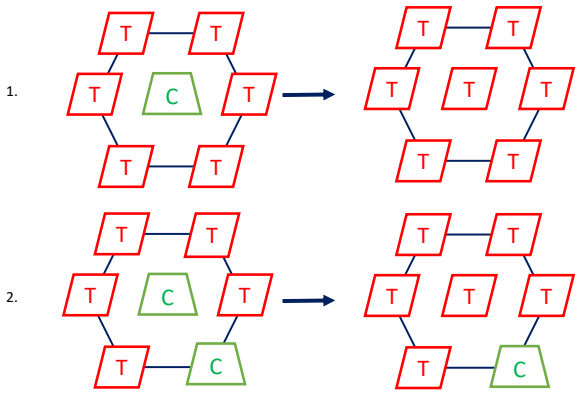

Figure 9.7: Ground state reactions studied at the DFT level.

Interaction energy decomposition. The interaction energies between separate monomers in their ground electronic state are small, as a logical consequence of their large separation. We performed a decomposition of the interaction energy in order to gain more insights into its origins. The dimers for respective calculations were extracted from the cell with 5 *trans* and 2 vicinal *cis* monomers (Figure 9.8). Our results are summarized in the Table 9.2. The *cis*/*trans* interaction is stronger due to both electrostatics (e.g., point charges, dipole-dipole) and dispersion effects. The cell was dominated by *cis*/*trans* interactions so the *cis*/*cis* interactions generate only a small portion of interaction energy. The antiparallel *cis*/*cis* arrangement is dominated by dispersion.

The calculations above imply an interaction of the *cis* with a neighboring *trans* isomer, which likely depends on the conformations of the two molecules. Because of the rigid nature of **1**, the conformational degrees of freedom of *trans* and *cis* isomers in the SAM are largely limited to rotations of the molecules around their principal axis. The resulting changes in conformation are insignificant for the *trans* isomers, whereas rotation of the *cis* isomers can lead to larger variations in the position relative to neighbor-

Motif	Total interaction	Electrostatics	Exchange repulsion	Induction	Dispersion
Two *trans* face-face	0.3	0.4	0.0	0.0	-0.1
Two *trans* face-side	-0.2	0.0	0.0	0.0	-0.1
Two *cis* parallel	0.2	0.4	0.0	0.0	-0.2
Two *cis* antiparallel	-0.3	0.1	0.0	0.0	-0.4
cis-trans	-5.3	-3.2	7.9	-1.3	-8.7

Table 9.2: Ground state interaction energy between different motifs decomposed at SAPT0/cc-pVDZ level of theory. All values are in kJ.mol^{-1}.

ing molecules and hence different intermolecular interactions. To further investigate this aspect, we performed additional PM7 relaxed geometrical scans, in which the rotational orientation of the *cis* isomer was varied. We find that the energy is minimal when the *cis* isomer is oriented towards one of the neighboring *trans* isomers and that the barrier for rotation to the next trans isomer is 5 kJ/mol, i.e., roughly twice of the thermal energy at room temperature. From a statistical point of view, the existence of an energetical minimum implies that the system will spend a larger portion of time in such arrangement, compared to other conformations (although rotation from one minimum to another is possible). Even though other arrangements are possible, the system will have a higher probability to be in this energetically most probable situation. We thus employ this geometry in our subsequent excited state calculations.

Excited state calculations. Let us now turn to the excited states. The experimental setup required irradiation of the surface for several minutes with 365 nm photons. Several previous studies have shown that the photodynamics of azobenzene is complex, but the main reactive channel follows excited states cascade $S_2 \rightarrow S_1 \rightarrow S_0$, i.e., the initially populated $\pi - \pi^*$ excited state decays into the lowest n-π^* excited state of AZB that actually performs the photochemical reaction [214, 215]. Therefore, we considered photoreactions following this process here. We have performed calculations starting from the Franck-Condon region of the differently arranged cells (see Figures 9.8 and 9.9):

1. 1 central *trans* + 6 peripheral *trans* → 1 central *cis* + 6 peripheral *trans*
2. 1 central *trans* + 1 peripheral *cis* + 5 peripheral *trans* → 1 central *cis* + 5 peripheral *trans* + 1 peripheral *cis*

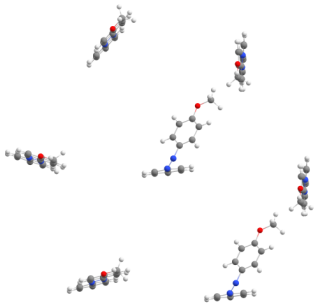

Figure 9.8: The cell consisting of two vicinal *cis* and 5 *trans* AZB isomers.

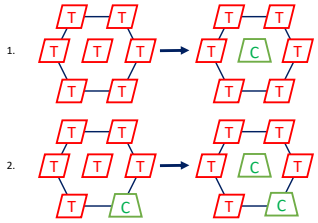

Figure 9.9: Schematic depiction of the studied photochemical reactions.

First, we have found that independently on the surrounding molecular environment the rotation around C-N=N-C dihedral angle is barrierless in the excited state and therefore can lead to the conical intersection directly. Nevertheless, it is worth to underline that this pathway is not systematically followed because other (larger) gradients are present at the FC point. These larger gradients may yield to a shallow excited state minimum corresponding to the inversion movement. For the photochemical reaction 1 of Figure 9.9 we observe that the switching *trans* AZB reached this local minimum while for 2 the system follows a direct path towards the conical intersection (see Fig. 9.10). In order to judge if this is a direct effect of the embedding

environment or an indirect effect from a reorientation of the central *trans* AZB in the ground state, we performed a geometry optimization of single AZB molecule starting from the same geometry as in case 2, but without the embedding charges. This optimization followed the path towards the local minimum. This supports the fact that the surrounding molecules, through their charge distribution, can influence the preferred relaxation path in the excited state, in the present case, leading to *cis* clusters. We observed the same behavior for the larger cell consisting of 13 *trans* and one *cis* isomer (see Figure 9.12).

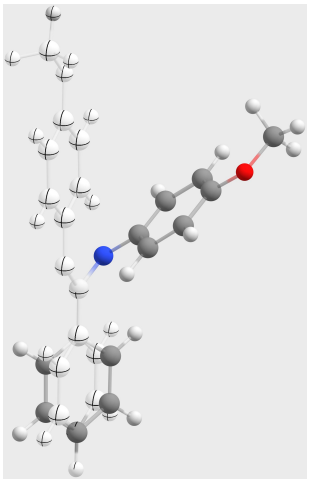

Figure 9.10: Overlay of the local minima structures reached on the excited state energy surface when the $n - \pi^*$ state is relaxed. White, crossed atoms depict structure optimized in all *trans* embedding. Standard color atoms show the structure optimized in the embedding with on *cis* isomer included. Note that the bent CNNC angle implies proximity of the ground state surface.

On top of these CAS calculations performed on the minimal possible cell, we have also performed excited state calculations with TD-DFT theory on a larger cell containing 14 AZB (see Figure 9.11). The localization of n-π^* states was studied for this model, considering one *cis* isomer and 13 *trans* (see Figure 9.11b). In this latter arrangement, the highest - in energy - n-π^* state is localized on one of the *trans* isomer interacting with the already switched *cis* (though by a small margin). The excitation energies and oscillator strengths of first 28 states of this system are summarized

in the Table 9.3 and the electron density difference for the highest excited state from the $n - \pi^*$ manifold is depicted in Figure 9.12. Therefore the initial energy accumulated in the $\pi - \pi^*$ state is preferably funneled to the (closest in energy) n-π^* state localized on the *trans* system vicinal to the *cis*, consistent with the formation of *cis* clusters.

$n - \pi^*$	f	$\pi - \pi^*$	f
2.6092	0.0243	4.0135	0.0110
2.6356	0.0000	4.0159	0.0287
2.6358	0.0001	4.0187	0.0043
2.6362	0.0001	4.0217	0.0096
2.6367	0.0000	4.0245	0.0265
2.6393	0.0008	4.0312	0.0293
2.6407	0.0011	4.0358	0.1177
2.6408	0.0009	4.0377	0.0404
2.6411	0.0014	4.0474	0.0361
2.6415	0.0008	4.0542	0.0062
2.6420	0.0016	4.0706	0.2603
2.6423	0.0013	4.0822	0.5067
2.6443	0.0017	4.1102	10.3514
2.6668	0.0002	4.6434	0.3108

Table 9.3: Excitation energies (in eV) and oscillator strengths f of the lowest 28 states of the model system consisting of 13 *trans* isomers and one *cis*. In bold the highest $n - \pi^*$ and the most intense $pi - \pi^*$ state.

Up to now, we treated the whole slab (modelled as several azobenzenes) as one supersystem. In such an approach, the cross sections (TD-DFT oscillator strengths) of individual molecules are inaccessible as $\pi - \pi^*$ states are delocalized. The $n - \pi^*$ states are localized on individual molecules, but the experimental setup uses $\pi - \pi^*$ excitation (365 nm). To determine if the magnitude of the oscillator of the $\pi - \pi^*$ transition depends on the nature of the neighbouring photochromes, we used a different description of our system: we treated a central *trans* azobenzene molecule at TD-DFT level and modelled all the rest via molecular mechanics (we used MM charges to embed TD-DFT). With this strategy we can access the oscillator strengths of all transitions on the central molecule, but are neglecting the quantum mechanical interactions between the photochromes. Interestingly, we found that even at this simple level of theory, the energy levels follow the ordering we

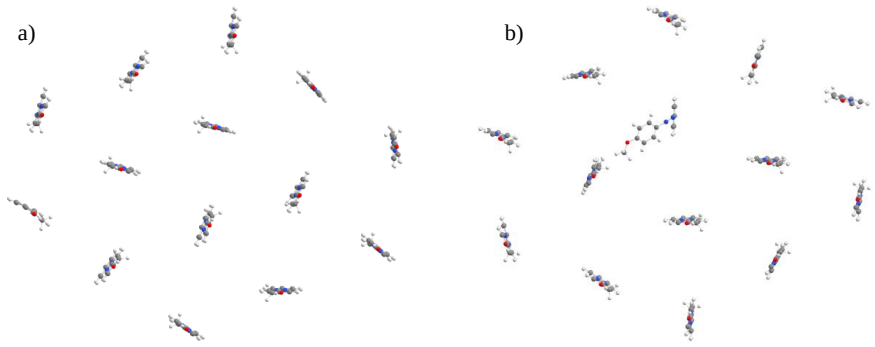

Figure 9.11: Large model system consisting of 14 photochromes: a) 14 *trans* isomers; b) 13 *trans* isomers and one *cis*. View from above.

outlined above, i.e., the localization of the exciton on the *trans* azobenzene which is interacting with the *cis* azobenzene. This calculation also showed that the oscillator strengths of individual *trans* molecules that do not interact with a *cis* photochrome are slightly larger than in *trans* molecules directly interacting with a *cis* photochrome. However, the difference is less than 1.5% for all *trans* molecules and therefore not significant, considering the compromises made in the methodology to be able to compute the oscillator strengths of a single molecule. Thus, the cross sections differences between different *trans* molecules is not large enough to explain the observed effects.

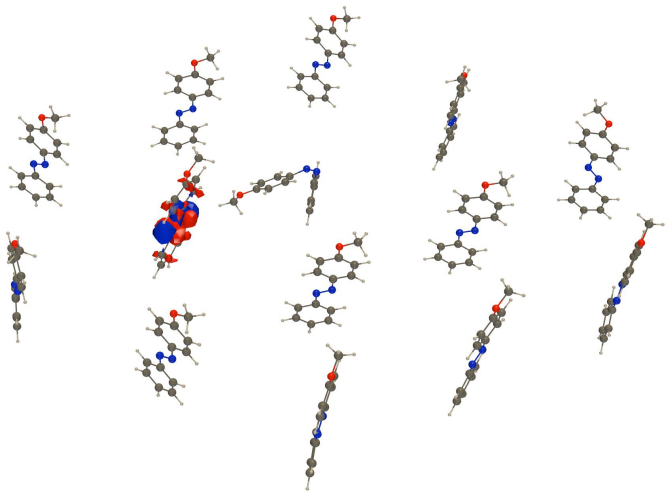

Figure 9.12: Electron density difference ($\rho^{ES} - \rho^{GS}$) determined on the Franck–Condon geometry for the highest n-π^* state. View from above.

9.2 Molecular Platforms as Versatile Building Blocks for Multifunctional Photoswitchable Surfaces

Synthesis of the Compounds

Synthesis of 4-trimethylsilylethinylpyridine [216]

1.00 g (5.14 mmol) 4-bromopyridine hydrochloride was solved under nitrogen atmosphere in 30 mL triethylamine and 30 mL THF. 300 mg (0.26 mmol) (bis(triphenylphosphine)-palladium(II)-chloride and 40 mg (0.22 mmol) copper(I)iodid were added to this solution. To this suspension were dropped 0.80 mL (5.66 mmol) trimethylsilylacetylene and stirred under reflux for 15 h. The solid was removed and the solvent was evaporated. The crude product was purified by column chromatography (cyclohexane/ethylacetate, 4:1). The product was obtained as light yellow oil (566 mg, 3.17 mmol, 62 %). ^{1}H-NMR (500.1 MHz, acetone-d_6, 300 K, acetone) δ = 8.58 (d, ^{3}J = 4.3 Hz, 2H), 7.37 (d, ^{3}J = 4.3 Hz, 2H), 0.26 (s, 9H) ppm.

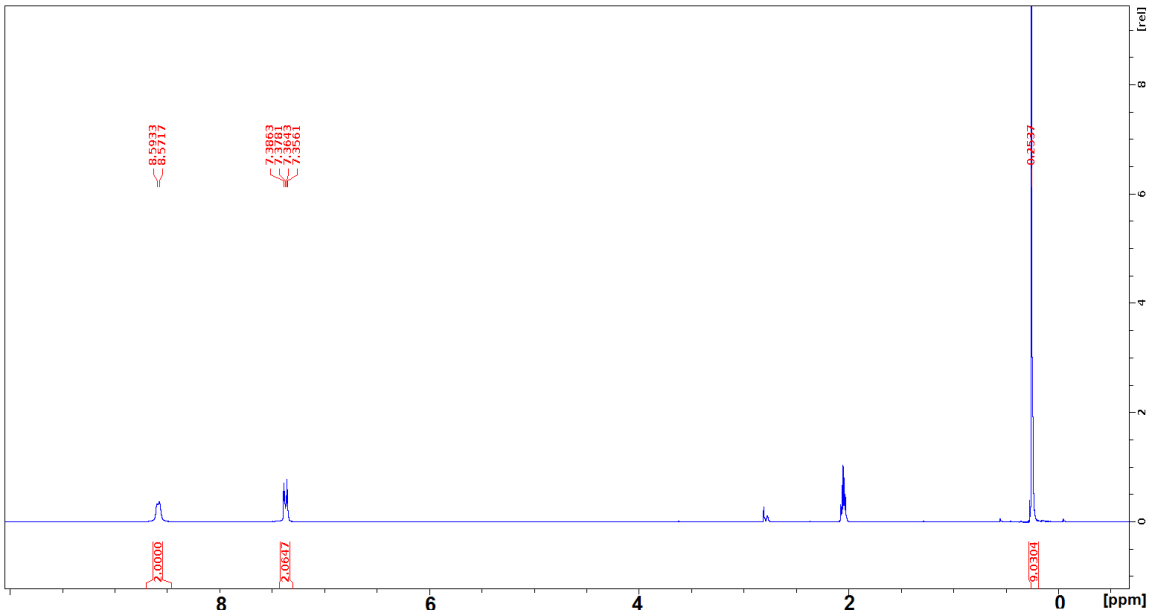

Figure 9.13: ^{1}H-NMR spectrum of 4-trimethylsilylethinylpyridine.

Synthesis of 12-(4(pyridine)ethinyl-4,8,12-tri-*n*-octyl-4,8,12-triazatriangulene Under nitrogen atmosphere 566 mg (3.17 mmol) 4-trimethylsilylethinylpyridine and 2.24 g (3.17 mmol) 4,8,12-tris-*n*-octyl-4,8,12-triazatriangulenium tetrafluorborat were suspended in 50 mL THF. To this suspension were added 1.24 g (22.2 mmol) fine powerded potassium hydroxide. The suspension was heated for 15 h under reflux. Afterwards the solution was poured onto water. For better phase separation brine was added, the phases were separated, extracted with dietyhl ether and the organic phases were dried above magnesium sulfate. The solvent was evaporated and the obtained oil was purified by column chromatography (flurosil, diethyl ether) to obtain a red oil. The oil was solved in a minimum of diethylether, overlayed with pentane and stored for 3 d at $-18°$C. The product precipitates as light pink solid (1.49 g, 2.07 mmol, 65 %). ^{1}H-NMR (500.1 MHz, acetone-d_6, 300 K, acetone) δ = 8.37 (d, ^{3}J= 4.5 Hz, 2H), 7.21 (t, ^{3}J = 8.3 Hz, 3H), 6.96 (d, ^{3}J = 4.5 Hz, 2H), 6.67 (d, ^{3}J = 8.3 Hz, 6H), 4.00 (t, ^{3}J = 7.6 Hz, 6H), 1.83 (ps. qui.,6H), 1.49 (ps.quint. 6H), 1.37 (ps.qui., 6H),1.32-1.21 (m, 18H), 0.86 (t, ^{3}J = 6.9 Hz, 9 H) ppm. ^{13}C-NMR (125.1 MHz, acetone-d_6, 300 K, acetone) δ =150.49, 141.48, 132.08, 129.60, 126.01, 110.54, 106.19, 99.28, 82.07, 46.68, 32.57, 30.39, 30.23, 30.08, 30.05, 27.46, 26.76, 23.29, 14.35 ppm. **MS** (ESI): m/z = 722.5 $[M+H]^{+}$, 618.6 $[TATA]^{+}$

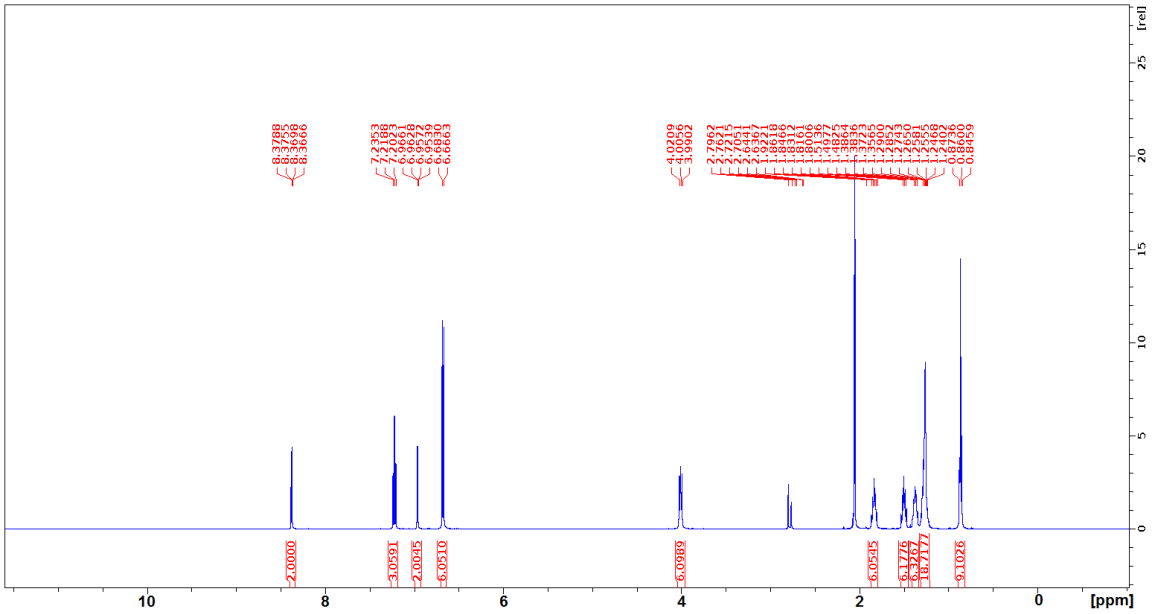

Figure 9.14: ^{1}H-NMR spectrum of 12-(4(pyridine)ethinyl-4,8,12-tri-n-octyl-4,8,12-triazatriangulene.

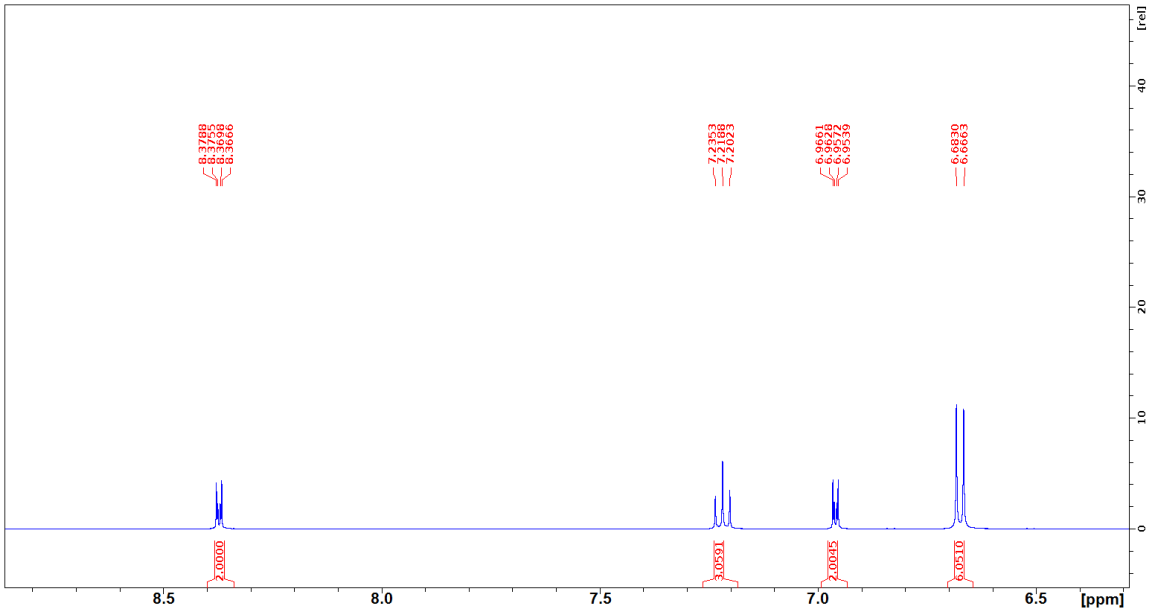

Figure 9.15: Aromatic region of ^{1}H-NMR spectrum of 12-(4(pyridine)ethinyl-4,8,12-tri-n-octyl-4,8,12-triazatriangulene.

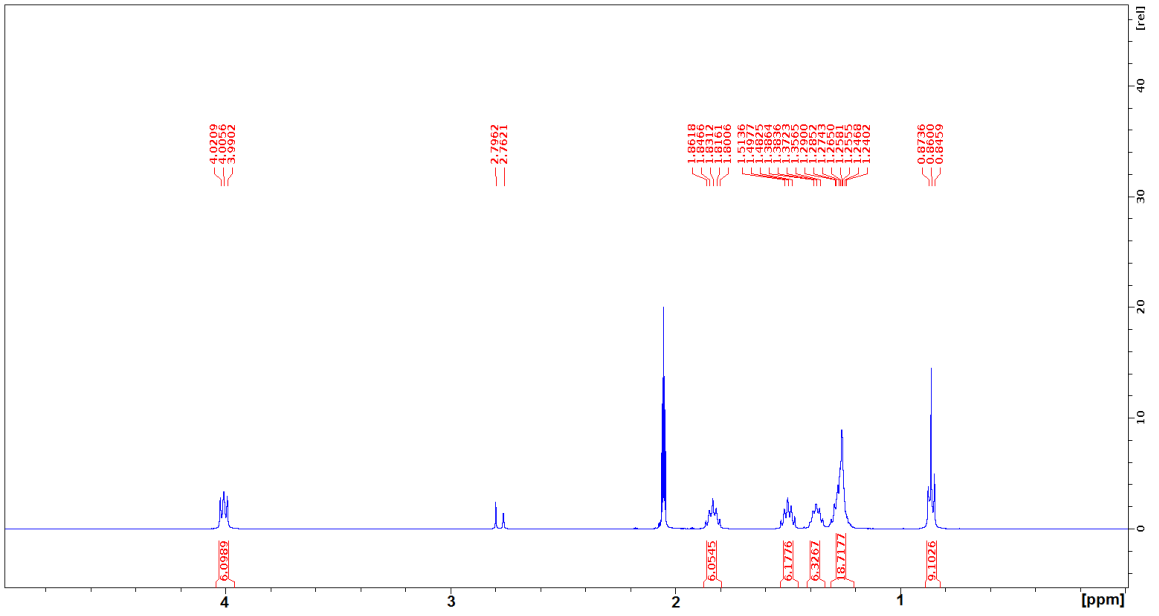

Figure 9.16: Aliphatic region of ^{1}H-NMR spectrum of 12-(4(pyridine)ethinyl-4,8,12-tri-n-octyl-4,8,12-triazatriangulene.

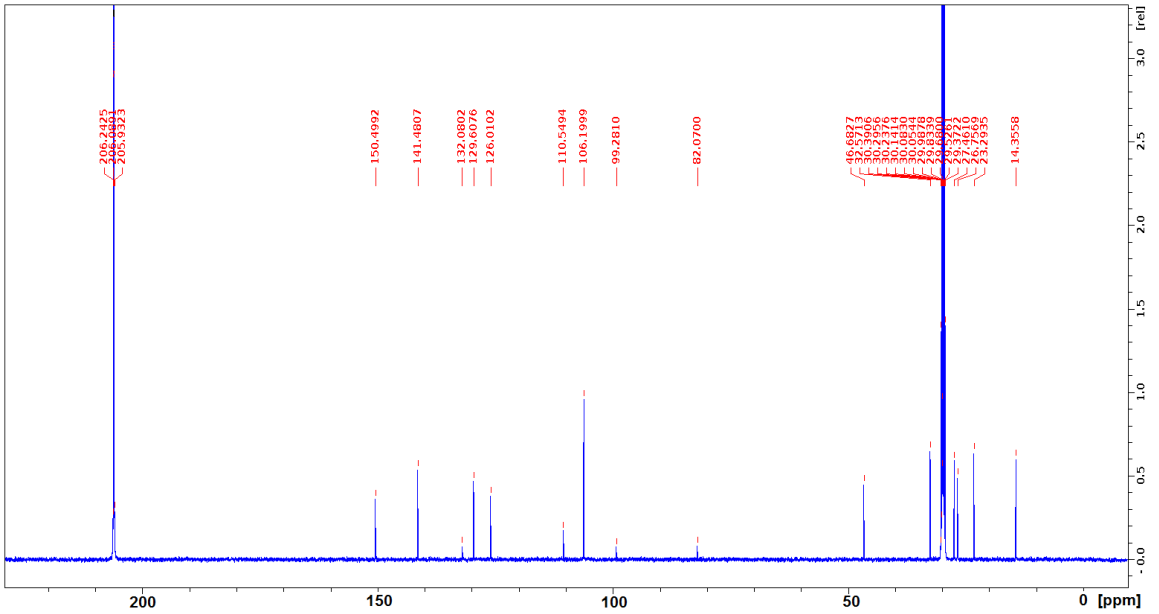

Figure 9.17: ^{13}C-NMR spectrum of 12-(4(pyridine)ethinyl-4,8,12-tri-n-octyl-4,8,12-triazatriangulene.

Sample Preparation

Au(111) single crystals with surface diameters of 10 mm, oriented within 0.3° (MaTeck) were used as substrates. The glassware used for the preparation of the SAMs was previously cleaned in piranha solution (1/3 hydrogen peroxide, 2/3 sulfuric acid). Directly before adlayer preparation, the substrates were flame annealed in butane gas. Then, the adsorbate layers were prepared by immersion in toluene solutions (3 ml) containing the respective compounds for 1 hour at temperatures between room temperature and 80 °C. These solutions were prepared by mixing 10 μM solutions of the pure compounds at the corresponding ratio. Afterwards, the samples were rinsed with pure toluene to remove excess molecules physisorbed on top of the SAM, dried under ambient conditions, and immediately afterwards mounted in the STM sample holder.

STM Measurements

STM studies were performed under ambient conditions with a PicoPlus STM (Agilent, Santa Clara, USA) and mechanically cut Pt/Ir (70:30) tips. The measurements were carried out in constant current mode at tunneling currents of 20 to 50 pA and bias voltages of 200 to 400 mV. The lattice constants and angles between rotational domains were analyzed using SPIP 6.7.6 (Image Metrology). STM images of highly oriented graphite were used for the in-plane calibration. Lateral drift was corrected with a dedicated software, developed by our group.

Quantitative Analysis of the STM Images

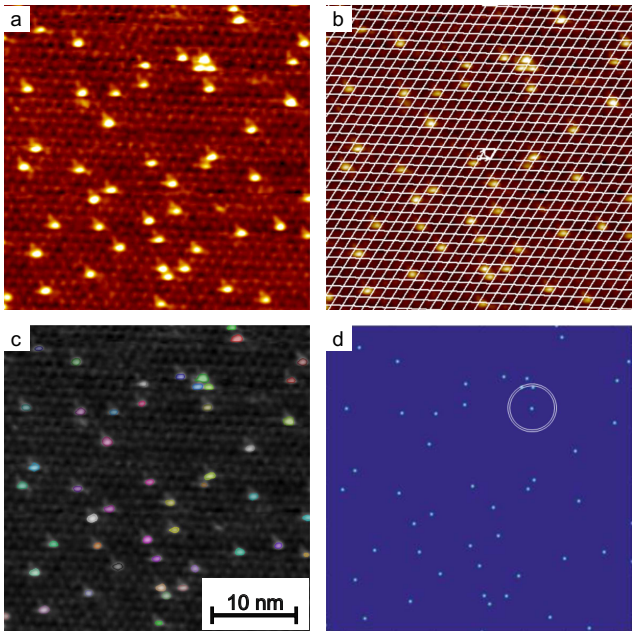

Figure 9.18: Evaluation steps for the analysis of the STM data of binary mixed adlayers on Au(111): (a) STM image after correction of lateral drift, (b) STM image with an overlaid lattice resulting from the fourier analysis, (c) detection of molecules obtained with SPIP (the colored circles show the detected molecules), (d) geometric centres of the in (c) detected molecules plotted with Matlab, the circular rings show exemplarily in which area the molecules were counted.

After the STM images had been corrected for lateral drift (Figure S5 a), the superstructure was determined using a fourier analysis (Figure S5 b).To determine the coverage ratio, one type of molecules was detected and counted by SPIP's particle analysis (Figure S5 c). The total number of adsorption sites could be concluded from the size of the image sections and the previously determined superstructure and thus the coverage could be calculated. The errors for the surface coverage were determined from the maximum deviation.

The Warren Cowley coefficient $\alpha(r)$ can be used as a measure of short-range order for binary mixed adlayers and was calculated as follows:

$$\alpha(r) = 1 - \frac{\rho_{1,i}(r)}{\theta_{1/2}} \tag{9.4}$$

Therein, $\rho_{1,i}(r)$ is the probability to find a molecule of type **2**, **3** or **4** in a defined distance to a molecule of type **1** and $\theta_{1/2}$ is the coverage ratio $\frac{\theta_1}{\theta_i}$ with i=2,3,4.

The Warren Cowley coefficients shown in Figure 3 and 9.21 show average values, obtained from 5 to 9 images respectively in the size range of 100 to 1600 nm^2, using Matlab and SPIP. The analysis was achieved by detecting the individual molecules on the STM images and calculating the geometric center. In order to determine the number of molecules of one type in the given distance to the other type, the relevant molecules were counted in the range of circular rings with a radius of the particular distance (1, $\sqrt{3}$, 2, $\sqrt{7}$, 3 nearest neighbour distances) and a width of 0.6 nm (see Figure S5 d). The errors plotted were calculated by error propagation using the standard deviation from the mean. For the calculation of the coverage ratio as well as for the Warren Cowley coefficients, only sections that do not show rotational domains or gold steps were selected, as these would falsify the calculations.

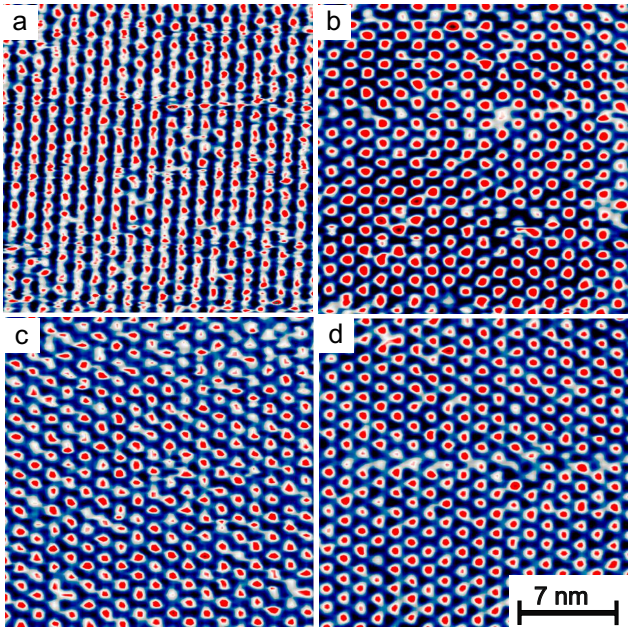

Figure 9.19: STM images (20 x 20) nm^2 of self-assembled monolayers of (a) **1**, (b) **2**, (c) **3** and (d) **4** on Au(111).

STM measurements reveal a hexagonally ordered superstructure with intermolecular distances of (1.27 $\pm$ 0.04) nm and rotational angles of 12° $\pm$ 2° for

adlayers of **3**. The lattice constant and the angle between different rotational domains are in agreement with a $(\sqrt{19} \times \sqrt{19})$ $R23.4°$ superstructure.

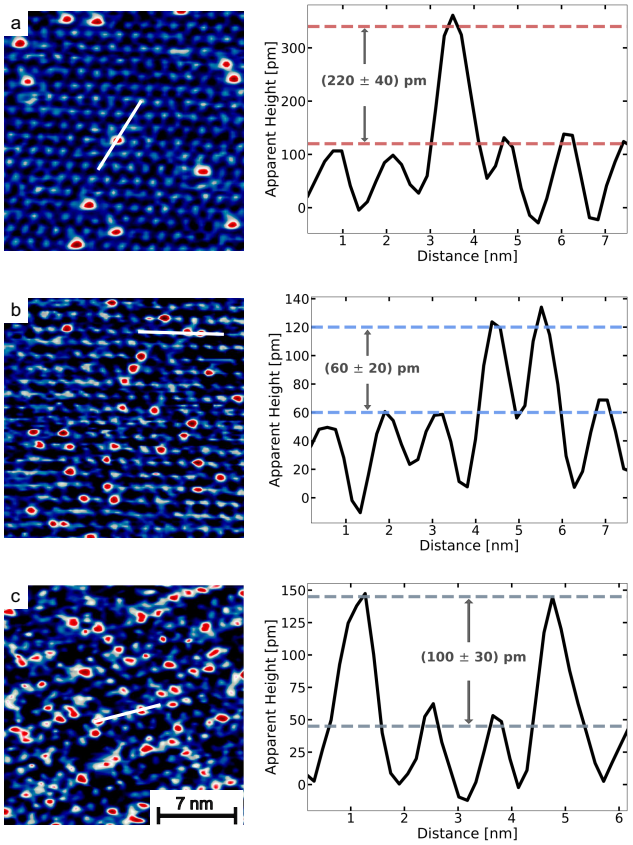

Figure 9.20: STM images of self-assembled monolayers on Au(111) prepared by coadsorption of (a) 9.8 μM **1** and 0.2 μM **2** solution, (b) 5 μM **1** and 5 μM **3** solution and (c) 5 μM **1** and 5 μM **4** solution (all images sections are 20 $\times$ 20 nm^2 large). The drawn white lines indicate where the crossections are, which are shown on the right. The dashed lines show average values for the different apparent heights from which the difference in apparent height was determined.

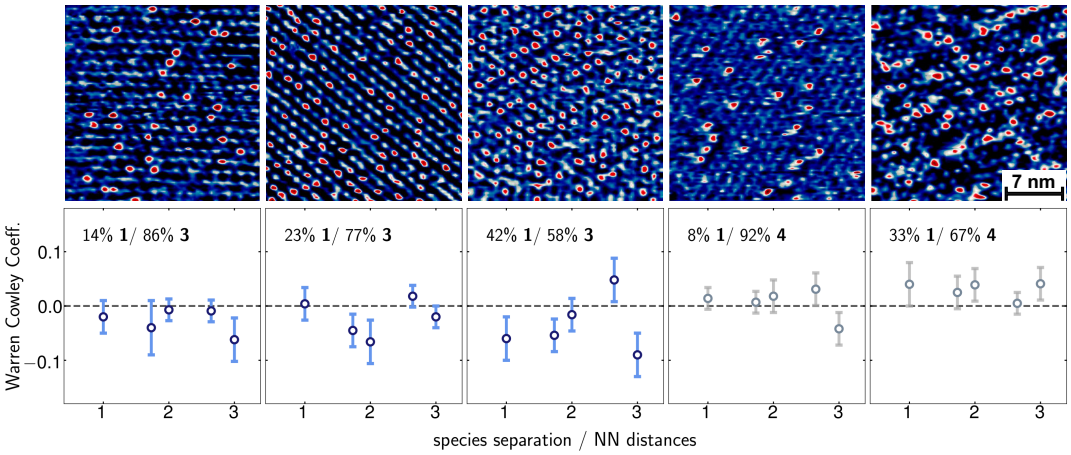

Figure 9.21: Top: Exemplary STM images of three different compositions of mixed monolayers consisting of **1** and **3** (image 1 to 3 from left to right) and two compositions of mixed monolayers consisting of **1** and **4** (image 4 and 5 from left to right), recorded at V = 0.3 V, I = 20 pA up to 50 pA, (20 x 20) nm^2. Bottom: Warren Cowley coefficients for different surface compositions and distances. The circles represent the coefficients calculated from the STM data and the error bars show the statistical scattering. The dashed line illustrates the value expected for a random distribution.

9.3 Ordered Adlayers of a Combined Lateral Switch and Rotor

Method	Source	θ in nm^{-2}
STM	Counted molecules	0.36 ± 0.02
UV/Vis	Absolut spectrum	0.79 ± 0.03
UV/Vis	Difference π-π^* band	0.37 ± 0.04
XPS	N 1s signal	0.45 ± 0.03
XPS	C 1s signal	0.32 ± 0.05
Theoretical	calculated from ideal $(\sqrt{31} \times \sqrt{31})$ $R8.9°$ superstructure (1 molecule per unit cell)	0.45
Theoretical	calculated from ideal $(\sqrt{31} \times \sqrt{31})$ $R8.9°$ superstructure (0.5 molecules per unit cell)	0.23

Table 9.4: Surface coverage of samples prepared after **(c)** determined by STM, UV/Vis spectroscopy, XPS and theoretically calculated.

STM

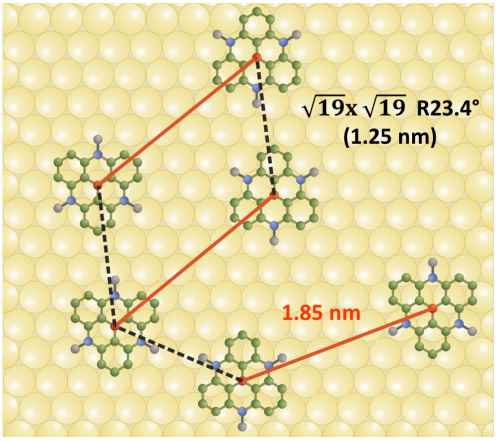

Figure 9.22: Model of the adsorbed molecules **1** in disordered areas (samples of type I). The red lines represent the vertical phenyl-azobenzene-phenyl units between the TATA platforms with an intramolecular distance of 1.85 nm. The dashed black lines indicate the distance corresponding to a $\sqrt{19} \times \sqrt{19}$) $R23.4°$ with an intermolecular distance of 1.25 nm

XPS

Compound	Transition	Excitation energy	Scans	Intensity	IPS	ratio
1	N 1s	500 eV	16	64000	4000	0.00079
1	Au 4f	500 eV	3	15253000	5084333	0.00079
1	C 1s	350 eV	5	1771000	354200	0.16877
1	Au 4f	350 eV	3	6296000	2098667	0.16877
2	N 1s	500 eV	10	63000	6300	0.00080
2	Au 4f	500 eV	3	23740000	7913333	0.00080
2	C 1s	350 eV	5	2007000	401400	0.11931
2	Au 4f	350 eV	3	10092000	3364333	0.11931

Table 9.5: Results obtained from quantitative XPS measurements.

Type	Measured Ratio **2**	Theoretical Ratio for **1** with 1 mol. per unit cell	Theoretical Ratio for **1** with 1/2 mol. per unit cell	Measured Ratio **1**
N 1s/Au 4f	0.00080	0.00079	0.00039	0.00079
C 1s/Au 4f	0.11931	0.14650	0.07320	0.16879

Table 9.6: Comparison of theoretical and experimental N 1s/ Au 4f and C 1s/ Au 4f ratios.

Component	Signal	Binding Energy (eV)	Area (%)	fwhm
TATA	N 1s	399.4	72.6	1.1
Azo	N 1s	399.9	27.4	1.1
Major Comp.	C 1s	284.6	82.8	1.3
Minor Comp.	C 1s	285.7	17.2	1.5

Table 9.7: Fitting parameters for XPS data

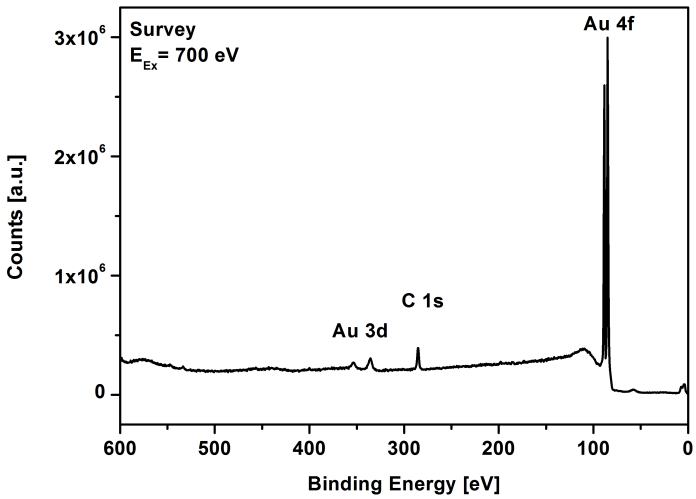

Figure 9.23: XP spectra of the **1** monolayer on Au(111) showing the survey recorded at a photon energy of hν = 700 eV.

NEXAFS

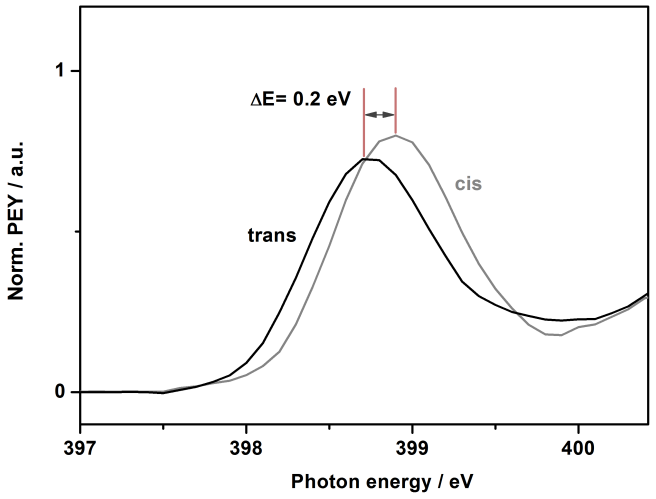

Figure 9.24: N 1s NEXAFS spectra of the LUMO resonance of the azo moiety after irradiation with light of 365 nm (grey) and after irradiation with light of 440 nm (black).

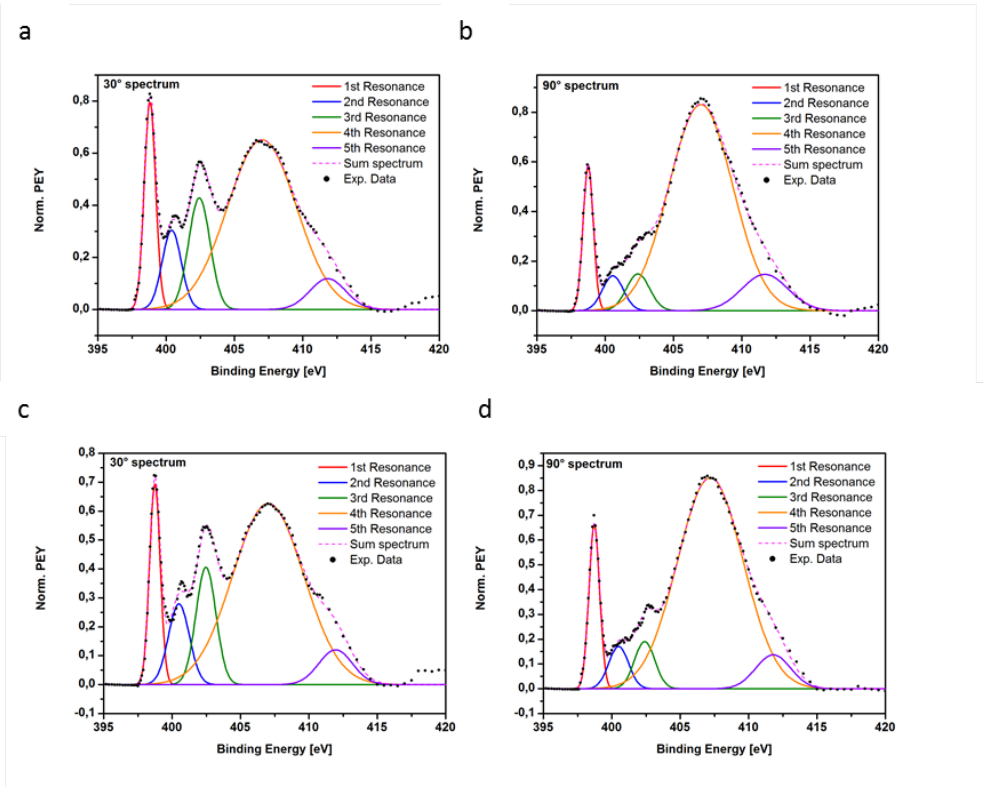

Figure 9.25: N-NEXAFS spectra (a and b *cis*, c and d *trans*) fitted with Gaussians to determine the intensity of the resonances. The spectra were baseline-substracted and afterwards fitted like described in the experimental section.

Computational Details

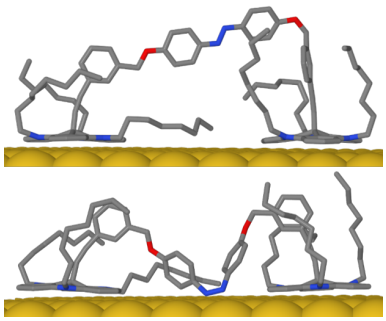

Figure 9.26: Local energy minima of *trans* (top) and *cis* isomer (bottom) conducted with the semiempiric approach.

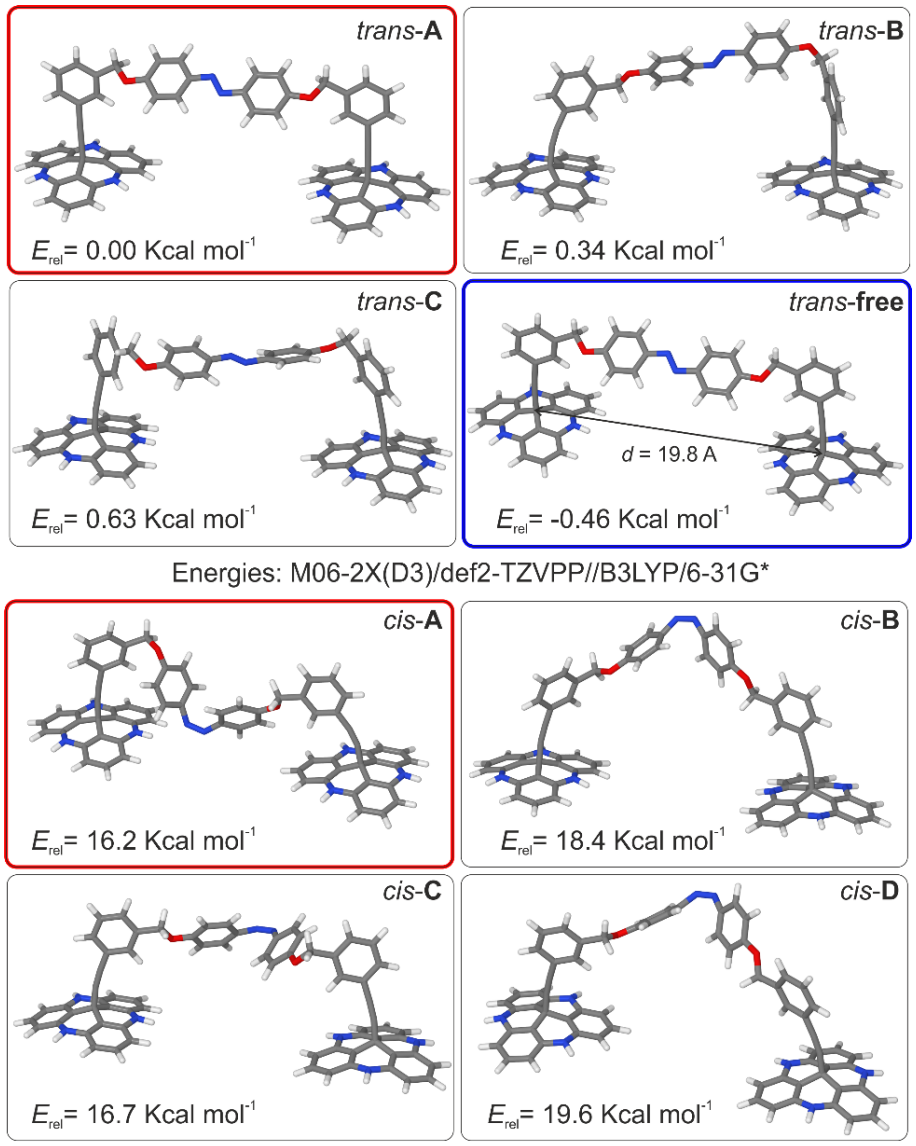

Figure 9.27: Local energy minima of 3 nearly isoenergetic *trans* isomers (top) and 4 *cis* isomers (bottom) with an intramolecular distance of 18.5 *Å*. Each most stable isomer is marked red. Additionally the most stable *trans* isomer was reoptimized without the constraint of intramolecular distance, yielding an also isoenergetic structure (marked blue) with a distance of 19.8 *Å*.

XYZ Coordinates 2nd approach

trans-**A**

$E_{M06\text{-}2X(D3)/def2\text{-}TZVPP}$ = -3206.059330528 Hartree

C	-9.2754571	1.8997519	-0.3944093	H	7.0861929	2.0482319	-0.3024893	H	-7.0099071	-2.9102381	4.1217507
C	-10.4880471	2.6169919	-0.4475393	H	11.2704329	4.6446219	-0.8764693	H	-5.9427171	-2.7965281	1.9588507
C	-8.0658671	2.6054719	-0.5048793	H	9.0816429	5.8144219	-0.8480193	C	-9.2419771	-0.7266181	-0.1090893
C	-8.0543971	3.9939919	-0.6590493	H	6.0285629	4.3819919	-1.5038893	C	-9.2674271	0.4799619	-0.2378093
C	-10.4766271	3.9994119	-0.6008193	H	6.7020729	5.7803819	-0.6394393	C	8.4108129	-2.8646181	4.1505807
C	-9.2656071	4.6897619	-0.7021693	H	4.2525529	5.6687719	-1.1832993	C	9.7393629	-2.7670081	3.7400407
C	-6.7362671	4.7127019	-0.8134993	H	1.7819029	5.7125619	-1.0093193	C	10.0224129	-2.5964381	2.3767707
O	-5.8887871	4.3400519	0.2773607	H	1.9544729	3.3492719	2.5540307	C	8.9763129	-2.5094181	1.4492407
C	-4.5517471	4.5809619	0.1909707	H	4.4608829	3.2693919	2.3836607	C	7.6489329	-2.6576381	1.8718907
C	-3.9350671	5.3371019	-0.8137093	C	-12.8323371	-3.5754981	-1.8436993	C	7.3610429	-2.8280281	3.2342207
C	-2.5463971	5.4696919	-0.8115893	C	-12.8455071	-3.2943481	-0.4784393	H	8.1895229	-2.9933081	5.2066607
C	-1.7621571	4.8691219	0.1786907	C	-11.6532071	-2.9057881	0.1506607	H	10.5488129	-2.8235781	4.4633507
C	-2.3974371	4.1384619	1.2042207	C	-10.4734271	-2.7878481	-0.5954593	N	11.3368029	-2.5153581	1.9095407
C	-3.7715971	3.9985519	1.2093807	C	-10.4664471	-3.1219781	-1.9558693	C	9.2757029	-2.1604581	-0.0009693
N	-0.3650771	5.0187219	0.0417707	C	-11.6564171	-3.5106381	-2.5892693	N	6.6362729	-2.6375781	0.9092407
H	-11.4262071	2.0771519	-0.3653193	H	-13.7555771	-3.8736681	-2.3332593	H	6.3312329	-2.9319781	3.5661907
H	-7.1291871	2.0593219	-0.4582693	H	-13.7648271	-3.3760881	0.0958307	C	8.2117629	-2.7670181	-0.9031293
H	-11.4150371	4.5462219	-0.6350593	N	-11.6065571	-2.6331681	1.5202807	C	6.8991529	-2.9115581	-0.4353993
H	-9.2641871	5.7716319	-0.8124393	C	-9.2241771	-2.2048481	0.0481907	C	5.8847129	-3.3299081	-1.3095093
H	-6.8804971	5.8016719	-0.8264593	N	-9.2560371	-3.0633981	-2.6509093	C	6.2061129	-3.6147481	-2.6356493
H	-6.2540671	4.4250119	-1.7583493	H	-11.6561971	-3.7595881	-3.6473693	C	7.5159329	-3.5224881	-3.1035393
H	-4.5183971	5.8160619	-1.5917793	C	-7.9867271	-2.7741781	-0.6285493	C	8.5269329	-3.1031081	-2.2260493
H	-2.0446171	6.0366319	-1.5901093	C	-8.0276671	-3.1141281	-1.9869793	C	10.6436329	-2.7034481	-0.3857293
H	-1.7853271	3.6781419	1.9715307	C	-6.8534871	-3.5024381	-2.6492193	C	11.6580929	-2.7853781	0.5769607
H	-4.2798071	3.4265519	1.9797207	C	-5.6584271	-3.5613581	-1.9341493	C	12.9612429	-3.1378381	0.1949907
C	9.2317729	1.9440919	-0.4420193	C	-5.6105071	-3.2723381	-0.5714093	C	13.2229329	-3.4205581	-1.1446593
C	10.4152429	2.6921019	-0.6071393	C	-6.7872871	-2.8848181	0.0868007	C	12.2137329	-3.3915281	-2.1057493
C	7.9996929	2.6187019	-0.4360493	C	-9.2026571	-2.5519681	1.5294307	C	10.9121229	-3.0383781	-1.7192093
C	7.9377529	4.0062719	-0.5850593	C	-10.4064171	-2.6768881	2.2349807	N	9.8594229	-3.0163981	-2.6373493
C	10.3537529	4.0738219	-0.7554293	C	-10.3897371	-2.8479781	3.6271907	H	12.0650529	-2.6853681	2.5894007
C	9.1211729	4.7329619	-0.7408593	C	-9.1644571	-2.9082181	4.2891207	H	5.7033929	-2.8487481	1.2357807
C	6.5911629	4.6878919	-0.6110293	C	-7.9578371	-2.8344281	3.5952207	H	4.8632829	-3.4322281	-0.9520493
O	5.8658129	4.2957019	0.5588607	C	-7.9794171	-2.6638581	2.2029407	H	5.4211229	-3.9363781	-3.3147893
C	4.5114829	4.4357619	0.5839207	N	-6.7995371	-2.6093381	1.4565407	H	7.7558729	-3.7740181	-4.1334593
C	3.7617229	5.1469719	-0.3691193	H	-12.4472371	-2.8315581	2.0451107	H	13.7527729	-3.1916781	0.9380707
C	2.3749129	5.1831519	-0.2715693	H	-9.2669771	-3.4124281	-3.5993393	H	14.2322729	-3.6913381	-1.4427693
C	1.7149029	4.5237119	0.7772107	H	-6.8805871	-3.7567381	-3.7056993	H	12.4273029	-3.6412681	-3.1418893
C	2.4784429	3.8494019	1.7450607	H	-4.7473571	-3.8591581	-2.4461393	H	10.0657529	-3.3623181	-3.5642893
C	3.8600829	3.8034119	1.6545107	H	-4.6762871	-3.3479181	-0.0209093	C	9.2727129	-0.6823781	-0.1601793
N	0.3156929	4.4409019	0.9371107	H	-11.3226871	-2.9342881	4.1783107	C	9.2698929	0.5244519	-0.2888393
H	11.3706429	2.1767919	-0.6147593	H	-9.1494971	-3.0371081	5.3680207				

trans-**B**

$E_{M06\text{-}2X(D3)/def2\text{-}TZVPP}$ = -3206.058788119 Hartree

C	-8.6701775	2.1760263	0.3540248	C	3.8042925	6.7743163	0.3067848	N	-7.1308975	-2.5311537	0.1476748
C	-9.3478275	3.3321763	0.7767248	C	5.1860125	6.8074063	0.1906448	H	-11.9953875	-2.7945537	3.0712348
C	-7.3263675	2.2916963	-0.0515452	N	1.6754625	5.7022763	0.0722048	H	-11.5587175	-1.9727437	-3.3686152
C	-6.6702275	3.5207363	-0.0547952	H	9.0412625	0.9420663	2.8592248	H	-9.4799975	-2.2312837	-4.5825052
C	-8.6877675	4.5608763	0.7848348	H	8.1650425	2.0259363	-1.2049152	H	-7.0405275	-2.6468937	-4.4336152
C	-7.3593575	4.6642963	0.3681248	H	8.9247125	3.3349363	3.5187748	H	-5.9115775	-2.8294137	-2.2336352
C	-5.2537975	3.5740863	-0.5737752	H	8.4267225	5.0738463	1.8149148	H	-10.1013375	-3.4284137	4.4313948
O	-4.4864275	4.5168463	0.1755548	H	7.6007425	4.3095863	-1.7668452	H	-7.6622175	-3.8680237	4.4991048
C	-3.1432075	4.5683663	-0.0532552	H	8.9774325	5.2160263	-1.1314952	H	-6.2441175	-3.4852737	2.5019348
C	-2.4628575	3.7633463	-0.9769952	H	5.6822325	3.6375963	-0.9850752	H	-6.1735275	-2.8542537	0.1716548
C	-1.0778175	3.8694363	-1.0861652	H	3.2162425	3.6291563	-0.8300652	C	-9.6327875	-0.2760137	0.2329648
C	-0.3549675	4.7816563	-0.3109152	H	3.2559625	7.6313263	0.6864048	C	-9.2686975	0.8791363	0.3213448
C	-1.0503775	5.6039363	0.5992048	H	5.7563225	7.6876063	0.4701248	C	8.9597425	-4.4386837	3.8437748
C	-2.4237275	5.4943363	0.7276548	C	-14.0418475	-2.6105637	-0.3301152	C	10.1137025	-4.2487737	3.0851948
N	1.0430925	4.7692763	-0.5004252	C	-13.4532975	-2.6524937	0.9326748	C	9.9983525	-3.7442737	1.7812448
H	-10.3816975	3.2580063	1.0993448	C	-12.0770675	-2.4087137	1.0545448	C	8.7375525	-3.4219937	1.2630748
H	-6.8031075	1.3927563	-0.3654752	C	-11.3145275	-2.1039037	-0.0807452	C	7.5840125	-3.6662537	2.0197448
H	-9.2161375	5.4499463	1.1186448	C	-11.9136775	-2.1070737	-1.3477552	C	7.6943725	-4.1705037	3.3242148
H	-6.8513675	5.6235363	0.3819648	C	-13.2894575	-2.3510937	-1.4743352	H	9.0469825	-4.8262237	4.8552548
H	-5.2370475	3.8645063	-1.6358452	H	-15.1073875	-2.8007637	-0.4264952	H	11.0919725	-4.4889437	3.4936448
H	-4.8007575	2.5774163	-0.4973652	H	-14.0470875	-2.8819637	1.8137548	N	11.1206825	-3.5555337	0.9703648
H	-2.9912075	3.0542363	-1.6023852	N	-11.4328475	-2.4785937	2.2931348	C	8.6268425	-2.7109737	-0.0778652
H	-0.5297575	3.2425563	-1.7832052	C	-9.8470775	-1.7393137	0.0640648	N	6.3396925	-3.4019537	1.4431948
H	-0.4881275	6.3092563	1.2013948	N	-11.1097375	-1.8795037	-2.4679552	H	6.8018125	-4.3501237	3.9180548
H	-2.9738875	6.1052363	1.4369948	H	-13.7564775	-2.3472137	-2.4558752	C	7.3009725	-3.0654837	-0.7352852
C	8.6164125	1.3241863	0.7810048	C	-9.0908375	-2.1478037	-1.1921352	C	6.1751825	-3.3215837	0.0585948
C	8.8314625	1.7071763	2.1184848	C	-9.7312875	-2.1036337	-2.4366752	C	4.9191725	-3.4984537	-0.5407052
C	8.3371025	2.3220763	-0.1730652	C	-8.9889975	-2.2803737	-3.6139852	C	4.8138725	-3.4328237	-1.9289652
C	8.2734825	3.6674663	0.1922648	C	-7.6179075	-2.5143637	-3.5225552	C	5.9324425	-3.2265337	-2.7348752
C	8.7632125	3.0494563	2.4827148	C	-6.9761275	-2.6163437	-2.2889952	C	7.1863225	-3.0505337	-2.1311252
C	8.4878525	4.0282163	1.5285548	C	-7.7221575	-2.4368537	-1.1146252	C	9.7744425	-3.1395537	-0.9795052
C	8.0315225	4.7388063	-0.8536652	C	-9.2569575	-2.4539237	1.2706148	C	11.0125725	-3.4835037	-0.4208852
O	7.2331125	5.8275163	-0.3828852	C	-10.0596475	-2.7226937	2.3862248	C	12.1072425	-3.7588937	-1.2539552
C	5.8768125	5.6858663	-0.2939352	C	-9.4828775	-3.2305037	3.5597048	C	11.9394025	-3.7052437	-2.6365652
C	5.1646125	4.5296163	-0.6530652	C	-8.1114075	-3.4778037	3.5898348	C	10.7028425	-3.4095737	-3.2078852
C	3.7781325	4.5145963	-0.5542052	C	-7.3076675	-3.2627937	2.4712948	C	9.6110225	-3.1350737	-2.3709352
C	3.0790425	5.6358963	-0.0804452	C	-7.8884575	-2.7528937	1.3008948	N	8.3431525	-2.8639137	-2.8936052

H	11.9980025	-3.9021837	1.3333048	H	5.8395125	-3.2048637	-3.8177052	H	8.2404925	-2.9759637	-3.8929652
H	5.5284725	-3.6824437	1.9766548	H	13.0706825	-4.0171737	-0.8219452	C	8.6703125	-1.2439337	0.1632448
H	4.0424025	-3.6861637	0.0737448	H	12.7864425	-3.9175437	-3.2833152	C	8.6529025	-0.0573137	0.4191148
H	3.8412225	-3.5666637	-2.3946952	H	10.5795125	-3.3977937	-4.2878352				

trans-**C**

$E_{M06\text{-}2X(D3)/def2\text{-}TZVPP}$ = -3206.058325100 Hartree

C	-8.6943899	2.0823093	-0.2561625	H	7.2738901	2.1196593	-1.3711325	H	-12.9612799	-3.1254107	2.5760975
C	-9.3420899	2.8559293	-1.2392525	H	9.5662801	4.7971093	2.1230375	H	-10.7257099	-2.7664407	3.3990075
C	-7.7758699	2.7066193	0.6094975	H	7.9400401	5.8813593	0.5988275	C	-9.1580599	-0.5139907	-0.0941625
C	-7.5004699	4.0702593	0.4946675	H	7.1703901	5.0817093	-2.3597725	C	-8.9529799	0.6810793	-0.1552725
C	-9.0652699	4.2145293	-1.3541225	H	6.1750601	5.6877693	-1.0280925	C	11.7632501	-3.1432607	-3.2306525
C	-8.1458599	4.8206593	-0.4963225	H	3.3997401	3.3843093	-3.2223425	C	10.3906201	-3.0132207	-3.4347625
C	-6.5853399	4.7734793	1.4791575	H	1.0925501	3.3272193	-2.2434125	C	9.5652001	-2.6874907	-2.3480625
O	-5.5325499	3.9679193	2.0139675	H	2.7054901	4.3616093	1.5847075	C	10.1248901	-2.4769407	-1.0805325
C	-4.3266899	3.9365193	1.3689775	H	5.0005601	4.4428693	0.6257875	C	11.5003101	-2.6554507	-0.8833825
C	-3.2206599	3.5922393	2.1673475	C	-7.6596399	-3.1548207	-3.8853225	C	12.3294101	-2.9806607	-1.9673125
C	-1.9472799	3.5607793	1.6248675	C	-9.0383499	-3.0052307	-3.7424925	H	12.4039101	-3.3949107	-4.0715625
C	-1.7509799	3.8583693	0.2622775	C	-9.5637199	-2.6946007	-2.4795725	H	9.9595701	-3.1683307	-4.4205025
C	-2.8628699	4.1603293	-0.5336125	C	-8.7057099	-2.5238407	-1.3862025	N	8.1804101	-2.5761607	-2.4935725
C	-4.1464699	4.2138293	0.0081475	C	-7.3273999	-2.7283907	-1.5351225	C	9.2470301	-2.0021707	0.0664875
N	-0.4966699	3.8713893	-0.3896325	C	-6.7973399	-3.0389207	-2.7963225	N	12.0134801	-2.5152507	0.4095175
H	-10.0506499	2.3764593	-1.9072025	H	-7.2498399	-3.3904907	-4.8637925	H	13.3981601	-3.1109507	-1.8175525
H	-7.2718299	2.1166593	1.3680075	H	-9.7008999	-3.1259007	-4.5957725	C	9.8157801	-2.4976707	1.3868575
H	-9.5611599	4.8044193	-2.1203425	N	-10.9392599	-2.5484607	-2.2766225	C	11.1984901	-2.6637207	1.5356575
H	-7.9317899	5.8829193	-0.5954325	C	-9.2524899	-1.9985807	-0.0666325	C	11.7370301	-2.9798407	2.7919575
H	-7.1616199	5.0747493	2.3619575	N	-6.5117999	-2.6175007	-0.4077325	C	10.8775001	-3.1447307	3.8769775
H	-6.1671899	5.6838493	1.0309575	H	-5.7271699	-3.1849007	-2.9183725	C	9.4956101	-3.0312407	3.7347275
H	-3.3923299	3.3709993	3.2163975	C	-8.3965699	-2.5127507	1.0812775	C	8.9614301	-2.7142407	2.4765975
H	-1.0853899	3.3174793	2.2364275	C	-7.0245899	-2.7207007	0.8867075	C	7.8339701	-2.5388107	-0.1148325
H	-2.6996299	4.3659593	-1.5873525	C	-6.2001599	-3.0273707	1.9795675	C	7.3159401	-2.7135607	-1.4041025
H	-4.9943199	4.4441693	-0.6272325	C	-6.7674599	-3.1362607	3.2481375	C	5.9578901	-3.0173407	-1.5789525
C	8.6961001	2.0800293	0.2530975	C	-8.1382599	-2.9819907	3.4492975	C	5.1437501	-3.1552207	-0.4557925
C	9.3446701	2.8507193	1.2379675	C	-8.9585599	-2.6755407	2.3534475	C	5.6564101	-3.0378607	0.8351275
C	7.7792101	2.7075493	-0.6119225	C	-10.6875099	-2.4659607	0.1150775	C	7.0149501	-2.7329807	1.0047575
C	7.5063601	4.0715293	-0.4950025	C	-11.5055099	-2.6688207	-1.0044525	N	7.5837901	-2.6135107	2.2747975
C	9.0699001	4.2095293	1.3553575	C	-12.8588999	-2.9978507	-0.8358225	H	7.8031901	-2.8213907	-3.3985625
C	8.1523001	4.8189093	0.4979075	C	-13.3681599	-3.1399507	0.4538675	H	12.9875101	-2.7570107	0.5302975
C	6.5928601	4.7783193	-1.4784825	C	-12.5572099	-2.9850307	1.5767875	H	12.8108801	-3.0984607	2.9119175
O	5.5399101	3.9753393	-2.0167625	C	-11.2040999	-2.6569207	1.4036075	H	11.2928401	-3.3880707	4.8512575
C	4.3335901	3.9424293	-1.3724325	N	-10.3413899	-2.5279607	2.4951175	H	8.8358101	-3.1896207	4.5839275
C	3.2277901	3.6016093	-2.1725225	H	-11.5335699	-2.7991207	-3.0548725	H	5.5487901	-3.1384907	-2.5787025
C	1.9542301	3.5682593	-1.6306625	H	-5.5372599	-2.8555407	-0.5289125	H	4.0897401	-3.3832907	-0.5893325
C	1.7575201	3.8606593	-0.2670425	H	-5.1332599	-3.1760707	1.8344375	H	5.0142501	-3.1744207	1.7014075
C	2.8691101	4.1598693	0.5302775	H	-6.1293799	-3.3688907	4.0964475	H	6.9938601	-2.8582307	3.0579075
C	4.1529101	4.2151293	-0.0107725	H	-8.5698299	-3.0960707	4.4403775	C	9.1521701	-0.5175307	0.0897375
N	0.5031201	3.8709393	0.3846575	H	-13.4964199	-3.1483307	-1.7033225	C	8.9516901	0.6783093	0.1508075
H	10.0522001	2.3689093	1.9053675	H	-14.4161799	-3.3948907	0.5863375				

trans-**free**

$E_{M06\text{-}2X(D3)/def2\text{-}TZVPP}$ = -3206.060070494 Hartree

C	9.6620019	2.0175336	0.1324547	C	-4.4455681	3.9665736	-0.4416953	C	6.7387219	-3.0632264	2.0101247
C	10.7881719	2.8593136	0.0371647	C	-3.6772881	4.7182036	0.4643447	C	7.5798019	-2.7562464	0.9301647
C	8.3924919	2.5987336	0.2934847	C	-2.2903081	4.7237436	0.3579247	C	9.2787719	-2.5650664	-1.3304253
C	8.2378819	3.9855636	0.3530147	C	-1.6473081	3.9897536	-0.6511353	C	10.1352919	-2.7523864	-2.4227653
C	10.6344119	4.2406836	0.0969347	C	-2.4281481	3.2603236	-1.5639053	C	9.6047419	-3.0269464	-3.6919353
C	9.3652719	4.8056236	0.2498647	C	-3.8099281	3.2461936	-1.4653753	C	8.2225319	-3.1263664	-3.8426853
C	6.8641419	4.5744336	0.5645047	N	-0.2506881	3.8953036	-0.8300653	C	7.3598919	-2.9909664	-2.7561653
O	5.9795719	4.0235736	-0.4157553	H	-11.6020681	2.5949836	0.5943547	C	7.8949919	-2.7165164	-1.4888553
C	4.6385519	4.2140436	-0.2795453	H	-7.3701981	1.8820236	0.3486047	N	7.0770519	-2.5930064	-0.3629353
C	4.0354519	5.0208136	0.6936847	H	-11.1681181	5.0256936	0.8656347	H	12.1028319	-2.9120264	-2.9952753
C	2.6437419	5.1070036	0.7410947	H	-8.8414981	5.8849236	0.8737847	H	11.2642919	-3.0205164	3.4548247
C	1.8415619	4.4094136	-0.1680353	H	-6.0488281	4.1307536	1.6230547	H	9.0925719	-3.3045964	4.4751047
C	2.4610719	3.6178636	-1.1575853	H	-6.4939781	5.5340936	0.6294047	H	6.6449119	-3.4693864	4.1148147
C	3.8381819	3.5230936	-1.2111053	H	-4.1532581	5.2971036	1.2479747	H	5.6674719	-3.1653064	1.8567247
N	0.4462419	4.5457136	0.0008047	H	-1.6845181	5.2911536	1.0560047	H	10.2666719	-3.1614464	-4.5435953
H	11.7719319	2.4168636	-0.0848353	H	-1.9178381	2.7002236	-2.3417253	H	7.8093019	-3.3353764	-4.8257453
H	7.5220119	1.9541936	0.3606447	H	-4.4239181	2.6790136	-2.1576153	H	6.2857319	-3.0972164	-2.8844253
H	11.5061719	4.8844336	0.0171147	C	13.9153619	-3.3817764	0.5130647	H	6.0978219	-2.8060164	-0.4940453
H	9.2527119	5.8866636	0.2859647	C	13.4158019	-3.1983564	-0.7752253	C	9.8452119	-0.6160064	0.0395547
H	6.8894219	5.6692936	0.4782347	C	12.0712519	-2.8336364	-0.9416553	C	9.7877119	0.5958036	0.0765747
H	6.4903019	4.3239736	1.5676847	C	11.2535819	-2.6390364	0.1792447	C	-13.9404081	-3.1676064	1.1267447
H	4.6312219	5.5768736	1.4083747	C	11.7582019	-2.8744564	1.4649047	C	-12.9269181	-3.1751364	2.0835947
H	2.1541219	5.7181836	1.4934847	C	13.1022319	-3.2387264	1.6361047	C	-11.6191381	-2.8458164	1.6967747
H	1.8357319	3.0818836	-1.8626253	H	14.9569419	-3.6627264	0.6437947	C	-11.3480081	-2.4957664	0.3675047
H	4.3349119	2.9112736	-1.9580153	H	14.0546819	-3.3405464	-1.6431053	C	-12.3686781	-2.5387964	-0.5912953
C	-9.5125081	2.0725436	0.4545347	N	11.5141219	-2.6647064	-2.2118253	C	-13.6779981	-2.8673164	-0.2089053
C	-10.5849581	2.9741636	0.6039347	C	9.8415619	-2.1024264	0.0052047	H	-14.9541581	-3.4213564	1.4248147
C	-8.1986081	2.5719236	0.4710447	N	10.8937819	-2.7471864	2.5551147	H	-13.1413181	-3.4377964	3.1163747
C	-7.9494681	3.9374236	0.6246947	H	13.4984319	-3.4120064	2.6333947	N	-10.5623181	-2.8667864	2.6103347
C	-10.3366181	4.3344936	0.7576747	C	8.9579619	-2.6095964	1.1353447	C	-9.9631181	-2.0010564	-0.0195253
C	-9.0257781	4.8187836	0.7638047	C	9.5073819	-2.8341064	2.4040147	N	-12.0468981	-2.2591264	-1.9219953
C	-6.5255281	4.4371336	0.6806747	C	8.6703119	-3.1417964	3.4868047	H	-14.4733081	-2.8922164	-0.9494853
O	-5.8036381	3.8703036	-0.4159453	C	7.2954719	-3.2352664	3.2764547	C	-9.6853381	-2.3439364	-1.4756253

C	-10.7385281	-2.3800164	-2.3982253	C	-6.9284181	-3.5740764	2.5850647	H	-7.0680481	-2.8296664	-3.6136053
C	-10.4689281	-2.5400764	-3.7654553	C	-6.6060381	-3.2927964	1.2583647	H	-8.4738481	-3.6960864	4.0908847
C	-9.1468281	-2.6786264	-4.1849653	C	-7.6123281	-2.8394664	0.3923747	H	-6.1494281	-3.9218364	3.2582147
C	-8.0917081	-2.6938964	-3.2741453	N	-7.3484581	-2.5619464	-0.9510953	H	-5.5898281	-3.4225764	0.8949647
C	-8.3661281	-2.5332264	-1.9078853	H	-10.7754281	-3.2183864	3.5336147	H	-6.4243981	-2.7980264	-1.2854753
C	-8.9174281	-2.6590664	0.8686047	H	-12.7837581	-2.3998264	-2.5993353	C	-9.8716481	-0.5273964	0.1554247
C	-9.2353481	-2.9930464	2.1911547	H	-11.2836281	-2.5566564	-4.4848953	C	-9.7341481	0.6707236	0.2928047
C	-8.2325181	-3.4469064	3.0607247	H	-8.9357081	-2.7991064	-5.2440853				

cis-**A**

$E_{M06\text{-}2X(D3)/def2\text{-}TZVPP}$ = -3206.033596869 Hartree

C	7.9566994	2.7018908	0.0412637	H	-6.5088706	2.3384708	-1.0767463	H	9.6082694	-2.1699092	-4.5143663
C	8.3923094	4.0337408	-0.0736963	H	-9.5646006	5.4720108	1.2509437	H	7.6786594	-1.9071392	-3.0878163
C	6.5773894	2.4437408	0.1785237	H	-7.4697606	6.3212408	0.2281537	C	9.4172194	0.5079608	0.0161137
C	5.6472394	3.4836108	0.1900337	H	-5.6019806	5.9637408	-1.2863263	C	8.8437894	1.5796908	0.0207437
C	7.4634594	5.0719108	-0.0608763	H	-5.3068506	4.3701808	-2.0156463	C	-12.8362306	-2.8536592	-0.1097763
C	6.0985394	4.8029408	0.0636937	H	-4.7308906	3.1092008	1.8437937	C	-12.2024606	-2.6954592	1.1216237
C	4.1756394	3.1956908	0.3964137	H	-3.7082806	0.8299608	2.0220737	C	-10.8469206	-2.3340792	1.1512937
O	3.8240294	2.0147408	-0.3294763	H	-1.7897506	1.4069008	-1.7791863	C	-10.1548306	-2.1117492	-0.0466063
C	2.5946894	1.4585208	-0.1548363	H	-2.8683606	3.6396108	-1.9823763	C	-10.7895606	-2.3351892	-1.2756863
C	2.4000694	0.2166908	-0.7840863	C	12.1690594	-1.9710092	3.4064237	C	-12.1450806	-2.6961792	-1.3099263
C	1.1930894	-0.4482992	-0.6471763	C	12.7806094	-1.7458692	2.1741537	H	-13.8868006	-3.1307092	-0.1344663
C	0.1220194	0.1273508	0.0614837	C	11.9827494	-1.4539392	1.0577837	H	-12.7457906	-2.8545692	2.0496037
C	0.3247094	1.3631208	0.6942837	C	10.5913894	-1.3663492	1.1927637	N	-10.1558506	-2.1968892	2.3577037
C	1.5520194	2.0214408	0.5964637	C	9.9889394	-1.6369792	2.4297637	C	-8.7375806	-1.5680392	-0.0137463
N	-1.0142706	-0.7364392	0.2070337	C	10.7831694	-1.9313292	3.5482737	N	-10.0417006	-2.2007292	-2.4477363
H	9.4526494	4.2418308	-0.1779363	H	12.7854894	-2.1990792	4.2717737	H	-12.6439506	-2.8556192	-2.2624763
H	6.2403994	1.4159508	0.2600237	H	13.8611594	-1.8060492	2.0721937	C	-7.9691806	-2.0496492	-1.2364063
H	7.8028594	6.0995508	-0.1585163	N	12.5442994	-1.2618492	-0.2088963	C	-8.6453006	-2.2798892	-2.4403663
H	5.3834294	5.6225808	0.0601437	C	9.7339894	-0.9519892	0.0107137	C	-7.9223606	-2.5792592	-3.6047463
H	3.5655894	4.0439308	0.0564437	N	8.5955194	-1.6179892	2.5130737	C	-6.5310706	-2.6488492	-3.5402863
H	3.9616994	3.0373108	1.4640037	H	10.3182594	-2.1347392	4.5095437	C	-5.8449806	-2.4541692	-2.3425963
H	3.2266694	-0.2153392	-1.3390463	C	8.3588894	-1.5989692	0.1232837	C	-6.5720706	-2.1612192	-1.1785163
H	1.0484394	-1.4304592	-1.0873263	C	7.7842394	-1.7756492	1.3882137	C	-8.0279606	-2.0463592	1.2459037
H	-0.4643106	1.8101508	1.2873637	C	6.4181594	-2.0740992	1.5008337	C	-8.7604806	-2.2747592	2.4168637
H	1.6822594	2.9698808	1.1053537	C	5.6546094	-2.2008992	0.3405437	C	-8.0933006	-2.5709692	3.6148137
C	-8.3380306	2.5296908	0.0387937	C	6.2282294	-2.0964692	-0.9267163	C	-6.7003706	-2.6389292	3.6170437
C	-9.2029206	3.4282408	0.6910037	C	7.5942894	-1.7943192	-1.0338163	C	-5.9578806	-2.4456192	2.4530337
C	-7.1691306	3.0317308	-0.5647963	C	10.3964494	-1.3825092	-1.2857863	C	-6.6295106	-2.1566992	1.2550637
C	-6.8435406	4.3884008	-0.4955263	C	11.7920394	-1.4637892	-1.3708363	N	-5.9419506	-1.9889592	0.0536437
C	-8.8904606	4.7846508	0.7468737	C	12.4057294	-1.7575892	-2.5976063	H	-10.6544606	-2.4740592	3.1920237
C	-7.7145506	5.2633608	0.1672037	C	11.6086894	-1.9904392	-3.7173863	H	-10.5007606	-2.4755192	-3.3051763
C	-5.5438406	4.8917908	-1.0799263	C	10.2175294	-1.9596692	-3.6390963	H	-8.4439006	-2.7535892	-4.5425163
O	-4.4319406	4.7582708	-0.1616863	C	9.6077594	-1.6634592	-2.4107463	H	-5.9693706	-2.8776992	-4.4421163
C	-3.8612806	3.5074508	-0.0762763	N	8.2190094	-1.6518692	-2.2731763	H	-4.7621006	-2.5345192	-2.3020363
C	-4.0807306	2.7278708	1.0635737	H	13.5353794	-1.4458592	-0.2859963	H	-8.6586206	-2.7442692	4.5270537
C	-3.5013506	1.4648708	1.1654537	H	8.1907494	-1.8725792	3.4032237	H	-6.1822206	-2.8656292	4.5450937
C	-2.6522006	0.9948508	0.1564937	H	5.9608794	-2.1882792	2.4802437	H	-4.8742506	-2.5269792	2.4631437
C	-2.4298706	1.7784808	-0.9849663	H	4.5933494	-2.4178292	0.4263437	H	-4.9319506	-2.0512392	0.0789837
C	-3.0375306	3.0261108	-1.1019263	H	5.6264794	-2.2330292	-1.8217363	C	-8.7287306	-0.0806692	-0.0119963
N	-2.2114506	-0.3723792	0.2489337	H	13.4891494	-1.8118092	-2.6671463	C	-8.5959406	1.1257908	0.0079837
H	-10.1101506	3.0504808	1.1522937	H	12.0823094	-2.2189692	-4.6683263				

cis-**B**

$E_{M06\text{-}2X(D3)/def2\text{-}TZVPP}$ = -3206.030037697 Hartree

C	-8.3541707	1.5039358	-0.6988618	C	8.2536593	3.4051958	-2.4019918	N	-11.0646707	-2.4939742	2.2425982
C	-9.2138707	2.4982858	-1.2007418	C	7.2499793	3.9981858	-1.6383518	C	-9.2448407	-2.4361842	0.0705482
C	-7.0139307	1.8406658	-0.4266218	C	5.6952293	4.0120858	0.3472682	N	-10.1781707	-3.5375042	-2.3680818
C	-6.5377807	3.1368958	-0.6293118	O	4.4949393	4.1733758	-0.4231418	H	-12.7813207	-4.1971942	-2.4600718
C	-8.7343607	3.7878358	-1.4138318	C	3.5169093	4.9869858	0.0676682	C	-8.3237807	-3.1900942	-0.8786818
C	-7.4073007	4.1141158	-1.1261418	C	3.5434693	5.5930858	1.3317682	C	-8.8068107	-3.6318442	-2.1166318
C	-5.1116607	3.4635358	-0.2358618	C	2.5329693	6.4839858	1.6849682	C	-7.9204707	-4.1556742	-3.0693618
O	-4.6758907	4.6320558	-0.9257018	C	1.4437193	6.7273158	0.8397782	C	-6.5645407	-4.2432542	-2.7585118
C	-3.5922807	5.3138758	-0.4477418	C	1.4041093	6.0841258	-0.4125618	C	-6.0766207	-3.8573642	-1.5108518
C	-3.4542307	6.6330258	-0.9076018	C	2.4337593	5.2350358	-0.7943718	C	-6.9663907	-3.3320242	-0.5624818
C	-2.4353307	7.4363258	-0.4207418	N	0.6037393	7.8111858	1.2588182	C	-8.7820207	-2.6486342	1.5048682
C	-1.4849507	6.9249658	0.4793882	H	9.5490693	1.6944758	-2.6422118	C	-9.7051907	-2.5769542	2.5554082
C	-1.6031307	5.5972558	0.9063682	H	6.8740993	1.5748458	0.7180882	C	-9.2582707	-2.5934642	3.8850482
C	-2.6552807	4.7951358	0.4550382	H	8.6393393	3.9166158	-3.2797618	C	-7.8921407	-2.6996142	4.1403582
N	-0.6334107	7.8961358	1.1073282	H	6.8486193	4.9678358	-1.9208618	C	-6.9654007	-2.8246242	3.1063682
H	-10.2468207	2.2470558	-1.4203518	H	6.0462193	5.0013058	0.6714182	C	-7.4168507	-2.8050442	1.7785182
H	-6.3516307	1.0660358	-0.0484518	H	5.4846393	3.4161158	1.2451182	N	-6.5313707	-2.9351542	0.7050982
H	-9.4015707	4.5510158	-1.8056818	H	4.3566493	5.4119158	2.0245582	H	-11.7065707	-2.5677642	3.0199182
H	-7.0388707	5.1200958	-1.2931618	H	2.5799093	7.0187558	2.6289982	H	-10.5078107	-3.9765642	-3.2167418
H	-4.4492207	2.6164758	-0.4653418	H	0.5906193	6.2816158	-1.1017918	H	-8.2902507	-4.4859042	-4.0366818
H	-5.0536207	3.6422058	0.8483682	H	2.4352093	4.7635058	-1.7722418	H	-5.8756207	-4.6444142	-3.4969718
H	-4.1905107	7.0202058	-1.6049618	C	-13.3172807	-3.7407342	-0.4170918	H	-5.0205107	-3.9572042	-1.2734318
H	-2.3684007	8.4801858	-0.7128818	C	-12.8892407	-3.2955642	0.8323782	H	-9.9715407	-2.5241342	4.7023182
H	-0.8932707	5.1941858	1.6219182	C	-11.5517207	-2.9059942	0.9989182	H	-7.5436807	-2.7090842	5.1696182
H	-2.7373207	3.7758158	0.8162182	C	-10.6681107	-2.9429742	-0.0881818	H	-5.9056107	-2.9345242	3.3219782
C	8.2748193	1.4847958	-0.9169218	C	-11.1043907	-3.4326442	-1.3267918	H	-5.5741707	-3.1595842	0.9397382
C	8.7692893	2.1593258	-2.0470618	C	-12.4410407	-3.8233142	-1.4978018	C	-9.1052807	-0.9868342	-0.2396618
C	7.2599593	2.0974158	-0.1527218	H	-14.3523207	-4.0449442	-0.5472718	C	-8.7993107	0.1667258	-0.4644818
C	6.7480693	3.3454958	-0.5033018	H	-13.5764507	-3.2608742	1.6738582	C	13.2378893	-3.2392242	1.4159382

C	12.9284693	-3.3749342	0.0637382	C	8.5938093	-2.5573242	2.5178082	H	11.9542993	-3.6763542	-2.3173918
C	11.6151493	-3.1321042	-0.3658118	C	7.6194493	-2.6478042	3.5231082	H	10.1860093	-2.3551442	3.8008882
C	10.6366593	-2.7343842	0.5552082	C	6.2955293	-2.8955342	3.1636282	H	7.8972393	-2.5239242	4.5666682
C	10.9550793	-2.6421742	1.9169682	C	5.9257793	-3.0937742	1.8341782	H	5.5383293	-2.9614142	3.9403482
C	12.2670393	-2.8843742	2.3508682	C	6.9035293	-3.0012742	0.8322982	H	4.8941293	-3.3144742	1.5723582
H	14.2540793	-3.4293042	1.7505882	C	8.9046093	-3.1981842	-1.1673518	H	10.3798893	-4.3993042	-4.0018618
H	13.6892093	-3.6775942	-0.6512818	C	9.9195193	-3.5476742	-2.0665118	H	8.0026993	-4.8409642	-4.5517318
N	11.2462893	-3.2959842	-1.7042718	C	9.5949793	-4.1389242	-3.2964218	H	6.2026993	-4.3171842	-2.9294318
C	9.2369493	-2.3872742	0.0766682	C	8.2566793	-4.3866942	-3.5978118	H	5.6503693	-3.5070242	-0.7191218
N	9.9379293	-2.3244042	2.8214882	C	7.2392893	-4.0929442	-2.6913218	C	9.0788293	-0.9450442	-0.2608518
H	12.5157593	-2.8072042	3.4062082	C	7.5685493	-3.5003642	-1.4633118	C	8.7435193	0.1822358	-0.5642418
C	8.2286493	-2.6992142	1.1735482	N	6.5907093	-3.1997142	-0.5133218				

cis-**C**

$E_{M06\text{-}2X(D3)/def2\text{-}TZVPP}$ = -3206.032771190 Hartree

C	8.3214377	2.1146398	-1.0841089	H	-6.3235623	1.3382598	-1.6607189	H	5.2144677	-3.3926302	-1.2673589
C	9.1050277	3.1071298	-1.7006589	H	-9.4127223	5.1958498	-1.2379989	H	5.7263477	-2.4086802	0.8827711
C	6.9673977	2.3875498	-0.8050289	H	-7.1366023	5.5300098	-2.1588789	C	9.2165477	-0.2810102	-0.4235789
C	6.4043577	3.6240998	-1.1212889	H	-4.9191223	4.7060598	-2.5771289	C	8.8529777	0.8337998	-0.7400589
C	8.5410777	4.3397698	-2.0193389	H	-5.2673723	3.3700798	-3.6818989	C	-12.8046623	-3.5364202	-1.2391489
C	7.2012977	4.6025298	-1.7281189	H	-4.8251823	4.8090098	-0.3208089	C	-12.7455023	-2.9672702	0.0318011
C	4.9418677	3.9078998	-0.8532089	H	-3.5288223	5.2562798	1.7392911	C	-11.5227123	-2.4628902	0.4996311
O	4.5342877	3.1922298	0.3103811	H	-0.8063923	2.0880398	0.7610811	C	-10.3843823	-2.5120902	-0.3159989
C	3.2898977	3.4049098	0.8264911	H	-2.1363223	1.5908698	-1.2747089	C	-10.4512423	-3.1264302	-1.5740889
C	3.0301177	2.7593098	2.0465711	C	13.4963577	-2.9571302	-0.3438689	C	-11.6719623	-3.6325402	-2.0455189
C	1.8230977	2.9593398	2.6954211	C	12.6343177	-3.1396702	-1.4237389	H	-13.7506123	-3.9290502	-1.6022789
C	0.8142977	3.7495498	2.1166111	C	11.2891777	-2.7611402	-1.2975789	H	-13.6306723	-2.9229702	0.6611811
C	1.0718877	4.3795098	0.8928311	C	10.8299877	-2.1836302	-0.1058989	N	-11.4031423	-1.9195202	1.7820711
C	2.3038177	4.2182498	0.2518811	C	11.7001777	-2.0460602	0.9841511	C	-9.0854323	-1.8755702	0.1497211
N	-0.2979423	4.0414298	2.9762811	C	13.0461977	-2.4230002	0.8621711	N	-9.2803423	-3.2340202	-2.3286089
H	10.1484577	2.9026798	-1.9192989	H	14.5378777	-3.2521002	-0.4390289	H	-11.7262423	-4.1029302	-3.0239689
H	6.3648577	1.6259698	-0.3233889	H	12.9919777	-3.5820402	-2.3500189	C	-7.9040323	-2.6210502	-0.4558689
H	9.1513577	5.1068398	-2.4883889	N	10.3771977	-2.9648002	-2.3368989	C	-8.0181723	-3.1889102	-1.7305689
H	6.7764777	5.5746298	-1.9688289	C	9.3949677	-1.6976602	-0.0000089	C	-6.8804123	-3.6916902	-2.3790889
H	4.3210877	3.5976398	-1.7084789	N	11.1916877	-1.5481802	2.1869211	C	-5.6475823	-3.6280902	-1.7313689
H	4.7871477	4.9859498	-0.7071489	H	13.7227177	-2.3105102	1.7055111	C	-5.5272323	-3.1155202	-0.4405589
H	3.8114677	2.1459898	2.4842611	C	8.9209377	-1.8076102	1.4419611	C	-6.6680023	-2.6141402	0.2040211
H	1.6398677	2.5178698	3.6705711	C	9.8303277	-1.6340702	2.4923311	C	-9.0008223	-1.9332802	1.6676111
H	0.3213477	5.0238698	0.4465711	C	9.3686577	-1.5534302	3.8144411	C	-10.1686723	-1.8710102	2.4376511
H	2.4839477	4.7354598	-0.6839589	C	8.0017277	-1.6649102	4.0635311	C	-10.0847223	-1.7697802	3.8341011
C	-8.2879823	1.9824798	-1.0446289	C	7.0893877	-1.8900402	3.0337511	C	-8.8287923	-1.7503302	4.4388211
C	-9.1582623	3.0835498	-0.9316589	C	7.5555977	-1.9676602	1.7132011	C	-7.6583323	-1.8605502	3.6900811
C	-6.9981723	2.1838098	-1.5737389	C	8.4999977	-2.5422302	-0.8963489	C	-7.7471923	-1.9612202	2.2937511
C	-6.5781823	3.4523798	-1.9771189	C	9.0048077	-3.0665402	-2.0924489	N	-6.6076923	-2.0967402	1.4987811
C	-8.7392723	4.3484098	-1.3337189	C	8.1386877	-3.6758102	-3.0123689	H	-12.2179523	-1.9973302	2.3752911
C	-7.4555823	4.5363898	-1.8504389	C	6.7806477	-3.7626202	-2.7101189	H	-9.3491523	-3.7582802	-3.1899589
C	-5.2192823	3.6510798	-2.6241089	C	6.2716077	-3.2932302	-1.5001089	H	-6.9627323	-4.1196702	-3.3748789
O	-4.1791623	2.8198098	-2.1036189	C	7.1413177	-2.6832202	-0.5842389	H	-4.7637223	-4.0109902	-2.2344989
C	-3.5371323	3.1839898	-0.9542189	N	6.6860677	-2.1998002	0.6446411	H	-4.5636023	-3.0983402	0.0620011
C	-3.9312523	4.2329298	-0.1139889	H	10.7246977	-3.4639002	-3.1442489	H	-10.9897923	-1.7100602	4.4331411
C	-3.2029223	4.4870498	1.0456111	H	11.8260177	-1.5489502	2.9739011	H	-8.7612723	-1.6683302	5.5202511
C	-2.0482223	3.7593698	1.3606911	H	10.0709277	-1.4047102	4.6306511	H	-6.6870223	-1.8697702	4.1777711
C	-1.6677123	2.6994098	0.5162411	H	7.6415277	-1.5983702	5.0865911	H	-5.7255423	-2.1876402	1.9831211
C	-2.4101123	2.4132998	-0.6210189	H	6.0293277	-2.0019402	3.2467611	C	-8.9615623	-0.4580002	-0.2886789
N	-1.5072023	4.0455298	2.6567211	H	8.5251577	-4.0709502	-3.9483489	C	-8.6847023	0.6738398	-0.6304589
H	-10.1532223	2.9336498	-0.5245289	H	6.1070477	-4.2296202	-3.4236189				

cis-**D**

$E_{M06\text{-}2X(D3)/def2\text{-}TZVPP}$ = -3206.059330528 Hartree

-3206.028099474 Basis = def2-TZVPP Functional = m06-2x

C	8.3078827	1.4300493	-1.4437177	H	1.0358627	6.0986293	-0.5988177	H	-4.0154373	7.0443893	-0.6718077
C	9.2088727	2.1852893	-2.2198077	H	2.8540327	4.8010393	-1.6202577	H	-2.1497173	8.1091993	0.6099623
C	7.0033127	1.9204593	-1.2459477	C	-8.1631973	1.5258193	-1.2922977	H	-0.5217873	4.2280193	1.4479223
C	6.6007427	3.1378993	-1.8012177	C	-8.7979073	2.4230393	-2.1699177	H	-2.3959573	3.1696993	0.2637723
C	8.8082327	3.3964993	-2.7741577	C	-6.8537273	1.8138993	-0.8596777	C	12.2275627	-2.3186507	3.1217223
C	7.5127927	3.8750793	-2.5641377	C	-6.1797873	2.9546293	-1.2966777	C	12.5133927	-2.6891507	1.8087223
C	5.1938127	3.6500393	-1.5945877	C	-8.1268473	3.5654993	-2.5995677	C	11.4769827	-2.7133707	0.8635523
O	4.9173527	3.6729793	-0.1901577	C	-6.8236573	3.8338093	-2.1749077	C	10.1773727	-2.3463607	1.2363823
C	3.8327027	4.3620293	0.2645323	C	-4.7573273	3.1836393	-0.8300377	C	9.8988127	-2.0172407	2.5701023
C	3.7726327	4.5307593	1.6581023	O	-4.4450073	4.5713793	-0.9178977	C	10.9321827	-1.9918607	3.5186623
C	2.7653327	5.2951793	2.2205923	C	-3.3342873	5.0459393	-0.2841677	H	13.0289227	-2.3004007	3.8553823
C	1.7474627	5.8520193	1.4247423	C	-3.2336873	6.4450493	-0.2160277	H	13.5234027	-2.9671307	1.5185323
C	1.7915627	5.6520193	0.0389623	C	-2.1936573	7.0314393	0.4846123	N	11.7052927	-3.1155407	-0.4561877
C	2.8306127	4.9194693	-0.5425477	C	-1.1852673	6.2481193	1.0747423	C	9.0764827	-2.2711307	0.1908623
N	0.9151227	6.8010293	2.1060123	C	-1.2709573	4.8537093	0.9740723	N	8.5779127	-1.7356307	2.9268323
H	10.2149427	1.8097893	-2.3784177	C	-2.3415473	4.2518093	0.3064923	H	10.7182727	-1.7299407	4.5517023
H	6.3091227	1.3438893	-0.6427077	N	-0.3143373	6.9673393	1.9595323	C	7.7337427	-2.5778807	0.8404723
H	9.5090227	3.9767893	-3.3681577	H	-9.8092873	2.2153493	-2.5050877	C	7.5001627	-2.1970107	2.1676823
H	7.2119427	4.8282493	-2.9923977	H	-6.3733373	1.1222393	-0.1723977	C	6.2062627	-2.2791907	2.7035423
H	4.4574827	3.0048993	-2.0970277	H	-8.6233873	4.2568793	-3.2752677	C	5.1699427	-2.7567607	1.9028423
H	5.0957127	4.6601793	-2.0123677	H	-6.3093673	4.7283593	-2.5088877	C	5.3975927	-3.1927307	0.5983823
H	4.5613827	4.0990193	2.2659223	H	-4.0479573	2.6097293	-1.4468477	C	6.6929227	-3.1070307	0.0666223
H	2.7541827	5.4972293	3.2875223	H	-4.6457873	2.8388993	0.2067923	C	9.3498427	-3.2794807	-0.9147377

C	10.6681227	-3.6103507	-1.2527177
C	10.9247527	-4.4295607	-2.3622477
C	9.8529527	-4.9221507	-3.1049077
C	8.5337627	-4.6424607	-2.7522377
C	8.2819027	-3.8219507	-1.6425577
N	6.9788327	-3.5324107	-1.2324477
H	12.6288227	-3.4741907	-0.6571377
H	8.4013827	-1.5810007	3.9098423
H	6.0178727	-1.9689007	3.7281023
H	4.1657927	-2.8152607	2.3142323
H	4.5842927	-3.5891007	-0.0041377
H	11.9477527	-4.6789407	-2.6321677
H	10.0496827	-5.5556407	-3.9656377
H	7.7073427	-5.0564007	-3.3243177
H	6.2354527	-4.0079607	-1.7247977
C	8.9560727	-0.9070507	-0.3937877
C	8.6883927	0.1735793	-0.8786977
C	-13.2360973	-3.7478107	-0.9179177
C	-13.1031773	-3.0540507	0.2836123
C	-11.8460573	-2.5474207	0.6462223
C	-10.7467473	-2.7175807	-0.2061077
C	-10.8891973	-3.4526307	-1.3911777
C	-12.1443573	-3.9613407	-1.7575177
H	-14.2083673	-4.1435807	-1.1986977
H	-13.9571673	-2.9171007	0.9420223
N	-11.6527873	-1.8858707	1.8624223
C	-9.4045573	-2.1022807	0.1488723
N	-9.7566373	-3.6795107	-2.1776377
H	-12.2560573	-4.5270407	-2.6789577
C	-8.2816273	-2.9570707	-0.4236577
C	-8.4700273	-3.6334007	-1.6352077
C	-7.3799573	-4.2400707	-2.2765777
C	-6.1202173	-4.1702007	-1.6841177
C	-5.9276373	-3.5492907	-0.4506677
C	-7.0200873	-2.9416607	0.1851523
C	-9.2608673	-2.0199507	1.6610223
C	-10.3920973	-1.8249207	2.4630523
C	-10.2455773	-1.5818107	3.8367923
C	-8.9660073	-1.5571807	4.3889423
C	-7.8334973	-1.8012007	3.6134723
C	-7.9848973	-2.0407207	2.2398923
N	-6.8831073	-2.3003307	1.4195523
H	-12.4457773	-1.8643807	2.4889223
H	-9.8823873	-4.2798407	-2.9809777
H	-7.5190573	-4.7521207	-3.2252477
H	-5.2733773	-4.6346807	-2.1822077
H	-4.9441473	-3.5281707	0.0120923
H	-11.1213473	-1.4166207	4.4590423
H	-8.8501673	-1.3659607	5.4523423
H	-6.8439673	-1.8054507	4.0634223
H	-5.9950873	-2.4169007	1.8881423
C	-9.2013273	-0.7375507	-0.4145877
C	-8.7856873	0.3235493	-0.8355677

trans-Au(111)-**A** Optimierung

$E_{PBE(D3)/def2\text{-}SVP}$ = -12164.64095368

Single Point w/o Au(111) surface

$E_{M06\text{-}2X(D3)/def2\text{-}TZVPP}$ = -3206.028039363 Hartree

Au	-10.6570346	4.5805559	3.9306543
Au	-14.8929346	1.9336559	3.9306543
Au	-12.0109346	2.0343559	3.9306543
Au	-13.3647346	-0.5118441	3.9306543
Au	-13.5391346	4.4798559	3.9306543
Au	-17.6006346	-3.1587441	3.9306543
Au	-14.7186346	-3.0580441	3.9306543
Au	-16.0724346	-5.6042441	3.9306543
Au	-16.2467346	-0.6125441	3.9306543
Au	-4.8930346	4.7818559	3.9306543
Au	-9.1289346	2.1349559	3.9306543
Au	-6.2469346	2.2356559	3.9306543
Au	-7.6007346	-0.3106441	3.9306543
Au	-7.7750346	4.6811559	3.9306543
Au	-11.8366346	-2.9574441	3.9306543
Au	-8.9546346	-2.8567441	3.9306543
Au	-10.3084346	-5.4029441	3.9306543
Au	-10.4827346	-0.4112441	3.9306543
Au	-14.5442346	-8.0498441	3.9306543
Au	-11.6622346	-7.9492441	3.9306543
Au	-13.1904346	-5.5036441	3.9306543
Au	0.8709654	4.9830559	3.9306543
Au	-3.3649346	2.3362559	3.9306543
Au	-0.4829346	2.4368559	3.9306543
Au	-1.8367346	-0.1093441	3.9306543
Au	-2.0110346	4.8824559	3.9306543
Au	-6.0726346	-2.7561441	3.9306543
Au	-3.1906346	-2.6555441	3.9306543
Au	-4.5444346	-5.2017441	3.9306543
Au	-4.7187346	-0.2099441	3.9306543
Au	-8.7802346	-7.8485441	3.9306543
Au	-5.8982346	-7.7479441	3.9306543
Au	-7.4264346	-5.3023441	3.9306543
Au	5.1067654	7.6299559	3.9306543
Au	7.9887654	7.7305559	3.9306543
Au	6.6349654	5.1843559	3.9306543
Au	2.3990654	2.5375559	3.9306543
Au	5.2810654	2.6381559	3.9306543
Au	3.9272654	0.0919559	3.9306543
Au	3.7529654	5.0837559	3.9306543
Au	-0.3086346	-2.5548441	3.9306543
Au	2.5733654	-2.4542441	3.9306543
Au	1.2195654	-5.0004441	3.9306543
Au	1.0452654	-0.0086441	3.9306543
Au	-1.6624346	-5.1010441	3.9306543
Au	10.8707654	7.8312559	3.9306543
Au	13.7527654	7.9318559	3.9306543
Au	12.3989654	5.3856559	3.9306543
Au	8.1630654	2.7388559	3.9306543
Au	11.0450654	2.8394559	3.9306543
Au	9.6912654	0.2932559	3.9306543
Au	9.5169654	5.2850559	3.9306543
Au	5.4554654	-2.3536441	3.9306543
Au	8.3374654	-2.2529441	3.9306543
Au	6.9835654	-4.7991441	3.9306543
Au	6.8092654	0.1926559	3.9306543
Au	4.1015654	-4.8997441	3.9306543
Au	13.9270654	2.9400559	3.9306543
Au	16.8090654	3.0407559	3.9306543
Au	15.4552654	0.4945559	3.9306543
Au	15.2809654	5.4862559	3.9306543
Au	11.2194654	-2.1523441	3.9306543
Au	14.1014654	-2.0516441	3.9306543
Au	12.7475654	-4.5978441	3.9306543
Au	12.5732654	0.3938559	3.9306543
Au	9.8655654	-4.6985441	3.9306543
C	-9.0850419	-1.2413496	-4.1402599
C	-10.2643082	-1.2941496	-4.9252368
C	-7.8271125	-1.2118525	-4.7898583
C	-7.7383391	-1.2383236	-6.1895503
C	-10.1720809	-1.3228255	-6.3218199
C	-8.9189350	-1.3002102	-6.9549841
C	-6.3885279	-1.1464557	-6.8649048
O	-5.4061781	-1.7263496	-6.0155278
C	-4.0875153	-1.5169496	-6.2605790
C	-3.5725286	-0.8553426	-7.3963298
C	-2.1890848	-0.6674461	-7.5108072
C	-1.3044299	-1.1347781	-6.5168357
C	-1.8331127	-1.8237747	-5.3923018
C	-3.2023204	-2.0118397	-5.2685275
N	0.0593322	-0.8535078	-6.7015259
H	-11.2437709	-1.3172670	-4.4260598
H	-6.9089422	-1.1783508	-4.1877331
H	-11.0893624	-1.3725317	-6.9279640
H	-8.8589182	-1.3348238	-8.0545937
H	-6.1391762	-0.0747211	-7.0553195
H	-6.4054742	-1.6598017	-7.8543295
H	-4.2375174	-0.4848818	-8.1880402
H	-1.7590947	-0.1434390	-8.3774584
H	-1.1295410	-2.1844203	-4.6285665
H	-3.6375472	-2.5313998	-4.4018017
C	9.5401564	1.8939679	-4.1299498
C	10.6057797	2.2874161	-4.9780376
C	8.3339870	1.4330025	-4.7105902
C	8.1855930	1.3598048	-6.1036017
C	10.4558346	2.2102342	-6.3678045
C	9.2566637	1.7454433	-6.9323705
C	6.8647103	0.9236270	-6.6964692
O	6.2614379	-0.0264262	-5.8251052
C	4.9384187	-0.3116128	-5.9344480
C	4.0969143	0.1557487	-6.9736437
C	2.7374698	-0.1639823	-6.9611131
C	2.1923669	-0.9582157	-5.9244975
C	3.0506376	-1.4459444	-4.9092508
C	4.4061006	-1.1307355	-4.9120760
N	0.8347262	-1.2886017	-5.7972886
H	11.5452706	2.6461288	-4.5332598
H	7.5074713	1.1188077	-4.0585669
H	11.2882745	2.5081306	-7.0232407
H	9.1549013	1.6788134	-8.0273981
H	7.0087781	0.4895670	-7.7128536
H	6.1983735	1.8120691	-6.8088509
H	4.5004346	0.7692240	-7.7913704
H	2.0590257	0.1971208	-7.7475644
H	2.6087741	-2.0660312	-4.1152201
H	5.0854436	-1.4895844	-4.1254619
C	-8.8392060	-5.3630735	0.8666338
C	-10.1116015	-4.7708993	0.8120060
C	-10.2098330	-3.3720333	0.6243570
C	-9.0319763	-2.6035364	0.4860198
C	-7.7572949	-3.2013519	0.6100482
C	-7.6614253	-4.6002637	0.7991431
H	-8.7628509	-6.4519796	1.0039258
H	-11.0203881	-5.3857919	0.8893317
N	-11.4392098	-2.7209420	0.5637275
C	-9.1362557	-1.1711417	-0.0014759
N	-6.6302238	-2.3880237	0.5365023
H	-6.6759062	-5.0833813	0.8713872
C	-7.9397764	-0.3651238	0.4654109
C	-6.6870972	-1.0002252	0.6000986
C	-5.5230295	-0.2133310	0.7896065
C	-5.6430664	1.1842550	0.8477107
C	-6.8933336	1.8200122	0.7828919
C	-8.0573841	1.0345715	0.5943986
C	-10.4234482	-0.5373523	0.4873822
C	-11.5749339	-1.3397390	0.6315751
C	-12.8359461	-0.7221101	0.8330105
C	-12.9075246	0.6778960	0.8991048
C	-11.7564951	1.4820089	0.8337252
C	-10.4965183	0.8657693	0.6205354
N	-9.3245271	1.6069747	0.5346491
H	-12.2727537	-3.2818681	0.7517121
H	-5.7255759	-2.8275796	0.7175498
H	-4.5366839	-0.6943222	0.8674980
H	-4.7376055	1.7939009	0.9857613
H	-6.9701904	2.9139128	0.8682734
H	-13.7465143	-1.3344380	0.9105460
H	-13.8865215	1.1576336	1.0451314
H	-11.8335614	2.5771314	0.9041326
H	-9.3920490	2.6099663	0.7189401
C	-9.1465984	-1.1895773	-1.4849476
C	-9.1405813	-1.2163667	-2.7137515
C	13.1506649	4.3792694	0.8976858
C	13.2881893	2.9838644	0.8251436
C	12.1322536	2.1866056	0.6241182
C	10.8727518	2.8094228	0.4914121
C	10.7364447	4.2068487	0.6329569
C	11.8927400	5.0027176	0.8423504
H	14.0486556	4.9986074	1.0392030
H	14.2808140	2.5141677	0.8905613
N	12.2030099	0.8013445	0.5458981
C	9.6921077	1.9938020	0.0040111
N	9.4674814	4.7663641	0.5523534
H	11.8052509	6.0963555	0.9211433
C	8.3898774	2.6110302	0.4766249
C	8.2971017	4.0135018	0.6061791
C	7.0288567	4.6149957	0.7902691
C	5.8880236	3.7977578	0.8525965
C	5.9771659	2.3978637	0.7964520
C	7.2448010	1.7950856	0.6101821
C	9.8052682	0.5593947	0.4831049
C	11.0840220	-0.0242181	0.6154709
C	11.1961288	-1.4211183	0.8144383
C	10.0265418	-2.1969506	0.8812759
C	8.7486641	-1.6177552	0.8159029
C	8.6352512	-0.2200322	0.6194748
N	7.3992914	0.4139111	0.5496489
H	13.1109327	0.3699405	0.7306953
H	9.3858641	5.7676536	0.7402910
H	6.9394728	5.7087776	0.8661192
H	4.9015008	4.2660081	0.9873020
H	5.0738817	1.7752520	0.8763372
H	12.1861896	-1.8925965	0.8986162
H	10.1135733	-3.2843989	1.0230678
H	7.8460154	-2.2424416	0.8879029
H	6.5723213	-0.1558477	0.7397173

C	9.6877587	1.9838593	-1.4796008	C	9.6505863	1.9520254	-2.7076798	

cis-Au(111)-**A** Optimization

$E_{PBE(D3)/def2\text{-}SVP}$ = -14609.61438845 Hartree

Single Point w/o Au(111) surface

$E_{M06\text{-}2X(D3)/def2\text{-}TZVPP}$ = -3205.998121241 Hartree

Au	-14.3918437	-7.4614089	-0.5044600	Au	7.2377957	5.0205980	-0.2869717	C	-12.3987964	-1.7015663	2.9114363
Au	-11.5081281	-7.4618861	-0.4994279	Au	10.1215112	5.0201208	-0.2819396	C	-13.6279931	-2.3734169	2.6953403
Au	-8.6244125	-7.4623634	-0.4943958	Au	13.0052268	5.0196435	-0.2769075	H	-14.5953344	-4.2958585	2.4631314
Au	-5.7406970	-7.4628406	-0.4893637	Au	15.8889424	5.0191663	-0.2718754	H	-12.4804468	-5.6247834	2.5842273
Au	-2.8569714	-7.4633178	-0.4843316	Au	-14.3897406	7.5212984	-0.2887628	N	-10.0157966	-4.5462541	2.9367727
Au	0.0267442	-7.4637950	-0.4792996	Au	-11.5060250	7.5208212	-0.2837308	C	-9.9424865	-1.7744361	3.5131721
Au	2.9104597	-7.4642723	-0.4742675	Au	-8.6223094	7.5203439	-0.2786987	N	-12.3247940	-0.3159553	2.9965979
Au	5.7941853	-7.4647495	-0.4692354	Au	-5.7385939	7.5198667	-0.2736666	H	-14.5648468	-1.8018073	2.6193530
Au	8.6779009	-7.4652267	-0.4642033	Au	-2.8548683	7.5193895	-0.2686345	C	-9.9133133	-0.3276970	3.0595209
Au	11.5616165	-7.4657039	-0.4591712	Au	0.0288473	7.5189123	-0.2636024	C	-11.1235938	0.3879380	2.9393856
Au	14.4453420	-7.4661812	-0.4541391	Au	2.9125628	7.5184350	-0.2585703	C	-11.0878751	1.7926908	2.7667381
Au	-15.8333509	-4.9640591	-0.4710266	Au	5.7962884	7.5179578	-0.2535382	C	-9.8444569	2.4432661	2.7153735
Au	-12.9496354	-4.9645363	-0.4659945	Au	8.6800040	7.5174806	-0.2485061	C	-8.6342696	1.7319890	2.7688186
Au	-10.0659198	-4.9650135	-0.4609624	Au	11.5637195	7.5170034	-0.2434740	C	-8.6688350	0.3281339	2.9336983
Au	-7.1822042	-4.9654908	-0.4559304	Au	14.4474451	7.5165261	-0.2384419	C	-8.7227374	-2.5149123	2.9941512
Au	-4.2984787	-4.9659680	-0.4508983	C	-9.0067559	-1.7996246	7.5236496	C	-8.7773141	-3.9190807	2.8610466
Au	-1.4147631	-4.9664452	-0.4458662	C	-9.8155023	-1.4264994	8.6260537	C	-7.5788144	-4.6507398	2.6683842
Au	1.4689525	-4.9669224	-0.4408341	C	-7.6632509	-2.1846699	7.7598976	C	-6.3598784	-3.9575860	2.6113960
Au	4.3526680	-4.9673997	-0.4358020	C	-7.1285377	-2.1909474	9.0579942	C	-6.3011937	-2.5545515	2.6787260
Au	7.2363936	-4.9678769	-0.4307699	C	-9.2800417	-1.4399237	9.9187724	C	-7.4985812	-1.8217331	2.8764761
Au	10.1201092	-4.9683541	-0.4257378	C	-7.9447799	-1.8159360	10.1415858	N	-7.5041404	-0.4359355	2.9768561
Au	13.0038248	-4.9688313	-0.4207057	C	-5.6794799	-2.5876664	9.2450203	H	-10.0425483	-5.5503738	2.7485429
Au	15.8875403	-4.9693086	-0.4156736	O	-5.4195287	-2.8307670	10.6221056	H	-13.1816687	0.2095111	2.8122835
Au	-17.2748682	-2.4666992	-0.4375931	C	-4.2344757	-3.3659613	11.0028856	H	-12.0238685	2.3663014	2.6961003
Au	-14.3911426	-2.4671765	-0.4325610	C	-4.1268042	-3.6988862	12.3752480	H	-9.8179967	3.5364560	2.5929081
Au	-11.5074271	-2.4676537	-0.4275289	C	-2.9822520	-4.3242527	12.8537320	H	-7.6716837	2.2588226	2.6927110
Au	-8.6237115	-2.4681309	-0.4224968	C	-1.8786464	-4.5771241	11.9972097	H	-7.6050717	-5.7471886	2.5868994
Au	-5.7399959	-2.4686082	-0.4174647	C	-1.9797449	-4.2163129	10.6308819	H	-5.4275294	-4.5248720	2.4710258
Au	-2.8562704	-2.4690854	-0.4124326	C	-3.1487176	-3.6294888	10.1334689	H	-5.3356415	-2.0310444	2.6167028
Au	0.0274452	-2.4695626	-0.4074005	N	-0.8509500	-5.3789116	12.5338036	H	-6.6228105	0.0493327	2.7988109
Au	2.9111608	-2.4700398	-0.4023685	H	-10.8597819	-1.1299542	8.4517245	C	-9.8167126	-1.7970958	4.9945679
Au	5.7948863	-2.4705171	-0.3973363	H	-7.0427408	-2.4824836	6.8996809	C	-9.4949111	-1.7903702	6.1815906
Au	8.6786019	-2.4709943	-0.3923043	H	-9.9124475	-1.1519582	10.7723716	C	11.9926511	-1.2660726	2.7265036
Au	11.5623175	-2.4714715	-0.3872722	H	-7.5291646	-1.8294244	11.1584829	C	12.0282016	0.1339680	2.8243087
Au	14.4460431	-2.4719487	-0.3822401	H	-5.0071189	-1.7788697	8.8693703	C	10.8196804	0.8417974	3.0265225
Au	17.3297586	-2.4724260	-0.3772080	H	-5.4594134	-3.5003259	8.6439272	C	9.6066411	0.1281674	3.1414056
Au	-15.8326499	0.0301834	-0.3991275	H	-4.9848552	-3.4926896	13.0311202	C	9.5741124	-1.2710231	2.9613419
Au	-12.9489343	0.0297061	-0.3940954	H	-2.9094849	-4.6468874	13.9028012	C	10.7833648	-1.9784622	2.7637205
Au	-10.0652188	0.0292289	-0.3890633	H	-1.1478731	-4.4302044	9.9442117	H	12.9334656	-1.8158901	2.5740291
Au	-7.1815032	0.0287517	-0.3840312	H	-3.2105336	-3.3881932	9.0636199	H	12.9824647	0.6763718	2.7521258
Au	-4.2977776	0.0282745	-0.3789991	C	7.3009163	0.4902570	7.5516977	N	10.7891283	2.2322370	3.1079186
Au	-1.4140621	0.0277972	-0.3739670	C	7.5744328	1.3883602	8.6113981	C	8.3521902	0.8481345	3.5901031
Au	1.4696535	0.0273200	-0.3689349	C	6.4293699	-0.6041527	7.7917045	N	8.3394190	-1.9201883	2.9748145
Au	4.3533691	0.0268428	-0.3639028	C	5.8482608	-0.8046756	9.0514589	H	10.7733656	-3.0719295	2.6442035
Au	7.2370946	0.0263655	-0.3588707	C	6.9820150	1.1931820	9.8666728	C	7.1171520	0.1551385	3.0396002
Au	10.1208102	0.0258883	-0.3538386	C	6.1251636	0.1060789	10.0922573	C	7.1265173	-1.2494560	2.8900813
Au	13.0045258	0.0254111	-0.3488065	C	4.9797668	-2.0135478	9.2995016	C	5.9009111	-1.9349692	2.6872216
Au	15.8882414	0.0249339	-0.3437745	O	3.7781826	-1.6143979	9.9683120	C	4.7029629	-1.1995086	2.6543974
Au	-17.2741672	2.5275432	-0.3656940	C	2.9338658	-2.5729538	10.4215687	C	4.6902191	0.2014092	2.7461026
Au	-14.3904416	2.5270660	-0.3606619	C	3.1231308	-3.9625626	10.2372402	C	5.9141979	0.8890395	2.9376673
Au	-11.5067260	2.5265887	-0.3556298	C	2.2262692	-4.8627655	10.8175966	C	8.3793321	2.2971794	3.1474492
Au	-8.6230105	2.5261115	-0.3505977	C	1.0880858	-4.4138170	11.5261148	C	9.6136586	2.9705221	3.0320842
Au	-5.7392949	2.5256343	-0.3455656	C	0.8883911	-3.0138392	11.6822990	C	9.6246732	4.3762061	2.8460817
Au	-2.8555693	2.5251571	-0.3405335	C	1.8054623	-2.1137773	11.1490350	C	8.4040851	5.0692420	2.7833301
Au	0.0281462	2.5246798	-0.3355014	N	0.3535746	-5.4078327	12.2039319	C	7.1712743	4.3998828	2.8342670
Au	2.9118618	2.5242026	-0.3304693	H	8.2449838	2.2415510	8.4339195	C	7.1591148	2.9944017	3.0093881
Au	5.7955874	2.5237254	-0.3254372	H	6.2075455	-1.2939445	6.9625976	N	5.9702761	2.2729186	3.0476737
Au	8.6793029	2.5232482	-0.3204051	H	7.1932181	1.9005955	10.6830072	H	11.6649607	2.7287748	2.9335415
Au	11.5630185	2.5227709	-0.3153730	H	5.6577105	-0.0391608	11.0778207	H	8.3366844	-2.9204040	2.7645956
Au	14.4467441	2.5222937	-0.3103409	H	5.5284814	-2.7462253	9.9375770	H	5.8864933	-3.0319143	2.6063729
Au	17.3304597	2.5218165	-0.3053088	H	4.7350254	-2.5236198	8.3405155	H	3.7517077	-1.7351947	2.5169075
Au	-15.8319489	5.0244158	-0.3272285	H	3.9813793	-4.3506313	9.6734445	H	3.7433707	0.7583367	2.6922255
Au	-12.9482333	5.0239386	-0.3221964	H	2.3901055	-5.9476259	10.7375700	H	10.5798906	4.9184905	2.7842029
Au	-10.0645177	5.0234613	-0.3171643	H	0.0277555	-2.6415546	12.2564620	H	8.4159112	6.1614449	2.6530118
Au	-7.1808022	5.0229841	-0.3121322	H	1.6877132	-1.0292952	11.2898705	H	6.2267487	4.9571086	2.7493183
Au	-4.2970766	5.0225069	-0.3071001	C	-13.6377992	-3.7763026	2.6159599	H	5.1044403	2.7904088	2.8832291
Au	-1.4133610	5.0220297	-0.3020680	C	-12.4544388	-4.5291974	2.6789702	C	8.1908286	0.7794064	5.0670820
Au	1.4703545	5.0215524	-0.2970359	C	-11.2242588	-3.8591750	2.8872179	C	7.8293110	0.6758198	6.2382920
Au	4.3540701	5.0210752	-0.2920038	C	-11.2119054	-2.4551543	3.0472107				

cis-Au(111)-**B** Optimization

$E_{PBE(D3)/def2\text{-}SVP}$ = -14609.64759805

Single Point w/o Au(111) surface

$E_{M06\text{-}2X(D3)/def2\text{-}TZVPP}$ = -3205.994729367 Hartree

Au	-14.3918209	-7.4965826	0.3034598	Au	-11.5081038	-7.4965179	0.2993902	Au	-8.6243866	-7.4964533	0.2953205

Au	-5.7406695	-7.4963886	0.2912509
Au	-2.8569424	-7.4963240	0.2871812
Au	0.0267747	-7.4962594	0.2831116
Au	2.9104919	-7.4961947	0.2790419
Au	5.7942190	-7.4961301	0.2749722
Au	8.6779361	-7.4960654	0.2709026
Au	11.5616532	-7.4960008	0.2668329
Au	14.4453804	-7.4959362	0.2627633
Au	-15.8337197	-4.9992699	0.3166762
Au	-12.9500025	-4.9992053	0.3126065
Au	-10.0662854	-4.9991406	0.3085369
Au	-7.1825683	-4.9990760	0.3044672
Au	-4.2988412	-4.9990114	0.3003975
Au	-1.4151240	-4.9989467	0.2963279
Au	1.4685931	-4.9988821	0.2922582
Au	4.3523102	-4.9988174	0.2881886
Au	7.2360374	-4.9987528	0.2841189
Au	10.1197545	-4.9986882	0.2800493
Au	13.0034716	-4.9986235	0.2759796
Au	15.8871887	-4.9985589	0.2719100
Au	-17.2756284	-2.5019473	0.3298926
Au	-14.3919013	-2.5018826	0.3258229
Au	-11.5081842	-2.5018180	0.3217532
Au	-8.6244670	-2.5017534	0.3176836
Au	-5.7407499	-2.5016887	0.3136139
Au	-2.8570228	-2.5016241	0.3095443
Au	0.0266943	-2.5015594	0.3054746
Au	2.9104115	-2.5014948	0.3014050
Au	5.7941386	-2.5014301	0.2973353
Au	8.6778557	-2.5013655	0.2932656
Au	11.5615728	-2.5013009	0.2891960
Au	14.4453000	-2.5012362	0.2851263
Au	17.3290171	-2.5011716	0.2810567
Au	-15.8338001	-0.0045600	0.3390393
Au	-12.9500829	-0.0044953	0.3349696
Au	-10.0663658	-0.0044307	0.3309000
Au	-7.1826487	-0.0043661	0.3268303
Au	-4.2989216	-0.0043014	0.3227606
Au	-1.4152044	-0.0042368	0.3186910
Au	1.4685127	-0.0041721	0.3146213
Au	4.3522298	-0.0041075	0.3105517
Au	7.2359570	-0.0040429	0.3064820
Au	10.1196741	-0.0039782	0.3024124
Au	13.0033912	-0.0039136	0.2983427
Au	15.8871083	-0.0038489	0.2942731
Au	-17.2757088	2.4927627	0.3522556
Au	-14.3919817	2.4928273	0.3481860
Au	-11.5082646	2.4928919	0.3441163
Au	-8.6245474	2.4929566	0.3400467
Au	-5.7408303	2.4930212	0.3359770
Au	-2.8571032	2.4930859	0.3319074
Au	0.0266139	2.4931505	0.3278377
Au	2.9103311	2.4932151	0.3237680
Au	5.7940582	2.4932798	0.3196984
Au	8.6777753	2.4933444	0.3156287
Au	11.5614924	2.4934091	0.3115591
Au	14.4452196	2.4934737	0.3074894
Au	17.3289367	2.4935384	0.3034198
Au	-15.8338805	4.9901399	0.3614023
Au	-12.9501633	4.9902046	0.3573327
Au	-10.0664462	4.9902692	0.3532630
Au	-7.1827291	4.9903339	0.3491933
Au	-4.2990020	4.9903985	0.3451237
Au	-1.4152848	4.9904632	0.3410540
Au	1.4684323	4.9905278	0.3369844
Au	4.3521494	4.9905924	0.3329147
Au	7.2358766	4.9906571	0.3288451
Au	10.1195937	4.9907217	0.3247754
Au	13.0033108	4.9907864	0.3207058
Au	15.8870279	4.9908510	0.3166361
Au	-14.3920621	7.4875272	0.3705490
Au	-11.5083450	7.4875919	0.3664794
Au	-8.6246278	7.4876565	0.3624097
Au	-5.7409107	7.4877212	0.3583401
Au	-2.8571836	7.4877858	0.3542704
Au	0.0265335	7.4878504	0.3502007
Au	2.9102507	7.4879151	0.3461311
Au	5.7939778	7.4879797	0.3420614
Au	8.6776949	7.4880444	0.3379918
Au	11.5614120	7.4881090	0.3339221
Au	14.4451392	7.4881736	0.3298525
C	7.5555013	-0.9695342	-7.1494071
C	7.7987720	-0.9821057	-8.5422995
C	6.2568014	-0.6411661	-6.6778771
C	5.2216937	-0.3298753	-7.5673013
C	6.7611526	-0.6651142	-9.4298734
C	5.4818250	-0.3366448	-8.9530117
C	3.8284862	-0.0518712	-7.0507341
O	3.9022260	0.5019942	-5.7337160
C	2.7631453	0.7534642	-5.0489976
C	2.9152483	1.3520967	-3.7750668
C	1.7935624	1.6554031	-3.0132285
C	0.4825223	1.3326885	-3.4532440
C	0.3387758	0.7492200	-4.7406595
C	1.4597001	0.4790531	-5.5304839
N	-0.5332616	1.7403404	-2.5535634
H	8.8009017	-1.2351165	-8.9170726
H	6.0745905	-0.6214556	-5.5949829
H	6.9534176	-0.6656175	-10.5134793
H	4.6811964	-0.0810142	-9.6654985
H	3.2431493	-1.0016662	-7.0209879
H	3.2907511	0.6486102	-7.7296351
H	3.9246143	1.6041988	-3.4174240
H	1.9017744	2.1568306	-2.0383120
H	-0.6503081	0.5254964	-5.1551079
H	1.3077649	0.0480638	-6.5287585
C	-7.4507369	-1.3015330	-7.2564353
C	-7.7145033	-0.9125084	-8.5884052
C	-6.1564586	-1.7765546	-6.9159610
C	-5.1290396	-1.8102317	-7.8619169
C	-6.6890117	-0.9784229	-9.5438020
C	-5.4020218	-1.4091966	-9.1875003
C	-3.7343814	-2.2644471	-7.4730109
O	-3.5567355	-2.5667278	-6.0904645
C	-3.2040063	-1.5671584	-5.2280032
C	-3.5689339	-0.2113924	-5.3872939
C	-3.1234893	0.7473128	-4.4628778
C	-2.2612194	0.3744023	-3.4130025
C	-1.9647363	-0.9927406	-3.2041828
C	-2.4435294	-1.9522834	-4.0999459
N	-1.7356750	1.3796050	-2.5518222
H	-8.7148410	-0.5469152	-8.8610395
H	-5.9591558	-2.0954026	-5.8824528
H	-6.8925299	-0.6726250	-10.5813703
H	-4.6026182	-1.4304822	-9.9459359
H	-2.9852196	-1.5026160	-7.7929699
H	-3.4887488	-3.2078050	-8.0062992
H	-4.2099059	0.0993603	-6.2239657
H	-3.3890972	1.8074769	-4.5907540
H	-1.3264097	-1.2906445	-2.3576135
H	-2.2019762	-3.0170956	-3.9656582
C	13.2247513	-3.3392614	-2.8400681
C	12.0952526	-4.1671185	-2.9192894
C	10.8190456	-3.5781036	-3.0990719
C	10.7080431	-2.1762862	-3.2270958
C	11.8411739	-1.3488772	-3.0684850
C	13.1160108	-1.9394503	-2.8775883
H	14.2162751	-3.7960547	-2.7042542
H	12.1948243	-5.2599904	-2.8425611
N	9.6613371	-4.3482340	-3.1450403
C	9.3846571	-1.5681922	-3.6279565
N	11.6737518	0.0313527	-3.0981641
H	14.0089752	-1.3060880	-2.7708533
C	9.2694689	-0.1452622	-3.1174258
C	10.4302119	0.6506763	-3.0082466
C	10.3010926	2.0478931	-2.8168805
C	9.0167459	2.6091080	-2.7282394
C	7.8571767	1.8163625	-2.7735690
C	7.9851262	0.4206350	-2.9615769
C	8.2331979	-2.4100523	-3.1100534
C	8.3846475	-3.8110115	-3.0273752
C	7.2413678	-4.6272649	-2.8424899
C	5.9790046	-4.0207786	-2.7494594
C	5.8241323	-2.6239266	-2.7643483
C	6.9668105	-1.8076829	-2.9516173
N	6.8743351	-0.4206116	-3.0162878
H	9.7617560	-5.3524270	-2.9848342
H	12.4964271	0.6067637	-2.9063909
H	11.1949046	2.6860597	-2.7553419
H	8.9168894	3.6967760	-2.5968343
H	6.8629054	2.2762220	-2.6731938
H	7.3408800	-5.7218711	-2.8034331
H	5.0889080	-4.6557220	-2.6255669
H	4.8261876	-2.1690179	-2.6775885
H	5.9661349	-0.0069141	-2.7950318
C	9.1389306	-1.4806468	-5.0980117
C	8.5242171	-1.2679696	-6.1442472
C	-13.2396319	-1.8952962	-2.8019378
C	-12.7923416	-0.5637196	-2.8395407
C	-11.4116219	-0.3057698	-3.0153564
C	-10.5160729	-1.3873232	-3.1571486
C	-10.9652559	-2.7199356	-3.0322314
C	-12.3476683	-2.9759133	-2.8673598
H	-14.3160366	-2.0931742	-2.6861559
H	-13.5063644	0.2683615	-2.7509172
N	-10.9058923	0.9922991	-3.0493429
C	-9.0918769	-1.1263921	-3.5858258
N	-10.0275750	-3.7491676	-3.0738886
H	-12.7150229	-4.0096868	-2.7853941
C	-8.1681042	-2.2173157	-3.0761063
C	-8.6567438	-3.5387421	-2.9751098
C	-7.7410329	-4.6056768	-2.8021233
C	-6.3661931	-4.3238183	-2.7389856
C	-5.8738771	-3.0084081	-2.7849090
C	-6.7869427	-1.9403996	-2.9597065
C	-8.6199289	0.2299177	-3.1017444
C	-9.5484403	1.2844733	-2.9738788
C	-9.0756944	2.6073102	-2.7784639
C	-7.6905833	2.8387766	-2.7234336
C	-6.7617751	1.7886808	-2.7887609
C	-7.2330728	0.4636291	-2.9725504
N	-6.3635829	-0.6183029	-3.0435125
H	-11.5603880	1.7543606	-2.8610656
H	-10.3681935	-4.6987959	-2.9121079
H	-8.1027276	-5.6427018	-2.7435277
H	-5.6556956	-5.1556022	-2.6206651
H	-4.7946125	-2.8078272	-2.7209936
H	-9.7853610	3.4430854	-2.6910531
H	-7.3263354	3.8675160	-2.5840966
H	-5.6816150	1.9841302	-2.7145701
H	-5.3644094	-0.4312427	-2.9248323
C	-8.9024346	-1.1538975	-5.0618801
C	-8.3698182	-1.1971330	-6.1704635

10 | Bibliography

[1] F. Schreiber. Self-assembled Monolayers: From Simple Model Systems to Biofunctionalized Interfaces. *Journal of Physics: Condensed Matter*, 16(28):R881–R900, 2004. doi: 10.1088/0953-8984/16/28/r01.

[2] J. C. Love, L. A. Estroff, J. K. Kriebel, R. G. Nuzzo, and G. M. Whitesides. Self-Assembled Monolayers of Thiolates on Metals as a Form of Nanotechnology. *Chem Rev.*, 105(4):1103–1170, 2005. doi: 10.1021/cr0300789.

[3] J. J. Gooding and S. Ciampi. The Molecular Level Modification of Surfaces: From Self-assembled Monolayers to Complex Molecular Assemblies. *Chemical Society Reviews*, 40(5):2704, 2011. doi: 10.1039/c0cs00139b.

[4] P. Tegeder. Optically and Thermally Induced Molecular Switching Processes at Metal Surfaces. *J. Phys. Condens. Matter*, 24(39):394001, 2012. doi: 10.1088/0953-8984/24/39/394001.

[5] E. Orgiu and P. Samorì. 25th Anniversary Article: Organic Electronics Marries Photochromism: Generation of Multifunctional Interfaces, Materials, and Devices. *Advanced Materials*, 26(12):1827–1845, 2014. doi: 10.1002/adma.201304695.

[6] D. A. Parthenopoulos and P. M. Rentzepis. Three-Dimensional Optical Storage Memory. *Science*, 245(4920):843–845, 1989. doi: 10.1126/science.245.4920.843.

[7] V. Balzani, A. Credi, and M. Venturi. Molecular Machines Working on Surfaces and at Interfaces. *ChemPhysChem*, 9(2):202–220, 2008. doi: 10.1002/cphc.200700528.

[8] D. Xiang, X. Wang, C. Jia, T. Lee, and X. Guo. Molecular-Scale Electronics: From Concept to Function. *Chemical Reviews*, 116(7):4318–4440, 2016. doi: 10.1021/acs.chemrev.5b00680.

[9] H. Jeong, D. Kim, D. Xiang, and T. Lee. High-Yield Functional Molecular Electronic Devices. *ACS Nano*, 11(7):6511–6548, 2017. doi: 10.1021/acsnano.7b02967.

[10] W. R. Browne and B. L. Feringa. Making Molecular Machines Work. *Nature Nanotechnology*, 1(1):25–35, 2006. doi: 10.1038/nnano.2006.45.

[11] J. M. Abendroth, O. S. Bushuyev, P. S. Weiss, and C. J. Barrett. Controlling Motion at the Nanoscale: Rise of the Molecular Machines. *ACS Nano*, 9(8): 7746–7768, 2015. doi: 10.1021/acsnano.5b03367.

[12] Press Release: The Nobel Prize in Chemistry 2016. `https://www.nobelprize.org/prizes/chemistry/2016/press-release/`, 05. October 2016.

[13] B. Baisch, D. Raffa, U. Jung, O. M. Magnussen, C. Nicolas, J. Lacour, J. Kubitschke, and R. Herges. Mounting Freestanding Molecular Functions onto Surfaces: The Platform Approach. *J. Am. Chem. Soc.*, 131(2):442–443, 2009. doi: 10.1021/ja807923f.

[14] U. Jung, S. Kuhn, U. Cornelissen, F. Tuczek, T. Strunskus, V. Zaporojtchenko, J. Kubitschke, R. Herges, and O. Magnussen. Azobenzene-Containing Triazatriangulenium Adlayers on Au(111): Structural and Spectroscopic Characterization. *Langmuir*, 27(10):5899–5908, 2011. doi: 10.1021/la104654p.

[15] U. Jung, J. Kubitschke, R. Herges, and O. Magnussen. Studies of the Molecular Switching of Azobenzene-Functionalized Platform Adlayers on Au(111) by Chronoamperometry. *Electrochim Acta*, 112:869–880, 2013. doi: 10.1016/j.electacta.2013.06.123.

[16] F. L. Otte, S. Lemke, C. Schütt, N. R. Krekiehn, U. Jung, O. M. Magnussen, and R. Herges. Ordered Monolayers of Free-Standing Porphyrins on Gold. *J. Am. Chem. Soc.*, 136(32):11248–11251, 2014. doi: 10.1021/ja505563e.

[17] H. Jacob, S. Ulrich, U. Jung, S. Lemke, T. Rusch, C. Schütt, F. Petersen, T. Strunskus, O. Magnussen, R. Herges, and F. Tuczek. Monitoring the Reversible Photoisomerization of an Azobenzene-Functionalized Molecular Triazatriangulene Platform on Au(111) by IRRAS. *Phys. Chem. Chem. Phys.*, 16(41):22643–22650, 2014. doi: 10.1039/c4cp03438d.

[18] S. Lemke, S. Ulrich, F. Claußen, A. Bloedorn, U. Jung, R. Herges, and O. M. Magnussen. Triazatriangulenium Adlayers on Au(111): Superstructure as a Function of Alkyl Side Chain Length. *Surf. Sci.*, 632:71–76, 2015. doi: 10.1016/j.susc.2014.08.028.

[19] G. Binnig, H. Rohrer, C. Gerber, and E. Weibel. Surface Studies by Scanning Tunneling Microscopy. *Physical Review Letters*, 49(1):57–61, 1982. doi: 10.1103/physrevlett.49.57.

[20] R. W. Hans-Joachim Güntherodt. *Scanning Tunneling Microscopy III*. Springer Berlin Heidelberg, 1996. ISBN 3540608249.

[21] W. Gärtner. Das Licht weise den Weg - oder: die Konformationsänderungen des Retinalchromophors im Sehpigment Rhodopsin nach Lichtanregung. *Angewandte Chemie*, 113(16):3065–3069, 2001. doi: 10.1002/1521-3757(20010817)113:16<3065::aid-ange3065>3.0.co;2-4.

[22] Z. F. Liu, K. Hashimoto, and A. Fujishima. Photoelectrochemical Information Storage Using an Azobenzene Derivative. *Nature*, 347(6294):658–660, 1990. doi: 10.1038/347658a0.

[23] T. Ikeda and O. Tsutsumi. Optical Switching and Image Storage by Means of Azobenzene Liquid-Crystal Films. *Science*, 268(5219):1873–1875, 1995. doi: 10.1126/science.268.5219.1873.

[24] A. C. Whalley, M. L. Steigerwald, X. Guo, and C. Nuckolls. Reversible Switching in Molecular Electronic Devices. *Journal of the American Chemical Society*, 129(42):12590–12591, 2007. doi: 10.1021/ja073127y.

[25] B. L. Feringa and W. R. Browne. *Molecular Switches*. Wiley VCH Verlag GmbH, 2011. ISBN 3527313656.

[26] M.-M. Russew and S. Hecht. Photoswitches: From Molecules to Materials. *Advanced Materials*, 22(31):3348–3360, 2010. doi: 10.1002/adma.200904102.

[27] G. S. HARTLEY. The Cis-form of Azobenzene. *Nature*, 140(3537):281–281, 1937. doi: 10.1038/140281a0.

[28] F. Krollpfeiffer, C. Mühlhausen, and G. Wolf. Zur Kenntnis der Lichtempfindlichkeit von Aryl-β-naphtylamin-azofarbstoffen. *Justus Liebigs Annalen der Chemie*, 508(1):39–51, 1934. doi: 10.1002/jlac.19345080106.

[29] G. Füchsel, T. Klamroth, J. Dokić, and P. Saalfrank. On the Electronic Structure of Neutral and Ionic Azobenzenes and Their Possible Role as Surface Mounted Molecular Switches. *The Journal of Physical Chemistry B*, 110(33): 16337–16345, 2006. doi: 10.1021/jp060969v.

[30] H. Rau and E. Lueddecke. On the Rotation-inversion Controversy on Photoisomerization of Azobenzenes. Experimental Proof of Inversion. *Journal of the American Chemical Society*, 104(6):1616–1620, 1982. doi: 10.1021/ja00370a028.

[31] T. Fujino, S. Y. Arzhantsev, and T. Tahara. Femtosecond Time-Resolved Fluorescence Study of Photoisomerization of trans-Azobenzene. *The Journal of Physical Chemistry A*, 105(35):8123–8129, 2001. doi: 10.1021/jp0110713.

[32] T. Schultz, J. Quenneville, B. Levine, A. Toniolo, T. J. Martínez, S. Lochbrunner, M. Schmitt, J. P. Shaffer, M. Z. Zgierski, and A. Stolow. Mechanism and Dynamics of Azobenzene Photoisomerization. *Journal of the American Chemical Society*, 125(27):8098–8099, 2003. doi: 10.1021/ja021363x.

[33] E. W.-G. Diau. A New Trans-to-Cis Photoisomerization Mechanism of Azobenzene on the S$-$1(n,π^*) Surface. *The Journal of Physical Chemistry A*, 108(6):950–956, 2004. doi: 10.1021/jp031149a.

[34] H. M. D. Bandara and S. C. Burdette. Photoisomerization in Different Classes of Azobenzene. *Chem. Soc. Rev.*, 41(5):1809–1825, 2012. doi: 10.1039/c1cs15179g.

[35] T. Ishikawa, T. Noro, and T. Shoda. Theoretical Study on the Photoisomerization of Azobenzene. *The Journal of Chemical Physics*, 115(16):7503–7512, 2001. doi: 10.1063/1.1406975.

[36] A. Cembran, F. Bernardi, M. Garavelli, L. Gagliardi, and G. Orlandi. On the Mechanism of the cis-trans Isomerization in the Lowest Electronic States of Azobenzene: S_0, S_1, and T_1. *J. Am. Chem. Soc.*, 126(10):3234–3243, 2004. doi: 10.1021/ja038327y.

[37] J.-M. Lehn. Supramolecular Chemistry. *Science*, 260(5115):1762+, 1993.

[38] R. Otero, J. M. Gallego, A. L. V. de Parga, N. Martín, and R. Miranda. Molecular Self-Assembly at Solid Surfaces. *Advanced Materials*, 23(44):5148–5176, 2011. doi: 10.1002/adma.201102022.

[39] A. Ulman. Formation and Structure of Self-Assembled Monolayers. *Chemical Reviews*, 96(4):1533–1554, 1996. doi: 10.1021/cr9502357.

[40] R. Klajn. Immobilized Azobenzenes for the Construction of Photoresponsive Materials. *Pure Appl. Chem.*, 82(12):2247–2279, 2010. doi: 10.1351/pac-con-10-09-04.

[41] N. Hauptmann, K. Scheil, T. G. Gopakumar, F. L. Otte, C. Schütt, R. Herges, and R. Berndt. Surface Control of Alkyl Chain Conformations and 2D Chiral Amplification. *J. Am. Chem. Soc.*, 135(24):8814–8817, 2013. doi: 10.1021/ja4036187.

[42] S. Lemke, C.-H. Chang, U. Jung, and O. M. Magnussen. Reversible Potential-Induced Switching of Alkyl Chain Aggregation in Octyl-Triazatriangulenium Adlayers on Au(111). *Langmuir*, 31(10):3115–3124, 2015. doi: 10.1021/acs.langmuir.5b00545.

[43] M. Elbing, A. Błaszczyk, C. von Hänisch, M. Mayor, V. Ferri, C. Grave, M. A. Rampi, G. Pace, P. Samorì, A. Shaporenko, and M. Zharnikov. Single Component Self-Assembled Monolayers of Aromatic Azo-Biphenyl: Influence of the Packing Tightness on the SAM Structure and Light-Induced Molecular Movements. *Adv. Funct. Mater.*, 18(19):2972–2983, 2008. doi: 10.1002/adfm.200800652.

[44] G. Pace, V. Ferri, C. Grave, M. Elbing, C. von Hanisch, M. Zharnikov, M. Mayor, M. A. Rampi, and P. Samori. Cooperative Light-Induced Molecular Movements of Highly Ordered Azobenzene Self-Assembled Monolayers. *Proc. Natl. Acad. Sci. U. S. A*, 104(24):9937–9942, 2007. doi: 10.1073/pnas.0703748104.

[45] L. Sosa-Vargas, E. Kim, and A.-J. Attias. Beyond "Decorative" 2D Supramolecular Self-assembly: Strategies Towards Functional Surfaces for Nanotechnology. *Materials Horizons*, 4(4):570–583, 2017. doi: 10.1039/c7mh00127d.

[46] M. Valášek, M. Lindner, and M. Mayor. Rigid Multipodal Platforms for Metal Surfaces. *Beilstein J. Nanotechnol.*, 7:374–405, 2016. doi: 10.3762/bjnano.7.34.

[47] M. Valášek and M. Mayor. Spatial and Lateral Control of Functionality by Rigid Molecular Platforms. *Chem. Eur. J.*, 23(55):13538–13548, 2017. doi: 10.1002/chem.201703349.

[48] S. Wagner, F. Leyssner, C. Kördel, S. Zarwell, R. Schmidt, M. Weinelt, K. Rück-Braun, M. Wolf, and P. Tegeder. Reversible Photoisomerization of an Azobenzene-functionalized Self-assembled Monolayer Probed by Sum-frequency Generation Vibrational Spectroscopy. *Physical Chemistry Chemical Physics*, 11(29):6242, 2009. doi: 10.1039/b823330f.

[49] S. Hagen, P. Kate, M. V. Peters, S. Hecht, M. Wolf, and P. Tegeder. Kinetic Analysis of the Photochemically and Thermally Induced Isomerization of an Azobenzene Derivative on Au(111) Probed by Two-Photon Photoemission. *Applied Physics A*, 93(2):253–260, 2008. doi: 10.1007/s00339-008-4831-5.

[50] K. Scheil, N. Lorente, M.-L. Bocquet, P. C. Hess, M. Mayor, and R. Berndt. Adatom Coadsorption with Three-Dimensional Cyclophanes on Ag(111). *J. Phys. Chem. C*, 121(45):25303–25308, 2017. doi: 10.1021/acs.jpcc.7b08953.

[51] P. Chinwangso, A. C. Jamison, and T. R. Lee. Multidentate Adsorbates for Self-Assembled Monolayer Films. *Accounts of Chemical Research*, 44(7):511–519, 2011. doi: 10.1021/ar200020s.

[52] L. Wei, H. Tiznado, G. Liu, K. Padmaja, J. S. Lindsey, F. Zaera, and D. F. Bocian. Adsorption Characteristics of Tripodal Thiol-Functionalized Porphyrins on Gold. *The Journal of Physical Chemistry B*, 109(50):23963–23971, 2005. doi: 10.1021/jp0537005.

[53] Y. Ie, T. Hirose, H. Nakamura, M. Kiguchi, N. Takagi, M. Kawai, and Y. Aso. Nature of Electron Transport by Pyridine-Based Tripodal Anchors: Potential for Robust and Conductive Single-Molecule Junctions with Gold Electrodes. *J. Am. Chem. Soc.*, 133(9):3014–3022, 2011. doi: 10.1021/ja109577f.

[54] T. Sebechlebská, J. Šebera, V. Kolivoška, M. Lindner, J. Gasior, G. Mészáros, M. Valášek, M. Mayor, and M. Hromadová. Investigation of the Geometrical Arrangement and Single Molecule Charge Transport in Self-assembled Monolayers of Molecular Towers Based on Tetraphenylmethane Tripod. *Electrochimica Acta*, 258:1191–1200, 2017. doi: 10.1016/j.electacta.2017.11.174.

[55] H. Jian and J. M. Tour. En Route to Surface-Bound Electric Field-Driven Molecular Motors. *J. Org. Chem.*, 68(13):5091–5103, 2003. doi: 10.1021/jo034169h.

[56] K.-Y. Chen, O. Ivashenko, G. T. Carroll, J. Robertus, J. C. M. Kistemaker, G. London, W. R. Browne, P. Rudolf, and B. L. Feringa. Control of Surface Wettability Using Tripodal Light-Activated Molecular Motors. *J. Am. Chem. Soc.*, 136(8):3219–3224, 2014. doi: 10.1021/ja412110t.

[57] S. Katano, Y. Kim, H. Matsubara, T. Kitagawa, and M. Kawai. Hierarchical Chiral Framework Based on a Rigid Adamantane Tripod on Au(111). *J. Am. Chem. Soc.*, 129(9):2511–2515, 2007. doi: 10.1021/ja065893v.

[58] T. Weidner, M. Zharnikov, D. G. Castner, and U. Siemeling. Adamantane-Based Tripodal Thioether Ligands Functionalized with a Redox-Active Ferrocenyl Moiety for Self-Assembled Monolayers. *The Journal of Physical Chemistry C*, 114(35):14975–14982, 2010. doi: 10.1021/jp104376p.

[59] T. Kitagawa, Y. Idomoto, H. Matsubara, D. Hobara, T. Kakiuchi, T. Okazaki, and K. Komatsu. Rigid Molecular Tripod with an Adamantane Framework and Thiol Legs. Synthesis and Observation of an Ordered Monolayer on Au(111). *The Journal of Organic Chemistry*, 71(4):1362–1369, 2006. doi: 10.1021/jo051863j.

[60] T. Kitagawa, H. Matsubara, K. Komatsu, K. Hirai, T. Okazaki, and T. Hase. Ideal Redox Behavior of the High-Density Self-Assembled Monolayer of a Molecular Tripod on a Au(111) Surface with a Terminal Ferrocene Group. *Langmuir*, 29(13):4275–4282, 2013. doi: 10.1021/la305092g.

[61] D. Takamatsu, Y. Yamakoshi, and K. ichi Fukui. Photoswitching Behavior of a Novel Single Molecular Tip for Noncontact Atomic Force Microscopy Designed for Chemical Identification. *The Journal of Physical Chemistry B*, 110 (5):1968–1970, 2006. doi: 10.1021/jp056986m.

[62] S. Zarwell and K. Rück-Braun. Synthesis of an Azobenzene-linker-conjugate with Tetrahedrical Shape. *Tetrahedron Letters*, 49(25):4020–4025, 2008. doi: 10.1016/j.tetlet.2008.04.086.

[63] J. Hierrezuelo, R. Rico, M. Valpuesta, A. Díaz, J. M. López–Romero, M. Rutkis, J. Kreigberga, V. Kampars, and M. Algarra. Synthesis of Azobenzene Substituted Tripod-shaped Bi(p-phenylene)s. Adsorption on Gold and CdS Quantum-dots Surfaces. *Tetrahedron*, 69(16):3465–3474, 2013. doi: 10.1016/j.tet.2013.02.054.

[64] K. Scheil, T. G. Gopakumar, J. Bahrenburg, F. Temps, R. J. Maurer, K. Reuter, and R. Berndt. Switching of an Azobenzene-Tripod Molecule on Ag(111). *J. Phys. Chem. Lett.*, 7(11):2080–2084, 2016. doi: 10.1021/acs.jpclett.6b01011.

[65] J. Henzl, M. Mehlhorn, H. Gawronski, K.-H. Rieder, and K. Morgenstern. Reversible cis-trans Isomerization of a Single Azobenzene Molecule. *Angew. Chem. Int. Ed.*, 45(4):603–606, 2006. doi: 10.1002/anie.200502229.

[66] B.-Y. Choi, S.-J. Kahng, S. Kim, H. Kim, H. W. Kim, Y. J. Song, J. Ihm, and Y. Kuk. Conformational Molecular Switch of the Azobenzene Molecule: A Scanning Tunneling Microscopy Study. *Physical Review Letters*, 96(15), 2006. doi: 10.1103/physrevlett.96.156106.

[67] M. J. Comstock, N. Levy, A. Kirakosian, J. Cho, F. Lauterwasser, J. H. Harvey, D. A. Strubbe, J. M. J. Fréchet, D. Trauner, S. G. Louie, and M. F. Crommie. Reversible Photomechanical Switching of Individual Engineered Molecules at a Metallic Surface. *Phys. Rev. Lett.*, 99(3), 2007. doi: 10.1103/physrevlett.99.038301.

[68] S. Hagen, F. Leyssner, D. Nandi, M. Wolf, and P. Tegeder. Reversible Switching of Tetra-Tert-Butyl-Azobenzene on a Au(111) Surface Induced by Light and Thermal Activation. *Chem. Phys. Lett.*, 444(1-3):85–90, 2007. doi: 10.1016/j.cplett.2007.07.005.

[69] M. Alemani, M. V. Peters, S. Hecht, K.-H. Rieder, F. Moresco, and L. Grill. Electric Field-Induced Isomerization of Azobenzene by STM. *J. Am. Chem. Soc.*, 128(45):14446–14447, 2006. doi: 10.1021/ja065449s.

[70] M. Alemani, S. Selvanathan, F. Ample, M. V. Peters, K.-H. Rieder, F. Moresco, C. Joachim, S. Hecht, and L. Grill. Adsorption and Switching Properties of Azobenzene Derivatives on Different Noble Metal Surfaces: Au(111), Cu(111), and Au(100). *J. Phys. Chem. C*, 112(28):10509–10514, 2008. doi: 10.1021/jp711134p.

[71] L. Óvári, M. Wolf, and P. Tegeder. Reversible Changes in the Vibrational Structure of Tetra-Tert-Butylazobenzene on a Au(111) Surface Induced by Light and Thermal Activation. *J. Phys. Chem. C*, 111(42):15370–15374, 2007. doi: 10.1021/jp075274o.

[72] P. Tegeder, S. Hagen, F. Leyssner, M. V. Peters, S. Hecht, T. Klamroth, P. Saalfrank, and M. Wolf. Electronic Structure of the Molecular Switch Tetra-*tert*-butyl-azobenzene Adsorbed on Ag(111). *Appl. Phys. A*, 88(3):465–472, 2007. doi: 10.1007/s00339-007-4047-0.

[73] C. Bronner, M. Schulze, S. Hagen, and P. Tegeder. The Influence of the Electronic Structure of Adsorbate–Substrate Complexes on Photoisomerization Ability. *New J. Phys.*, 14(4):043023, 2012. doi: 10.1088/1367-2630/14/4/043023.

[74] F. Matino, G. Schull, F. Kohler, S. Gabutti, M. Mayor, and R. Berndt. Electronic Decoupling of a Cyclophane from a Metal Surface. *Proc. Natl. Acad. Sci. U. S. A*, 108(3):961–964, 2010. doi: 10.1073/pnas.1006661107.

[75] B. W. Laursen and F. C. Krebs. Synthesis, Structure, and Properties of Azatriangulenium Salts. *Chem. Eur. J.*, 7(8):1773–1783, 2001. doi: 10.1002/1521-3765(20010417)7:8<1773::aid-chem17730>3.0.co;2-f.

[76] C. Nicolas and J. Lacour. Triazatriangulenium Cations: Highly Stable Carbocations for Phase-Transfer Catalysis. *Organic Letters*, 8(19):4343–4346, 2006. doi: 10.1021/ol0617392.

[77] S. Kuhn, U. Jung, S. Ulrich, R. Herges, and O. Magnussen. Adlayers Based on Molecular Platforms of Trioxatriangulenium. *Chemical Communications*, 47(31):8880, 2011. doi: 10.1039/c1cc12598b.

[78] S. Kuhn, B. Baisch, U. Jung, T. Johannsen, J. Kubitschke, R. Herges, and O. Magnussen. Self-Assembly of Triazatriangulenium-Based Functional Adlayers on Au(111) Surfaces. *Phys. Chem. Chem. Phys.*, 12(17):4481, 2010. doi: 10.1039/b922882a.

[79] U. Jung, O. Filinova, S. Kuhn, D. Zargarani, C. Bornholdt, R. Herges, and O. Magnussen. Photoswitching Behavior of Azobenzene-Containing Alkanethiol Self-Assembled Monolayers on Au Surfaces. *Langmuir*, 26(17):13913–13923, 2010. doi: 10.1021/la1015109.

[80] J. Kubitschke, C. Näther, and R. Herges. Synthesis of Functionalized Triazatriangulenes for Application in Photo-Switchable Self-Assembled Monolayers. *Eur. J. Org. Chem.*, 2010(26):5041–5055, 2010. doi: 10.1002/ejoc.201000650.

[81] U. Jung, C. Schütt, O. Filinova, J. Kubitschke, R. Herges, and O. Magnussen. Photoswitching of Azobenzene-Functionalized Molecular Platforms on Au Surfaces. *J. Phys. Chem. C*, 116(49):25943–25948, 2012. doi: 10.1021/jp310451c.

[82] M. Hammerich, T. Rusch, N. R. Krekiehn, A. Bloedorn, O. M. Magnussen, and R. Herges. Imine-Functionalized Triazatriangulenium Platforms: Towards an Artificial Ciliated Epithelium. *ChemPhysChem*, 17(12):1870–1874, 2016. doi: 10.1002/cphc.201600147.

[83] A. Schlimm, R. Löw, T. Rusch, F. Röhricht, T. Strunskus, T. Tellkamp, F. Sönnichsen, U. Manthe, O. Magnussen, F. Tuczek, and R. Herges. Long-Distance Rate Acceleration by Bulk Gold. *Angew. Chem. Int. Ed.*, 58(20):6574–6578, 2019. doi: 10.1002/anie.201814342.

[84] R. Löw, T. Rusch, F. Röhricht, O. M. Magnussen, and R. Herges. Diazocine Functionalized TATA Platforms. *Beilstein J. Org. Chem.*, Seite DOI: 10.3762/bxiv.2019.11.v1, 2019. doi: 10.3762/bxiv.2019.11.v1.

[85] R. Löw, T. Rusch, T. Moje, F. Röhricht, O. M. Magnussen, and R. Herges. Norbornadiene Functionalized Triaza-triangulenium and Trioxa-triangelium Platforms. *Beilstein J. Org. Chem.*, 15:1815–1821, 2019. doi: 10.3762/bxiv.2019.5.v1.

[86] T. R. Rusch, M. Hammerich, R. Herges, and O. M. Magnussen. Molecular Platforms as Versatile Building Blocks for Multifunctional Photoswitchable Surfaces. *Chemical Communications*, 55(64):9511–9514, 2019. doi: 10.1039/c9cc04528g.

[87] N. R. Krekiehn, M. Müller, U. Jung, S. Ulrich, R. Herges, and O. M. Magnussen. UV/Vis Spectroscopy Studies of the Photoisomerization Kinetics in Self-Assembled Azobenzene-Containing Adlayers. *Langmuir*, 31(30):8362–8370, 2015. doi: 10.1021/acs.langmuir.5b01645.

[88] S. Ulrich, U. Jung, T. Strunskus, C. Schütt, A. Bloedorn, S. Lemke, E. Ludwig, L. Kipp, F. Faupel, O. Magnussen, and R. Herges. X-Ray Spectroscopy Characterization of Azobenzene-Functionalized Triazatriangulenium Adlayers on Au(111) Surfaces. *Phys. Chem. Chem. Phys.*, 17(26):17053–17062, 2015. doi: 10.1039/c5cp01447f.

[89] The Nobel Prize in Physics 1986. `http://www.nobelprize.org/nobel_prizes/physics/laureates/1986/press.html`, 15. October 1986.

[90] N. D. Lang. Theory of Single-Atom Imaging in the Scanning Tunnelling Microscope. In *Solvay Conference on Surface Science*, Seite 216–221. Springer Berlin Heidelberg, 1988. doi: 10.1007/978-3-642-74218-7_18.

[91] P. O. Gartland, S. Berge, and B. J. Slagsvold. Photoelectric Work Function of a Copper Single Crystal for the (100), (110), (111), and (112) Faces. *Physical Review Letters*, 28(12):738–739, 1972. doi: 10.1103/physrevlett.28.738.

[92] C. J. M. Brugman, P. J. van Scherpenzeel, R. P. H. Rettschnick, and G. J. Hoijtink. On the Lower Excited Electronic States of Decacyclene. *The Journal of Chemical Physics*, 58(8):3468–3471, 1973. doi: 10.1063/1.1679678.

[93] T. Sano, H. Fujii, Y. Nishio, Y. Hamada, H. Takahashi, and K. Shibata. Organic Electroluminescent Devices Doped with Condensed Polycyclic Aromatic Compounds. *Synthetic Metals*, 91(1-3):27–30, 1997. doi: 10.1016/s0379-6779(97)03969-6.

[94] N. D. Lang. Apparent Size of an Atom in the Scanning Tunneling Microscope as a Function of Bias. *Physical Review Letters*, 58(1):45–48, 1987. doi: 10.1103/physrevlett.58.45.

[95] L. M. Wesoloski, A. Z. Stieg, M. Kunitake, S. C. Dultz, and J. K. Gimzewski. Observations of Image Contrast and Dimerization of Decacyclene by Low Temperature Scanning Tunneling Microscopy. *The Journal of Chemical Physics*, 127(17):174703, 2007. doi: 10.1063/1.2799991.

[96] N. Néel, J. Kröger, R. Berndt, T. O. Wehling, A. I. Lichtenstein, and M. I. Katsnelson. Controlling the Kondo Effect inCoCunClusters Atom by Atom. *Physical Review Letters*, 101(26), 2008. doi: 10.1103/physrevlett.101.266803.

[97] M. Ziegler, N. Ruppelt, N. Néel, J. Kröger, and R. Berndt. Control of Spin-polarized Current in a Scanning Tunneling Microscope by Single-atom Transfer. *Applied Physics Letters*, 96(13):132505, 2010. doi: 10.1063/1.3377917.

[98] L. Gross, F. Mohn, N. Moll, G. Meyer, R. Ebel, W. M. Abdel-Mageed, and M. Jaspars. Organic Structure Determination Using Atomic-resolution Scanning Probe Microscopy. *Nature Chemistry*, 2(10):821–825, 2010. doi: 10.1038/nchem.765.

[99] P. Jelínek. High Resolution SPM Imaging of Organic Molecules with Functionalized Tips. *Journal of Physics: Condensed Matter*, 29(34):343002, 2017. doi: 10.1088/1361-648x/aa76c7.

[100] M. J. Comstock, J. Cho, A. Kirakosian, and M. F. Crommie. Manipulation of Azobenzene Molecules on Au(111) Using Scanning Tunneling Microscopy. *Physical Review B*, 72(15), 2005. doi: 10.1103/physrevb.72.153414.

[101] N. D. Follin, K. D. Taylor, C. J. Musalo, and M. L. Trawick. Three-axis Correction of Distortion due to Positional Drift in Scanning Probe Microscopy. *Review of Scientific Instruments*, 83(8):083711, 2012. doi: 10.1063/1.4738646.

[102] R. Wiesendanger and H.-J. Güntherodt, editors. *Scanning Tunneling Microscopy II*. Springer Berlin Heidelberg, 1992. doi: 10.1007/978-3-642-97363-5.

[103] H.-J. Güntherodt and R. Wiesendanger, editors. *Scanning Tunneling Microscopy I*. Springer Berlin Heidelberg, 1992. doi: 10.1007/978-3-642-97343-7.

[104] D. Bonnell. *Scanning Probe Microscopy and Spectroscopy*. Wiley-Blackwell, 2001. ISBN 047124824X.

[105] C. J. Chen. *Introduction to Scanning Tunneling Microscopy*. Oxford University Press, 2007. doi: 10.1093/acprof:oso/9780199211500.001.0001.

[106] M. Hammerich and R. Herges. Laterally Mounted Azobenzenes on Platforms. *J. Org. Chem.*, 80(22):11233–11236, 2015. doi: 10.1021/acs.joc.5b02262. PMID: 26551306.

[107] G. Ertl, H. Knözinger, F. Schüth, and J. Weitkamp. Handbook of Heterogeneous Catalysis. Wiley-VCH, Weinheim, 2008.

[108] G. Ertl. Reactions at Surfaces: From Atoms to Complexity (Nobel Lecture). *Angew. Chem. Int. Ed.*, 47(19):3524–3535, 2008. doi: 10.1002/anie.200800480.

[109] B. G. Gowenlock. Arrhenius Factors (Frequency Factors) in Unimolecular Reactions. *Q. Rev. Chem. Soc.*, 14(2):133, 1960. doi: 10.1039/qr9601400133.

[110] A. Hauser. Intersystem Crossing in Fe(II) Coordination Compounds. *Coord. Chem. Rev.*, 111:275–290, 1991. doi: 10.1016/0010-8545(91)84034-3.

[111] J. N. Harvey. Understanding the Kinetics of Spin-forbidden Chemical Reactions. *Phys. Chem. Chem. Phys.*, 9(3):331–343, 2007. doi: 10.1039/b614390c.

[112] Peter R. Schreiner and Hans Peter Reisenauer and Frank C. Pickard IV and Andrew C. Simmonett and Wesley D. Allen and Edit Mátyus and Attila G. Császár. Capture of Hydroxymethylene and Its Fast Disappearance Through Tunnelling. *Nature*, 453(7197):906–909, 2008. doi: 10.1038/nature07010.

[113] A. Mishchenko, D. Vonlanthen, V. Meded, M. Bürkle, C. Li, I. V. Pobelov, A. Bagrets, J. K. Viljas, F. Pauly, F. Evers, M. Mayor, and T. Wandlowski. Influence of Conformation on Conductance of Biphenyl-Dithiol Single-Molecule Contacts. *Nano Letters*, 10(1):156–163, 2010. doi: 10.1021/nl903084b.

[114] A. Mishchenko, L. A. Zotti, D. Vonlanthen, M. Bürkle, F. Pauly, J. C. Cuevas, M. Mayor, and T. Wandlowski. Single-Molecule Junctions Based on Nitrile-Terminated Biphenyls: A Promising New Anchoring Group. *Journal of the American Chemical Society*, 133(2):184–187, 2011. doi: 10.1021/ja107340t.

[115] M. L. Kirk, D. A. Shultz, D. E. Stasiw, G. F. Lewis, G. Wang, C. L. Brannen, R. D. Sommer, and P. D. Boyle. Superexchange Contributions to Distance Dependence of Electron Transfer/Transport: Exchange and Electronic Coupling in Oligo(para-Phenylene)- and Oligo(2,5-Thiophene)-Bridged Donor–Bridge–Acceptor Biradical Complexes. *Journal of the American Chemical Society*, 135(45):17144–17154, 2013. doi: 10.1021/ja4081887.

[116] R. G. Greenler. Infrared Study of Adsorbed Molecules on Metal Surfaces by Reflection Techniques. *The Journal of Chemical Physics*, 44(1):310–315, 1966. doi: 10.1063/1.1726462.

[117] X. Yu, Z. Wang, M. Buchholz, N. Füllgrabe, S. Grosjean, F. Bebensee, S. Bräse, C. Wöll, and L. Heinke. Cis-to-Trans Isomerization of Azobenzene Investigated by Using Thin Films of Metal–organic Frameworks. *Physical Chemistry Chemical Physics*, 17(35):22721–22725, 2015. doi: 10.1039/c5cp03091a.

[118] S. D. Evans, S. R. Johnson, H. Ringsdorf, L. M. Williams, and H. Wolf. Photoswitching of Azobenzene Derivatives Formed on Planar and Colloidal Gold Surfaces. *Langmuir*, 14(22):6436–6440, 1998. doi: 10.1021/la980450t.

[119] M. Kaneta, T. Honda, K. Onda, and M. Han. Repeated Photoswitching Performance of Azobenzenes Adsorbed on Gold Surfaces: A Balance Between Space, Intermolecular Interactions, and Phase Separation. *New Journal of Chemistry*, 41(4):1827–1833, 2017. doi: 10.1039/c6nj03121h.

[120] A. Muždalo, P. Saalfrank, J. Vreede, and M. Santer. Cis-to-Trans Isomerization of Azobenzene Derivatives Studied with Transition Path Sampling and Quantum Mechanical/Molecular Mechanical Molecular Dynamics. *Journal of Chemical Theory and Computation*, 14(4):2042–2051, 2018. doi: 10.1021/acs.jctc.7b01120.

[121] T. Moldt, D. Przyrembel, M. Schulze, W. Bronsch, L. Boie, D. Brete, C. Gahl, R. Klajn, P. Tegeder, and M. Weinelt. Differing Isomerization Kinetics of Azobenzene-Functionalized Self-Assembled Monolayers in Ambient Air and in Vacuum. *Langmuir*, 32(42):10795–10801, 2016. doi: 10.1021/acs.langmuir.6b01690.

[122] X. Tong, M. Pelletier, A. Lasia, and Y. Zhao. FastCis–Trans Isomerization of an Azobenzene Derivative in Liquids and Liquid Crystals under a Low

Electric Field. *Angewandte Chemie International Edition*, 47(19):3596–3599, 2008. doi: 10.1002/anie.200705699.

[123] A. Goulet-Hanssens, M. Utecht, D. Mutruc, E. Titov, J. Schwarz, L. Grubert, D. Bléger, P. Saalfrank, and S. Hecht. Electrocatalytic Z $\rightarrow$ E Isomerization of Azobenzenes. *Journal of the American Chemical Society*, 139(1):335–341, 2016. doi: 10.1021/jacs.6b10822.

[124] G. L. Hallett-Tapley, C. D'Alfonso, N. L. Pacioni, C. D. McTiernan, M. González-Béjar, O. Lanzalunga, E. I. Alarcon, and J. C. Scaiano. Gold Nanoparticle Catalysis of the Cis–Trans Isomerization of Azobenzene. *Chemical Communications*, 49(86):10073, 2013. doi: 10.1039/c3cc41669k.

[125] E. Titov, L. Lysyakova, N. Lomadze, A. V. Kabashin, P. Saalfrank, and S. Santer. Thermal Cis-to-Trans Isomerization of Azobenzene-Containing Molecules Enhanced by Gold Nanoparticles: An Experimental and Theoretical Study. *The Journal of Physical Chemistry C*, 119(30):17369–17377, 2015. doi: 10.1021/acs.jpcc.5b02473.

[126] C. Bronner and P. Tegeder. Photo-induced and thermal reactions in thin films of an azobenzene derivative on Bi(111). *New Journal of Physics*, 16(5): 053004, 2014. doi: 10.1088/1367-2630/16/5/053004.

[127] P. Bortolus, L. Flamigni, S. Monti, M. Bolte, and G. Guyot. Silver(I) Perturbation of (E)–(Z) Photoisomerization of Stilbene and Azobenzene. *J. Chem. Soc., Faraday Trans.*, 87(9):1303–1309, 1991. doi: 10.1039/ft9918701303.

[128] R. A. van Delden, M. K. J. ter Wiel, M. M. Pollard, J. Vicario, N. Koumura, and B. L. Feringa. Unidirectional molecular motor on a gold surface. *Nature*, 437(7063):1337–1340, 2005. doi: 10.1038/nature04127.

[129] T. Kudernac, N. Ruangsupapichat, M. Parschau, B. Maciá, N. Katsonis, S. R. Harutyunyan, K.-H. Ernst, and B. L. Feringa. Electrically Driven Directional Motion of a Four-wheeled Molecule on a Metal Surface. *Nature*, 479(7372): 208–211, 2011. doi: 10.1038/nature10587.

[130] D. P. Goronzy, M. Ebrahimi, F. Rosei, Arramel, Y. Fang, S. D. Feyter, S. L. Tait, C. Wang, P. H. Beton, A. T. S. Wee, P. S. Weiss, and D. F. Perepichka. Supramolecular Assemblies on Surfaces: Nanopatterning, Functionality, and Reactivity. *ACS Nano*, 12(8):7445–7481, 2018. doi: 10.1021/acsnano.8b03513.

[131] J. Mielke, S. Selvanathan, M. Peters, J. Schwarz, S. Hecht, and L. Grill. Molecules with multiple switching units on a Au(111) surface: self-organization and single-molecule manipulation. *Journal of Physics: Condensed Matter*, 24(39):394013, 2012. doi: 10.1088/0953-8984/24/39/394013.

[132] M. Wolf and P. Tegeder. Reversible molecular switching at a metal surface: A case study of tetra-tert-butyl-azobenzene on Au(111). *Surface Science*, 603 (10-12):1506–1517, 2009. doi: 10.1016/j.susc.2008.11.049.

[133] S. Jaekel, A. Richter, R. Lindner, R. Bechstein, C. Nacci, S. Hecht, A. Kühnle, and L. Grill. Reversible and Efficient Light-Induced Molecular Switching on an Insulator Surface. *ACS Nano*, 12(2):1821–1828, 2018. doi: 10.1021/acsnano.7b08624.

[134] C. Nacci, M. Baroncini, A. Credi, and L. Grill. Reversible Photoswitching and Isomer-Dependent Diffusion of Single Azobenzene Tetramers on a Metal Surface. *Angew. Chem. Int. Ed.*, 57(46):15034–15039, 2018. doi: 10.1002/anie.201806536.

[135] T. Weidner, F. Bretthauer, N. Ballav, H. Motschmann, H. Orendi, C. Bruhn, U. Siemeling, and M. Zharnikov. Correlation between the Molecular Structure and Photoresponse in Aliphatic Self-Assembled Monolayers with Azobenzene Tailgroups. *Langmuir*, 24(20):11691–11700, 2008. doi: 10.1021/la802454w.

[136] V. Ferri, M. Elbing, G. Pace, M. Dickey, M. Zharnikov, P. Samorì, M. Mayor, and M. Rampi. Light-Powered Electrical Switch Based on Cargo-Lifting Azobenzene Monolayers. *Angew. Chem. Int. Ed.*, 47(18):3407–3409, 2008. doi: 10.1002/anie.200705339.

[137] C. Liu, D. Zheng, W. Hu, Q. Zhu, Z. Tian, J. Zhao, Y. Zhu, and J. Ma. Tuning the collective switching behavior of azobenzene/Au hybrid materials: flexible versus rigid azobenzene backbones and Au(111) surfaces versus curved Au nanoparticles. *Nanoscale*, 9(43):16700–16710, 2017. doi: 10.1039/c7nr03421k.

[138] V. Cantatore, G. Granucci, G. Rousseau, G. Padula, and M. Persico. Photoisomerization of Self-Assembled Monolayers of Azobiphenyls: Simulations Highlight the Role of Packing and Defects. *The Journal of Physical Chemistry Letters*, 7(19):4027–4031, 2016. doi: 10.1021/acs.jpclett.6b02018.

[139] K. M. McElhinny, J. Park, Y. Ahn, P. Huang, Y. Joo, A. Lakkham, A. Pateras, H. Wen, P. Gopalan, and P. G. Evans. Photoisomerization Dynamics in a Densely Packed Optically Transformable Azobenzene Monolayer. *Langmuir*, 34(37):10828–10836, 2018. doi: 10.1021/acs.langmuir.8b01524.

[140] T. Moldt, D. Brete, D. Przyrembel, S. Das, J. R. Goldman, P. K. Kundu, C. Gahl, R. Klajn, and M. Weinelt. Tailoring the Properties of Surface-Immobilized Azobenzenes by Monolayer Dilution and Surface Curvature. *Langmuir*, 31 (3):1048–1057, 2015. doi: 10.1021/la504291n.

[141] S. Yokoyama, T. Hirose, and K. Matsuda. Photochemical Cleavage of the Axial Group Attached to the Central Carbon Atom of Triazatriangulene. *Chemistry Letters*, 44(1):76–78, 2015. doi: 10.1246/cl.140897.

[142] J. M. Cowley. X-Ray Measurement of Order in Single Crystals of Cu3Au. *Journal of Applied Physics*, 21(1):24–30, 1950. doi: 10.1063/1.1699415.

[143] M. Avrami. Kinetics of Phase Change. II Transformation-Time Relations for Random Distribution of Nuclei. *The Journal of Chemical Physics*, 8(2):212–224, 1940. doi: 10.1063/1.1750631.

[144] U. Retter. Two-dimensional One-step Nucleation According to an Exponential Law in the Formation of Condensed Adsorption Films. *Journal of Electroanalytical Chemistry and Interfacial Electrochemistry*, 179(1-2):25–29, 1984. doi: 10.1016/s0022-0728(84)80271-5.

[145] D. Beljonne, C. Curutchet, G. D. Scholes, and R. J. Silbey. Beyond Förster Resonance Energy Transfer in Biological and Nanoscale Systems. *The Journal of Physical Chemistry B*, 113(19):6583–6599, 2009. doi: 10.1021/jp900708f.

[146] R. van Grondelle and V. I. Novoderezhkin. Energy Transfer in Photosynthesis: Experimental Insights and Quantitative Models. *Phys. Chem. Chem. Phys.*, 8:793–807, 2006. doi: 10.1039/b514032c.

[147] G. D. Scholes and G. R. Fleming. On the Mechanism of Light Harvesting in Photosynthetic Purple Bacteria: B800 to B850 Energy Transfer. *The Journal of Physical Chemistry B*, 104(8):1854–1868, 2000. doi: 10.1021/jp993435l.

[148] K. G. Yager and C. J. Barrett. Novel Photo-switching Using Azobenzene Functional Materials. *Journal of Photochemistry and Photobiology A: Chemistry*, 182(3):250–261, 2006. doi: 10.1016/j.jphotochem.2006.04.021.

[149] W. R. Browne and B. L. Feringa. Making Molecular Machines Work. In *Nanoscience and Technology*, Seite 79–89. Co-Published with Macmillan Publishers Ltd, UK, 2009. doi: 10.1142/9789814287005_0009.

[150] V. S. Miguel, C. G. Bochet, and A. del Campo. Wavelength-Selective Caged Surfaces: How Many Functional Levels Are Possible? *Journal of the American Chemical Society*, 133(14):5380–5388, 2011. doi: 10.1021/ja110572j.

[151] D. Bléger, J. Dokić, M. V. Peters, L. Grubert, P. Saalfrank, and S. Hecht. Electronic Decoupling Approach to Quantitative Photoswitching in Linear Multiazobenzene Architectures. *The Journal of Physical Chemistry B*, 115(33):9930–9940, 2011. doi: 10.1021/jp2044114.

[152] M. Dommaschk, C. Schütt, S. Venkataramani, U. Jana, C. Näther, F. D. Sönnichsen, and R. Herges. Rational Design of a Room Temperature Molecular Spin Switch. The Light-driven Coordination Induced Spin State Switch (LD-CISSS) Approach. *Dalton Trans.*, 43(46):17395–17405, 2014. doi: 10.1039/c4dt03048f.

[153] M. M. Lerch, M. J. Hansen, W. A. Velema, W. Szymanski, and B. L. Feringa. Orthogonal Photoswitching in a Multifunctional Molecular System. *Nature Communications*, 7(1):DOI: 10.1038/ncomms12054, 2016. doi: 10.1038/ncomms12054.

[154] M. Ito, T. X. Wei, P.-L. Chen, H. Akiyama, M. Matsumoto, K. Tamada, and Y. Yamamoto. A Novel Method for Creation of Free Volume in a One-Component Self-Assembled Monolayer. Dramatic Size Effect of Para-Carborane. *J. Mater. Chem.*, 15(4):478, 2005. doi: 10.1039/b411121d.

[155] D. Bléger, F. Mathevet, D. Kreher, A.-J. Attias, A. Bocheux, S. Latil, L. Douillard, C. Fiorini-Debuisschert, and F. Charra. Janus-Like 3D Tectons: Self-Assembled 2D Arrays of Functional Units at a Defined Distance from the Substrate. *Angew. Chem. Int. Ed.*, 50(29):6562–6566, 2011. doi: 10.1002/anie.201008212.

[156] S.-E. Zhu, Y.-M. Kuang, F. Geng, J.-Z. Zhu, C.-Z. Wang, Y.-J. Yu, Y. Luo, Y. Xiao, K.-Q. Liu, Q.-S. Meng, L. Zhang, S. Jiang, Y. Zhang, G.-W. Wang, Z.-C. Dong, and J. G. Hou. Self-Decoupled Porphyrin with a Tripodal Anchor for Molecular-Scale Electroluminescence. *J. Am. Chem. Soc.*, 135(42):15794–15800, 2013. doi: 10.1021/ja4048569.

[157] A. S. Kumar, T. Ye, T. Takami, B.-C. Yu, A. K. Flatt, J. M. Tour, and P. S. Weiss. Reversible Photo-Switching of Single Azobenzene Molecules in Controlled Nanoscale Environments. *Nano Letters*, 8(6):1644–1648, 2008. doi: 10.1021/nl080323+. PMID: 18444688.

[158] D. T. Valley, M. Onstott, S. Malyk, and A. V. Benderskii. Steric Hindrance of Photoswitching in Self-Assembled Monolayers of Azobenzene and Alkane Thiols. *Langmuir*, 29(37):11623–11631, 2013. doi: 10.1021/la402144g.

[159] T. R. Rusch, A. Schlimm, N. R. Krekiehn, B. M. Flöser, F. Röhricht, M. Hammerich, I. Lautenschläger, T. Strunskus, R. Herges, F. Tuczek, and O. M. Magnussen. Ordered Adlayers of a Combined Lateral Switch and Rotor. *J. Phys. Chem. C*, 123(22):13720–13730, 2019. doi: 10.1021/acs.jpcc.9b02469.

[160] J. Kubitschke. *Schaltbare Moleküle auf Oberflächen - das Plattform-Konzept*. Dissertation, Kiel University, 2010.

[161] A. Schlimm, N. Stucke, B. M. Flöser, T. Rusch, J. Krahmer, C. Näther, T. Strunskus, O. M. Magnussen, and F. Tuczek. Influence of a Metal Substrate on Small-Molecule Activation Mediated by a Surface-Adsorbed Complex. *Chemistry - A European Journal*, 24(42):10732–10744, 2018. doi: 10.1002/chem.201800911.

[162] G. Zuo, H. Yuan, J. Yang, R. Zuo, and X. Lu. Study of Orientation Mode of Cobalt-Porphyrin on the Surface of Gold Electrode by Electrocatalytic Dioxygen Reduction. *J. Mol. Catal. Chem.*, 269(1-2):46–52, 2007. doi: 10.1016/j.molcata.2006.11.041.

[163] R. Madueno, M. T. Räisänen, C. Silien, and M. Buck. Functionalizing Hydrogen-bonded Surface Networks with Self-assembled Monolayers. *Nature*, 454(7204):618–621, 2008. doi: 10.1038/nature07096.

[164] T. Kudernac, S. Lei, J. A. A. W. Elemans, and S. D. Feyter. Two-dimensional Supramolecular Self-assembly: Nanoporous Networks on Surfaces. *Chem. Soc. Rev.*, 38(2):402–421, 2009. doi: 10.1039/b708902n.

[165] S. Stepanow, M. Lingenfelder, A. Dmitriev, H. Spillmann, E. Delvigne, N. Lin, X. Deng, C. Cai, J. V. Barth, and K. Kern. Steering Molecular Organization and Host–Guest Interactions Using Two-dimensional Nanoporous Coordination Systems. *Nature Materials*, 3(4):229–233, 2004. doi: 10.1038/nmat1088.

[166] K. Cui, K. S. Mali, D. Wu, X. Feng, K. Müllen, M. Walter, S. D. Feyter, and S. F. L. Mertens. Reversible Anion-Driven Switching of an Organic 2D Crystal at a Solid-Liquid Interface. *Small*, 13(46):1702379, 2017. doi: 10.1002/smll.201702379.

[167] T. F. Magnera and J. Michl. Altitudinal Surface-Mounted Molecular Rotors. In *Molecular Machines*, Seite 63–97. Springer-Verlag, 2005. doi: 10.1007/128_014.

[168] G. T. Carroll, M. M. Pollard, R. van Delden, and B. L. Feringa. Controlled Rotary Motion of Light-Driven Molecular Motors Assembled on a Gold Film. *Chem. Sci.*, 1(1):97, 2010. doi: 10.1039/c0sc00162g.

[169] L. Kobr, K. Zhao, Y. Shen, A. Comotti, S. Bracco, R. K. Shoemaker, P. Sozzani, N. A. Clark, J. C. Price, C. T. Rogers, and J. Michl. Inclusion Compound Based Approach to Arrays of Artificial Dipolar Molecular Rotors. A Surface Inclusion. *J. Am. Chem. Soc.*, 134(24):10122–10131, 2012. doi: 10.1021/ja302173y.

[170] F. von Wrochem, F. Scholz, D. Gao, H.-G. Nothofer, A. Yasuda, J. M. Wessels, S. Roy, X. Chen, and J. Michl. High-Band-Gap Polycrystalline Monolayers of a 12-Vertex p-Carborane on Au(111). *J. Phys. Chem. Lett.*, 1(24):3471–3477, 2010. doi: 10.1021/jz101215h.

[171] Y. Yao and J. M. Tour. Facile Convergent Route to Molecular Caltrops. *J. Org. Chem.*, 64(6):1968–1971, 1999. doi: 10.1021/jo982085g.

[172] X. Zheng, M. E. Mulcahy, D. Horinek, F. Galeotti, T. F. Magnera, and J. Michl. Dipolar and Nonpolar Altitudinal Molecular Rotors Mounted on an Au(111) Surface. *J. Am. Chem. Soc.*, 126(14):4540–4542, 2004. doi: 10.1021/ja039482f.

[173] G. London, G. T. Carroll, T. F. Landaluce, M. M. Pollard, P. Rudolf, and B. L. Feringa. Light-Driven Altitudinal Molecular Motors on Surfaces. *Chem. Commun.*, 13:1712–1714, 2009. doi: 10.1039/b821755f.

[174] G. T. Carroll, G. London, T. F. Landaluce, P. Rudolf, and B. L. Feringa. Adhesion of Photon-Driven Molecular Motors to Surfaces via 1,3-Dipolar Cycloadditions: Effect of Interfacial Interactions on Molecular Motion. *ACS Nano*, 5(1):622–630, 2011. doi: 10.1021/nn102876j.

[175] C. J. Murphy, Z. C. Smith, A. Pronschinski, E. A. Lewis, M. L. Liriano, C. Wong, C. J. Ivimey, M. Duffy, W. Musial, A. J. Therrien, S. W. Thomas III, and E. C. H. Sykes. Ullmann Coupling Mediated Assembly of an Electrically Driven Altitudinal Molecular Rotor. *Phys. Chem. Chem. Phys.*, 17(47): 31931–31937, 2015. doi: 10.1039/C5CP05294G.

[176] J. Visser, N. Katsonis, J. Vicario, and B. L. Feringa. Two-Dimensional Molecular Patterning by Surface-Enhanced Zn-Porphyrin Coordination. *Langmuir*, 25(10):5980–5985, 2009. doi: 10.1021/la804196r.

[177] D. Bléger, A. Ciesielski, P. Samorì, and S. Hecht. Photoswitching Vertically Oriented Azobenzene Self-Assembled Monolayers at the Solid-Liquid Interface. *Chem. Eur. J.*, 16(48):14256–14260, 2010. doi: 10.1002/chem.201002834.

[178] S. Grimme, C. Bannwarth, and P. Shushkov. A Robust and Accurate Tight-Binding Quantum Chemical Method for Structures, Vibrational Frequencies, and Noncovalent Interactions of Large Molecular Systems Parametrized for All spd-Block Elements (Z = 1–86). *J Chem Theory Comput.*, 13(5):1989–2009, 2017. doi: 10.1021/acs.jctc.7b00118.

[179] J.-P. Ryckaert, G. Ciccotti, and H. J. C. Berendsen. Numerical Integration of the Cartesian Equations of Motion of a System with Constraints: Molecular Dynamics of n-Alkanes. *J. Comput. Phys.*, 23(3):327–341, 1977. doi: 10.1016/0021-9991(77)90098-5.

[180] F. Neese. Software Update: The ORCA Program System, Version 4.0. *Wiley Interdiscip. Rev. Comput. Mol. Sci.*, 8(1):e1327, 2017. doi: 10.1002/wcms.1327.

[181] J.-D. Chai and M. Head-Gordon. Long-Range Corrected Hybrid Density Functionals with Damped Atom–Atom Dispersion Corrections. *Phys. Chem. Chem. Phys.*, 10(44):6615, 2008. doi: 10.1039/b810189b.

[182] F. Weigend and R. Ahlrichs. Balanced Basis Sets of Split Valence, Triple Zeta Valence and Quadruple Zeta Valence Quality for H to Rn: Design and Assessment of Accuracy. *Phys. Chem. Chem. Phys.*, 7(18):3297, 2005. doi: 10.1039/b508541a.

[183] L. Goerigk, A. Hansen, C. Bauer, S. Ehrlich, A. Najibi, and S. Grimme. A Look at the Density Functional Theory Zoo with the Advanced GMTKN55 Database for General Main Group Thermochemistry, Kinetics and Noncovalent Interactions. *Phys. Chem. Chem. Phys.*, 19(48):32184–32215, 2017. doi: 10.1039/c7cp04913g.

[184] F. Neese, F. Wennmohs, A. Hansen, and U. Becker. Efficient, Approximate and Parallel Hartree–Fock and Hybrid DFT Calculations. A 'Chain-of-Spheres' Algorithm for the Hartree–Fock Exchange. *Chem. Phys.*, 356(1-3): 98–109, 2009. doi: 10.1016/j.chemphys.2008.10.036.

[185] F. Weigend. Accurate Coulomb-Fitting Basis Sets for H to Rn. *Phys. Chem. Chem. Phys.*, 8(9):1057, 2006. doi: 10.1039/b515623h.

[186] A. D. Becke. Density-Functional Thermochemistry. III. The Role of Exact Exchange. *J. Chem. Phys*, 98(7):5648–5652, 1993. doi: 10.1063/1.464913.

[187] R. Ditchfield, W. J. Hehre, and J. A. Pople. Self-Consistent Molecular-Orbital Methods. IX. An Extended Gaussian-Type Basis for Molecular-Orbital Studies of Organic Molecules. *J. Chem. Phys*, 54(2):724–728, 1971. doi: 10.1063/1.1674902.

[188] M. J. Frisch, G. W. Trucks, H. B. Schlegel, G. E. Scuseria, M. A. Robb, J. R. Cheeseman, G. Scalmani, V. Barone, and G. A. et al Petersson. Gaussian 16 Revision B.01. 2016.

[189] Y. Zhao and D. G. Truhlar. The M06 Suite of Density Functionals for Main Group Thermochemistry, Thermochemical Kinetics, Noncovalent Interactions, Excited States, and Transition Elements: Two New Functionals and Systematic Testing of Four M06-Class Functionals and 12 Other Functionals. *Theor. Chem. Acc.*, 120(1-3):215–241, 2007. doi: 10.1007/s00214-007-0310-x.

[190] S. Grimme, J. Antony, S. Ehrlich, and H. Krieg. A Consistent and Accurate Ab Initio Parametrization of Density Functional Dispersion Correction (DFT-D) for the 94 Elements H-Pu. *J. Chem. Phys*, 132(15):154104, 2010. doi: 10.1063/1.3382344.

[191] TURBOMOLE V7.0 2015, a Development of University of Karlsruhe and Forschungszentrum Karlsruhe GmbH, 1989-2007, TURBOMOLE GmbH, since 2007; Available from
http://www.turbomole.com Accessed: May 13, 2019.

[192] P. A. M. Dirac. Quantum Mechanics of Many-Electron Systems. *Proc. Royal Soc. A*, 123(792):714–733, 1929. doi: 10.1098/rspa.1929.0094.

[193] J. C. Slater. A Simplification of the Hartree-Fock Method. *Phys. Rev.*, 81(3): 385–390, 1951. doi: 10.1103/physrev.81.385.

[194] J. P. Perdew and Y. Wang. Accurate and Simple Analytic Representation of the Electron-Gas Correlation Energy. *Phys. Rev. B*, 45(23):13244–13249, 1992. doi: 10.1103/physrevb.45.13244.

[195] J. P. Perdew, K. Burke, and M. Ernzerhof. Generalized Gradient Approximation Made Simple. *Phys. Rev. Lett.*, 77(18):3865–3868, 1996. doi: 10.1103/physrevlett.77.3865.

[196] V. Chandrasekaran, H. Jacob, F. Petersen, K. Kathirvel, F. Tuczek, and T. K. Lindhorst. Synthesis and Surface-Spectroscopic Characterization of Photoisomerizable Glyco-SAMs on Au(111). *Chem. Eur. J.*, 20(28):8744–8752, 2014. doi: 10.1002/chem.201402075.

[197] R. J. Maurer and K. Reuter. Bistability Loss as a Key Feature in Azobenzene (Non-)Switching on Metal Surfaces. *Angew. Chem. Int. Ed.*, 51(48):12009–12011, 2012. doi: 10.1002/anie.201205718.

[198] R. J. Maurer and K. Reuter. Computational Design of Metal-Supported Molecular Switches: Transient Ion Formation during Light- and Electron-Induced iIsomerisation of Azobenzene. *J. Phys. Condens. Matter*, 31(4):044003, 2018. doi: 10.1088/1361-648x/aaf0e1.

[199] M. Marschall, J. Reichert, K. Seufert, W. Auwärter, F. Klappenberger, A. Weber-Bargioni, S. Klyatskaya, G. Zoppellaro, A. Nefedov, T. Strunskus, C. Wöll, M. Ruben, and J. V. Barth. Supramolecular Organization and Chiral Resolution of p-Terphenyl-m-Dicarbonitrile on the Ag(111) Surface. *ChemPhysChem*, 11(7):1446–1451, 2010. doi: 10.1002/cphc.200900938.

[200] M. F. Sykes and M. Glen. Percolation processes in two dimensions I. Low-density series expansions. *J. Phys. A: MAth. Gen.*, 9(1):87–95, 1976.

[201] E. B. Wilson. Probable Inference, the Law of Succession, and Statistical Inference. *J. Am. Stat. Assoc.*, 22(158):209–212, 1927. doi: 10.1080/01621459.1927.10502953.

[202] A. Hauser. Cooperative Effects on the HS→LS Relaxation in the [Fe(ptz)6](BF4)2 Spin-crossover System. *Chemical Physics Letters*, 192(1):65–70, 1992. doi: 10.1016/0009-2614(92)85429-e.

[203] R. Hinek, P. Gutlich, and A. Hauser. Cooperative Effects in the [Fe(mtz)6](BF4)2 Spin-crossover System: Fine Tuning the Energy Gap. *Inorganic Chemistry*, 33(3):567–572, 1994. doi: 10.1021/ic00081a027.

[204] N. Moliner, L. Salmon, L. Capes, M. C. Muñoz, J.-F. Létard, A. Bousseksou, J.-P. Tuchagues, J. J. McGarvey, A. C. Dennis, M. Castro, R. Burriel, and J. A. Real. Thermal and Optical Switching of Molecular Spin States in the [FeL[H2B(pz)2]2 Spin-Crossover System (L = bpy, phen). *The Journal of Physical Chemistry B*, 106(16):4276–4283, 2002. doi: 10.1021/jp013872b.

[205] S. Grimme, S. Ehrlich, and L. Goerigk. Effect of the Damping Function in Dispersion Corrected Density Functional Theory. *Journal of Computational Chemistry*, 32(7):1456–1465, 2011. doi: 10.1002/jcc.21759.

[206] M. J. Frisch, G. W. Trucks, H. B. Schlegel, G. E. Scuseria, M. A. Robb, J. R. Cheeseman, G. Scalmani, V. Barone, G. A. Petersson, H. Nakatsuji, and et al. Gaussian~16 Revision C.01, 2016. Gaussian Inc. Wallingford CT.

[207] B. Jeziorski, R. Moszynski, and K. Szalewicz. Perturbation Theory Approach to Intermolecular Potential Energy Surfaces of van der Waals Complexes. *Chemical Reviews*, 94(7):1887–1930, 1994. doi: 10.1021/cr00031a008.

[208] T. M. Parker, L. A. Burns, R. M. Parrish, A. G. Ryno, and C. D. Sherrill. Levels of Symmetry Adapted Perturbation Theory (SAPT). I. Efficiency and Performance for Interaction Energies. *The Journal of Chemical Physics*, 140(9): 094106, 2014.

[209] R. M. Parrish, L. A. Burns, D. G. A. Smith, A. C. Simmonett, A. E. DePrince, E. G. Hohenstein, U. Bozkaya, A. Y. Sokolov, and et al. Psi4 1.1: An Open-Source Electronic Structure Program Emphasizing Automation, Advanced Libraries, and Interoperability. *Journal of Chemical Theory and Computation*, 13 (7):3185–3197, 2017. doi: 10.1021/acs.jctc.7b00174.

[210] J. J. P. Stewart. Optimization of Parameters for Semiempirical Methods VI: More Modifications to the NDDO Approximations and Re-optimization of Parameters. *Journal of Molecular Modeling*, 19:1–32, 2013. doi: 10.1007/s00894-012-1667-x.

[211] B. O. Roos, P. R. Taylor, and P. E. M. Sigbahn. A Complete Active Space SCF Method (CASSCF) Using a Density Matrix Formulated Super-CI Approach. *Chemical Physics*, 48(2):157 – 173, 1980. doi: https://doi.org/10.1016/0301-0104(80)80045-0.

[212] K. Andersson, P. Malmqvist, and B. O. Roos. Second-order Perturbation Theory with a Complete Active Space Self-consistent Field Reference Function. *The Journal of Chemical Physics*, 96(2):1218–1226, 1992. doi: 10.1063/1.462209.

[213] F. Aquilante, J. Autschbach, R. K. Carlson, L. F. Chibotaru, M. G. Delcey, L. De Vico, I. Fdez. Galván, N. Ferré, L. M. Frutos, and et al. Molcas 8: New Capabilities for Multiconfigurational Quantum Chemical Calculations Across the Periodic Table. *Journal of Computational Chemistry*, 37(5):506–541, 2016. doi: 10.1002/jcc.24221.

[214] M. Quick, A. L. Dobryakov, M. Gerecke, C. Richter, F. Berndt, I. N. Ioffe, A. A. Granovsky, R. Mahrwald, N. P. Ernsting, and S. A. Kovalenko. Photoisomerization Dynamics and Pathways of trans- and cis-Azobenzene in Solution from Broadband Femtosecond Spectroscopies and Calculations. *The Journal of Physical Chemistry B*, 118(29):8756–8771, 2014. doi: 10.1021/jp504999f.

[215] C. Xu, L. Yu, F. L. Gu, and C. Zhu. Probing the $\pi - \pi^*$ Photoisomerization Mechanism of Trans-azobenzene by Multi-state ab initio on-the-fly Trajectory Dynamics Simulations. *Physical Chemistry Chemical Physics*, 20:23885–23897, 2018. doi: 10.1039/C8CP02767F.

[216] W.-Y. Gao, W. Yan, R. Cai, K. Williams, A. Salas, L. Wojtas, X. Shi, and S. Ma. A Pillared Metal–Organic Framework Incorporated with 1,2,3-Triazole Moieties Exhibiting Remarkable Enhancement of CO2 Uptake. *Chemical Communications*, 48(71):8898, 2012. doi: 10.1039/c2cc34380k.

Sworn Declaration

I hereby declare that I have written the present thesis independently under the guidance of my supervisor Prof. Dr. O. M. Magnussen and that I have not used any other sources and aids than those stated. This thesis was prepared adhering to the Rules of Good Scientific Practice of the German Research Foundation. This work has never fully or in part been used in another dissertation and comprises my first one. I was not deprived of an academic degree. Parts of the thesis have already been published or submitted as manuscripts for publication. My own contributions to these publications are summarized below.

Angew. Chem. Int. Ed. 2019, 58, 1-6, Chapter 4: Sample preparation, STM measurements and analysis of the STM data. Preparation of the corresponding figures and contributions to writing the manuscript.

Submitted to Angew. Chem. Int. Ed., Chapter 5: Sample preparation, STM measurements as well as analysis and interpretation of the STM data. Preparation of the corresponding graphics and substantial contributions to writing the manuscript.

Chem. Commun. 2019,55, 9511-9514., Chapter 6: Sample preparation, STM measurements as well as analysis and interpretation of the STM data. Creation of the corresponding figures and substantial contributions to writing the manuscript.

J. Phys. Chem. C 2019, 123, 22, 13720-13730., Chapter 7: Sample preparation, STM measurements as well as analysis and interpretation of the STM data. Creation of the figures except Fig. 1, Fig. 2, Fig. 7 and Fig. 8. Contributions to writing the manuscript.

Kiel,

Talina Rusch

Acknowledgements

Since this work is not the work of a single person, I would like to take this opportunity to thank all the people who have supported me over the past years with this thesis.
First of all, I would like to express my sincere gratitude to my supervisor Prof. Dr. Olaf Magnussen, not only for the opportunity to work on this exciting topic, but especially for the confidence, patience and support I've received from him in the recent years. No matter what the issue was, with his ideas and ability to express complex matters in simple terms, he has provided me with an invaluable service. I have always enjoyed working in the AG Magnussen.
Moreover I would like to thank

- Prof. Dr. Rainer Herges and the members of his research group for the exceptionally fruitful collaboration and the always helpful discussions during the project B09 meetings. Especially I thank Dr. Roland Löw and Dr. Melanie Hammerich for the synthesis of those amazing molecules. I also would like to thank Fynn Röhricht for the calculations and his patience.
- Prof. Dr. Felix Tuczek and his research group, particularly Dr. Alexander Schlimm, Benedikt Flöser, Dr. Nadja Stucke and Kai Uwe Clausen, for the great IRRAS, XPS and NEXAFS measurements, calculations and the many helpful discussions in the already mentioned B09/C13 meetings.
- Alex und Roland also for the amazing cooperation within the IGK and during our joint presentations. It has been a pleasure working with you.
- Nicolai Krekiehn for great UV/Vis spectra and the numerous discussions that have brought our project forward.
- my current and former office mates Dr. Martin Ruge, Dr. Finn Reikowski, Nicolai Krekiehn and Reihaneh Amirbeigiarab for the great time, the

team spirit and the encouragement. Mett Wednesdays, office ham and discussions about pretty much everything made sure that it never got boring with you.

- Dr. Sonja Lemke for the introduction to STM measurements and the numerous tips she gave me.
- Matthias Greve for his ideas and help with the implementation of the quartz fibers into the STM setup as well as the staff of the central workshop for the realization of the setup.
- Karsten Tarhouni, Arnd Seeger and Joost Jakobs for their technical support.
- Monika Seeger, Wiebke Wagner and Claudia Läufer for their support in administrative matters.

I am also deeply grateful for all the people who supported me outside of university. I want to express my gratitude to all my friends, especially Claudia.

The deepest thanks go to my family for their love and unconditional support: Sven, Mama, Papa, Thaisen, Arianna, Helene and Karin thank you so much for always being there!

Scientific Contributions

Publications

This thesis is based on the following publications:

- **Long-Distance Rate Acceleration by Bulk Gold**
  Alexander Schlimm, Roland Löw, Talina Rusch, Fynn Röhricht, Thomas Strunskus, Tobias Tellkamp, Frank Sönnichsen, Uwe Manthe, Olaf M. Magnussen, Felix Tuczek, Rainer Herges
  Angew. Chem. Int. Ed. 2019, 58, 1-6.

- **Observation of collective photoswitching in free-standing TATA-based azobenzenes on Au(111)**
  Talina R. Rusch, Alexander Schlimm, Nicolai R. Krekiehn, Tobias Tellkamp, Šimon Budzák, Denis Jacquemin, Felix Tuczek, Rainer Herges, Olaf M. Magnussen.
  submitted to Angew. Chem. Int. Ed.

- **Molecular platforms as versatile building blocks for multifunctional photoswitchable surfaces**
  Talina R. Rusch, Melanie Hammerich, Rainer Herges, Olaf M. Magnussen
  Chem. Commun. 2019,55, 9511-9514.

- **Ordered Adlayers of a Combined Lateral Switch and Rotor**
  Talina R. Rusch, Alexander Schlimm, Nicolai R. Krekiehn, Benedikt M. Flöser, Fynn Röhricht, Melanie Hammerich, Irene Lautenschläger, Thomas Strunskus, Rainer Herges, Felix Tuczek, Olaf M. Magnussen
  J. Phys. Chem. C 2019, 123, 22, 13720-13730.

Furthermore, I have contributed to the following publications during my time as a graduate student:

- **Imine-Functionalized Triazatriangulenium Platforms: Towards an Artificial Ciliated Epithelium**
  Melanie Hammerich, Talina Rusch, Nicolai R. Krekiehn, Andreas Bloedorn, Olaf M. Magnussen, Rainer Herges
  Phys. Chem. Chem. Phys. 2016, 17, 12, 1870-1874.

- **Influence of a Metal Substrate on Small-Molecule Activation Mediated by a Surface-Adsorbed Complex**
  Alexander Schlimm, Nadja Stucke, Benedikt M. Flöser, Talina Rusch, Jan Krahmer, Christian Näther, Thomas Strunskus, Olaf M. Magnussen, Felix Tuczek
  Chem. Eur. J. 2018, 24, 42, 10732-10744.

- **Diazocine-functionalized TATA platforms**
  Roland Löw, Talina Rusch, Fynn Föhricht, Olaf M. Magnussen, Rainer Herges
  Beilstein J. Org. Chem. 2019, 15, 1485–1490.

- **Norbornadiene-functionalized triazatriangulenium and trioxatriangulenium platforms**
  Roland Löw, Talina Rusch, Tobias Moje, Fynn Föhricht, Olaf M. Magnussen, Rainer Herges
  Beilstein J. Org. Chem. 2019, 15, 1815–1821.

Oral Presentations

- **7th SFB 677 Summer School**
  "STM Studies of Adsorbate Layers on Au (111)"
  Talina Rusch, Melanie Hammerich, Olaf M. Magnussen, Rainer Herges
  Ahrensburg 2016

- **Molecular Switches: Elementary Processes and Applications**
  "Investigation of Azobenzene TATA Platforms on Au(111)"
  Roland Löw, Talina Rusch, Alexander, Rainer Herges, Felix Tuczek, Olaf M. Magnussen
  Plön 2017

- **DPG Spring Meeting: Molecular Nanostructures on surfaces – New Concepts towards Complex Architectures**
  "STM Studies of Switchable Platform Molecules on Au(111)"
  Talina R. Rusch, Roland Löw, Alexander Schlimm, Felix Tuczek, Rainer Herges, Olaf M. Magnussen
  Berlin 2018

- **EMRS Spring Meeting: Scanning Probe Frontiers in Molecular 2D-Architecture World**
  "STM Studies of Switchable Platform Molecules on Au(111)"
  Talina R. Rusch, Nicolai R. Krekiehn, Roland Löw, Alexander Schlimm, Felix Tuczek, Rainer Herges, Olaf M. Magnussen
  Straßburg 2018

Poster Presentations

- **6th Baltic Electrochemistry Conference**
  "In situ STM Studies of Functional Platform Adlayers on Au(111) Surfaces"
  Sonja Lemke, Talina R. Rusch, Sandra Ulrich, Chi-Hao Chang, Ulrich Jung, Rainer Herges, Olaf M. Magnussen
  Helsinki 2016

- **ECHEMS - Electrochemistry in Ingenious Molecules, Surfaces and Devices**
  "STM Studies of Functional Platform Adlayers on Au(111) Surfaces"
  Talina Rusch, Melanie Hammerich, Roland Löw, Alexander Schlimm, Felix Tuczek, Rainer Herges, Olaf M. Magnussen
  Milano Marittima 2017

- **Molecular Switches: Elementary Processes and Applications**
  "STM Investigation of Switchable Platforms Adlayers on Au(111)"
  Talina Rusch, Roland Löw, Alexander Schlimm, Melanie Hammerich, Felix Tuczek, Rainer Herges, Olaf M. Magnussen
  Plön 2017

- **8th SFB 677 Summer School**
  "STM Investigation of Switchable Platforms Adlayers on Au(111)"
  Talina Rusch, Roland Löw, Alexander Schlimm, Felix Tuczek, Rainer Herges, Olaf M. Magnussen
  Hohwacht 2017

- **14th International Fischer Symposium**
  "STM Investigation of Switchable Platforms Adlayers on Au(111)"
  Talina Rusch, Roland Löw, Alexander Schlimm, Felix Tuczek, Rainer Herges, Olaf M. Magnussen
  Seeon 2018

- **9th SFB 677 Summer School**
  "STM Investigation of Switchable Platforms Adlayers on Au(111)"
  Talina Rusch, Roland Löw, Alexander Schlimm, Felix Tuczek, Rainer Herges, Olaf M. Magnussen
  Alt Duvenstedt 2018

Awards

- **Young Author Poster Prize**
  ECHEMS - Electrochemistry in Ingenious Molecules, Surfaces and Devices
  Milano Marittima 2017